SYNTHESIS AND CHARACTERIZATION OF YNEDIYL-BRIDGED PINCER COMPLEXES AND CONJUGATED BIS(PINCER) COMPLEXES FOR NOVEL METALLAPOLYMER PREPARATION

A Dissertation

by

CHENG-HAN YU

Submitted to the Office of Graduate and Professional Studies of
Texas A&M University
in partial fulfillment of the requirements for the degree of

DOCTOR OF PHILOSOPHY

Chair of Committee,	Oleg V. Ozerov
Committee Members,	Lei Fang
	David C. Powers
	Jaime C. Grunlan
Head of Department,	Simon W. North

December 2020

Major Subject: Chemistry

ABSTRACT

Since the discover of polyacetylene in the mid-19th century, organic conductive polymers have received a great deal of attention, especially in recent times. The emerging technologies, such as lithium batteries, organic semiconductors, solar cells, and luminescent probes, just to name a few, stimulate chemists to invent more advanced functional materials in order to fulfill the requirements. Concurrently, the understanding and development of conductive metallapolymers have flourished thanks to the maturity of organic synthesis and polymer chemistry. More and more studies demonstrate that the beneficial synergistic effect brought by metallapolymers can be applied in a wide range of fields.

The Ozerov group has been working with diarylamido (PNP) pincers as well as bis(pincer) complexes. Their physical and chemical features, such as the ligand-based redox behavior, numerous available modifications of functional groups and preference for coplanar coordination, are in common with many conventional ligands used in metallapolymers. Unavoidably, it spurred to think of an idea: could we incorporate these PNP complexes into conductive metallapolymers?

To put this idea into practice, first we examined the possibility of conjugation extension from the fourth coordination site of pincer group 10 metal complexes (^{Me}PNP)MCl. We successfully found a synthetic method to construct homo- and heterobimetallic ynediyl-bridged complexes. The bridged pincer dimer could be treated as a mixed-valence (MV) model. Physical methods such as cyclic voltammetry (CV), light absorption spectroscopy, electron paramagnetic resonance (EPR) spectroscopy and theoretical calculation using density functional theory (DFT) were used to study the electron delocalization phenomenon between two (^{Me}PNP)M moieties bridged by a μ-ethynediyl linker. With different chelated metals, we found the order of redox coupling is Pt > Ni

> Pd. The results are consistent with those obtained with *N,N′*-bis(salicylidene)ethylenediamine (salen) ligated group 10 complexes and further expand the knowledge from a monoatomic metal "stepping stone" to bimetallic ynediyl bridges.

Another direction involves extension of the π-system of the PNP ligand backbone. To this end, we envisioned bis(pincers) connected by π-conjugated linkers as promising candidates. We chose diphenyl ether, biphenyl, phenylene, and indolocarbarzole as the central bis(pincer) backbones and were able to synthesize and characterize bis(pincer) complexes. The mixed valence study showed that the π-delocalization was as good as in the organic analogues while the stability of the oxidized species was enhanced, leading to the successful isolation of their single crystals and X-ray crystallography characterization.

The combination of these two projects led to the exploration of a polymerization pathway derived from metal-to-metal bridging linkage. Bis(pincer) Pd complexes were selected to build up μ-ethynediyl-connected metallapolymers. Preliminary results of polymerization showed the highest M_n among the metallapolymers we obtained could be up to 18000, corresponding to 16 repeating units. On the other hand, the tetrametallic pincer complexes were also successfully synthesized. Lastly, the CV and UV-vis-NIR absorption spectra of tetrametallic complexes and metallapolymers were collected to understand the detailed electronic properties.

DEDICATION

To my beloved family and friends

ACKNOWLEDGEMENTS

I would like to thank my committee chair, Dr. Ozerov, for his continuous support during these five years. I appreciate his guiding in patience on English oral presentation, essay writing skill as well as thoughtful suggestions in chemistry expertise. My project is a little adventurous because it requires physical inorganic concepts and techniques that I was not familiar with. Dr. Ozerov gave me many helpful advises that sharpens my senses of this area.

Also, I would like to thank my committee members, Dr. Fang, Dr. Powers, and Dr. Grunlan, for their guidance and support throughout the course of this research and the revision of dissertation. Special thanks is given to Dr. Fang for the use of chemicals and equipment. I appreciate that we had chance to collaborate.

My colleagues in the Ozerov group, Chandra, Loren, Wei-Chun, Chris, Alex, Bryan, Qingheng, Ming-Uei, Olivia, Yihan, Yanwu, Mario, Brandy, Derek, Vinh, and Sam are the best. I met you guys in my PhD career. I will never forget in my life. I also appreciate Sakura Fu, Chen-Hao Wang, and Oscar, who came together with me from Taiwan to College Station at the same year. Katherine, Gina and Henry, thank you all and now it is your turn to struggle. I believe you guys can make it.

Friends in Taiwanese student association and Christian fellowship in College Station are with me all the time no matter my life was on the peaks or down to the valleys. Even the hard time like now under the COVID-19 pandemic, we are still connected online.

I would like to thank many friends in Taiwan, especially Mon-Chie Wang. I miss you a lot and I hope we can have time sharing our stories in the nearest future.

Finally, thanks to my mother and father for their encouragement and support. I miss you always. And thanks to my brother Cheng-Xuan, who generously provided PS4 for me.

CONTRIBUTORS AND FUNDING SOURCES

This work was supervised by a thesis (or) dissertation committee consisting of Professor Oleg V. Ozerov, Professor Lei Fang, Professor David C. Powers of the Department of Chemistry and Professor Jaime C. Grunlan of the Department of Mechanical Engineering.

The computational data analyzed for Chapter 2 was provided by Xin Yang as a graduate student from the Michael B. Hall group. The EPR data collected for Chapter 2 and 3 and GPC analysis for Chapter 4 were helped by Xiaozhou Ji and Che-Hsuan Chang as graduate students from the Lei Fang group. The Raman spectra conducted for Chapter 2 was collected by Chen-Hao Wang as a graduate student from the David C. Powers group in the Department of Chemistry at Texas A&M University. The XRD structures in Chapter 2 and 3 were solved by Dr. Nattamai Bhuvanesh who is a staff crystallographer in the Department of Chemistry at Texas A&M University. Synthesis of compound **72** was accomplished by Dr. Wei Hu as a postdoctoral research associate and Congzhi Zhu as a graduate student from the Lei Fang group. The computational data analyzed for Chapter 3 was provided by Congzhi Zhu and Xiaozhou Ji as graduate students. The EPR simulation for Chapter 3 was completed by Haomiao Xie as a graduate student from the Kim R. Dunbar group in the Department of Chemistry at Texas A&M University.

All other work conducted for the thesis (or) dissertation was completed by the student independently.

This work was also made possible in part by the support from the Welch Foundation (grants A-0648, A-1907, A-1717) and National Science Foundation under Grant Number DMR-1654029.

NOMENCLATURE

ACN	Acetonitrile
Ar	Aryl
BAr^F_4	Tetrakis[3,5-bis(trifluoromethyl)phenyl]borate
COD	Cyclooctadiene
Cp	Cyclopentadiene
CV	Cyclic voltammetry
DCM	Dichloromethane
DFT	Density functional theory
DMF	Dimethylformamide
DPPF	1,1'-Bis(diphenylphosphino)ferrocene
EPR	Electron paramagnetic resonance
Et	Ethyl
Fc	Ferrocene
G	Gauss
HOMO	Highest occupied molecular orbital
^iPr	isopropyl
IVCT	Inter-valence charge transfer
L	Ligand
LDA	Lithium diisopropylamide
LLCT	Ligand to ligand charge transfer
LMCT	Ligand to metal charge transfer
LUMO	Lowest unoccupied molecular orbital

MLCT	Metal to ligand charge transfer
MV	Mixed-valence
NBS	*N*-bromosuccinimide
^{n}Bu	*n*-butyl
NIR	Near infrared
NMR	Nuclear magnetic resonance
OAc	Acetate
OTf	Triflate
Ph	Phenyl
RT	Room temperature
^{t}Bu	*tert*-butyl
THF	Tetrahydrofuran
XRD	X-ray diffraction

TABLE OF CONTENTS

LIST OF SCHEMES

LIST OF FIGURES

LIST OF TABLES

CHAPTER I

INTRODUCTION AND LITERATURE REVIEW

1.1 Redox Non-innocent Ligands and Pincer Complexes

1.1.1 Redox Non-Innocent Ligands and Stable Metal-Organic Radicals

Redox non-innocent ligands are capable of expanding the redox sphere beyond the metal center. In other words, during reduction/oxidation of the complex, partial or total redox events could happen on the ligand. This phenomenon can be demonstrated by a classical system, nickel(II) bis(dithiolene) complex[1,2] in Figure **I-1**. The three stable oxidation states of Ni bis(stilbenedithiolate) complexes could be isolated, causing a confusion on how to assign the oxidation state of Ni in this type of complexes, although geometrically one can think about Ni(II) square planar at first glance. Recently, spectroscopic evidence obtained from X-ray absorption together with DFT calculations confirmed that they are all higher ligand valence "inverted" complexes and can be assigned as Ni(II).[3,4] In other words, during the oxidation, the radical anion is generated on the thiolate ligand without oxidizing the Ni(II) to Ni(III) or Ni(IV). The ligand non-innocence reactivity was illustrated by the observation of addition of alkenes to the ligand instead of interacting with the metal (Figure I-2).[2,5]

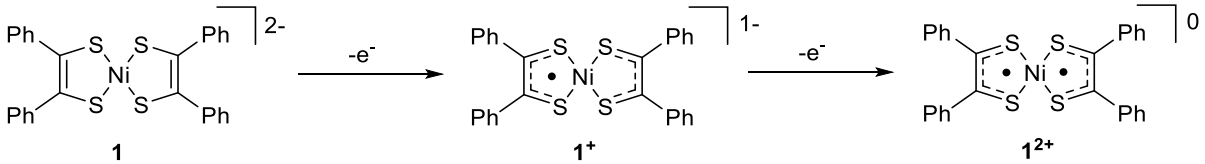

Figure **I-1**. Sequential oxidation of nickel(II) bis(stilbenedithiolate).

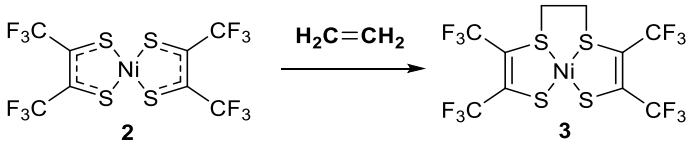

Figure **I-2**. Addition of the ethylene to $Ni[S_2C_2(CF_3)_2]_2$.

Redox non-innocent behavior of ligands is also observed in biochemistry, where some metalloenzymes utilize the metal and the ligand radical synergistically to catalyze chemical reactions. For example, galactose oxidase,[6] which contains copper(II) tyrosinyl radical on one of the peptide sequences, is capable of catalyzing oxidation of primary alcohols into aldehydes with turnover frequency up to 800 s^{-1}. Efficient reactivity is due to the fast hydrogen atom transfer (HAT) from the α-hydrogen of hydroxyl group to the tyrosinyl radical, followed by the catalyst regeneration with dioxygen.

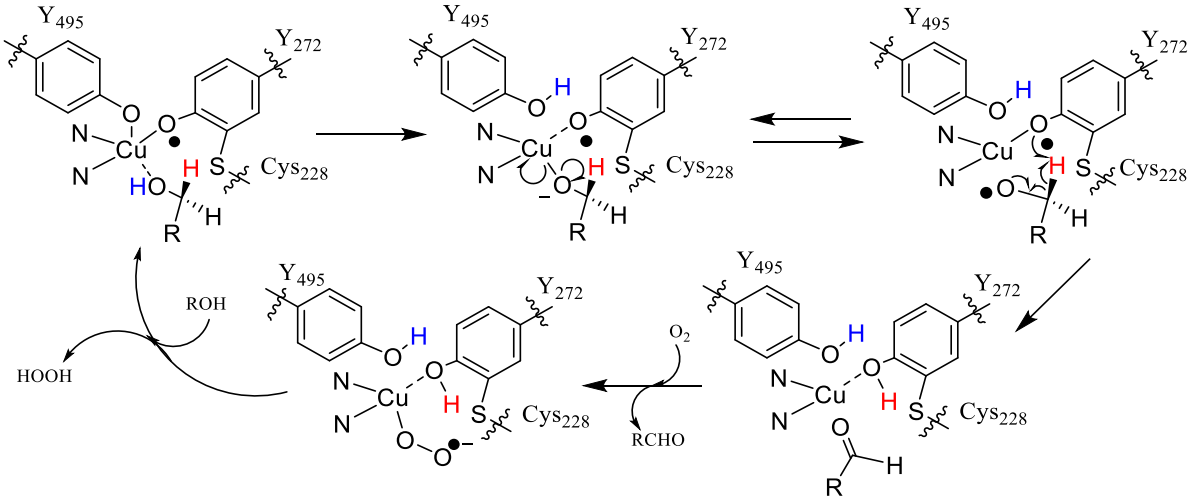

Figure I-3. Simplified mechanism of alcohol oxidation by galactose oxidase.

Compounds which contain a radical or multiple radicals are often highly reactive and cannot be easily characterized or isolated. Nevertheless, radical species are of interest because they appear

as intermediates in many chemical or biological process. Some radical compounds, however, are exceptionally stable which makes it possible to characterize, isolate or store them. A pioneer landmark discovery of this area is Gomberg's trityl radical (Figure I-4).[7] The trityl radical can dimerize under deoxygenated environment. The equilibrium is facile due to the intradimer bond is only ca. 11 kcal/mol,[8] resulting that this radical is persistent and easy to observe but can never be isolated as a pure radical form. The stability of trityl radical is attributed to its steric protection from three propeller phenyl rings as well as spin delocalization via π orbitals. The steric protection can be further enhanced by using the perchlorophenyl rings. In this way, the dimerization will be blocked and the radical will be isolable.[9,10]

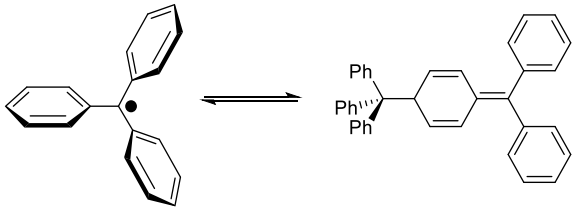

Figure I-4. Gomberg's trityl radical dimerization equilibrium.

Another strategy to stabilize radical species is via coordination to metals. Taking advantage of the mixing between metal d orbitals with the orbital of unpaired electron, the attached radical can form electronic isomers/valence tautomers that enhance the stability. This method led to the successful isolation of the oxyl and aminyl radical complexes by Tanaka[11] and Grützmacher,[12] respectively (Figure I-5). Notably, single crystals of those radical complexes were obtained and the solid state structures were determined by X-ray crystallography. Ru−O• bond length in this oxyl radical complex was measured 2.043(7) Å, which is clearly shorter than its H_2O adduct 2.099(3) Å. Meanwhile, the Rh−N• bond length was measured 1.936(3) Å comparing to the neutral

Rh−N bond 2.045(3) Å before oxidation. These are very impressive milestones that help advance the understanding of the physical properties of radicals.

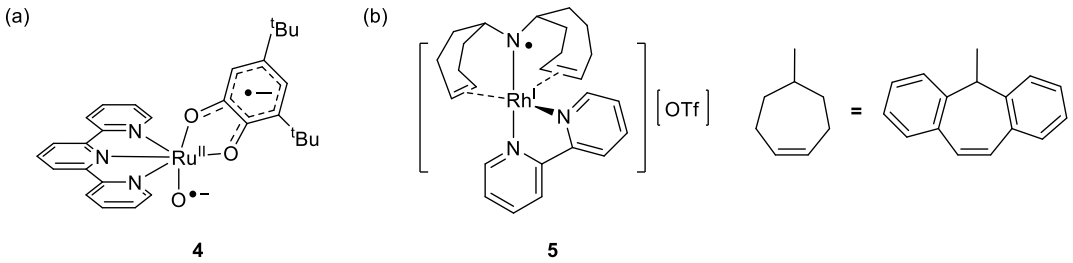

Figure I-5. Ru(II) oxyl radical complex **4** and Rh(I) aminyl complex **5**.

1.1.2 Valence Tautomerism

In the previous section, we mentioned the electronic isomer/valence tautomerism arising from the mixing of orbitals between a radical and a metal. The nature of this observation could be illustrated by cobalt catecholate derivatives.[13] In Figure I-6, the low-spin Co(III) complex was found as the ground state under lower temperature with a semiquinone radical anion and a neutral catecholate ligand. Upon raising the temperature, one electron from the neutral catecholate transfers to Co, thereby "reducing" Co(III) to Co(II). The ground state under this circumstance becomes two semiquinone radical anions with high-spin Co(II). The oxidation state determination method was again X-ray absorption/emission spectroscopy.

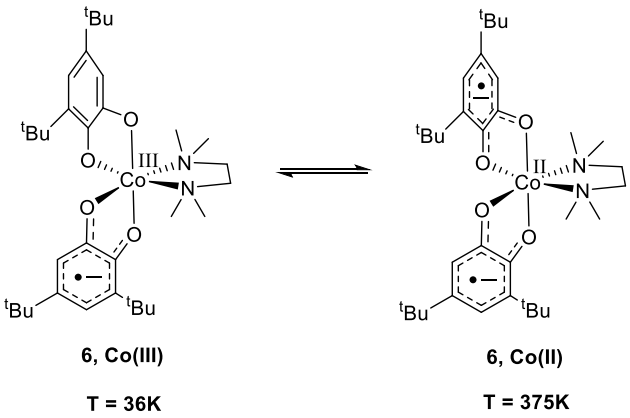

Figure I-6. Valence tautomerization of a cobalt diamino bis(catecholate) complex.

The example demonstrated above belongs to the discrete localized oxidation state. That is, the assignment of Co(II, III) with ligand oxidation states is distinct. Another model complex was demonstrated with bis(salicylidene) ethylenediamine (salen) ligand.[14] In 2007, Shimazaki *et al*. prepared group 10 salen complexes and investigated their oxidation products in detail. The oxidized Ni salen complex exhibited valence tautomerization between Ni(II)−phenoxyl radical and Ni(III)−phenolate species according to its ESR and X-ray absorption spectrum. In fact, the Ni(III) involved is minimal in this case, so it can still be claimed that the major form is Ni(II)−phenoxyl radical. The Pd complex, on the other hand, did not show significant difference in the Pd XPS data between neutral and mono-cation state. It is safe to conclude that Pd(II)−phenoxyl radical is the only existing state. Lastly, the oxidized Pt salen complex exhibited charge distribution in which the oxidation state of Pt becomes hard to determine. In this complex, the measured $4f_{5/2}$ and $4f_{7/2}$ binding energies of the neutral Pt(II) complex were 76.0 and 72.6 eV, respectively. On the other hand, the $4f_{5/2}$ and $4f_{7/2}$ binding energies collected from the mono-oxidized form were 76.3 and 72.9 eV, respectively. The difference between them was only 0.3 eV. Typically, the $4f_{5/2}$ and $4f_{7/2}$ binding energies of a Pt(III) or Pt(IV) complex would have at least 2 eV difference comparing to

a Pt(II) complex. As the result, the authors tended to assign the valence tautomers with non-integer oxidation states, of which Pt had +2.14 to +2.5. All in all, the valence tautomerization is an important study for understanding the metal-radical interaction.

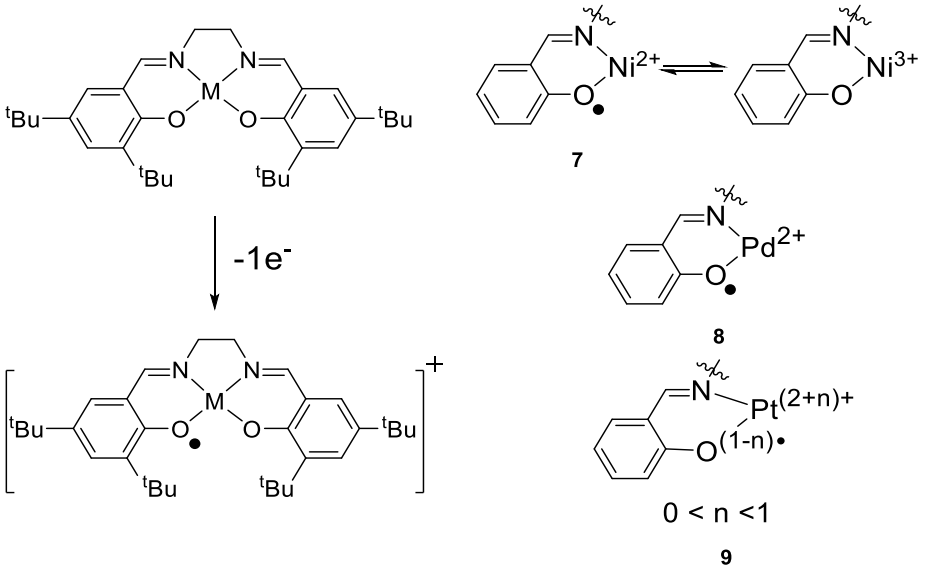

Figure I-7. The electronic properties of salen radical cation complexes.

1.1.3 Pincer Ligands and Complexes

A pincer ligand under a broad definition contains a central donor and two side arms which strongly prefer three-coordinated meridional fashion while chelating with metals.[15–17] Pioneer pincer ligands were synthesized by Shaw[18,19] and van Koten *et al*.[20] They reported carbanion center pincers with amines or phosphines as side arms that could be utilized to coordinate to group 9 or group 10 metals (Figure I-8).

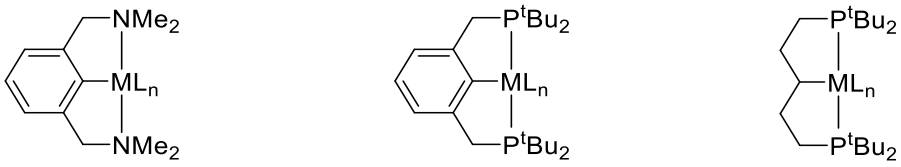

Figure I-8. Examples of pincer complexes from the 1970s.

A nomenclature of pincer ligands was suggested by Peris and Crabtree[15] according to their symmetry (palindromic and non-palindromic) and the nature of binding motifs (neutral and anionic as L and X). There is also a common naming feature of pincer ligands according to their donor atoms. For example, the ligands showing in Figure I-8 would all be called PCP ligands. Summary of types and simplified examples are illustrated in Figure I-9.

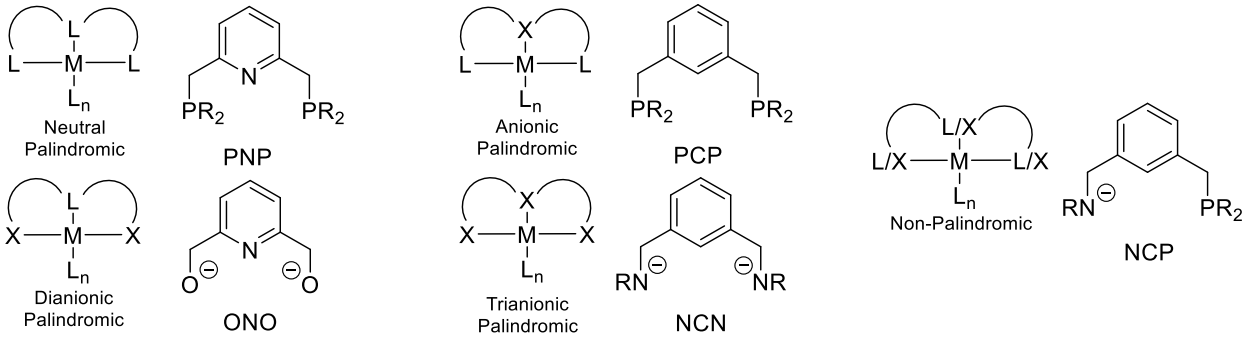

Figure I-9. Nomenclature and examples of pincer ligands.

By virtue of the versatility of donor atoms, pincer ligands are capable of chelating a wide variety of metals. A designer's blueprint is depicted in Figure I-10 The peripheral donors L with their substituents R_n can be easily modified to increase/decrease the steric effect on the metal reaction center.[21,22] Meanwhile, replacing a soft σ-donor atom like phosphorus or sulfur with a hard one like nitrogen or oxygen may cause the side arm to become labile.[23,24] The size of two chelating metallocycles can also be altered. In some cases, the common type 5,5-membered pincer

complexes can be forged into 5,6-membered or 6,6-membered pincer[25] without breaking their meridional coordination, thereby introducing new properties. In addition, ring sizes can be intentionally made too big to maintain the planar structure.[26]

The nature of the central donor X is of particular importance in influencing the structure and the reactivity of a pincer complex. For example, the PNP amido nitrogen is a weaker σ donor compared to the boryl of the PBP ligand, therefore, the position trans to X will experience different *trans* influence, resulting in the different rates of ligand exchange, coordination preference or complex geometry.[16]

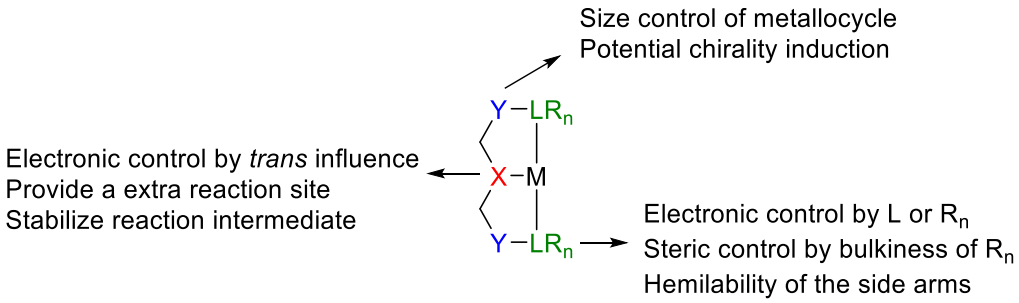

Figure I-10. Fine-tuning strategy on a pincer ligand.

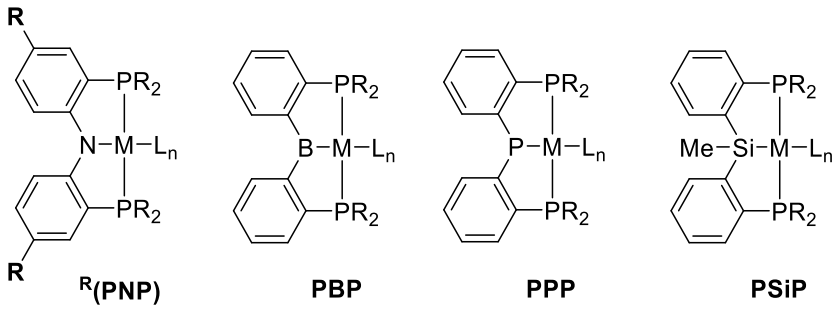

Figure I-11. Variations of the central donor on a diphenyl PXP pincer ligand.

1.1.4 Non-Innocent Chemical Reactivity of Pincer Ligands

Besides direct influence of electron donating ability toward the metal, pincer ligands can facilitate the overall reaction by the indirect ways. Cooperation modes between ligand and metal are depicted in Figure I-12.[27] In type A, the reactant A–B bond is broken heterolytically while the oxidation states of ligand and metal remain unchanged. In most cases, while encountering the reactant A–B, the more reactive site, either on the ligand or metal, will coordinate to the reactant to polarize it. Then the heterolytic bond activation happens. Notably, the oxidation states of L and M do not change after reaction. In type B, the ligand is involved in the oxidation/reduction partially or totally instead of only happening on the metal. The last case is the ligand chemical non-innocence reaction. Examples of this type are often found in proton coupled electron transfer (PCET) homolytic bond activation. Upon reacting with A–B, L and M prefers homolytic bond activation. One can think that this type is more like oxidation/reduction than nucleophilic/electrophilic attack.

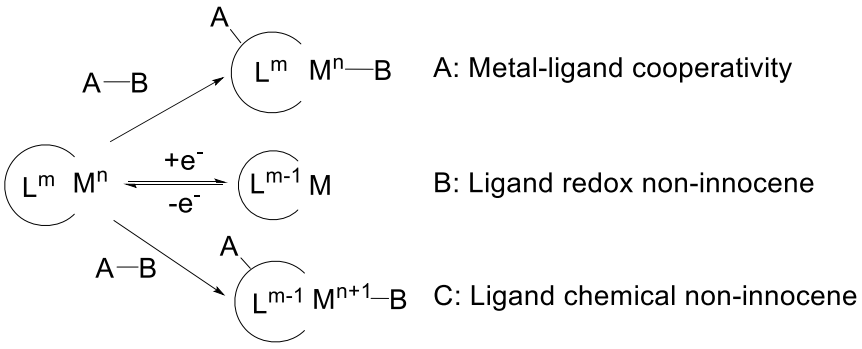

Figure I-12. Potential bond breaking processes of a cooperative complex.

Those types are just simplified illustrations. In fact, many reactions could proceed by more complicated mechanisms. Type A would be discussed in this section and type B in the next. The type C reaction is beyond this thesis so not included.[28] As shown in Figure I-13, (^{Me}PNP)PdOTf utilizes the Lewis basic non-bonding orbitals on the nitrogen, with an electron deficient Pd(II)

triflate motif, to effect the heterolytic bond breaking of H_2.[29] On the other hand, the boryl PBP Ir(I) dicarbonyl complex can be protonated by H_2O, followed by the capture of hydroxide ion with the Lewis acidic boron.[30] In addition, the cooperativity could happen with the participation of a remote position in the supporting ligand. For instance, Milstein[31–35] and our group[36] have separately published reports on the de-aromatization of lutidine- (**15**) and benzene-based ligands (**17**) by deprotonating the benzylic CH_2 group in the side arm. After de-aromatization, the nucleophilic carbon side arm is generated, which can be used as a tool for H_2 shuffling or CO_2 activation (Figure I-14).

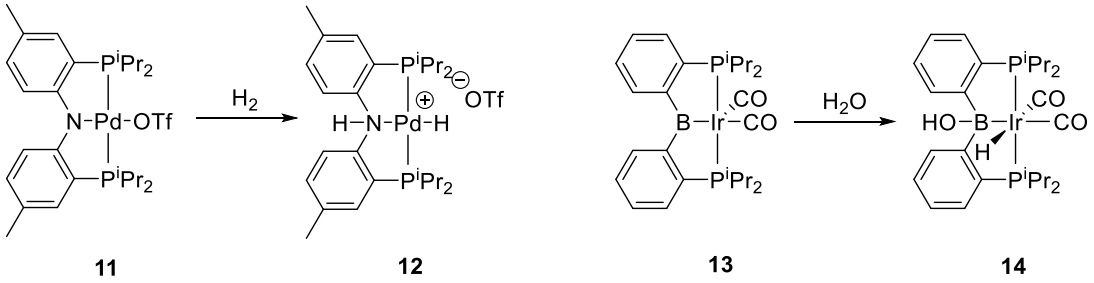

Figure I-13. Heterolytic bond activation (type A) on (^{Me}PNP)Pd and PBPIr complexes.

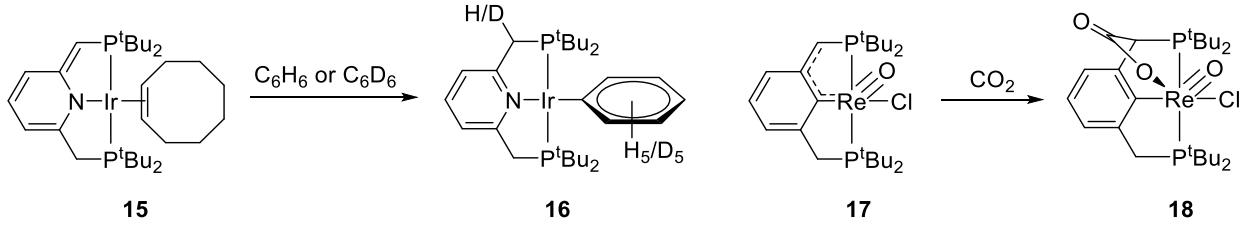

Figure I-14. Small molecule activation on side arms of lutidine-based PNPIr and benzene-based PCPRe complexes.

1.1.5 Non-Innocent Reduction/Oxidation on Pincer Ligands

The redox sphere expanded by the ligand can be utilized to avoid unwanted radical pathways in catalysis, stabilize the reaction intermediate, or control the physical properties.[37] In this section,

two types of non-innocent ligands corresponding to electron donor and acceptor will be discussed. The first example is the ditolylamido PNP ligand studied by Mindiola.[38] The nitrogen lone pair on the PNP ligand backbone could act as a redox center, so it is important to know how non-innocent could this charge be while it is complexed with metal. (^{Me}PNP)NiCl was then prepared and oxidized into mono-cationic state with ferrocenium triflate. This aminyl radical complex was stable enough to be isolated and studid by single crystal X-ray crystallography, XPS and EPR spectroscopy. These experimental data suggested the ligand-based aminyl radical with small amount of Ni(III). On the other hand, the computational result also showed SOMO orbital and spin density spreading mainly on PNP ligand framework (68%) and partly on nickel center (26%). Comparing to the Ni salen complex, the amount of Ni(III) is larger in the PNP complex. The significant reactivity with Mn(I) and Re(I) PNP aminyl radical was done by our group together with Nocera,[39] showing spin density was still mainly localized on the ligand backbone so it underwent de-aromatization allylation with allyltributylstannane.

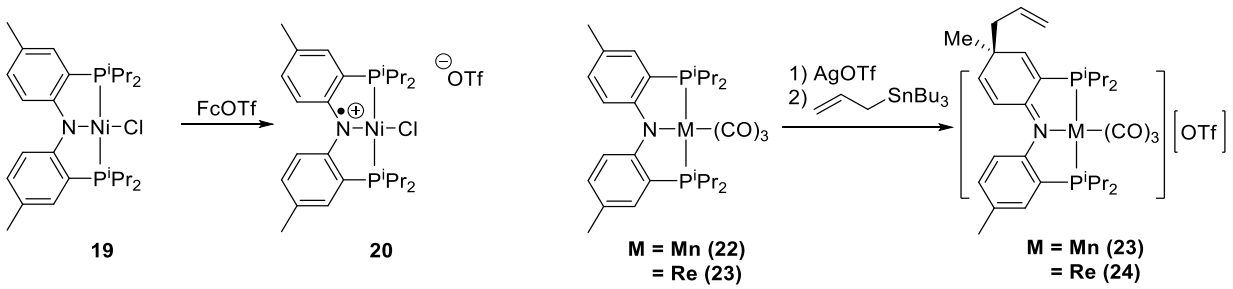

Figure I-15. (^{Me}PNP)NiCl oxidation and (^{Me}PNP)Mn and Re oxidation radical trapping experiment.

The second example is the bis(imino)pyridine (PDI) ligand.[37,40] The π* orbitals of imino groups are capable of accepting two electrons. After the first reduction with Na/Hg amalgam, a chloride ion dissociates from the Fe(II) center, forming compound **26**. Compound **26** can be reduced again using Na/Hg amalgam. The chloride ion dissociates and N_2 binds to the iron center. Detailed

analysis of the crystal metrical data, Mössbauer parameters, and computational studies showed that the spin density of unpaired electron of **26** and **27** was mainly located on the ligand backbone instead of on the metal center. The oxidation state of iron is mostly Fe(II) intact. Another example of a PDI coordinated complex was prepared by Rohde with Ni(II).[41] They found that after one-electron reduction, the ligand-based radical can react with dioxygen, resulting in the C–C bond cleavage oxygenation.

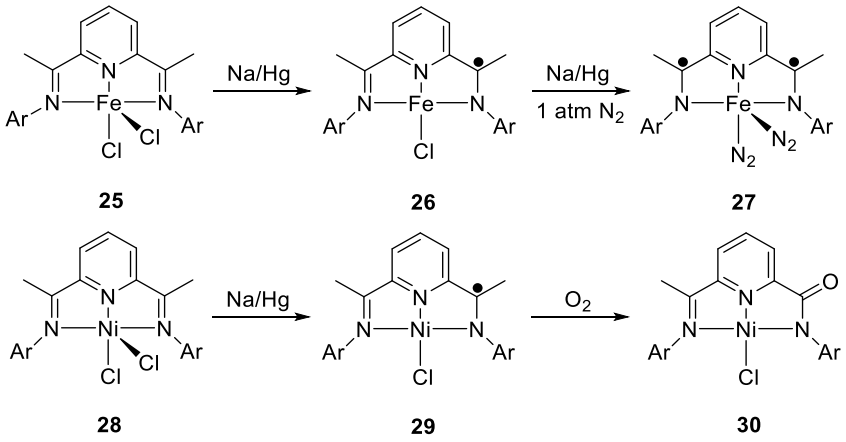

Figure I-16. (PDI)$FeCl_2$ sequential reduction and (PDI)$NiCl_2$ reduction activation of dioxygen.

1.2 Introduction of Mixed-valence Compounds.

1.2.1 Creutz-Taube Complex

The study of mixed-valence (MV) compounds can be traced back to early 1960s when penta-amminediruthenium with a bridging pyrazine, the well-known Creutz-Taube complex was prepared (Figure I-17).[42] Later Dr. Taube was awarded the Nobel Prize for research on electron transfer. The interesting point of this complex is the valence assignment of two Ru oxidation states. We know the sum of them are five so one must be Ru (II) and the other must be Ru (III). However, one cannot actually differentiate on which side is the Ru center +2 or +3 because it is a totally symmetric molecule. So is there a real Ru +2.5 state? In order to answer this ambiguous question,

a new concept had to be introduced.[43,44] That is, if the compound is mixed-valence, it is capable of hybridizing two degenerate states into a pair of localized-delocalized states, just as the inner electron transfer described in Marcus theory. In consequence, the orbitals of two Ru (III) with its bridge will merge into a new delocalized state for this incoming electron. One could say, it looks like two Ru +2.5 states, but more accurately, it should be one, called the Ru(II)/Ru(III) mixed-valence state.

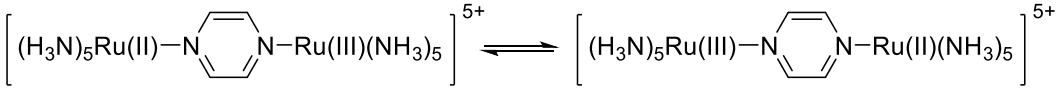

31

Figure I-17. The Creutz-Taube complex.

1.2.2 Robin-Day Classification

The mixed-valence compounds can be subdivided into three categories according to Robin and Day classification.[44,45] Class I describes the trapped valence on one side. That is, no bridge exists for the valence transferring from A to A'. In this case, A and A' will form two distinct states that they do not communicate to each other. It is also called the charge isolated state. Class II compounds are intermediate. The charge is moderately delocalized between redox centers. It is also known as the localized state. In class II, one can imagine two distinct state are partially hybridized, making their energy lower and share the character of each. Here the electron coupling energy is defined with Marcus-Hush theory[46] as H_{AB} which means the energy gained by orbital mixing for delocalization. This system exhibits an intervalence transition (IV-CT) shown as the red arrow. The existence of this transition, usually found in the near infrared (NIR) region, means the energy is required for interconverting the two distinct oxidation states. The H_{AB} can be calculated through mathematical operation on the IV-CT energy. For MV compounds belong to

class III, a totally delocalized state is postulated that is merged from the original two oxidation states. In this situation, the distinct states cannot be assigned anymore, and the transition represented by the red arrow becomes the charge resonance band from the total delocalized to localized orbital. In a more precise analysis, the transition from class II to III is not a discrete step. In fact, many cases can be assigned to be borderline between class II and III. One can notice, in class III compound, the two original separated ground states of A and A' merge into one delocalized state. The graph in Figure I-18 implies a less diffuse ground state. In some cases, especially organic MV compounds, the ground state composed by A and A' could be not very orientated. Taking tetraphenylphenylenediamine radical as an example, peripheral π orbitals on arenes along the travel way of the radical cation would introduce many vibration modes, leading to a unusual spectral feature.[47] Overall, one must be very careful in assigning the Robin-Day class if a new system is going to be introduced.

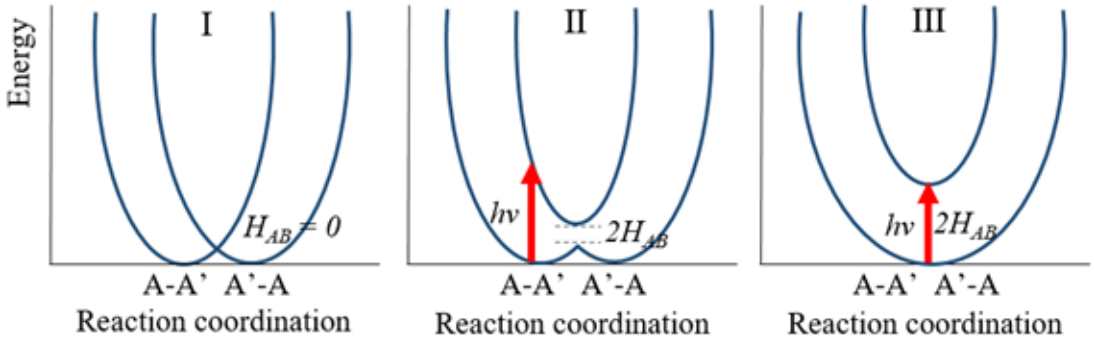

Figure I-18. Potential energy surface of Robin and Day classification.

1.2.3 Physical Methods for Mixed-Valence Investigation

Electron delocalization will affect many physical properties of a molecule. For example, for Robin-Day class III MV compounds, owing to that totally delocalized orbital, molecular structure determined by X-ray crystallography analysis a be close to symmetrical.[48,49] However, due to solid

state packing, while the molecules are close to each other, the distortion may happen in order to account for the interactions in the lattice. Although the symmetry could be instructive for determining class III compounds, the difference between class II and class I compounds could be minor. Besides the solid-state structural analysis, EPR spectroscopy could also be enlightening. MV compounds contain an unpaired electron that could be characterized by its coupling with the spins of the nuclei. This information could qualitatively characterize Class I-III MV compounds, but for the compounds at the borderline of II-III, due to the fast rate of electron transport, the relaxation of spin cannot really catch up the real situation of orbitals. That is, even if the EPR signal of a MV compound is found to reflect coupling to every surrounding nucleus, the real charge distribution could still be localized.

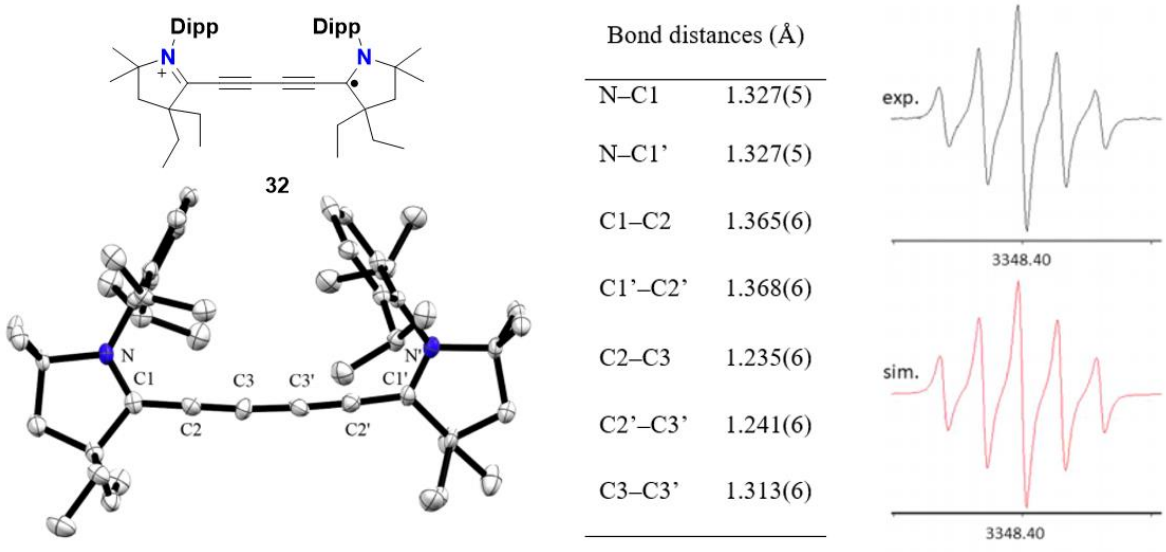

Bond distances (Å)	
N–C1	1.327(5)
N–C1'	1.327(5)
C1–C2	1.365(6)
C1'–C2'	1.368(6)
C2–C3	1.235(6)
C2'–C3'	1.241(6)
C3–C3'	1.313(6)

Figure I-19. A mixed-valence carbene crystal structure and its EPR spectrum published by the Bertrand group.[49] Counter anion $[SbF_6]^-$ is omitted for clarity. Dipp = 2,6-Diisopropylphenyl. Reprinted with permission from the ref. 49.

Electrochemical analysis with cyclic voltammetry could be a way to estimate the degree of electronic coupling. Taking diferrocene compounds[50] (Figure I-20) as examples, there are two potential oxidation events for Fe(II) to Fe(III).[51] While scanning these neutral compounds on CV,

it is possible to observe only one wave or two waves with a separation ΔE. Given that each wave on CV is corresponding to generation of the diferrocenyl cationic species, those phenomena can be explained: only one wave observed means the monocation and dication are generated at the same potential and the observation of two waves means they are generated at different potentials. The ΔE between the first and the second waves are the indication of monocation stability comparing to the sum of neutral and dicationic forms. One factor that can affect the monocation stability is the mixed-valence delocalization state. As was discussed above, the more delocalized MV state will provide more stability by lowering the energy level of the monocationic species. Therefore, it will result in a larger ΔE separating the redox events. Notably, even though it is a good guideline for MV classification, more precise analysis should take into consideration that the intrinsic energy difference between monocation and dication will also contribute to ΔE, not only the energy contributed from electron coupling.

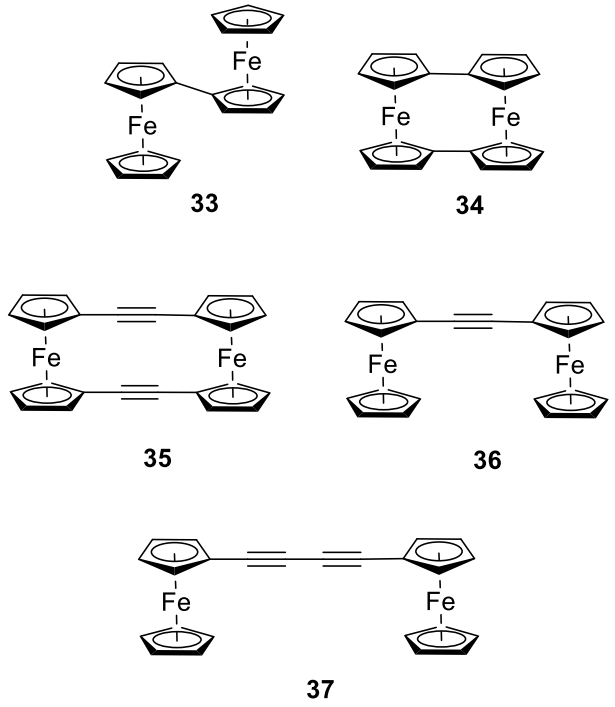

Complex	$E^1_{1/2}$ (V)	$E^2_{1/2}$ (V)	ΔE (V)
33	0.435	0.785	0.350
34	0.265	0.855	0.590
35	0.620	0.975	0.355
36	0.625	0.755	0.130
37	~0.58	~0.68	~0.10

Figure I-20. Diferrocene MV compounds and their CV data published by Cowan.[51]

The IR and Raman spectra arise from the absorptions that correspond to the bond stretching and bending modes.[47,52] A symmetrical vibration is the necessary feature for a total charge delocalized, Robin-Day class III compound. However, it is also important to be awared that the time scale of vibration is slower than the electron transition. With that, class II features can be determined by asymmetrical vibrational bands but class III compounds will need additional supporting evidence. Theoretical calculation using density functional theory (DFT) to simulate unpaired electron is more mature today. With the proper basis set, the degree of electron delocalization could be finely described and visualized by isosurface plots.[53,54] Time-dependent density functional theory (TD-DFT) became a common tool for predicting electronic transitions.[55] This calculation mode could help correlated the essential absorption peaks to the frontier molecular orbitals. Usually, the calculation method works well enough for simple organic compounds. To organometallic complexes, the proper method is sometimes hard to find.

The IVCT band is the most determinative feature of a MV compound. This transition corresponding to the valence interconversion usually appears in the near-infrared (NIR) region. For Robin-Day class I molecules, since the charge is isolated, the IVCT band would be absent. The MV compounds between class II and class III will have different band parameters that one can utilize to calculate the Hush electron coupling energy *V*, which is the quantitative indication about how high is the barrier to move the valence. Typical class III compounds will have *V* at around 3000-4000 cm^{-1}. The higher *V*, the greater separation between the localized and delocalized states, meaning the higher stabilization contributed by the delocalization. Although the IVCT band analysis is a very reliable method, some difficulties still exist. For example, there could be multiple absorptions in the same region where the IVCT band should appear. Determining the correct band is sometimes problematic. This challenge often happens while analyzing metal complexes because

their d orbitals provide extra pathways. Another potential difficulty is the identification of Robin-Day III MV compounds. The IVCT band itself cannot provide the direct information of orbital mixing. Instead, it can only tell us the electron coupling energy by assuming their class at first. By comparing this information to the analogs, we can then decide whether the previous assignment is reasonable. As a result, if a new type MV compound is introduced and it is at the borderline of II-III, IVCT spectral analysis alone cannot certainly determine whether it is class III or not. The overall features of experimental evidences above should be consistent to give the accurate answer.

1.3 Introduction of Coplanarized Compounds

1.3.1 Synthesis of Fully Conjugated "Ladder" Polymers

Conjugated polymers which have fully fused aromatic backbones are considered as the one dimensional micro graphene.[56–58] The development of this area has drawn much attention[57,59–61] in recent years because the molecules or polymers with ladder structure show unique optical, physical and chemical properties comparing to their unlocked relatives. An early method for synthesizing ladder polymers was demonstrated by Swager.[62] This reaction was simply based on the electrophilic substitution on backbone phenyl group. Surprisingly, it was very successful and could convert this polymer (M_n = 45000 ~ 50000 g/mol) to its ladder form in nearly quantitative yields.

A similar approach using electrophilic cyclization was done by Fang.[63] With this method, the quinacridone functional group can be readily introduced in the ladder in contrast to all-carbon polymer. Notably, inter-molecular hydrogen bonds as well as the π-π stacking makes this polymer highly insoluble. The characterization has to be done via replacing N–H by *tert*-butyl carbamate (Boc) groups. In recent development, the method for building up ladder molecule is not restricted

to covalent bond only. Non-covalent interactions such as hydrogen bonding, Lewis acid-base adduct formation, and metal coordination could be utilized to construct a ladder type compound.

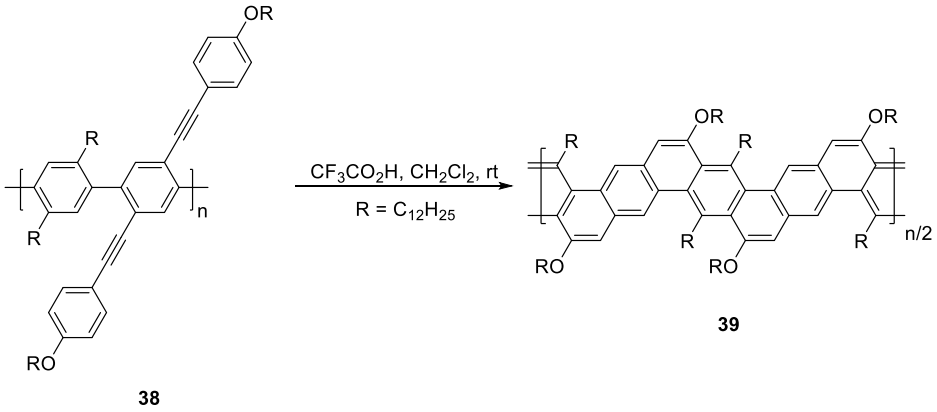

Figure I-21. Coplanarization of phenyl-based polymer

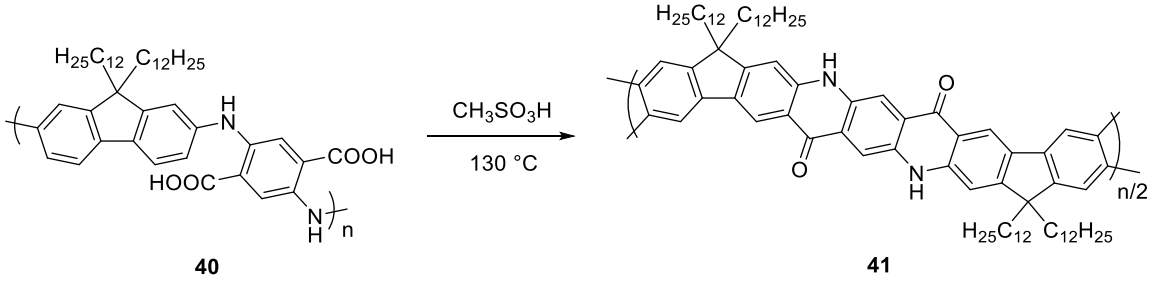

Figure I-22. Coplanarization of quinacridone-fluorene polymer

1.3.2 Effects Derived from Intramolecular Coplanar Locking

The manufacture of semiconductor band gap is essential for approaching desired physical properties. Factors that affect the energy of band gap (E_g) are summarized into the formula below. $E^{\delta r}$ is the bond-length alteration. The difference between single bonds and double bonds in the π-conjugated system. E^{θ} is the contribution by interannular rotation. E^{res} is the aromatic resonance energy. There could be two competition way on it. One is the confined localized ring current, and another is resonance traveling throughout the backbone. E^{sub} is derived from the substituents. Finally, E^{int} represents the interaction between chains such as π-π or dipole-dipole interaction.

$$E_g = E^{\delta r} + E^{\theta} + E^{res} + E^{sub} + E^{int}$$

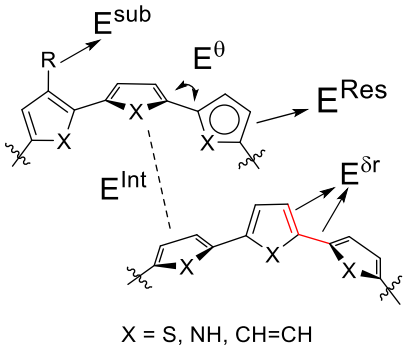

Figure I-23. Factors of controlling the bandgap.

After summarizing the major physical factors that influence E_g, It becomes clear that how coplanarization will affect the band gap. First, the $E^{\delta r}$ and E^{θ} would be minimized. The bond-length alteration between bonds would be reduced because of the enhanced double bond character on intra-arene single bonds. The conformation locked by the ladder structure leads the torsional angle close to 0°. E^{res} and E^{int} will benefit the compression of the band gap, as well. One of the drawbacks of increasing E^{int} is that the solubility could decline drastically due to the enhanced π-π interaction. Besides the strong connection on band gap, the fully fused π-conjugation also would lead to the bathochromic shift of optical absorption, amplified thermal excitation, higher charge carrier mobility as well as the carrier stability.

1.4 Conjugated metallapolymer: Idea, Preparation, and Their Applications

1.4.1 Conducting Metallapolymer

π-Conjugated conducting metallapolymers are a subgroup of conjugated polymers and metallapolymers. In the area of simple organic conjugated polymers, the polymer is tuned by organic functional groups, heteroatoms such as N, O, S, *etc*. and the structural design in order to

achieve the desired optoelectronic properties. On the other hand, the idea behind metallapolymers is to try to anchor the desired property of metal complexes on the polymer carriage. Taking advantage of macro-physical properties of the polymer, some challenges of using small molecules can be overcome. For example, a dendrimeric macromolecule was synthesized by Astruc[64] to adapt the copper catalyst. This design forced the reactive site into a "nano-reactor", making the click reaction water-friendly and the catalyst recyclable. The design of conducting metallapolymer was targeting at the interaction between metal and electric current on the polymer backone. In 2017, Nann et al. reported the Pt(II)-containing polythiophene,[65] in which the Pt(II) metals were chelated by side-arm terpyridine ligands. This metallapolymer allows the catalytic oxygen reduction and hydrogen evolution reaction that driven by electricity. The loading amount of Pt(II) on polymer is far less than that used in conventional platinum catalyst system. Althuogh the idea is intriguing, there are still few applicable conducting metallapolymers, since the metal, polymer backbone, and the coordination sphere will have to cooperate to establish the desired properties. Regardless of difficulties, the possibility in this area is appealing as a playground for chemists.

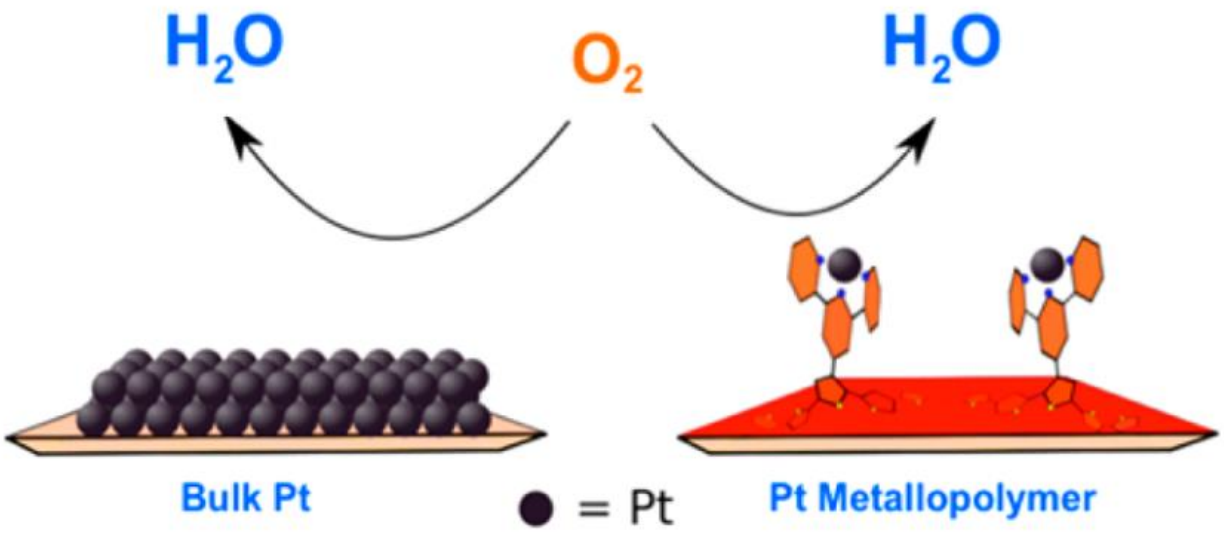

Figure I-24. The bulk platinum and Pt metallapolymer coated electrode for oxygen reduction reaction. Reproduced with permission from ref. 65.

1.4.2 Wolf Classification of Conducting Metallapolymer

Generally, conducting metallapolymers can be categorized into three classes. The classification is aimed to clarify the carrier transportation among the polymer. The metal nodes on type I metallapolymer are mainly on the side arms with non-conjugated or conjugated linkers. Since the chelated metals and the polymer backbone are quite remote, the polymerization reaction mostly can be well-manfactured. The Wolf type II metallapolymer contains the chelated metals on the adjacent side ligands as a part of polymer backbone. Under this structure, the metal redox or chemical events would strongly couple with the electronic properties on the main strand. It is worth noting that the metal node here would also have great impact on the polymer aggregation structure if multiple coordination sites are open or free for ligand exchange.

Type III metallapolymers have the metal nodes directly embedded in the main chain. The electronic environment of metal, such as oxidation states and binding ligands, will strongly influence the electric current flowing through the backbone. Meanwhile, the coordination sphere will have to be robust otherwise ligand dissociation could lead to depolyemrization. To date, the class II and III metallapolymer mostly include metallocenes, porphyrin complexes, or platinum-polyynes as the building blocks

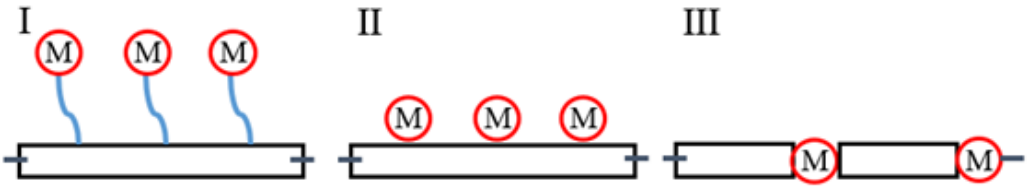

Figure I-25. Different Wolf types of conducting metallapolymers.

1.4.3 The Logic of Designing and Potential Application of PNP Metallapolymer

The key for successful application of a metallapolymer relies heavily on the function of the incorporated metal complex. For a complex molecule like porphyrin, the only extension possible is via its organic backbone. Therefore, it is easy to modify the functional groups to adapt it into Wolf type I and type III metallapolymers, and the choice of metal could be pre- or post-polymerization due to its saturated coordination sphere. Although there could be some obvious synthetic advantages on polymerizing specific metal complexes into metallapolymer like porphyrins or salen complexes. One needs to think in depth what benefit this metal complex gains being a metallapolymer instead of just small molecule, or what knowledge could we learn from preparing this into metallapolymer. Take a representative complex, ferrocene, as an example.[66] It is known that Fe(II)/Fe(III) redox couple can be interconverted by external applied voltage. With the different oxidation state of Fe, the electric current will face different resistances, causing a resistance memory effect. That is, if we give an impulse signal to oxidize Fe(II) to Fe(III), or *vice versa*, this metallapolymer will remember that pulse by showing different current densities.

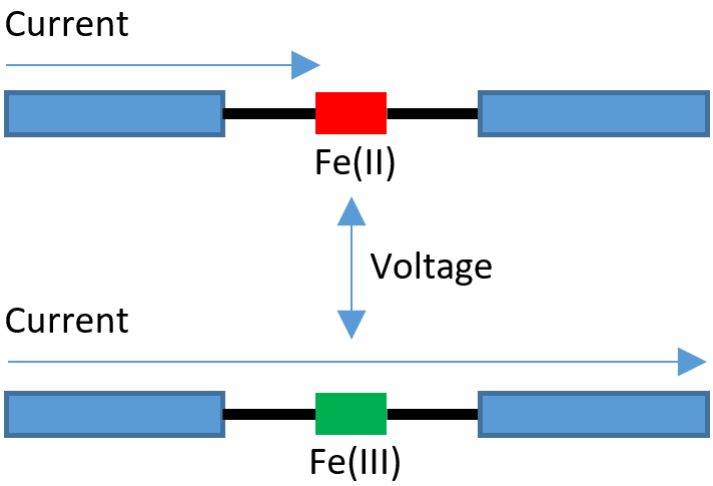

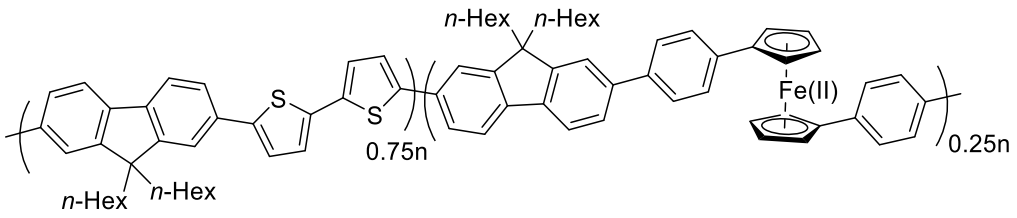

42

Figure I-26. Ferrocene-containing metallapolymer as a memory device.

Our PNP group 10 metal complexes share the redox stability with the ferrocene/ferrocenium couple and in addition, more delocalized orbitals on ligand backbone. We hypothesize that if those complexes are put into a conjugated metallapolymer, the charge doping density would be controllable with two separated stages. Also, if we could prepare the Wolf type II metallapolymers of PNP complexes, using the pre-functional groups as Y in Figure, they could be utilized as an optical or chemical sensor with X as a chromophore or reaction center, respectively. All in all, the thesis aims to find out ways to polymerize PNP group 10 metal complexes, and focus on evaluating the physical properties.

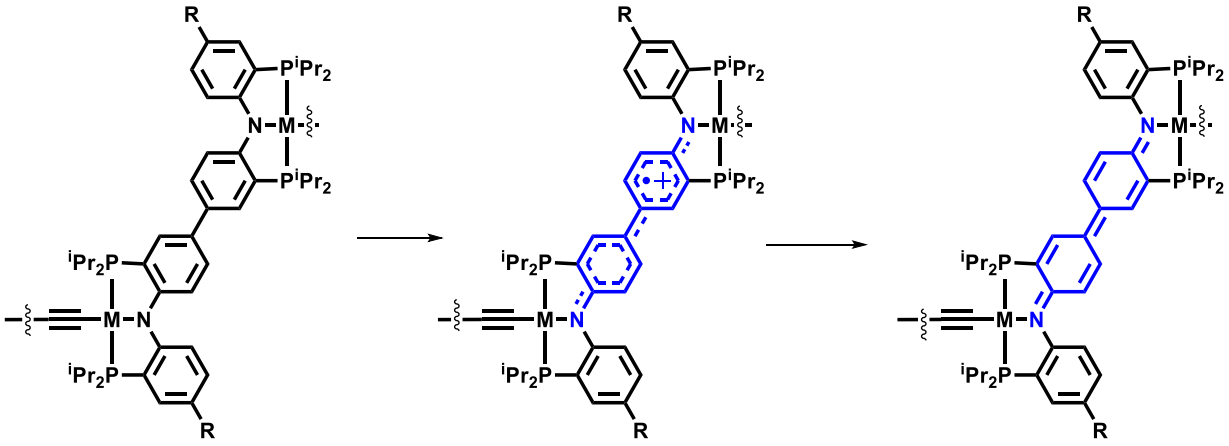

Figure I-27. Sequential oxidation of designed PNP group 10 (M =Ni, Pd, Pt) metallapolymer.

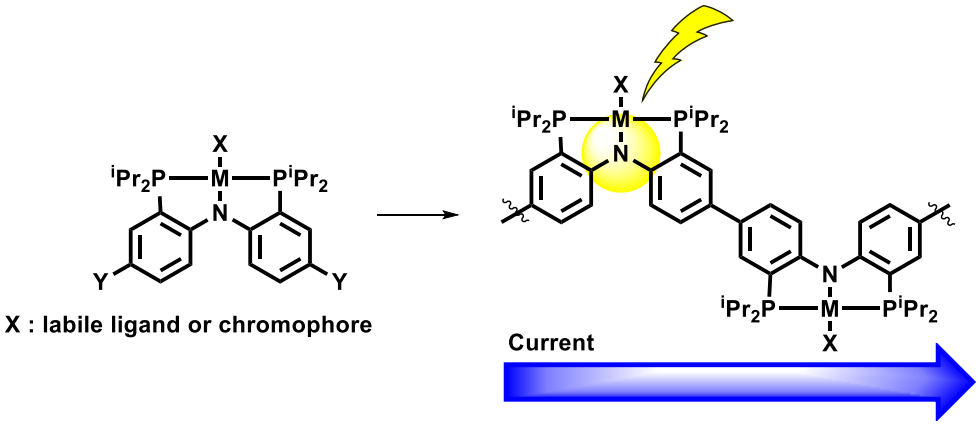

Figure I-28. Wolf type II metallapolymer rational design for PNP complexes.

CHAPTER II

Redox Communication Between Two Diarylamido/Bis(Phosphine) (PNP)M Moieties Bridged By Ynediyl Linkers (M = Ni, Pd, Pt)*

2.1 Introduction

The study of mixed-valence (MV) compounds is of continued interest because of its relevance to the broader questions pertaining to the study of electron transfer[67,68] in biology[69] and material science.[70] MV compounds also attract interest from a more fundamental point of view because of the exciting challenges in properly characterizing and understanding the nature of the MV, as well as because of the synthetic interest in designing new types of MV systems. The history of the MV compounds can be traced to the 1969 work by Creutz and Taube and their diruthenium complex **A** (Figure II-1).[42] Bis(ferrocene) systems have also been broadly studied.[50] Although this origin is tied to inorganic MV states, purely organic MV compounds have received a lot of attention, as well. A pivotal study was carried out by Lambert et al. in 1999 on a series of organic MV compounds of type **B** (Figure II-1), where the two triarylamine redox sites were connected by a variety of conjugating organic linkers.[71] MV compounds can be categorized according to the Robin-Day classification, depending on the degree of delocalization between the two redox sites.[44] For class I, the interaction between redox centers is small and so they behave mostly as separate sites; in class III, redox sites are strongly coupled to the extent that the delocalization can be considered complete. Class II systems exhibit intermediate properties, characterized by significant, but incomplete delocalization. The degree of delocalization can be assessed by the separation of

*Reproduced in part from "Redox Communication between Two Diarylamido/Bis(Phosphine) (PNP)M Moieties Bridged by Ynediyl Linkers (M = Ni, Pd, Pt)" by Yu, C.-H.; Yang, X.; Ji, X.; Wang, C.-H.; Lai, Q.; Bhuvanesh, N.; Ozerov, O. V. *Inorg. Chem.* **2020**, *59*, 10153-10162. DOI: 10.1021/acs.inorgchem.0c01281. Copyright [2020] by The American Chemical Society.

redox potential in a cyclic voltammogram (CV),[72] or by analyzing intervalence charge transfer (IV-CT) bands based on Marcus-Hush theory.[46] The redox potential separation is a seemingly very convenient and frequently used measure; however, its use alone is fraught with potential for misinterpretation, as was elegantly delineated by Winter in a 2014 review.[72]

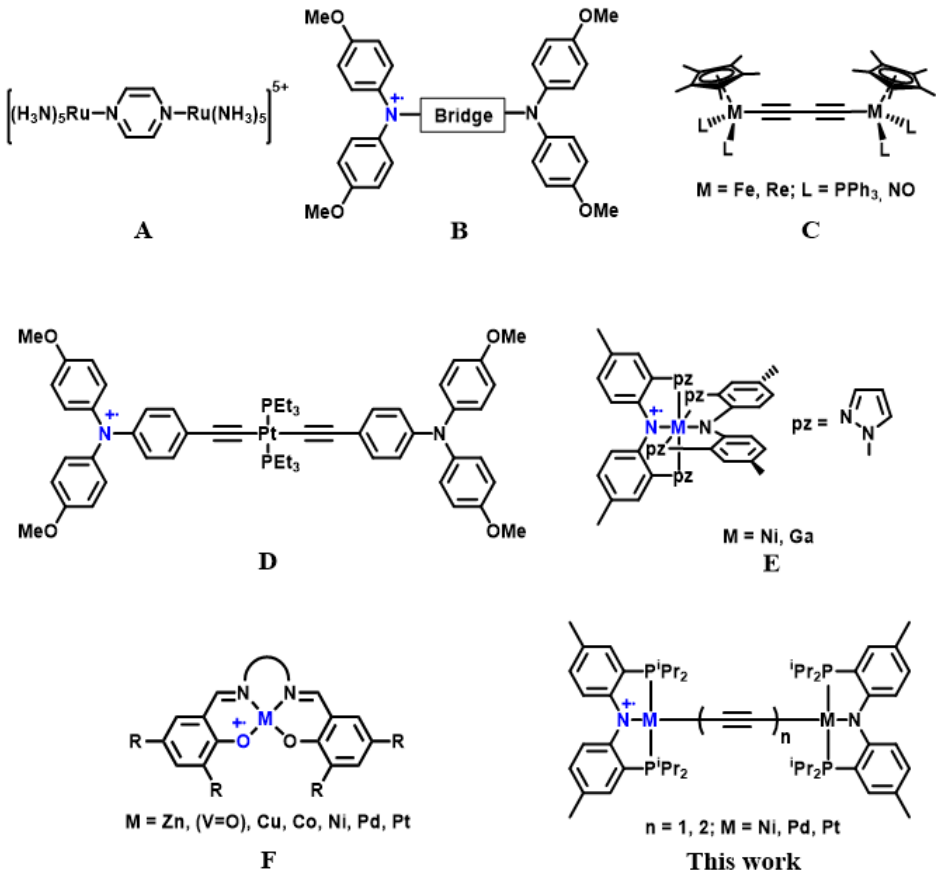

Figure II-1. Examples of MV compound: Creutz-Taube complex (**A**), Bis-triphenylamines (**B**), Half-sandwiched metal alkynediyl complexes (**C**), Bis-triphenylamine with the platinum containing bridge (**D**), metal-radical resonance complexes (**E**, **F**).

Within transition metal-containing MV systems, a few different types can be identified. The Creutz-Taube compound **A** represents a situation where the redox sites are metal-based and are connected by an organic linker. Ynediyl linkers, such as in **C** by Gladysz et al.,[73,74] are a common synthetic refrain. Attached directly to the redox-active metal centers, they are able to provide effective conjugation maintaining approximate linearity.[75] Compound **D** by Marder et al.[76]

represents a design where the two remote organic redox sites are connected via a transition metal-anchored linker. Systems such as **E**[77,78] and **F** are examples of a situation where the transition metal is intimately connected to two ligand-based redox sites, and although the metal is not necessarily redox active itself, it defines the spatial and electronic communication. The redox communication of the **F** design has been studied by Yamauchi et al.,[14] as well as Shimazaki et al.[79] and Thomas et al.[80] It was determined that the delocalization in the monooxidized species decreased in the order Pt > Ni > Pd among group 10 metals, with the Pt and Ni complexes falling into the Robin-Day class III. Structures of type **F** have also been incorporated into conjugated conducting polymers.[81-83] The interest in MV compounds, and in metal-stabilized radicals in general is often rooted in the studies of conducting polymeric materials[84-86] and relevance to enzyme reactivity.[87,88]

Our group has been interested in the complexes of the diarylamido/bis(phosphine) PNP ligands for a considerable period of time.[89–92] Our work and that of others showed that (PNP)M complexes can be reversibly oxidized, with the oxidation taking place primarily on the diarylamido ligand framework.[38,39,93] This has been especially thoroughly studied for the square-planar group 10 metal systems.[21,38] Other diarylamido-based pincer ligands have also been studied and found to be redox-active;[94–98] Gardinier's compounds of the type **E** are an example of that.[77,78] The oxidation of diarylamido ligands can be related to other metal-bound aminyl radicals.[12,99] We became interested in investigating the properties of group 10 bimetallic complexes in which the two (^{Me}PNP)M sites are connected by ynediyl linkers (Figure II-1). We reasoned that such a design is an amalgam of the types of systems exemplified by compounds **A**-**F** in that the two intimately metal-bound redox sites are connected by an organic and potentially conjugating linker, but where

the metal centers themselves are not expected to undergo oxidation. Here we report a comprehensive study of the electronic communication in these systems.

2.2 Results and Discussion

2.2.1 Synthesis of Bridged Bimetallic PNP Pincer Complexes.

In order to prepare μ-ethynediyl bimetallic complexes, we first synthesized and isolated (^{Me}PNP)MCCH in good yields (**46-48**) from the reactions of (^{Me}PNP)MCl (**43-45**) with slight excess of LiCCH (**Scheme II-1**). (^{Me}PNP)MCCH was then reacted with one equivalent of LDA in THF at room temperature. Although we assume deprotonation of the ethynyl C−H, we have not attempted to establish the composition of the resultant mixture. After 5 to 10 min, this reaction mixture was combined directly with (^{Me}PNP)MCl to yield homobimetallic C_2-bridged-(^{Me}PNP)MCCM(PNP^{Me}) products **49-51**. Good isolated yields were obtained after recrystallization. This approach also lent itself well to the preparation of the hetero-bimetallic analogs (^{Me}PNP)MCCM'(PNP^{Me}) **52-54** by changing the reacting partner to (^{Me}PNP)M'Cl. Notably, although the polyynediyl-bridged heterobimetallic complexes (M−$(CC)_n$−M') are many,[100] the examples with only σ-C_2-bridges are relatively rare.[101] To construct the C_4 butadiyne-diyl bridge, we employed slightly different strategies. For Ni and Pd, reaction of two equiv. of (^{Me}PNP)MOAc with bis(trimethylsilyl)butadiene in the presence of $NaOBu^t$ conveniently furnished the homobimetallic C_4-bridged complexes **57** and **58**. For Pt, we first prepared compound **60** from a 1:1:1 reaction of (^{Me}PNP)PtOTf (**59**) with bis(trimethylsilyl)butadiene and $NaOBu^t$, and then desilylated it to yield **61**. Treatment of **61** first with LDA and then with (^{Me}PNP)PtCl led to the successful formation and isolation of the bimetallic complex **62**. The longest bridge in this series, in compound **64**, was accessed via the reaction of two equiv. of

(^{Me}PNP)NiOTf with 1,4-diethynylbenzene in the presence of Et_3N. This synthesis was based on the previously reported reactivity of (^{Me}PNP)PdOTf toward terminal alkynes.[29] (^{Me}PNP)NiOTf appears to react similarly here, allowing the isolation of **64** in an excellent yield.

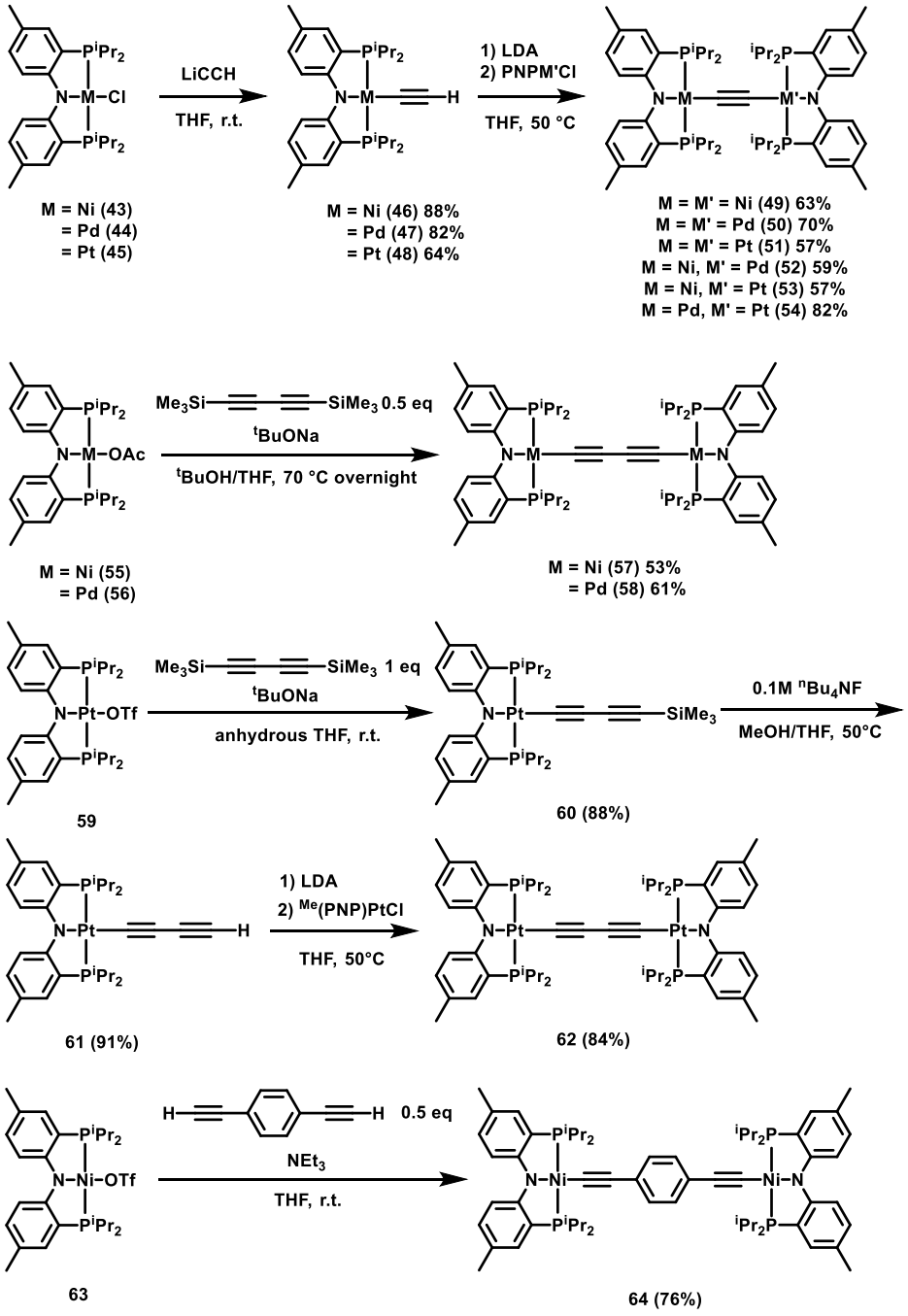

Scheme II-1. Synthesis of PNP group 10 ynediyl bridging complexes.

2.2.2 NMR and IR/Raman Spectroscopy.

The ^{1}H, ^{13}C, and ^{31}P NMR spectra of the (^{Me}PNP)MCCH complexes **46-48** are consistent with C_{2v} symmetry in solution. The diagnostic terminal ethynyl hydrogens present at around 2.6-2.7 ppm. The ^{13}C NMR chemical shifts of the α-ethynyl carbons are metal-dependent, covering the range of ca. 100-112 ppm, whereas the β-ethynyl carbons resonate in the 78-89 ppm range. For the all the bimetallic complexes (**49-51**, **52-54**, **57, 58, 62**, **64**), the local symmetry in each mono-pincer unit is also C_{2v} by NMR spectroscopy. For the homobimetallic complexes, this translates into the overall D_{2d} molecular symmetry on the NMR timescale.

The ethynediyl carbons resonate in the 100-120 ppm range in the ^{13}C NMR spectrum of **49-51**, with a clear difference of about 10 ppm between the metals in the Ni-Pd-Pt series. In the heterobimetallic complexes **52-54**, the two (^{Me}PNP)MC "halves" show ^{13}C NMR chemical shifts for the α-carbons that are reasonably similar to the same "half" in a homobimetallic analog. The corresponding ^{31}P NMR chemical shifts also correlate well, as do the $J_{P\text{-}Pt}$ values. The corresponding data for the homobimetallic complexes with the longer bridges (**57, 58, 62**, **64**) correlate more closely with those for the ethynyl complexes **46-48**.

Table II-1. Selected NMR Data for (^{Me}PNP)MCCM'(PNP^{Me}) (δ, ppm).

Complex	^{31}P NMR (C_6D_6)	^{13}C NMR (C_6D_6) M***C***CM'	^{13}C NMR (C_6D_6) MC***C***M'
49	37.52	120.3	
50	45.22	110.2	
51	42.60 (2710 Hz)[a]	101.6	
52	37.54, 44.82	125.5	105.1
53	37.83, 40.68 (2713 Hz)[a]	117.9	101.4
54	41.89 (2705 Hz),[a] 46.89	107.5	102.5

[a] $J_{P\text{-}Pt}$ coupling constant

The CC triple bond stretching frequencies of those complexes were identified in the solid-state FT-IR and Raman spectra (see Section 2.4.4). For **46-48**, the stretching frequencies of the CC

triple bond and the terminal C-H increased slightly in Ni < Pd ~ Pt order. Compared to 1-hexyne, a significant decrease in the CC stretching frequency can be noted, suggesting a decrease in the CC bond order. Raman spectra of **49-51** also support the same trend. Notably, CC triple bond stretching observed in between PNP metal were considerably lower compared to bis(trimethylsilyl)acetylene (2108 cm^{-1})[102] and bis(diphenylphosphino)acetylene (2097 cm^{-1}).[103]

Table II-2. CC and CH stretching frequencies by FT-IR and Raman.

IR	**CC (cm^{-1})**	**CH (cm^{-1})**	**Raman**	**CC (cm^{-1})**
46	1957	3258	**49**	1926
47	1969	3281	**50**	1987
48	1972	3285	**51**	1994
1-hexyne	2120	3311	**C_2H_2**[104]	1974

2.2.3 Solid-State Characterization

Single crystals of **50** and **51** were obtained by slowly diffusing hexane into the toluene solutions, while **49** was crystallized under CH_2Cl_2 layered with pentane. Oxidation of **49-51** with ca. 0.9 equiv. of ferrocenium carborane $[Fc]CH_{12}B_{11}$ was individually carried out in CH_2Cl_2 and X-ray quality crystals of the corresponding monocations **[49-51]$CH_{12}B_{11}$** were obtained by layering pentane or isooctane over the CH_2Cl_2 solution and cooling to -35 °C. We did not attempt isolation of **[49-51]$CH_{12}B_{11}$** on a preparative scale.

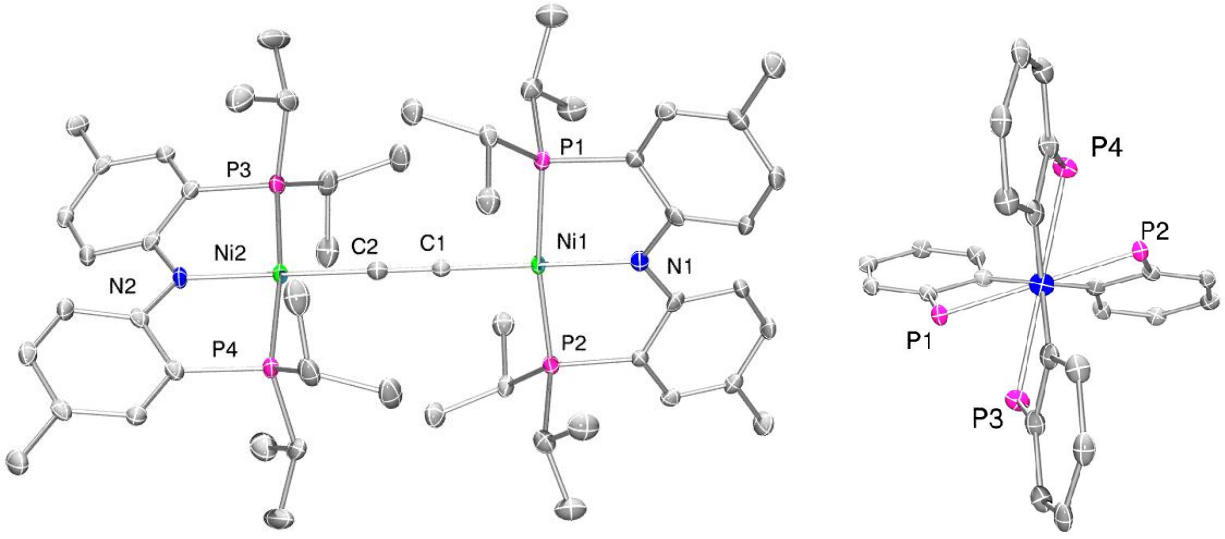

Figure II-2. Solid-state structure of **49**. Truncated view down the N-Ni-CC-Ni-N axis shown on the right. Displacement ellipsoids are shown at the 50% probability level and all solvent and hydrogen atoms have been removed for clarity.

Selected crystal structural data are summarized in Table II-3. The isomorphous structures of **50** and **51** contained two independent molecules in the asymmetric unit with insignificant differences in bond distances and angles. The N–M and M–C bond distances in nickel **complex 49** (Figure II-2) are about 0.1 Å shorter than those in **50** and **51** due to the smaller size of Ni(II). The N–M distances in **49** and **50** are slightly longer than the N–M distances in the previously reported structures of (^{Me}PNP)MCl (M = Ni, Pd) complexes,[89] likely owing to the stronger *trans*-influence of –CC– group. The C(1)–C(2) triple bond distances in **49**, **50**, **51** are similar to each other and to that in free acetylene (1.20 Å).[105] The dihedral angles P(1)–M(1)–M(2)–P(3) can be taken as a proxy for the angle between the two (^{Me}PNP)M planes and it varies from 60º to 90º among **49-51** and **[49-51]CH$_{12}$B$_{11}$**. The M(1)–C(1)–C(2)–M(2) angles in these structures are close to 180º, except for **[50]CH$_{12}$B$_{11}$** where it deviates from linearity by 7º. The structures of **49** (Figure 2) and of **[49]CH$_{12}$B$_{11}$** (Figure 3) are shown as examples. The N–M and M–C bond distances appear to

decrease slightly upon oxidation of **49-51** to the corresponding **[49-51]$CH_{12}B_{11}$**, whereas the C-C (triple bond) distances do not seem to change much. However, it is difficult to analyze these small differences from the X-ray data because the uncertainties in the values are not insignificant. Because of this, it is also difficult to analyze whether the monocations are truly dissymmetric. In addition, the structures of **[49-51]$CH_{12}B_{11}$** contain one anion which may influence the apparent dissymmetry. In the structure of **[49]$CH_{12}B_{11}$**, however, the anion is disordered over an element of symmetry, resulting in a monocation with two halves equivalent by crystallographic symmetry. However, it is possible to say that those changes cumulatively result in a decrease of the N…N distance by about 0.1 Å. It seems more appropriate to evaluate the individual bond distance differences using the calculated structures (*vide infra*). The solid-state structure of **58** was also determined for comparison (Figure 4). In contrast to **49-51**, the two P/N/P/Pd planes in **58** are approximately parallel with each other. The C(1)…C(4) distance in the C_4 bridge measured 3.8154(3). Gladysz's group in 2008 prepared a closely related $(C_6F_5)(R_3P)_2PtC_4Pt(PR_3)_2)(C_6F_5)$ in which the analogous C…C distance was determined to be 3.859(7).[106]

Table II-3. Selected bond distances (Å), and dihedral angles (º) derived from the XRD structural determinations (top row for each metric) and DFT calculations (bottom row), as well as crystal data for **49-51** and [**49-51**]$CH_{12}B_{11}$.

	49	**50**	**51**	**[49]$CH_{12}B_{11}$**	**[50]$CH_{12}B_{11}$**	**[51]$CH_{12}B_{11}$**
N(1)–M(1)	1.926(4)	2.075(4); 2.062(4)	2.068(6); 2.076(6)	1.872(2)	2.060(5)	2.028(6)
	1.944	2.102	2.122	1.914	2.083	2.097
N(2)–M(2)	1.929(3)	2.067(4); 2.061(4)	2.079(6); 2.085(6)	1.916(2)	2.029(5)	2.073(7)
	1.948	2.099	2.122	1.928	2.088	2.103
M(1)–C(1)	1.850(5)	1.984(5); 1.965(5)	1.975(8); 1.972(8)	1.838(3)	1.975(6)	1.941(9)
	1.849	1.982	1.985	1.835	1.965	1.967
M(2)–C(2)	1.864(5)	1.979(5); 1.965(6)	1.987(8); 1.972(7)	1.848(3)	1.959(7)	1.941(8)
	1.848	1.982	1.985	1.833	1.964	1.967
C(1)–C(2)	1.220(6)	1.208(7); 1.233(7)	1.209(11); 1.214(11)	1.237(4)	1.207(9)	1.237(11)
	1.246	1.241	1.240	1.249	1.242	1.247
P(1)–M(1)–M(2)–P(3)	60.817(6)	98.291(4); 95.818(4)	89.336(5); 84.408(4)	89.141(4)	107.123(3)	91.415(4)
N(1), N(2) distance	8.7887(7)	9.3108(3); 9.2843(3)	9.3138(4); 9.3167(4)	8.7072(7)	9.2003(5)	9.2162(6)
	8.835	9.402	9.454	8.759	9.343	9.375
Crystal system, space group	Monoclinic, *C*12/*c*1	Triclinic, $P\bar{1}$	Triclinic, $P\bar{1}$	Monoclinic, *C*12/*c*1	Monoclinic, $P12_1/c1$	Monoclinic, *C*12/*c*1

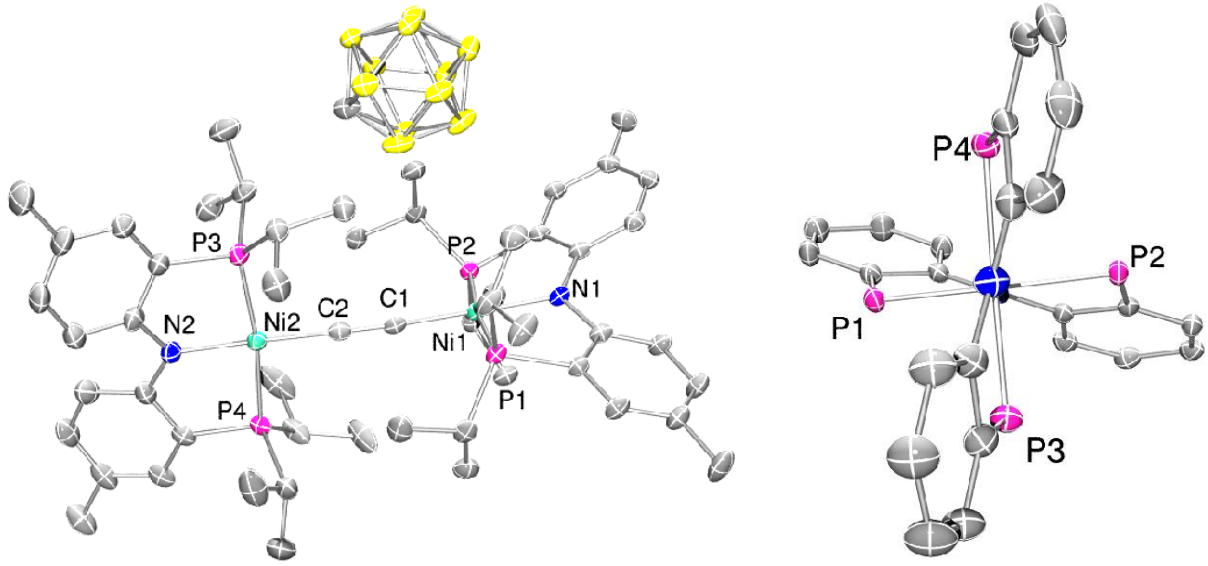

Figure II-3. Solid-state structure of **[49]$CH_{12}B_{11}$**. Truncated view down the N-Ni-CC-Ni-N axis shown on the right. Displacement ellipsoids are shown at the 50% probability level and all solvent and hydrogen atoms have been removed for clarity.

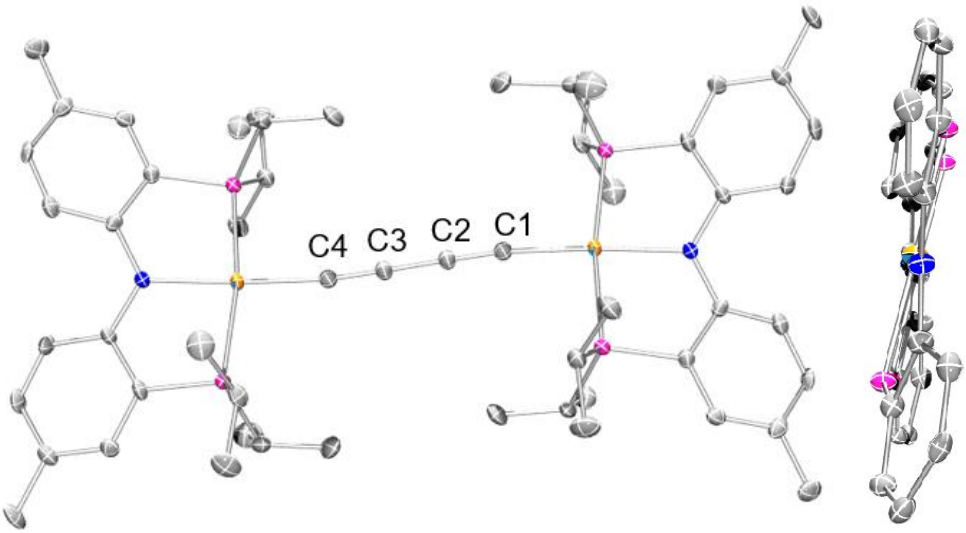

Figure II-4. Solid-state structure of **58**. Truncated view down the N-Pd-CC-Pd-N axis shown on the right. Displacement ellipsoids are shown at the 50% probability level and all solvent and hydrogen atoms have been removed for clarity.

2.2.4 Theoretical Calculation

DFT calculations were carried out using Gaussian 09 at the M06/def2-SVP level for describing the molecular orbital diagrams of **49-51** and **[49-51]**$^+$ (see Section 2.4.3 for the details and references). XRD-determined molecular structures of **49-51** molecules were imported as starting geometries for optimization. The DFT-optimized geometries (Table II-3) for **49-51** and their oxidized form **[49-51]**$^+$ (without an anion) reproduce the general features and the metrics from the corresponding X-ray diffraction structures quite well. The neutral bimetallic complexes **49-51** were calculated to be essentially symmetric, but for **[49-51]**$^+$, an asymmetry can be noted. However, this asymmetry is very modest. For example the two M-N distances are different by 0.005-0.014 Å in the three cations, while the two M-C distances within each cation hardly diverge at all (≤0.002 Å). Both the M-N distances and the M-C distances are shorter in the cations than in the neutral compounds (by 0.015-0.030 Å and by 0.015-0.018 Å, respectively). Curiously, the calculations reproduced the deviation from linearity in the N-M-C-C-M-N linkage in **[50]**$^+$**.**

Examination of the calculated HOMO for the neutral molecules and the SOMO for the cations in Figure II-5 evinces contributions from both (^{Me}PNP)M fragments and from the π-bonding orbitals of the C≡C bond. The nature of the HOMO can be viewed as an anti-bonding interaction between a combination of the delocalized lone pairs on N and the π-bonding electrons of the C≡C bond on the one hand, and the filled d_π orbitals at the d^8 metal center on the other. The removal of an electron from the HOMO is thus consistent with the modest shortening of the M-N and the M-C bonds. The HOMOs, LUMOs of **49**, **50** and **51**, and the depictions SOMO orbitals as well as the spin density maps for the corresponding oxidized cations **[49]**$^+$, **[50]**$^+$, **[51]**$^+$ can be found in the Figure II-19.

Table 4 shows the calculated percentages of spin density assignable to the atoms in the NMCCMN sequence in **[49-51]**$^+$. The differences among M = Ni/Pd/Pt are modest, but a few numbers deserve attention. Of the three cations, **[50]**$^+$ has the lowest total percentage of spin density in the NMCCMN unit (ca. 55%) vs. ca. 62-63% for Ni and Pt. Moreover, **[50]**$^+$ has the highest percentage on the N atoms. Arguably, this presages the greater degree of communication between the two halves in **[49]**$^+$ and **[51]**$^+$ gleaned from the electrochemistry experiments (*vide infra*). The percentage of spin density on the –C≡C– unit is greatest for **[51]**$^+$, which can be rationalized by the more effective orbital overlap with the 5d orbitals of Pt.

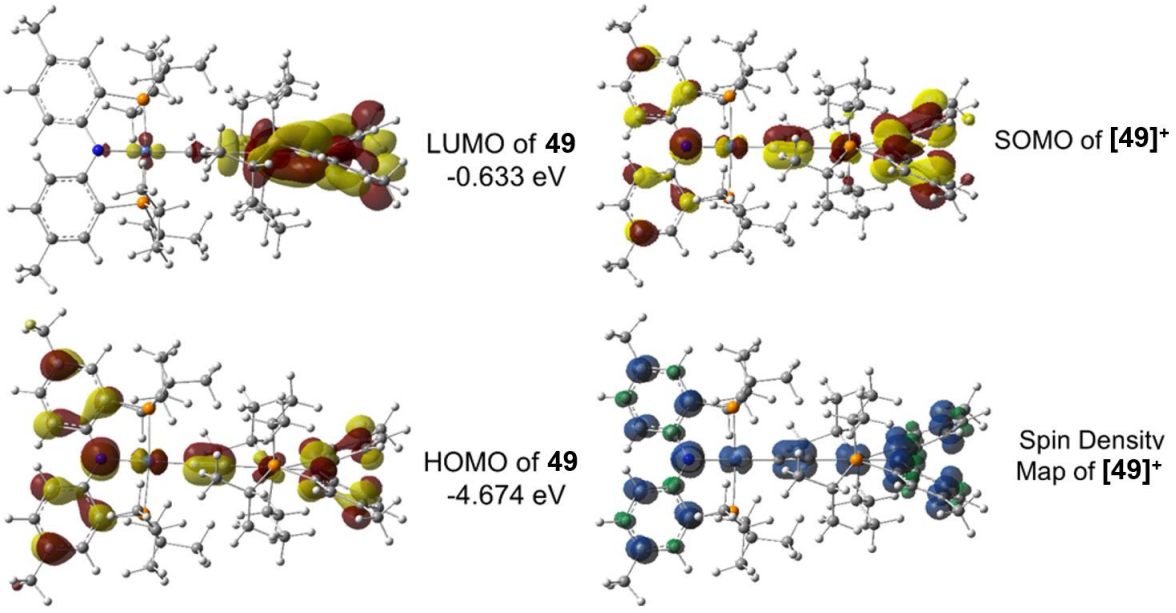

Figure II-5. The frontier molecular orbitals of **49**, as well as SOMO and the spin density map of **[49]**$^+$ calculated by DFT at the M06/def2-SVP level of theory (isovalue = 0.004).

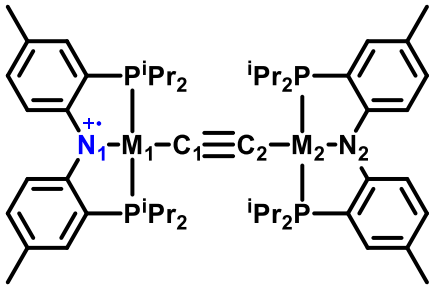

Table II-4. Selected spin density (%) of atoms in **[49-51]$^+$.**

Complex	N_1	M_1	C_1	C_2	M_2	N_2
[49]$^+$	18.6	10.1	4.8	3.2	7.4	18.6
[50]$^+$	21.5	3.5	3.6	3.2	2.4	20.3
[51]$^+$	18.6	6.3	8.3	7.3	4.7	16.7

2.2.5 Electron Paramagnetic Resonance Spectroscopy (EPR)

EPR spectra of **[49-51]$^+$** were collected on samples produced by in situ one-electron oxidation of **49-51** using ferrocenium carborane in CH_2Cl_2. The observed order of g_{iso} values was **[51]$^+$** > **[49]$^+$** > **[50]$^+$**. The broadness caused by long-range delocalization of radical obviates the detection of the hyperfine splitting features in all of the solution spectra. On the other hand, in the solid-state, g factors depend on the orientation in the magnetic field. An axial spectrum with a larger g_1 and a smaller g_2 values were found in the EPR spectrum of solid **[49]$^+$**. In Mindiola's EPR study of solid **[43][OTf]**,[38] a rhombic signal was found with an large anisotropy in the g values (g_1 = 2.040(4), g_2 = 2.016(4), g_3 = 2.005(4)),[31] interpreted as originating from a non-negligible contribution of Ni(III) in a low-symmetry environment. In the case of **[49]$^+$**, the higher D_{2d} symmetry likely results in the merging of two of the three g values in the mononuclear **[43][OTf]** into one in **[49]$^+$**.

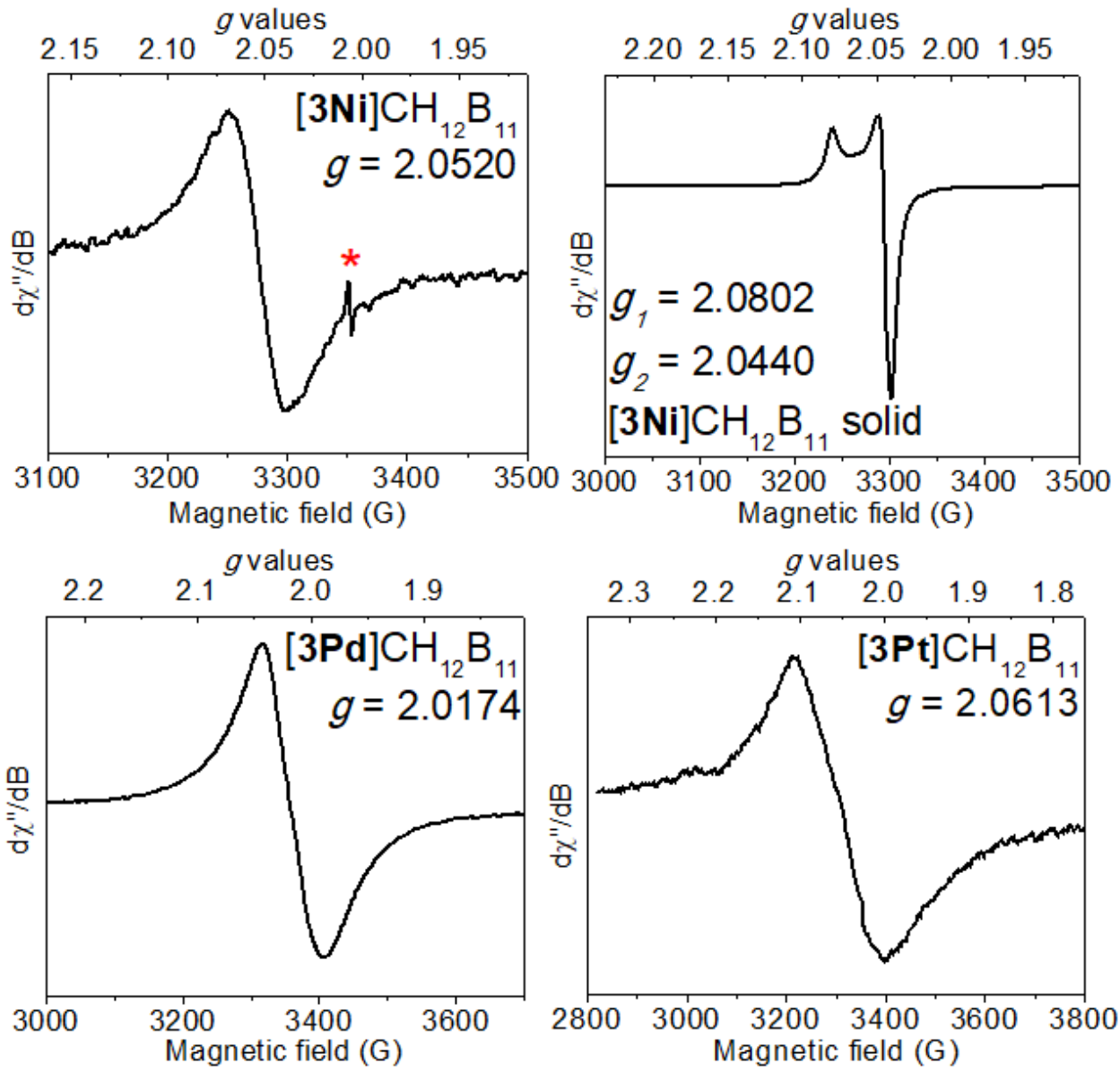

Figure II-6. The X-band EPR spectra were recorded at 292 K of **[49]$CH_{12}B_{11}$** solid and **[49-51]$CH_{12}B_{11}$** solution in CH_2Cl_2 (20 mM) and with a microwave frequency of 9.38 GHz, microwave power 0.6 mW, and modulation width 1G. The spectrum was collected over multiple runs. The asterisk labeled the instrumental noise that decreased the intensity while collecting runs.

2.2.6 Electrochemical Studies

Cyclic voltammograms were collected in order to understand the degree of electronic communication. First, **46-48** were investigated with 0.1 M $^{n}Bu_4NBAr^{F}_4$ as the supporting electrolyte in CH_2Cl_2. Quasi-reversible waves were observed, centered at -0.1 to -0.2 V versus the ferrocenium/ferrocene external standard. Compared to the previously reported values for (^{Me}PNP)MCl,[21] **46-48** were slightly easier to oxidize, presumably owing to the more electron-releasing properties of –CCH vs. –Cl. Next, the bimetallic complexes **49-51** were investigated in the same manner. Two quasireversible oxidation waves were observed; they all occurred at more negative potentials than the corresponding oxidations for **46-48**. The CV data for **49-51** were also collected using $^{n}Bu_4NBAr^{F}_4$ as the supporting electrolyte (Figure II-7, Table II-5). The separation between the two waves ΔE can be converted to the comproportionation equilibrium constant *K*c according to **formula I**.[72,107,108] Greater separation of the redox waves, and thus greater K_c values, indicative of greater apparent electronic communication between the two sites and greater electronic delocalization in the radical. The CV of **64** yielded only a single quasireversible wave at a potential similar to that of **46**. This evidences the lack of communication between the redox sites in **64**. The C_4-bridged bimetallics (**57, 58, 62**) gave rise to more closely spaced waves compared to the C_2-bridged bimetallics (**49-51** and **52-54**). A greater degree of communication in the C_2-bridged compounds compared to the C_4-bridged compounds should be expected. Within the homobimetallic C_2-bridged complexes, the order of K_c values is **51** ≈ **49** > **50**. Within the homobimetallic C_4-bridged analogs, it is **62** > **57** > **58**. In both cases, the dipalladium complex displayed weakest communication. Based on the K_c values alone, **49** and **51** can be assigned at the borderline of Robin-Day Class II-III, whereas **50** and **57, 58, 62** fall more squarely into Class II. For the heterobimetallic compounds **52-54**, K_c should not be calculated directly from the ΔE values because of the intrinsic dissymmetry. Presumably the first oxidation in **52** and **53** is based

to a greater degree on the Ni half because of the easier oxidation of (^{Me}PNP)MX for M = Ni vs. Pd or Pt. Considering the 0.10 V difference between the $E_{1/2}$ values for **46** vs. **47** ≈ **51**, one could expect a 0.10 V difference in the ΔE values for **52** and **53** vs **54**, which happens to be exactly the case. The ΔE value for **54** of 0.20 V is also approximately the average of the ΔE values for **50** (Pd/Pd) and **51** (Pt/Pt).

$$Kc = e^{\frac{-nF\Delta E}{RT}} \qquad \textbf{(I)}$$

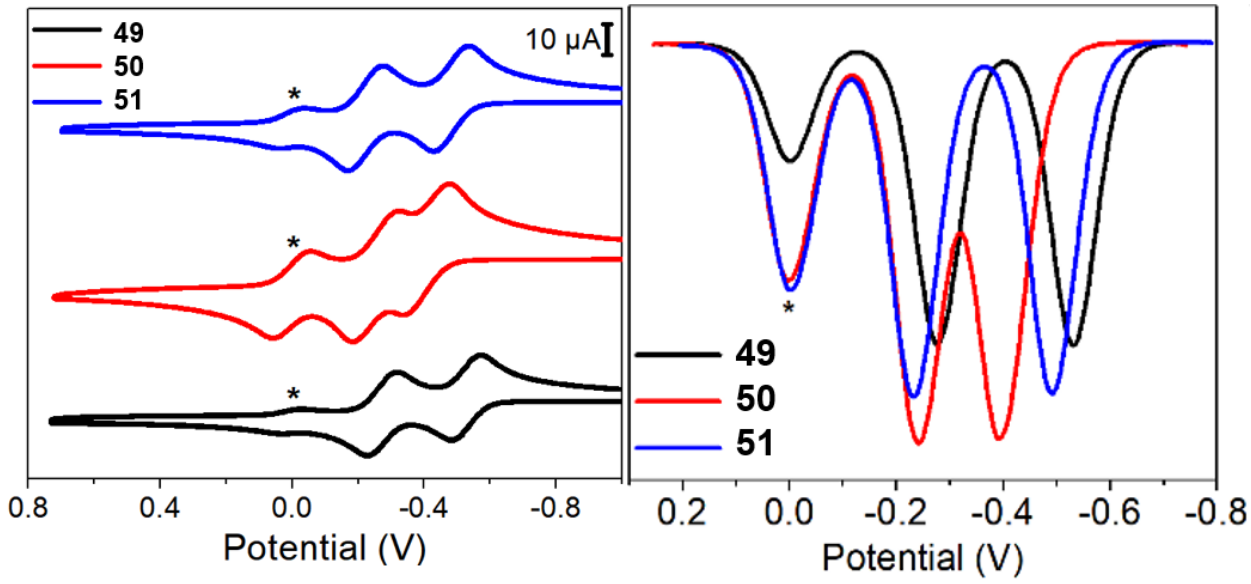

Figure II-7. Cyclic voltammograms (left) and differential pulse voltammograms (right) of ca. 1 x 10^{-3} M PNPMC$_2$MPNP **49-51** with ferrocene as the internal standard. (^{n}Bu$_4$NBAr$^{F}_4$ 0.1 M in CH_2Cl_2, with a Ag/$AgNO_3$ reference electrode, at a scan rate of 100 mV s^{-1}, vs Fc^+/Fc). The asterisks label the internal ferrocene standard.

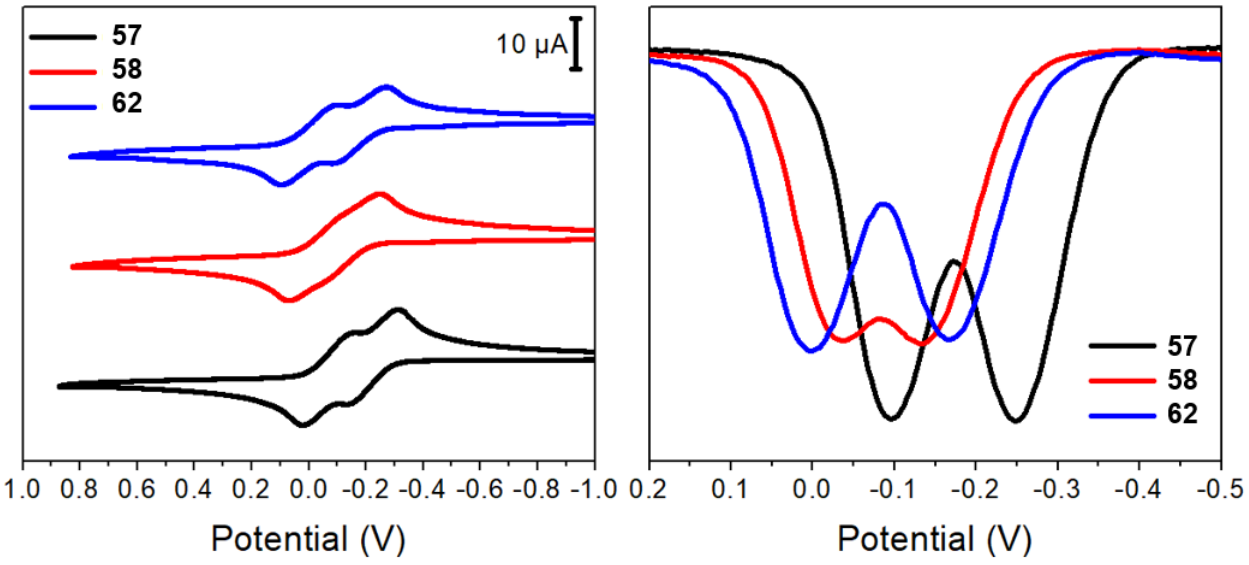

Figure II-8. Cyclic voltammograms (left) and differential pulse voltammograms (right) of ca. 1 x 10^{-3} M PNPMC$_4$MPNP **57, 58, 62**. (^{n}Bu$_4$NBAr$^F{}_4$ 0.1 M in CH_2Cl_2, with a Ag/$AgNO_3$ reference electrode, at a scan rate of 100 mV s^{-1}, vs. Fc^+/Fc).

Table II-5. Summary of oxidation potential*.

Compound	$E^1_{1/2}$ (V)	$E^2_{1/2}$ (V)	ΔE (V)	Kc
49	-0.53	-0.27	0.26	2.5×10^4
50	-0.40	-0.25	0.15	3.4×10^2
51	-0.50	-0.24	0.26	2.5×10^4
52	-0.53	-0.19	0.34	
53	-0.57	-0.23	0.34	
54	-0.47	-0.23	0.24	
57	-0.25	-0.10	0.15	3.4×10^2
58	-0.14	-0.04	0.10	4.9×10^1
62	-0.17	0.00	0.17	7.5×10^2

* The $E^1_{1/2}$ (V) of **46-48** and **64** was found -0.21, -0.09, -0.07, and -0.15 V respectively.

2.2.7 UV-vis-NIR Spectroscopy

The UV-vis-NIR spectra of **46-48** and the oxidized **[46-48]**$^+$ recorded in CH_2Cl_2 solution are shown in Figure II-9. The spectra of neutral **46-48** shares the similar absorption feature with a shoulder at 400-500 nm. Upon one electron oxidation, **[46-48]**$^+$ exhibit an intense metal-to-ligand charge transfer (MLCT) band at 600-700 nm in general. The additional near-infrared band found

in **[46]**$^{+}$ is at 870 nm. Similar bands were previously reported in **[43]**$^{+}$, as well as an mono-oxidized divinylamido-centered Ni(II) pincer complex.[27,38] Taking into account the interpretations from the literature, this is presumably a combination of MLCT and LLCT transition owing to the closer d-π energy match of Ni(II) with the oxidized ligand backbone.[14,27,109–112] Absorption spectra of **49-51**, **[49-51]**$^{+}$, and **[49-51]**$^{2+}$ were collected in a similar manner (Figure II-10). Neutral **49-51** exhibited multiple strong absorptions ranging at around 300 nm for typical π-conjugated arylamines, and the shoulder or minor band at 400-500 nm likely contains the HOMO-LUMO transition. In **[49-51]**$^{+}$, two additional bands appeared along with the decline of bands at around 300 nm. The longer wavelength band with λ_{max} at around 1200-1600 nm is proposed to be the IV-CT transition, while the shorter wavelength band at λ_{max} of 500-600 nm could correspond to MLCT, which was observed in **[46-48]**$^{+}$ as well.[38] [**49**]$^{+}$ and [**51**]$^{+}$ gave rise to IV-CT transitions of similar λ_{max}, whereas it was observed at a shorter wavelength for Pd [**50**]$^{+}$. Removal of the second electron and formation of **[49-51]**$^{2+}$ resulted in the increase of MLCT band absorbance and the disappearance of IV-CT band. Additionally, another long-wavelength band with λ_{max} at around 1000-1200 nm appeared. We propose it may be attributed to the same type of π-π* transition as found in **[43-45]**$^{+}$ and **[46-48]**$^{+}$ but at a longer wavelength because of the increased effective nuclear charge of the ligand atoms in the dication.[38]

In order to gain additional insight into the nature of the transitions in **[49]**$^{0/+}$, TD-DFT calculations were carried out (see Figure II-20). The computed absorption patterns for **[49]** and **[49]**$^{+}$ match the experimental spectra reasonably well, although the computed NIR band is red-shifted by about 200 nm to 1749 nm. Analysis of the orbitals involved supports the notion of an LLCT type IV-CT transition. On the other hand, the computed transition at 704 nm is consistent with a mostly localized MLCT. In order to quantify the degree of delocalization in **[49-51]**$^{+}$, Marcus-Hush

analysis (**formula II**) was applied for a Robin-Day class II MV compound. The shapes of IV-CT bands were close to Gaussian which indicated a double adiabatic stage transition that depicted the same situation in theory.[113]

$$V = \frac{0.0206}{r}\sqrt{\tilde{\upsilon}_{max}\tilde{\upsilon}_{1/2}\varepsilon} \qquad \textbf{(II)}$$

Hush electronic coupling integral *V* is the energy barrier between two adiabatic stages which indicate the degree of electron delocalization.[45] It is determined by the wavenumber at maximum absorption of IVCT ($\tilde{\upsilon}_{max}$), band half-width ($\tilde{\upsilon}_{1/2}$), extinction coefficient **ε**, and effective transition distance **r**. The effective transition distance **r** mostly has to be estimated. We performed two calculations, one with the M(1)-M(2) distance, the other with the N(1)-N(2) distance from the X-ray structures of **[49-51]**$^+$ in crystal structures are picked for comparison (Table II-6). The calculated *V* values from both **r** distances suggest the electron communication decreases in the order Pt > Ni > Pd within the range of a few hundred cm^{-1}. However, the *V* values based on the M(1)-M(2) distance are too large compared to a typical Robin-Day class II compound. On the other hand, using the N(1)-N(2) distance leads to the more reasonable *V* values at around 800-1100 cm^{-1}. Using the N-N distance also appears appropriate, given that the DFT calculations identified the nitrogens as the atoms with the most spin density in the monocations. Figure II-9 also provides a relevant illustration. Compound **[67]**$^+$ is related to **[65]**$^+$ via "replacement" of the *para*-phenylene connector in **65** with a Pt center.[71,76] Likewise, **[66]**$^+$ and **[51]**$^+$ can also be viewed as related by a "replacement" of two *para*-phenylene linkers in **66** with two Pt centers in **51**. The *V* values indicate that Pt is a comparable but slightly less effective connector than *para*-phenylene in both cases. *V*

values of **[49-51]**$^{+}$ confirm the assumption that **50** matches the Robin-Day class II, whereas **49** and **51** are at the borderline of Robin-Day classes II and III. In order to ensure they do not approach the complete delocalization of class III, further verifications were conducted using the solvatochromic effect and IR spectroscopy of **[49]**$^{+}$ and [**51**]$^{+}$ (Figure II-22). The change in solvent polarity is expected to cause a considerable shift of IVCT band in Robin-Day class II MV compounds in contrast to class III.[45] We observed the $\Delta\tilde{\nu}$(CH_2Cl_2/acetonitrile) order **[50]**$^{+}$ > **[51]**$^{+}$ ≈ **[49]**$^{+}$ in agreement with **50** as closest to class II. However, the magnitude of ca. 300-900 cm^{-1} is not aligned with class II compound **[66]**$^{+}$ (2170 cm^{-1})[114] as well as the other simple organic analog,[47,71] so this determination is not definitive. The stretching band of the C≡C bond was present in the IR spectra of both **[49]**$CH_{12}B_{11}$ and **[51]**$CH_{12}B_{11}$ with little broadening, which suggested that the positive charge was not completely delocalized.

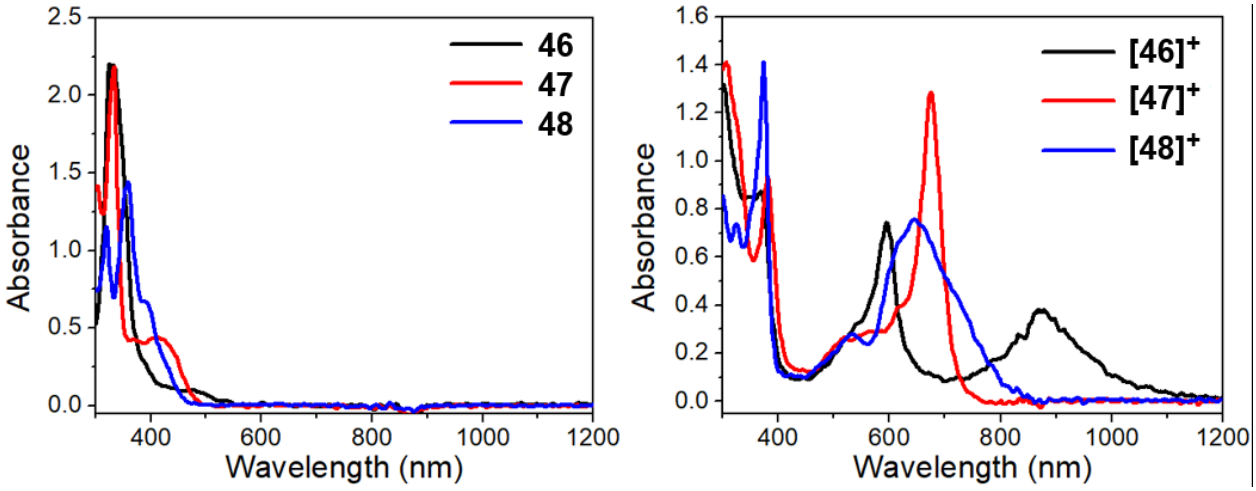

Figure II-9. UV-vis-NIR spectra of ca. 1 × 10^{-4} M **46-48** and [**46-48**]$CH_{12}B_{11}$. [**46-48**]$CH_{12}B_{11}$ were obtained by *in situ* oxidation using 1.2 eq [Fc]$CH_{12}B_{11}$ as the oxidant in CH_2Cl_2 solution.

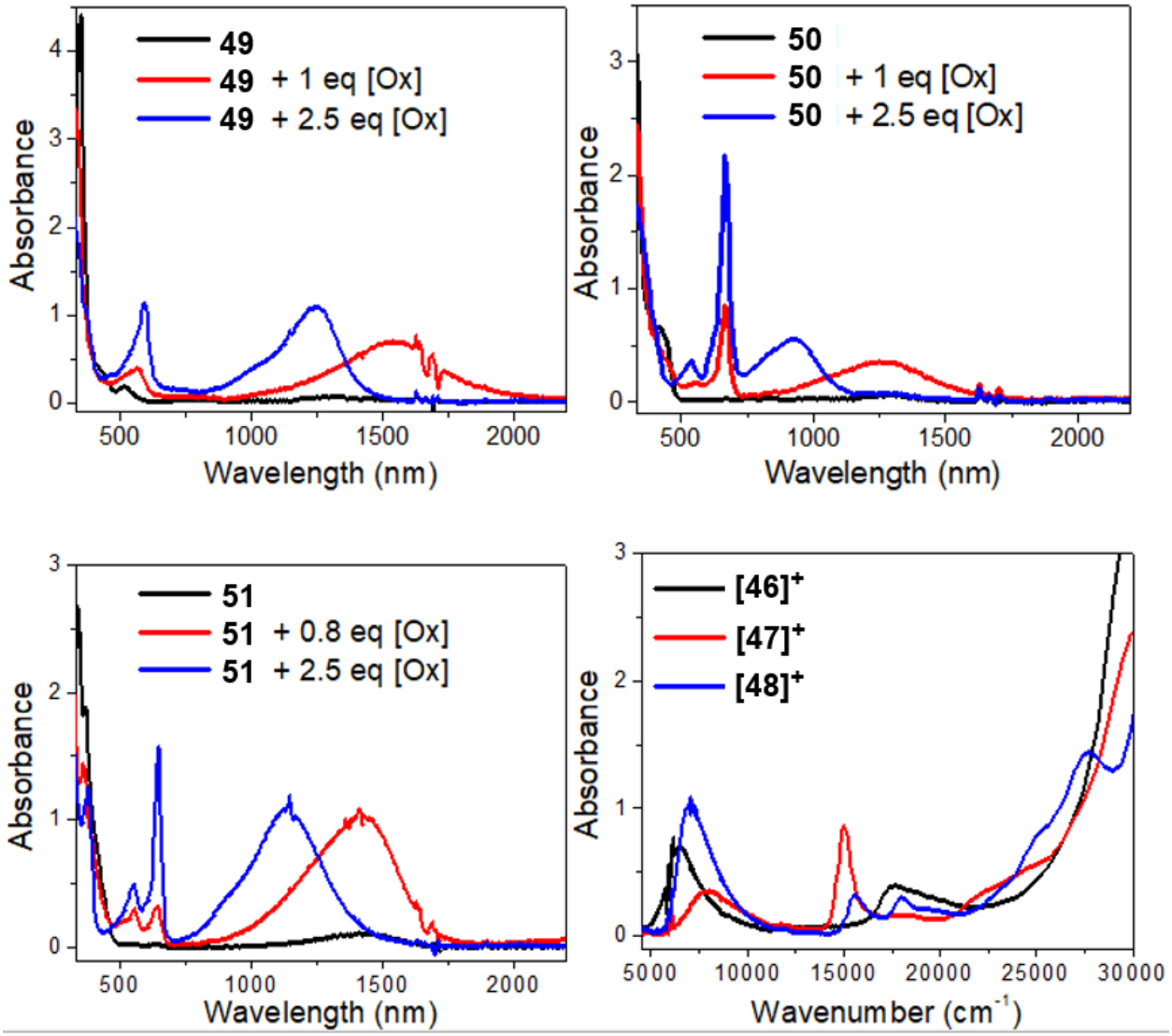

Figure II-10. UV-vis-NIR spectra of ca. 6 × 10^{-5} M **49-51,** [**49-51**] $CH_{12}B_{11}$ and [**49-51**][$CH_{12}B_{11}$]$_2$. [**49-51**]$CH_{12}B_{11}$ and [**49-51**][$CH_{12}B_{11}$]$_2$ were obtained by in situ oxidation using [Fc]$CH_{12}B_{11}$ as the oxidant [Ox] in CH_2Cl_2 solution.

Table II-6. Summary of parameters in NIR band analysis.

Complex	$\tilde{\upsilon}_{max}$ [cm^{-1}]	$\tilde{\upsilon}_{1/2}$ [cm^{-1}]	ε [$M^{-1}cm^{-1}$]	r [Å]	V [cm^{-1}]
[49]$^+$	6494	2055	11551	8.707[a] (4.921)[b]	930 (1640)
[50]$^+$	7937	3146	5207	9.201[a] (5.129)[b]	810 (1450)
[51]$^+$	7037	1982	17640	9.216[a] (5.117)[b]	1110 (2000)

[a] Distance from N(1) to N(2).

[b] Distance from M(1) to M(2).

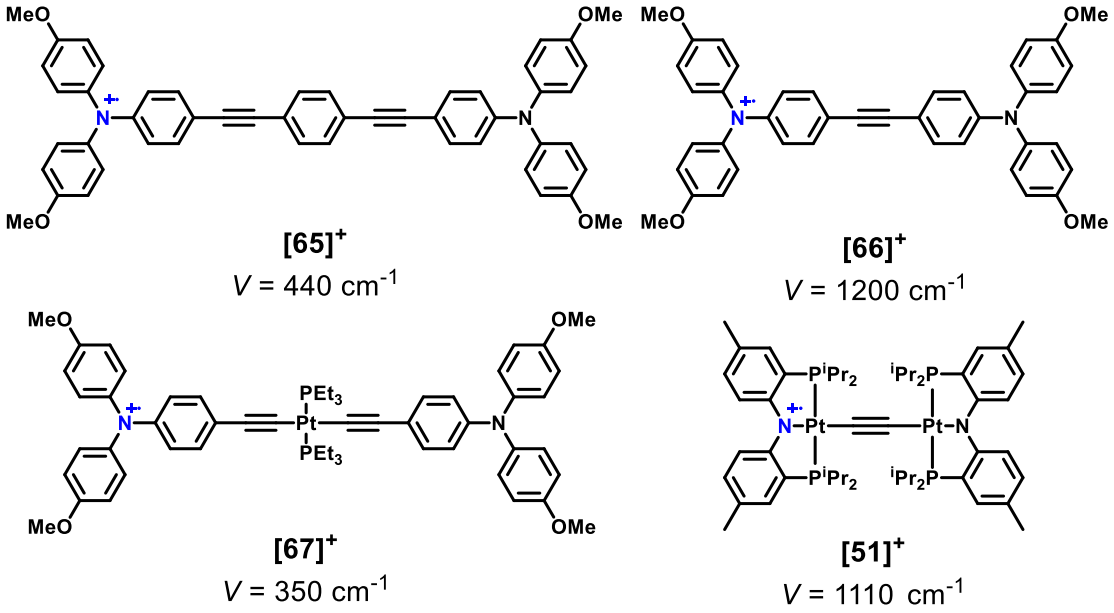

Figure II-11. Comparison of ***V*** values of compounds in literature.

2.3 Conclusion

In summary, a detailed investigation of a series of bimetallic (^{Me}PNP)M complexes was carried out. The redox sites in these group 10 metal complexes are largely based on the PNP ligands, in concert with the previous reports on the oxidation of PNP complexes. Alkynediyl linkers bound to the transition metals were used to connect the redox sites. It was found that communication between the two sites was marginal for a –C≡C-C≡C- linker, and non-existent for the longer linker.

The shortest -C≡C- linkers allowed for stronger communication, which was weakest for Pd, and more pronounced for Ni and Pt. Electrochemical analysis of the redox peak separation gave similar results for Ni and Pt, but the analysis of the IV-CT band in the NIR spectrum suggested a higher degree of delocalization for Pt. In the analysis of the electronic coupling in the Ni/Pd/Pt series of complexes of the type **F** (Figure 1), Shimazaki et al. concluded that the order of Pd < Ni < Pt reflected the order of the energies of the corresponding filled d_π orbital at the metal and how well it can overlap with the ligand orbital.[18] We interpret the situation in the Ni/Pd/Pt compounds presented in this work similarly. Pt provides the best opportunity for electronic communication via stronger orbital interactions, while Pd is least effective. In addition, we propose that the communication in the bis(nickel) compounds benefits from the closer physical proximity of the two redox sites owing to the shorter Ni-C and Ni-N bonds.

2.4 Experimental section

2.4.1 General Considerations

Unless specified otherwise, all manipulations were performed under an Ar atmosphere using standard Schlenk line or glovebox techniques. Toluene, diethyl ether, pentane, and isooctane were dried and deoxygenated (by purging) using a solvent purification system (Innovative Technology Pure Solv MD-5 Solvent Purification System) and stored over molecular sieves in an Ar-filled glove box. C_6D_6 was dried over NaK/Ph_2CO/18-crown-6, distilled or vacuum transferred and stored over molecular sieves in an Ar-filled glovebox. CH_2Cl_2, $CDCl_3$, and CD_2Cl_2 were dried over CaH_2, distilled or vacuum transferred and stored over molecular sieves in an Ar-filled glove box. (^{Me}PNP)MCl (as **43-45**, M = Ni, Pd, Pt), (^{Me}PNP)NiOAc (**55**) and (^{Me}PNP)PdOAc (**56**) (^{Me}PNP)NiOTf (**63**) were prepared via literature procedures[89,90,115] as well as tetra(*n*-

butyl)ammonium tetrakis(3,5-bis(trifluoromethyl)phenyl)borate[116] [$^{n}Bu_4N$][BAr^{F}_4]. All other chemicals were used as received from commercial vendors.

2.4.2 Physical Methods

NMR spectra were recorded on a Varian Inova 300, Mercury 300 (^{1}H NMR, 299.952 MHz; ^{13}C NMR, 75.421 MHz; ^{31}P NMR, 121.422 MHz), Bruker 400 (^{1}H NMR, 399.535 MHz; ^{11}C NMR, 100.582 MHz; ^{31}P NMR, 161.734 MHz) and Varian Inova 500 (^{1}H NMR, 499.703 MHz; ^{13}C NMR, 125.697 MHz; ^{31}P NMR, 202.265 MHz) spectrometer. Chemical shifts are reported in δ (ppm). For ^{1}H and ^{13}C NMR spectra, the residual solvent peak was used as an internal reference (^{1}H NMR: δ 7.16 for C_6D_6, 7.24 for $CDCl_3$; ^{13}C NMR: δ 128.06 for C_6D_6, 77.16 for $CDCl_3$). ^{31}P NMR spectra were referenced externally with 85% phosphoric acid at δ 0. Infrared spectra were collected on an Agilent CARY FT-IR spectrometer. Raman spectra were obtained from a Horiba Jobin-Yvon LabRam HR spectrometer with a 633 nm laser (300 gr/mm). Data were collected between 100 and 3000 cm^{-1}. Measured power at the sampling level was controlled at about 0.6 mW. Acquisition time was 15 seconds, optical filter density was D 1, and confocal pinhole was 200 μm. UV-vis-NIR spectra were collected on a Hitachi U-4100 UV-vis-NIR spectrophotometer. Electron paramagnetic resonance spectra were recorded in a continuous wave X-band EleXsys EPR spectrometer at 288 K. Electrochemical studies were carried out using a CH Instruments Model 700 D Series. Electrochemical Analyzer and Workstation in conjunction with a three electrode cell. The working electrode was a CHI 104 glassy carbon disk with a 3.0 mm diameter and the auxiliary electrode was composed of platinum wire. The third electrode, the reference electrode, was a $Ag/AgNO_3$ electrode. This was prepared as a bulk solution composed of 0.01 M $AgNO_3$ and 0.1 M $^{n}Bu_4NPF_6$ in dichloromethane. This was separated from solution by a fine

porosity frit. CVs and DPVs were conducted in dichloromethane with 0.1 supporting electrolyte mentioned in footnotes and were reported with a scan rate of 100 mV/s. The concentration of the analyte solutions were approximately 1.00×10^{-3} M. CVs were referenced to $Fe(\eta^5\text{-}Cp)_2$/ $Fe(\eta^5\text{-}Cp)^+$ redox couple. Elemental analyses were performed by CALI Labs, Inc. (Highland Park, NJ).

2.4.3 Computational Details

DFT calculations were carried out using Gaussian 09,[117] Revision D.01. X-ray crystal structures of **49, 50,** and **51** were imported as starting geometries for optimization. Previous studies indicate that the M06 functional is well-performing on closely related complexes.[118–120] Hence, the M06[121] functional was chosen for all the calculations, in combination with the def2-SVP[122] basis set for all the atoms and the corresponding pseudopotentials for the Pd and Pt atoms. The integration grid was set to be ultrafine. Based on the optimized structures of **49** and **[49]**$^+$, transition energies were calculated by Time-Dependent DFT (TD-DFT) at the level of M06/def2-SVP with CH_2Cl_2 PCM solvation.

2.4.4 Synthesis and Characterization Details

(^{Me}PNP)Ni(CCH) (46). (^{Me}PNP)NiCl (43) (100 mg, 191 μmol) was dissolved in THF solution (5.0 mL) and lithium acetylide, ethylene diamine complex ($LiCCH \cdot NH_2CH_2CH_2NH_2$) (53 mg, 573 μmol) was added to it under room temperature. The solution color changed immediately from green to red. After stirring 1 hour, the volatiles were removed under vacuum, and the residue was extracted with toluene and filtered through a plug of silica gel. The filtrate was collected and the volatiles were removed under vacuum, yielding red solid (86 mg, 88%). ATR-IR: $\nu_{C\equiv C}$ 1958 cm^{-1},

$\nu_{C\text{-}H}$ 3258 cm^{-1}. ^{1}H NMR (500 MHz, C_6D_6): δ 7.69 (dvt, $J_{2,\,H\text{-}P}$ = 2 Hz, $J_{H\text{-}H}$ = 10 Hz, 2H, Ar-*H*), 6.97 (s, 2H, Ar-*H*), 6.82 (dd, $J_{2,\,H\text{-}H}$ = 2 Hz, $J_{H\text{-}H}$ = 10 Hz, 2H, Ar-*H*), 2.74 (t, $J_{H\text{-}P}$ = 5 Hz, 1H, CC-*H*), 2.40 (m, 4H, C*H*Me_2), 2.17 (s, 3H, CH_3), 1.51 (dvt, 12H, CH*Me*$_2$), 1.21 (dvt, 12H, CH*Me*$_2$). ^{31}P {^{1}H} NMR (202 MHz, C_6D_6): δ 44.05. ^{13}C {^{1}H} NMR (125 MHz, C_6D_6): δ 162.2 (vt, $J_{C\text{-}P}$ = 14 Hz, Ar-*C*), 132.5 (s, Ar-*C*), 132.2 (s, Ar-*C*), 124.7 (vt, $J_{C\text{-}P}$ = 4 Hz, Ar-*C*), 121.0 (vt, $J_{C\text{-}P}$ = 16 Hz, Ar-*C*), 115.7 (vt, $J_{C\text{-}P}$ = 5 Hz, Ar-*C*), 111.6 (s, Ni*C*CH), 89.31 (t, $J_{C\text{-}P}$ = 43 Hz, NiC*C*H), 24.63 (vt, $J_{C\text{-}P}$ = 13 Hz, *C*HMe_2), 20.53 (s, Ar-*C*H_3), 18.88 (s, CH*Me*$_2$), 18.07 (s, CH*Me*$_2$). Elem. Anal. Calcd. for $C_{28}H_{41}NP_2Ni$: C, 65.65; H, 8.07; N, 2.73. Found: C, 65.66; H, 8.26; N, 2.88.

(^{Me}PNP)Pd(CCH) (47). **(^{Me}PNP)PdCl (44)** (100 mg, 175 μmol) was dissolved in THF solution (5.0 mL) and lithium acetylide, ethylene diamine complex (LiCCH · $NH_2CH_2CH_2NH_2$) (48 mg, 526 μmol) was added to it. The solution color changed immediately from purple to yellow. After stirring 1 hour, the volatiles were removed under vacuum, and the residue was extracted with toluene and filtered through a plug of silica gel. The filtrate was collected and the volatiles were removed under vacuum, yielding yellow solid (84 mg, 82%). ATR-IR: $\nu_{C\equiv C}$ 1969 cm^{-1}, $\nu_{C\text{-}H}$ 3281 cm^{-1}. ^{1}H NMR (500 MHz, C_6D_6): δ 7.78 (d, $J_{H\text{-}H}$ = 10 Hz, 2H, Ar-*H*), 6.88 (s, 2H, Ar-*H*), 6.84 (d, $J_{H\text{-}H}$ = 5 Hz, 2H, Ar-*H*), 2.66 (s, 1H, CC-*H*), 2.33 (m, 4H, C*H*Me_2), 2.16 (s, 3H, CH_3), 1.46 (dvt, 12H, CH*Me*$_2$), 1.11 (dvt, 12H, CH*Me*$_2$). ^{31}P {^{1}H} NMR (202 MHz, C_6D_6): δ 50.25. ^{13}C {^{1}H} NMR (125 MHz, C_6D_6): δ 161.9 (vt, $J_{C\text{-}P}$ = 11 Hz, Ar-*C*), 133.0 (s, Ar-*C*), 132.6 (s, Ar-*C*), 124.9 (t, $J_{C\text{-}P}$ = 4 Hz, Ar-*C*), 120.3 (vt, $J_{C\text{-}P}$ = 18 Hz, Ar-*C*), 115.9 (vt, $J_{C\text{-}P}$ = 5 Hz, Ar-*C*), 101.6 (t, $J_{C\text{-}P}$ = 4 Hz, Pd*C*CH), 88.72 (t, $J_{C\text{-}P}$ = 16 Hz, PdC*C*H), 25.18 (vt, $J_{C\text{-}P}$ = 13 Hz, *C*HMe_2), 20.48 (s, Ar-*C*H_3), 19.03 (vt, $J_{C\text{-}P}$ = 3 Hz, CH*Me*$_2$), 18.19 (s, CH*Me*$_2$). Elem. Anal. Calcd. for $C_{28}H_{41}NP_2Pd$: C, 60.05; H, 7.38; N, 2.50. Found: C, 59.72; H, 7.23; N, 2.39.

(^{Me}PNP)Pt(CCH) (48). (^{Me}PNP)PtCl (45) (100 mg, 152 μmol) was dissolved in THF solution (5.0 mL) and lithium acetylide, ethylene diamine complex ($LiCCH \cdot NH_2CH_2CH_2NH_2$) (42 mg, 455 μmol) was added to it. The solution color changed immediately from orange to yellow. After stirring 5 minutes, the volatiles were removed under vacuum, and the residue was extracted with toluene and filtered through a plug of silica gel. The filtrate was collected and the volatiles were removed under vacuum, yielding yellow solid (63 mg, 64%). ATR-IR: $\nu_{C\equiv C}$ 1972 cm^{-1}, ν_{C-H} 3285 cm^{-1}. ^{1}H NMR (500 MHz, C_6D_6): δ 7.83 (d, J_{H-H} = 10 Hz, 2H, Ar-*H*), 6.90 (s, 2H, Ar-*H*), 6.83 (d, J_{H-H} = 10 Hz, 2H, Ar-*H*), 2.76 (t, J_{H-P} = 2 Hz, 1H, CC-*H*), 2.50 (m, 4H, C*H*Me_2), 2.17 (s, 3H, CH_3), 1.45 (dvt, 12H, CH*Me*$_2$), 1.11 (dvt, 12H, CH*Me*$_2$). ^{31}P {^{1}H} NMR (202 MHz, C_6D_6): δ 44.56 (s, J_{P-Pt} = 2586 Hz). ^{13}C{^{1}H} NMR (125 MHz, C_6D_6): δ 162.7 (vt, J_{C-P} = 8 Hz, Ar-*C*), 133.1 (s, Ar-*C*), 132.6 (s, Ar-*C*), 125.5 (vt, J_{C-P} = 4 Hz, Ar-*C*), 120.4 (vt, J_{C-P} = 23 Hz, Ar-*C*), 116.1 (vt, J_{C-P} = 5 Hz, Ar-*C*), 99.9 (dt, J_{C-P} = 3 Hz, J_{C-Pt} = 350 Hz, Pt*C*CH), 78.24 (t, J_{C-P} = 13 Hz, PtC*C*H), 25.75 (vt, J_{C-P} = 15 Hz, *C*HMe_2), 20.41 (s, Ar-*C*H_3), 18.75 (s, CH*Me*$_2$), 18.16 (s, CH*Me*$_2$). Elem. Anal. Calcd. for $C_{28}H_{41}NP_2Pt$: C, 51.85; H, 6.37; N, 2.16. Found: C, 51.55; H, 6.07; N, 2.10.

(^{Me}PNP)Ni(CC)Ni(PNP^{Me}) (49). (^{Me}PNP)Ni(CCH) (46) (100 mg, 195 μmol) was dissolved in THF solution (5.0 mL) and fresh prepared lithium diisopropylamide (31 mg, 293 μmol) was added to it. After stirring 1 minutes, **(^{Me}PNP)NiCl (43)** (102 mg, 195 μmol) was added and immediately its green color diminished into red solution. Further after stirring for 30 minutes, the volatiles were removed under vacuum and the product was extracted with toluene and filtered through a plug of silica gel. The filtrate was collected and the volatiles were removed under vacuum, yielding orange solid (123 mg, 63%). The crystal can be obtained by CH_2Cl_2 solution layered with ethanol (1/1) in

a -35 ºC freezer over a week. Raman: $\nu_{C\equiv C}$ 1926, 1936 cm^{-1}. ^{1}H NMR (500 MHz, C_6D_6): δ 7.68 (d, $J_{H\text{-}H}$ = 5 Hz, 4H, Ar-*H*), 6.99 (s, 4H, Ar-*H*), 6.81 (d, $J_{H\text{-}H}$ = 5 Hz, 4H, Ar-*H*), 2.50 (m, 8H, C*H*Me_2), 2.20 (s, 12H, C*H*$_3$), 1.71 (dvt, 24H, CH*Me*$_2$), 1.30 (dvt, 24H, CH*Me*$_2$). ^{31}P {^{1}H} NMR (202 MHz, C_6D_6): δ 37.52. ^{13}C {^{1}H} NMR (125 MHz, CD_2Cl_2): δ 161.6 (vt, $J_{C\text{-}P}$ = 13 Hz, Ar-*C*), 132.4 (s, Ar-*C*), 131.6 (s, Ar-*C*), 124.1 (s, Ar-*C*), 121.8 (vt, $J_{C\text{-}P}$ = 16 Hz, Ar-*C*), 119.9 (t, $J_{C\text{-}P}$ = 44 Hz, Ni-*CC*-Ni), 114.9 (s, Ar-*C*), 24.23 (vt, $J_{C\text{-}P}$ = 13 Hz, *C*HMe_2), 20.40 (s, Ar-*C*H$_3$), 19.36 (s, CH*Me*$_2$), 17.84 (s, CH*Me*$_2$). Elem. Anal. Calcd. for $C_{54}H_{80}N_2P_4Ni_2$: C, 64.95; H, 8.08; N, 2.81. Found: C, 64.86; H, 8.02; N, 2.56.

(^{Me}PNP)Pd(CC)Pd(PNP^{Me}) (50). (^{Me}PNP)Pd(CCH) (47) (100 mg, 179 μmol) was dissolved in THF solution (5.0 mL) and fresh prepared lithium diisopropylamide (28 mg, 269 μmol) was added to it. After stirring 1 minutes, **(^{Me}PNP)PdCl (44)** (102 mg, 179 μmol) was added and immediately its light green color diminished into red solution. Further after stirring for 30 minutes, the volatiles were removed under vacuum and the product was extracted with toluene and filtered through a plug of silica gel. The filtrate was collected and the volatiles were removed under vacuum, yielding orange solid (150 mg, 70%). The crystal can be obtained by toluene solution layered with pentane (1/3) in a -35 °C freezer over a week. Raman: $\nu_{C\equiv C}$ 1987 cm^{-1}. ^{1}H NMR (500 MHz, C_6D_6): δ 7.86 (d, $J_{H\text{-}H}$ = 10 Hz, 4H, Ar-*H*), 6.99 (s, 4H, Ar-*H*), 6.87 (d, $J_{H\text{-}H}$ = 10 Hz, 4H, Ar-*H*), 2.48 (m, 8H, C*H*Me_2), 2.21 (s, 12H, C*H*$_3$), 1.62 (dvt, 24H, CH*Me*$_2$), 1.24 (dvt, 24H, CH*Me*$_2$). ^{31}P {^{1}H} NMR (202 MHz, C_6D_6): δ 45.22. ^{13}C {^{1}H} NMR (125 MHz, CD_2Cl_2): δ 162.0 (vt, $J_{C\text{-}P}$ = 10 Hz, Ar-*C*), 133.1 (s, Ar-*C*), 132.4 (s, Ar-*C*), 124.2 (vt, $J_{C\text{-}P}$ = 4 Hz, Ar-*C*), 121.0 (vt, $J_{C\text{-}P}$ = 18 Hz, Ar-*C*), 115.8 (vt, $J_{C\text{-}P}$ = 6 Hz, Ar-*C*), 110.2 (tt, $J_{C\text{-}P1}$ = 16 Hz, $J_{C\text{-}P2}$ = 4 Hz, Pd-*CC*-Pd), 25.09 (vt, $J_{C\text{-}P}$ =

13 Hz, *C*HMe$_2$), 20.58 (s, Ar-*C*H$_3$), 19.37 (vt, $J_{C\text{-}P}$ = 3 Hz, CH*Me*$_2$), 18.24 (s, CH*Me*$_2$). Elem. Anal. Calcd. for $C_{54}H_{80}N_2P_4Pd_2$: C, 59.29; H, 7.37; N, 2.56. Found: C, 59.27; H, 7.14; N, 2.51.

(^{Me}PNP)Pt(CC)Pt(PNP^{Me}) (51). (^{Me}PNP)Pt(CCH) (48) (100 mg, 154 μmol) was dissolved in THF solution (5.0 mL) and fresh prepared lithium diisopropylamide (16.5 mg, 154 μmol) was added to it. After stirring 1 minute, **(^{Me}PNP)PtCl (45)** (102 mg, 154 μmol) was added. Further after heating to 50 ºC for 1 hour, the volatiles were removed under vacuum and the product was extracted with toluene and filtered through a plug of silica gel. The filtrate was collected and the volatiles were removed under vacuum, yielding yellow solid (112 mg, 57%). The crystal can be obtained by toluene solution layered with pentane (1/3) in a -35 ºC freezer over a week. Raman: $\nu_{C\equiv C}$ 1994 cm^{-1}. ^{1}H NMR (500 MHz, C_6D_6): δ 7.91 (d, $J_{H\text{-}H}$ = 10 Hz, 4H, Ar-*H*), 7.01 (s, 4H, Ar-*H*), 6.86 (d, $J_{H\text{-}H}$ = 10 Hz, 4H, Ar-*H*), 2.65 (m, 8H, C*H*Me$_2$), 2.23 (s, 12H, C*H*$_3$), 1.62 (dvt, 24H, CH*Me*$_2$), 1.25 (dvt, 24H, CH*Me*$_2$). ^{31}P {^{1}H} NMR (202 MHz, C_6D_6): δ 42.60 (s, $J_{P\text{-}Pt}$ = 2710 Hz). ^{13}C{^{1}H} NMR (125 MHz, C_6D_6): δ 162.8 (vt, $J_{C\text{-}P}$ = 10 Hz, Ar-*C*), 133.3 (s, Ar-*C*), 132.3 (s, Ar-*C*), 124.7 (vt, $J_{C\text{-}P}$ = 4 Hz, Ar-*C*), 121.0 (vt, $J_{C\text{-}P}$ = 21 Hz, Ar-*C*), 116.1 (vt, $J_{C\text{-}P}$ = 5 Hz, Ar-*C*), 101.6 (t, $J_{C\text{-}P}$ = 13 Hz, Pt-*CC*-Pt), 25.68 (vt, $J_{C\text{-}P}$ = 16 Hz, *C*HMe$_2$), 20.53 (s, Ar-*C*H$_3$), 19.02 (s, CH*Me*$_2$), 18.21 (s, CH*Me*$_2$). Elem. Anal. Calcd for $C_{54}H_{80}N_2P_4Pt_2$: C, 51.02; H, 6.34; N, 2.20 Found: C, 50.97; H, 6.39; N, 2.05.

(^{Me}PNP)Ni(CC)Pd(PNP^{Me}) (52). 46 (100 mg, 195 μmol) was dissolved in THF solution (5.0 mL) and fresh prepared lithium diisopropylamide (20.9 mg, 195 μmol) was added to it. After stirring 1 minute, **44** (111 mg, 195 μmol) was added. Further after stirring for 30 minutes, the volatiles were removed under vacuum and the product was extracted with toluene and filtered

through a plug of silica gel. The filtrate was collected and the volatiles were removed under vacuum, yielding orange-red solid. The product was recrystallized with acetonitrile/dichloromethane, yielding orange-red crystal (120 mg, 59%). ^{1}H NMR (400 MHz, C_6D_6): δ 7.81 (d, $J_{H\text{-}H}$ = 8 Hz, 2H, Ar-*H*), 7.74 (d, $J_{H\text{-}H}$ = 8 Hz, 2H, Ar-*H*), 7.03 (s, 2H, Ar-*H*), 6.96 (s, 2H, Ar-*H*), 6.85-6.83 (m, 4H, Ar-*H*), 2.53 (m, 4H, C*H*Me$_2$), 2.45 (m, 4H, C*H*Me$_2$), 2.22 (s, 6H, C*H*$_3$), 2.20 (s, 6H, C*H*$_3$), 1.71 (dvt, 12H, CH*Me*$_2$), 1.60 (dvt, 12H, CH*Me*$_2$), 1.33 (dvt, 12H, CH*Me*$_2$), 1.21 (dvt, 12H, CH*Me*$_2$). ^{31}P {^{1}H} NMR (202 MHz, C_6D_6): δ 44.82 (s, 1P), 37.54 (s, 1P). ^{13}C{^{1}H} NMR (101 MHz, C_6D_6): δ 162.3 (vt, $J_{C\text{-}P}$ = 13 Hz, Ar-*C*), 161.9 (vt, $J_{C\text{-}P}$ = 10 Hz, Ar-*C*), 133.1 (s, Ar-*C*), 132.5 (s, Ar-*C*), 132.2 (two s, Ar-*C*), 125.5 (t, $J_{C\text{-}P}$ = 16 Hz, Ni-*C*C-Pd), 124.2 (vt, $J_{C\text{-}P}$ = 4 Hz, Ar-*C*), 124.0 (vt, $J_{C\text{-}P}$ = 3 Hz, Ar-*C*), 121.8 (vt, $J_{C\text{-}P}$ = 16 Hz, Ar-*C*), 120.5 (vt, $J_{C\text{-}P}$ = 17 Hz, Ar-*C*), 115.8 (vt, $J_{C\text{-}P}$ = 6 Hz, Ar-*C*), 115.6 (vt, $J_{C\text{-}P}$ = 5 Hz, Ar-*C*), 105.1 (t, $J_{C\text{-}P}$ = 42 Hz, Ni-C*C*-Pd), 24.86 (vt, $J_{C\text{-}P}$ = 12 Hz, *C*HMe$_2$), 24.39 (vt, $J_{C\text{-}P}$ = 12 Hz, *C*HMe$_2$), 20.63 (s, Ar-*C*H$_3$), 20.57 (s, Ar-*C*H$_3$), 19.36 (s, CH*Me*$_2$), 19.35 (s, CH*Me*$_2$), 17.98 (s, CH*Me*$_2$), 17.94 (s, CH*Me*$_2$). Elem. Anal. Calcd for $C_{54}H_{80}N_2P_4NiPd$: C, 61.99; H, 7.71; N, 2.68 Found: C, 61.88; H, 7.88; N, 2.49.

(^{Me}PNP)Ni(CC)Pt(PNP^{Me}) (53). 48 (100 mg, 154 μmol) was dissolved in THF solution (5.0 mL) and fresh prepared lithium diisopropylamide (16.5 mg, 154 μmol) was added to it. After stirring 1 minute, **43** (80.5 mg, 154 μmol) was added. Further after heating to 50 ºC for 1 hour, the volatiles were removed under vacuum and the product was extracted with toluene and filtered through a plug of silica gel. The filtrate was collected and the volatiles were removed under vacuum, yielding orange solid. The product was recrystallized with acetonitrile/dichloromethane, yielding orange crystal (100 mg, 57%). ^{1}H NMR (400 MHz, C_6D_6): δ 7.86 (d, $J_{H\text{-}H}$ = 8 Hz, 2H, Ar-*H*), 7.75 (d, $J_{H\text{-}}$

$_{H}$ = 8 Hz, 2H, Ar-*H*), 7.04 (s, 2H, Ar-*H*), 6.98 (s, 2H, Ar-*H*), 6.84 (d, J_{H-H} = 8 Hz, 4H, Ar-*H*), 2.62 (m, 4H, C*H*Me$_2$), 2.53 (m, 4H, C*H*Me$_2$), 2.22 (s, 12H, C*H*$_3$), 1.73 (dvt, 12H, CH*Me*$_2$), 1.59 (dvt, 12H, CH*Me*$_2$), 1.34 (dvt, 12H, CH*Me*$_2$), 1.21 (dvt, 12H, CH*Me*$_2$). ^{31}P {^{1}H} NMR (202 MHz, C_6D_6): δ 40.68 (s, J_{P-Pt} = 2713 Hz, 1P), 37.83 (s, 1P). ^{13}C{^{1}H} NMR (101 MHz, C_6D_6): δ 162.8 (vt, J_{C-P} = 10 Hz, Ar-*C*), 162.3 (vt, J_{C-P} = 13 Hz, Ar-*C*), 133.1 (s, Ar-*C*), 132.4 (s, Ar-*C*), 132.2 (s, Ar-*C*), 128.6 (s, Ar-*C*), 124.8 (vt, J_{C-P} = 4 Hz, Ar-*C*), 124.0 (vt, J_{C-P} = 3 Hz, Ar-*C*), 121.9 (vt, J_{C-P} = 15 Hz, Ar-*C*), 120.6 (vt, J_{C-P} = 23 Hz, Ar-*C*), 117.9 (s, Ni-*C*C-Pt), 116.1 (m, Ar-*C*), 115.5 (m, Ar-*C*), 25.50 (vt, J_{C-P} = 15 Hz, *C*HMe$_2$), 24.41 (vt, J_{C-P} = 12 Hz, *C*HMe$_2$), 20.63 (s, Ar-*C*H$_3$), 20.49 (s, Ar-*C*H$_3$), 19.29 (s, CH*Me*$_2$), 19.06 (s, CH*Me*$_2$), 17.97 (s, CH*Me*$_2$), 17.92 (s, CH*Me*$_2$). Elem. Anal. Calcd for $C_{54}H_{80}N_2P_4NiPt$: C, 57.15; H, 7.11; N, 2.47 Found: C, 56.64; H, 7.04; N, 2.39.

(^{Me}PNP)Pt(CC)Pd(PNP^{Me}) (54). 48 (100 mg, 154 μmol) was dissolved in THF solution (5.0 mL) and fresh prepared lithium diisopropylamide (16.5 mg, 154 μmol) was added to it. After stirring 1 minute, **44** (88.0 mg, 154 μmol) was added. Further after heating to 50 ºC for 1 hour, the volatiles were removed under vacuum and the product was extracted with toluene and filtered through a plug of silica gel. The filtrate was collected and the volatiles were removed under vacuum, yielding yellow solid. The product was recrystallized with acetonitrile/dichloromethane, yielding yellow crystal (150 mg, 82%). ^{1}H NMR (400 MHz, C_6D_6): δ 7.91 (d, J_{H-H} = 8 Hz, 2H, Ar-*H*), 7.87 (d, J_{H-H} = 8 Hz, 2H, Ar-*H*), 7.01-7.00 (m, 4H, Ar-*H*), 6.88-6.86 (m, 4H, Ar-*H*), 2.65 (m, 4H, C*H*Me$_2$), 2.49 (m, 4H, C*H*Me$_2$), 2.22 (two s, 12H, C*H*$_3$), 1.62 (m, 24H, CH*Me*$_2$), 1.25 (m, 24H, CH*Me*$_2$). ^{31}P{^{1}H} NMR (202 MHz, C_6D_6): δ 46.89 (s, 1P), 41.89 (s, J_{P-Pt} = 2705 Hz, 1P). ^{13}C{^{1}H} NMR (101 MHz, C_6D_6): δ 162.5 (vt, J_{C-P} = 10 Hz, Ar-*C*), 161.6 (vt, J_{C-P} = 10 Hz, Ar-*C*), 132.9 (s, Ar-*C*), 132.8 (s, Ar-*C*), 132.1 (s, Ar-*C*), 132.0 (s, Ar-*C*), 124.4 (vt, J_{C-P} = 3 Hz, Ar-*C*),

123.8 (vt, $J_{C\text{-}P}$ = 3 Hz, Ar-*C*), 120.7 (vt, $J_{C\text{-}P}$ = 23 Hz, Ar-*C*), 120.6 (vt, $J_{C\text{-}P}$ = 17 Hz, Ar-*C*), 107.5 (m, Pd-*C*C-Pt), 102.5 (m, Pd-C*C*-Pt), 25.32 (vt, $J_{C\text{-}P}$ = 16 Hz, *C*HMe$_2$), 24.71 (vt, $J_{C\text{-}P}$ = 16 Hz, *C*HMe$_2$), 20.20 (s, Ar-*C*H$_3$), 20.13 (s, Ar-*C*H$_3$), 18.94 (m, CH*Me*$_2$), 18.69 (m, CH*Me*$_2$), 17.86 (s, CH*Me*$_2$), 17.82 (s, CH*Me*$_2$). Elem. Anal. Calcd for $C_{54}H_{80}N_2P_4PdPt$: C, 54.84; H, 6.82; N, 2.37 Found: C, 54.52; H, 6.68; N, 2.33.

(^{Me}PNP)Ni(CCCC)Ni(PNP^{Me}) (57). 55 (300 mg, 549 μmol), bis(trimethylsilyl)butadiyne (53.4 mg, 275 μmol), sodium *tert*-butoxide (67 mg, 686 μmol), were mixed in *tert*-butanol/THF solution (1:1, 5.0 mL) After heating to 70 ºC overnight, the solution color changed from red to orange red. The volatiles were removed under vacuum, and the residue was extracted with toluene and filtered through a plug of silica gel with CH_2Cl_2. The filtrate was collected and the volatiles were removed under vacuum, yielding red solid. Recrystallization in CH_2Cl_2 solution layered with ethanol (1/1) in a -35 ºC freezer overnight yielded red crystals (150 mg, 53%). ^{1}H NMR (500 MHz, C_6D_6): δ 7.69 (d, $J_{H\text{-}H}$ = 10 Hz, 1H, Ar-*H*), 6.98 (s, 4H, Ar-*H*), 6.82 (d, $J_{H\text{-}H}$ = 10 Hz, 4H, Ar-*H*), 2.38 (m, 8H, C*H*Me$_2$), 2.18 (s, 12H, C*H*$_3$), 1.54 (dvt, 24H, CH*Me*$_2$), 1.23 (dvt, 24H, CH*Me*$_2$). ^{31}P{^{1}H} NMR (202 MHz, C_6D_6): δ 44.10. ^{13}C{^{1}H} NMR (125 MHz, CD_2Cl_2): δ 161.6 (s, Ar-*C*), 132.4 (s, Ar-*C*), 132.0 (s, Ar-*C*), 124.9 (s, Ar-*C*), 121.1 (s, Ar-*C*), 115.0 (s, Ar-*C*), 113.5 (s, Ni-*C*CC*C*-Ni), 78.3 (s, Ni-C*CC*C-Ni), 24.63 (s, *C*HMe$_2$), 20.36 (s, Ar-*C*H$_3$), 18.71 (s, CH*Me*$_2$), 18.05 (s, CH*Me*$_2$). $C_{56}H_{80}N_2Ni_2P_4$: C, 65.78; H, 7.89; N, 2.74. Found: C, 65.55; H, 7.78; N, 2.69.

(^{Me}PNP)Pd(CCCC)Pd(PNP^{Me}) (58). 56 (260 mg, 438 μmol), bis(trimethylsilyl)butadiyne (42.5 mg, 219 μmol), sodium *tert*-butoxide (53 mg, 548 μmol), were mixed in *tert*-butanol/THF solution (1:1, 5.0 mL) After heating to 70 ºC overnight, the solution color changed from red to yellow. The

volatiles were removed under vacuum, and the residue was extracted with toluene and filtered through a plug of silica gel with CH_2Cl_2. The filtrate was collected and the volatiles were removed under vacuum, yielding yellow solid. Recrystallization in CH_2Cl_2 solution layered with ethanol (1/1) in a -35 ºC freezer overnight yielded yellow crystals (150 mg, 61%). ^{1}H NMR (500 MHz, C_6D_6): δ 7.41 (s, 4H, Ar-*H*), 6.92 (s, 4H, Ar-*H*), 6.87 (d, $J_{H\text{-}H}$ = 10 Hz, 4H, Ar-*H*), 2.52 (m, 8H, C*H*Me$_2$), 2.20 (s, 12H, C*H*$_3$), 1.40 (dvt, 24H, CH*Me*$_2$), 1.18 (dvt, 24H, CH*Me*$_2$). ^{31}P{^{1}H} NMR (202 MHz, C_6D_6): δ 50.28. ^{13}C{^{1}H} NMR (125 MHz, CD_2Cl_2): δ 161.3 (s, Ar-*C*), 133.2 (s, Ar-*C*), 132.2 (s, Ar-*C*), 125.1 (s, Ar-*C*), 120.2 (s, Ar-*C*), 115.3 (s, Ar-*C*), 103.0 (s, Pd-*C*C*C*-Pd), 78.8 (m, Pd-C*CC*C-Pd), 25.13 (m, *C*HMe$_2$), 20.31 (s, Ar-*C*H$_3$), 18.81 (s, CH*Me*$_2$), 18.19 (s, CH*Me*$_2$). Elem. Anal. Calcd for $C_{56}H_{80}N_2Pd_2P_4$: C, 60.16; H, 7.21; N, 2.51 Found: C, 59.80; H, 7.37; N, 2.46.

(^{Me}PNP)PtOTf (59). 45 (300 mg, 455 mmol), lithium aluminum hydride (27 mg, 683 mmol) were mixed in ether (10 mL). The solution color steadily changed from yellow to brownish yellow. After 1 hour, the volatiles were removed under vacuum, and the corresponding product (^{Me}PNP)PtH was extracted with toluene and filtered through a plug of silica gel. The filtrate was collected and the volatiles were removed under vacuum, yielding light yellow solid (260 mg, 92%). (^{Me}PNP)PtH can be used directly without further purification. (^{Me}PNP)PtH (260 mg, 416 μmol) and MeOTf (68 mg, 416 μmol) were mixed in toluene solution (5 mL). After heating to 50 ºC for 1 hour under argon atmosphere, the volatiles were removed under vacuum, and the product **59** was extracted with toluene and filtered through celite. Further purification was conducted by recrystallization with diethyl ether layered pentane, yielding orange solid (280 mg, 87 %). Synthesis procedure was modified from the previous publication.[115]

(^{Me}PNP)PtCCCCTMS (60). 59 (260 mg, 337 μmol) and bis(trimethylsilyl)butadiyne (72 mg, 371 μmol) were mixed in THF solution (5.0 mL) and sodium *tert*-butoxide (39 mg, 404 μmol) was added to the solution. The color changed immediately from orange to yellow. After stirring 5 minutes, the volatiles were removed under vacuum, and the residue was extracted with toluene and filtered through celite. The filtrate was collected and the volatiles were removed under vacuum, yielding yellow solid. The product can be further purified by recrystallization with pentane in a -35 ºC freezer overnight, yielding yellow crystals (220 mg, 88%). ^{1}H NMR (500 MHz, C_6D_6): δ 7.77 (d, $J_{H\text{-}H}$ = 5 Hz, 2H, Ar-*H*), 6.83 (s, 2H, Ar-*H*), 6.80 (d, $J_{H\text{-}H}$ = 5 Hz, 2H, Ar-*H*), 2.34 (m, 4H, C*H*Me$_2$), 2.13 (s, 6H, C*H*$_3$), 1.32 (dvt, 12H, CH*Me*$_2$), 0.99 (dvt, 12H, CH*Me*$_2$), 0.22 (s, 9H, Si*Me*$_3$). ^{31}P{^{1}H} NMR (202 MHz, C_6D_6): δ 47.08 (s, $J_{P\text{-}Pt}$ = 2526 Hz). ^{13}C{^{1}H} NMR (125 MHz, C_6D_6): δ 162.6 (vt, $J_{C\text{-}P}$ = 10 Hz, Ar-*C*), 133.1 (s, Ar-*C*), 132.7 (s, Ar-*C*), 125.9 (vt, $J_{C\text{-}P}$ = 4 Hz, Ar-*C*), 119.9 (vt, $J_{C\text{-}P}$ = 23 Hz, Ar-*C*), 116.2 (vt, $J_{C\text{-}P}$ = 5 Hz, Ar-*C*), 98.02 (s, Pt-***C***CCC-TMS), 94.76 (s, Pt-CC***C***C-TMS), 83.79 (t, $J_{C\text{-}P}$ = 13 Hz, Pt-C***C***CC-TMS), 77.09 (s, Pt-CCC***C***-TMS), 25.70 (vt, $J_{C\text{-}P}$ = 16 Hz *C*HMe$_2$), 20.33 (s, Ar-*C*H$_3$), 18.67 (s, CH*Me*$_2$), 18.02 (s, CH*Me*$_2$), 0.63 (s, Si*Me*$_3$).

(^{Me}PNP)PtCCCCH (61). 60 (220 mg, 295 μmol) was dissolved in methanol/THF solution (1:1, 5.0 mL) and tetra-*n*-butylammonium fluoride (TBAF) solution (1.0 M, 0.6 ml) was added to it. After heating to 50 ºC for 3 hours, the volatiles were removed under vacuum, and the residue was extracted with toluene and filtered through a plug of silica gel. The filtrate was collected and the volatiles were removed under vacuum. Further added small amount of pentane to help solidification, yielding yellow solid (180 mg, 91%). ^{1}H NMR (500 MHz, C_6D_6): δ 7.75 (d, $J_{H\text{-}H}$ =

5 Hz, 2H, Ar-*H*), 6.83 (s, 2H, Ar-*H*), 6.79 (d, $J_{H\text{-}H}$ = 10 Hz, 2H, Ar-*H*), 2.34 (m, 4H, C*H*Me$_2$), 2.13 (s, 6H, C*H*$_3$), 1.79 (s, 1H, Pt-CCCC-H), 1.34 (dvt, 12H, CH*Me*$_2$), 1.00 (dvt, 12H, CH*Me*$_2$). ^{31}P{^{1}H} NMR (121 MHz, C_6D_6): δ 45.15 (s, $J_{P\text{-}Pt}$ = 2534 Hz). ^{13}C{^{1}H} NMR (125 MHz, C_6D_6): δ 162.6 (vt, $J_{C\text{-}P}$ = 10 Hz, Ar-*C*), 133.1 (d, $J_{C\text{-}Pt}$ = 5 Hz, Ar-*C*), 132.7 (s, Ar-*C*), 125.9 (vt, $J_{C\text{-}P}$ = 4 Hz, Ar-*C*), 119.9 (t, $J_{C\text{-}P}$ = 23 Hz, Ar-*C*), 116.14 (m, Ar-*C*), 96.70 (t, $J_{C\text{-}P}$ = 3 Hz, Pt-***C***CCC-H), 80.40 (t, $J_{C\text{-}P}$ = 13 Hz, Pt-CC***C***C-H), 73.53 (m, Pt-C***C***CC-H), 61.28 (d, $J_{C\text{-}Pt}$ = 11 Hz, Ar-*C*, Pt-CCC***C***-H), 25.70 (m, *C*HMe$_2$), 20.35 (dvt, Ar-*C*H$_3$), 18.61 (dvt, CH*Me*$_2$), 18.00 (dvt, CH*Me*$_2$).

(^{Me}PNP)Pt(CCCC)Pt(PNP^{Me}) (62). 61 (130 mg, 194 μmol) was dissolved in THF solution (5.0 mL) and fresh prepared lithium diisopropylamide (21 mg, 200 μmol) was added to it. After stirring 1 minutes, **45** (128 mg, 194 μmol) was added to the solution and heating to 70 ºC overnight, the volatiles were removed under vacuum and the product was extracted with toluene and filtered through a plug of silica gel with CH_2Cl_2. The filtrate was collected and the volatiles were removed under vacuum, yielding yellow solid. Further purification by recrystallization with CH_2Cl_2 layered with pentane yielded yellow crystalline powders (210 mg, 84%). ^{1}H NMR (500 MHz, CD_2Cl_2): δ 7.49 (d, $J_{H\text{-}H}$ = 10 Hz, 4H, Ar-*H*), 6.95 (s, 4H, Ar-*H*), 6.89 (d, $J_{H\text{-}H}$ = 10 Hz, 4H, Ar-*H*), 2.68 (m, 8H, C*H*Me$_2$), 2.23 (s, 12H, C*H*$_3$), 1.39 (dvt, 12H, CH*Me*$_2$), 1.18 (dvt, 12H, CH*Me*$_2$). ^{31}P{^{1}H} NMR (202 MHz, C_6D_6): δ 46.49 (s, $J_{P\text{-}Pt}$ = 2594 Hz). ^{13}C{^{1}H} NMR (125 MHz, CD_2Cl_2): δ 162.2 (vt, $J_{C\text{-}P}$ = 10 Hz, Ar-*C*), 133.4 (s, Ar-*C*), 132.2 (s, Ar-*C*), 125.7 (vt, $J_{C\text{-}P}$ = 4 Hz, Ar-*C*), 120.3 (vt, $J_{C\text{-}P}$ = 23 Hz, Ar-*C*), 115.6 (vt, $J_{C\text{-}P}$ = 5 Hz, Ar-*C*), 102.2 (s, Pt-***C***CC***C***-Pt), 70.07 (s, Pt-C***CC***C-Pt), 25.70 (vt, $J_{C\text{-}P}$ = 16 Hz,, *C*HMe$_2$), 20.28 (s, Ar-*C*H$_3$), 18.51 (s, CH*Me*$_2$), 18.16 (s, CH*Me*$_2$). Elem. Anal. Calcd for $C_{56}H_{80}N_2Pt_2P_4$: C, 51.93; H, 6.23; N, 2.16. Found: C, 51.61; H, 5.97; N, 2.08.

(^{Me}PNP)Ni(CCPhCC)Ni(PNP^{Me}) (64). 63 (120 mg, 188 μmol) was dissolved in THF solution (5.0 mL) and 1,4-diethynylbenzene (11.4 mg, 90 μmol), triethylamine (20 mg, 200 μmol) were added to it subsequently. The solution color changed from blue to red. After stirring 5 minutes, the volatiles were removed under vacuum, and the residue was extracted with toluene and filtered through a plug of silica gel. The filtrate was collected and the volatiles were removed under vacuum, yielding red solid. The product can be further purified by recrystallization with ethanol/dichloromethane in a -35 ºC freezer overnight, yielding red crystals (75 mg, 76%). ^{1}H NMR (400 MHz, CD_2Cl_2): δ 7.36 (d, $J_{H\text{-}H}$ = 8 Hz, 4H, Ar-*H*), 7.00 (s, 4H, Ar-*H*), 6.86 (d, $J_{H\text{-}H}$ = 8 Hz, 4H, Ar-*H*), 2.54 (m, 8H, C*H*Me$_2$), 2.21 (s, 12H, C*H*$_3$), 1.46 (dvt, 24H, CH*Me*$_2$), 1.29 (dvt, 24H, CH*Me*$_2$). ^{31}P{^{1}H} NMR (202 MHz, CD_2Cl_2): δ 45.55. ^{13}C{^{1}H} NMR (101 MHz, CD_2Cl_2): δ 161.7 (vt, $J_{C\text{-}P}$ = 10 Hz, Ar-*C*), 132.5 (s, Ar-*C*), 132.2 (s, Ar-*C*), 130.2 (s, Ar-*C*), 125.6 (s, Ar-*C*), 125.6 (s, Ar-*C*), 125.0 (s, Ar-*C*), 121.0 (vt, $J_{C\text{-}P}$ = 17 Hz, Ar-*C*), 115.2 (s, Ni-C*C*Ph*C*C-Ni), 97.62 (t, $J_{C\text{-}P}$ = 43 Hz, Ni-*C*CPhC*C*-Ni). 24.75 (vt, $J_{C\text{-}P}$ = 13 Hz, *C*HMe$_2$), 20.38 (s, Ar-*C*H$_3$), 18.78 (s, CH*Me*$_2$), 18.17 (s, CH*Me*$_2$). Elem. Anal. Calcd for $C_{62}H_{84}N_2P_4Ni_2$: C, 67.78; H, 7.71; N, 2.55. Found: C, 67.33; H, 7.60; N, 2.40.

Ferrocenium 1-carbadodecaborate (FcCH$_{12}$B$_{11}$). A Schlenk flask was charged with Cs[$CH_{12}B_{11}$] (0.26 g, 1.0 mmol), ferrocene (0.18 g, 1.0 mmol), PhI(OAc)$_2$ (0.16 mg, 0.50 mmol), and acetonitrile (10 mL). Me$_3$SiCl (126 μL, 1.0 mmol) was then added to the orange solution resulting in a color change to royal blue. The solution was stirred for 30 min and then the volatiles were removed extensively under vacuum. The resulting blue powder was dissolved in acetonitrile and filtered through a pad of Celite. The solution was then layered with benzene/heptane (1/1) and

slow diffusion at room temperature resulted in a paramagnetic blue block crystal (0.20 g, 0.61 mmol, 61%). Elem. Anal. Calcd. for FeC11H22B11: C 40.15; H 6.74; found: C 39.87; H 6.37.

[49-51]$CH_{12}B_{11}$ crystals. Complex **49-51** (10 mg) was dissolved in CH_2Cl_2 (or THF) and mixed with approximately 0.9 equivalent of ferrocenium carba-*closo*-dodecaborate in a glass vial. The solution color changed immediately. The reaction mixture was layered by isooctane (or pentane) and put into a -35 ºC freezer overnight, yielding the black color crystal. The crystal was then subjected to X-ray crystallography.

2.4.5 X-ray Structural Determination Details

X-Ray data collection, solution, and refinement for (49). (CCDC number: 1915573)

A Leica MZ 75 microscope was used to identify a suitable red plate with very well defined faces with dimensions (max, intermediate, and min) 0.457 x 0.428 x 0.035 mm^3 from a representative sample of crystals of the same habit. The crystal mounted on a nylon loop was then placed in a cold nitrogen stream (Oxford) maintained at 110 K. A BRUKER APEX 2 Duo X-ray (three-circle) diffractometer was employed for crystal screening, unit cell determination, and data collection. The X-ray radiation employed was generated from a Mo sealed X-ray tube (K_α = 0.71073Å with a potential of 40 kV and a current of 40 mA). All diffractometer manipulations, including data collection, integration and scaling were carried out using the Bruker APEXII software.[123] An absorption correction was applied using SADABS.[124] Systematic reflection conditions and statistical tests of the data suggested the space group *C*2/*c*. A solution was obtained readily (Z=4; Z'=0.5) using XT/XS in APEX2.[123,125] Hydrogen atoms were placed in idealized positions and were set riding on the respective parent atoms. 2 molecules of DCM were found solvated per

molecule of Ni_2 complex. Final Formula: $C_{54}H_{80}N_2Ni_2P_4 \cdot 2(CH_2Cl_2)$. All non-hydrogen atoms were refined with anisotropic thermal parameters. Q-peaks close to DCM suggested disorder, and was modeled between two positions with an occupancy ratio of 0.93:0.07. Absence of additional symmetry and voids were confirmed using PLATON (ADDSYM). The structure was refined (weighted least squares refinement on F^2) to convergence.[125,126] ORTEP-3 and POV-Ray were employed for the final data presentation and structure plots.[127,128]

X-Ray data collection, solution, and refinement for (50). (CCDC number: 1915574)

A Leica MZ 75 microscope was used to identify a suitable green block with very well defined faces with dimensions (max, intermediate, and min) 0.258 x 0.239 x 0.162 mm^3 from a representative sample of crystals of the same habit. The crystal mounted on a nylon loop was then placed in a cold nitrogen stream (Oxford) maintained at 110 K. A BRUKER Quest X-ray (fixed-Chi geometry) diffractometer was employed for crystal screening, unit cell determination, and data collection. The X-ray radiation employed was generated from a Mo-Iμs X-ray tube (K_α = 0.71073Å). All diffractometer manipulations, including data collection, integration and scaling were carried out using the Bruker APEXII software.[122] An absorption correction was applied using SADABS.[123] Systematic reflection conditions and statistical tests of the data suggested the space group $P2_1/c$. A solution was obtained readily using XT/XS in APEX3.[122,124] Half a molecule of hexane is found solvated per molecule of Pd-complex. Final Formula: $C_{54}H_{80}N_2P_4Pd_2 \cdot 0.5(C_6H_{14})$. Hydrogen atoms were placed in idealized positions and were set riding on the respective parent atoms. All non-hydrogen atoms were refined with anisotropic thermal parameters. Q-peaks near C25, C27, C45B, C47B indicated possible disorder which were modeled between two positions each with an occupancy ratio of 0.86:0.14. Appropriate restraints and / or constraints were used to

keep the bond distances, angles, and thermal ellipsoids meaningful. Absence of additional symmetry and voids were confirmed using PLATON (ADDSYM). The structure was refined (weighted least squares refinement on F^2) to convergence.[124,125] ORTEP-3 and POV-Ray were employed for the final data presentation and structure plots.[126,127]

X-Ray data collection, solution, and refinement for (51). (CCDC number: 1915575)

A Leica MZ 75 microscope was used to identify a suitable yellow block with very well defined faces with dimensions (max, intermediate, and min) 0.183 x 0.134 x 0.084 mm^3 from a representative sample of crystals of the same habit. The crystal mounted on a nylon loop was then placed in a cold nitrogen stream (Oxford) maintained at 110 K. A BRUKER Quest X-ray (fixed-Chi geometry) diffractometer was employed for crystal screening, unit cell determination, and data collection. The X-ray radiation employed was generated from a Mo-Iμs X-ray tube (K_α = 0.71073Å). All diffractometer manipulations, including data collection, integration and scaling were carried out using the Bruker APEXII software.[122] An absorption correction was applied using SADABS.[123] Systematic reflection conditions and statistical tests of the data suggested the space group *P*-1. A solution was obtained readily (Z=4; Z'=2) using XT/XS in APEX3.[122,124] A molecule of pentane was found solvated. Hydrogen atoms were placed in idealized positions and were set riding on the respective parent atoms. All non-hydrogen atoms were refined with anisotropic thermal parameters. Some of the carbon atoms showed unusual thermal ellipsoids. Appropriate restraints were added to keep them meaningful. Absence of additional symmetry and voids were confirmed using PLATON (ADDSYM). The structure was refined (weighted least squares refinement on F^2) to convergence.[124,125] ORTEP-3 and POV-Ray were employed for the final data presentation and structure plots.[126,127]

X-Ray data collection, solution, and refinement for (58). (CCDC number: 1915568)

A Leica MZ 75 microscope was used to identify a suitable yellow block with very well defined faces with dimensions (max, intermediate, and min) 0.219 x 0.082 x 0.076 mm^3 from a representative sample of crystals of the same habit. The crystal mounted on a nylon loop was then placed in a cold nitrogen stream (Oxford) maintained at 110 K. A BRUKER Quest X-ray (fixed-Chi geometry) diffractometer with a PHOTON II detector was employed for crystal screening, unit cell determination, and data collection. The X-ray radiation employed was generated from a Mo-Iμs X-ray tube (K_α = 0.71073Å). All diffractometer manipulations, including data collection, integration and scaling were carried out using the Bruker APEXII software.[122] An absorption correction was applied using SADABS.[123] Systematic reflection conditions and statistical tests of the data suggested the space group *P*-1. A solution was obtained readily (Z=1; Z'=0.5) using XT/XS in APEX3.[122,124] Hydrogen atoms were placed in idealized positions and were set riding on the respective parent atoms. All non-hydrogen atoms were refined with anisotropic thermal parameters. Absence of additional symmetry and voids were confirmed using PLATON (ADDSYM). The structure was refined (weighted least squares refinement on F^2) to convergence.[124,125] ORTEP-3 and POV-Ray were employed for the final data presentation and structure plots.[126,127]

X-Ray data collection, solution, and refinement for [49] $CH_{12}B_{11}$. (CCDC number: 1915572)

A Leica MZ 75 microscope was used to identify a suitable brown block with very well defined faces with dimensions (max, intermediate, and min) 0.261 x 0.084 x 0.073 mm^3 from a

representative sample of crystals of the same habit. The crystal mounted on a nylon loop was then placed in a cold nitrogen stream (Oxford) maintained at 110 K. A BRUKER Quest X-ray (fixed-Chi geometry) diffractometer with a PHOTON II detector was employed for crystal screening, unit cell determination, and data collection. The X-ray radiation employed was generated from a Mo-Iμs X-ray tube (K_α = 0.71073Å). All diffractometer manipulations, including data collection, integration and scaling were carried out using the Bruker APEXII software.[122] An absorption correction was applied using SADABS.[123] Systematic reflection conditions and statistical tests of the data suggested the space group *C*2/*c*. A solution was obtained readily using XT/XS in APEX3.[122,124] Several solvent molecules were found which were significantly disordered. Hydrogen atoms were placed in idealized positions and were set riding on the respective parent atoms. All non-hydrogen atoms were refined with anisotropic thermal parameters. For the final least squares refinement, the solvent molecules were MASKed using OLEX2. Absence of additional symmetry was confirmed using PLATON (ADDSYM). The structure was refined (weighted least squares refinement on F^2) to convergence.[124,125] ORTEP-3 and POV-Ray were employed for the final data presentation and structure plots.[126,127]

X-Ray data collection, solution, and refinement for [50] $CH_{12}B_{11}$. (CCDC number: 1984910)

A Leica MZ 75 microscope was used to identify a suitable black plate with very well defined faces with dimensions (max, intermediate, and min) 0.438 x 0.263 x 0.094 mm^3 from a representative sample of crystals of the same habit. The crystal mounted on a nylon loop was then placed in a cold nitrogen stream (Oxford) maintained at 110 K. A BRUKER Quest X-ray (fixed-Chi geometry) diffractometer with a PHOTON II detector was employed for crystal screening, unit cell determination, and data collection. The X-ray radiation employed was generated from a

Mo-Iμs X-ray tube (K_α = 0.71073Å). All diffractometer manipulations, including data collection, integration and scaling were carried out using the Bruker APEXII software.[122] An absorption correction was applied using SADABS.[123] Systematic reflection conditions and statistical tests of the data suggested the space group *C*2/*c*. A solution was obtained readily using XT/XS in APEX3.[122,124] Several solvent molecules were found which were significantly disordered. Hydrogen atoms were placed in idealized positions and were set riding on the respective parent atoms. All non-hydrogen atoms were refined with anisotropic thermal parameters. For the final least squares refinement, the solvent molecules were MASKed using OLEX2. Absence of additional symmetry was confirmed using PLATON (ADDSYM). The structure was refined (weighted least squares refinement on F^2) to convergence.[124,125] ORTEP-3 and POV-Ray were employed for the final data presentation and structure plots.[126,127]

X-Ray data collection, solution, and refinement for [51] $CH_{12}B_{11}$. (CCDC number: 1984911)

A Leica MZ 75 microscope was used to identify a suitable brown plate with very well defined faces with dimensions (max, intermediate, and min) 0.238 x 0.182 x 0.01 mm^3 from a representative sample of crystals of the same habit. The crystal mounted on a nylon loop was then placed in a cold nitrogen stream (Oxford) maintained at 110 K. A BRUKER Quest X-ray (fixed-Chi geometry) diffractometer with a PHOTON II detector was employed for crystal screening, unit cell determination, and data collection. The X-ray radiation employed was generated from a Mo-Iμs X-ray tube (K_α = 0.71073Å). All diffractometer manipulations, including data collection, integration and scaling were carried out using the Bruker APEXII software.[122] An absorption correction was applied using SADABS.[123] Systematic reflection conditions and statistical tests of the data suggested the space group *C*2/*c*. A solution was obtained readily using XT/XS in

APEX3.[122,124] Several solvent molecules were found which were significantly disordered. Hydrogen atoms were placed in idealized positions and were set riding on the respective parent atoms. All non-hydrogen atoms were refined with anisotropic thermal parameters. For the final least squares refinement, the solvent molecules were MASKed using OLEX2. Absence of additional symmetry was confirmed using PLATON (ADDSYM). The structure was refined (weighted least squares refinement on F^2) to convergence.[124,125] ORTEP-3 and POV-Ray were employed for the final data presentation and structure plots.[126,127]

2.4.6 Electrochemical Analysis.

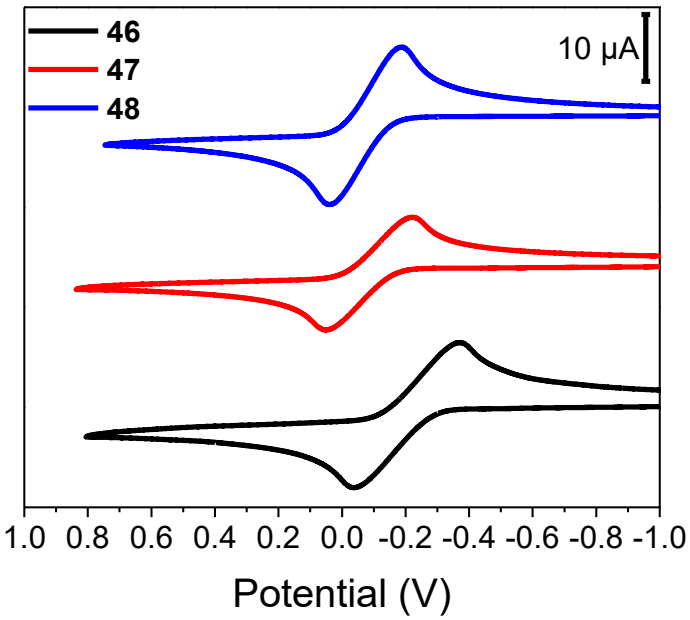

Figure II-12. Cyclic voltammogram (CV) of complexes **46-48** in CH_2Cl_2 with 0.1 M $^{n}Bu_4NBAr^{F}{}_4$ as the supporting electrolyte.

Table II-7. Electrochemical data of complexes **46-48**.

vs Fc/Fc^+	$E_{1/2}$ (V)
46	**-0.21**
47	**-0.09**
48	**-0.07**

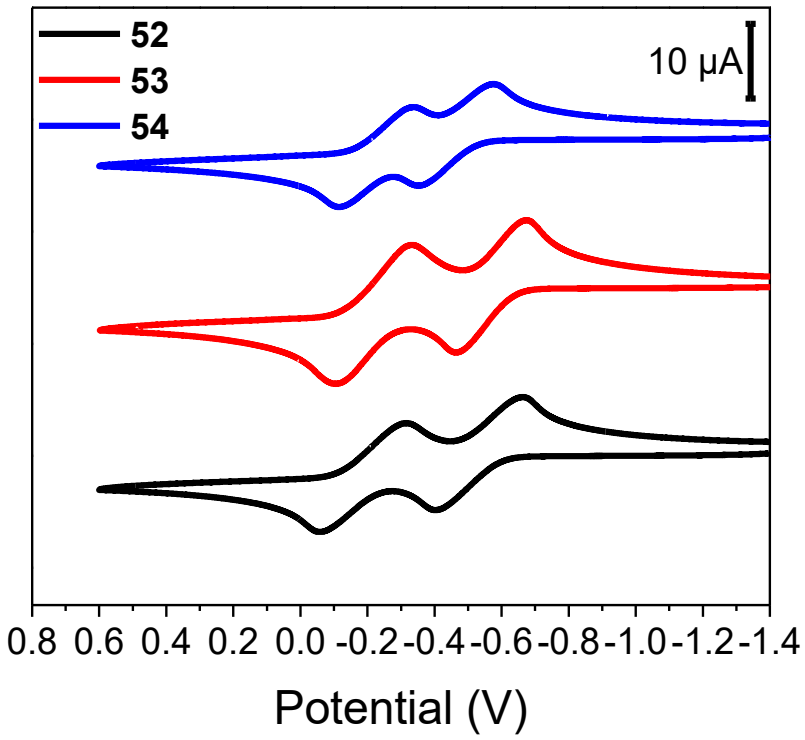

Figure II-13. Cyclic voltammogram of complexes **52-54** in CH_2Cl_2 with 0.1 M $^{n}Bu_4NBAr^{F}_4$ as the supporting electrolyte.

Table II-8. Electrochemical data of complexes **52-54**.

vs Fc/Fc^+	$E^1_{1/2}$ (V)	$E^2_{1/2}$ (V)	ΔE (V)
52	**-0.53**	**-0.19**	**0.34**
53	**-0.57**	**-0.23**	**0.34**
54	**-0.47**	**-0.23**	**0.24**

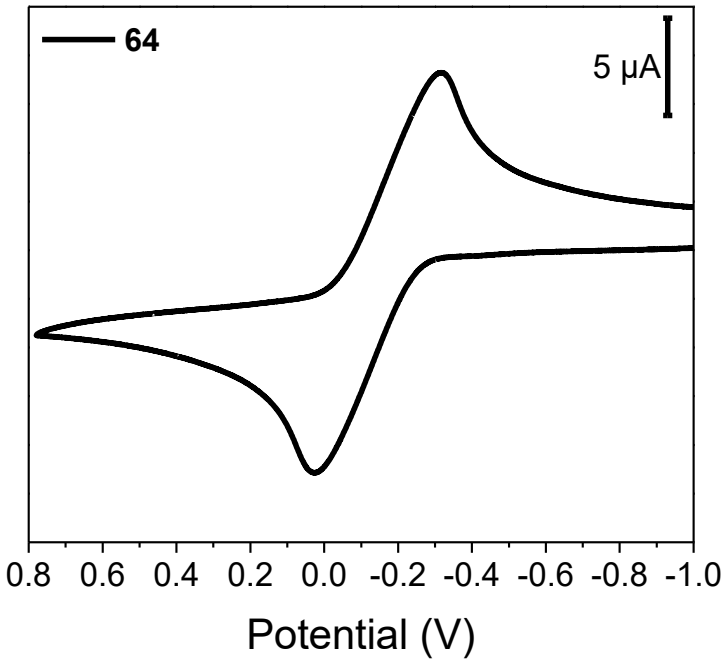

Figure II-14. Cyclic voltammogram of **64** in CH_2Cl_2 with 0.1 M $^{n}Bu_4NBAr^{F}_4$ as the supporting electrolyte.

Table II-9. Electrochemical data of **64**.

vs Fc/Fc^+	$E_{1/2}$ (V)
64	**-0.15**

2.4.7 UV-vis-NIR Spectrum

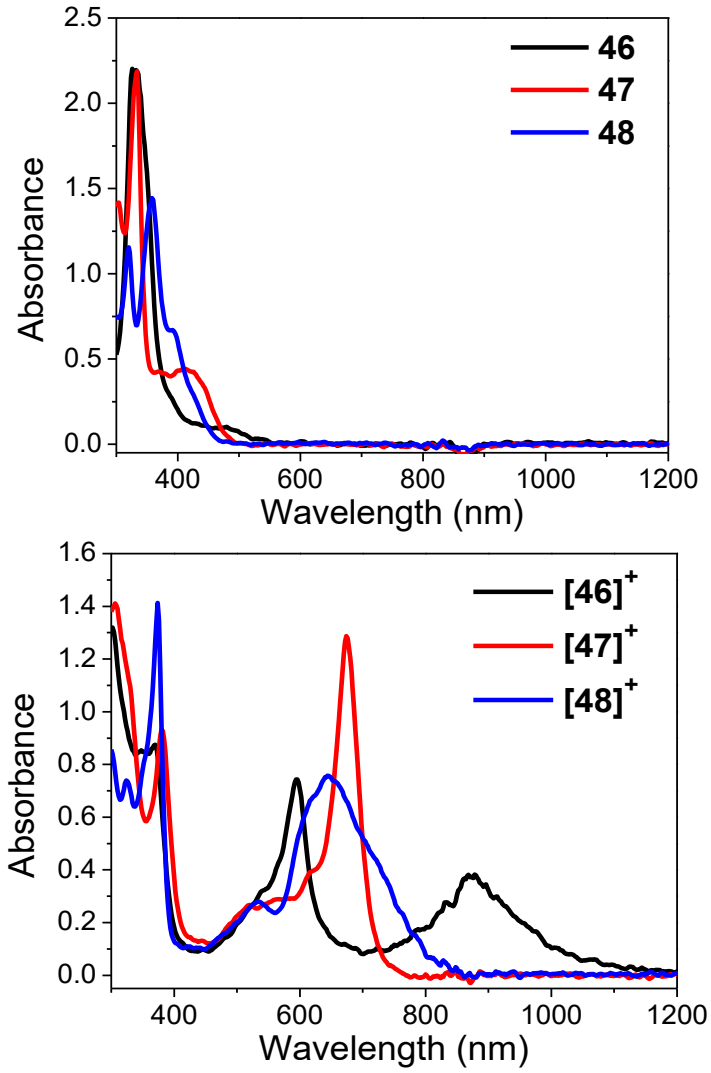

Figure II-15. UV-vis-NIR spectrum of ca. 1 x 10^{-4} M **46-48** (up) and **[46-48]**$^{+}$ (down) in CH_2Cl_2 solution at room temperature. **[46]**$^{+}$ were prepared by adding 1.2 eq [Fc]$CH_{12}B_{11}$ as the oxidant into **46-48**.

Table II-10. Selected absorption wavelengths of **[46-48]**$^{+}$.

Complex	λ (nm)
[46]$^{+}$	595, 870
[47]$^{+}$	674
[48]$^{+}$	645

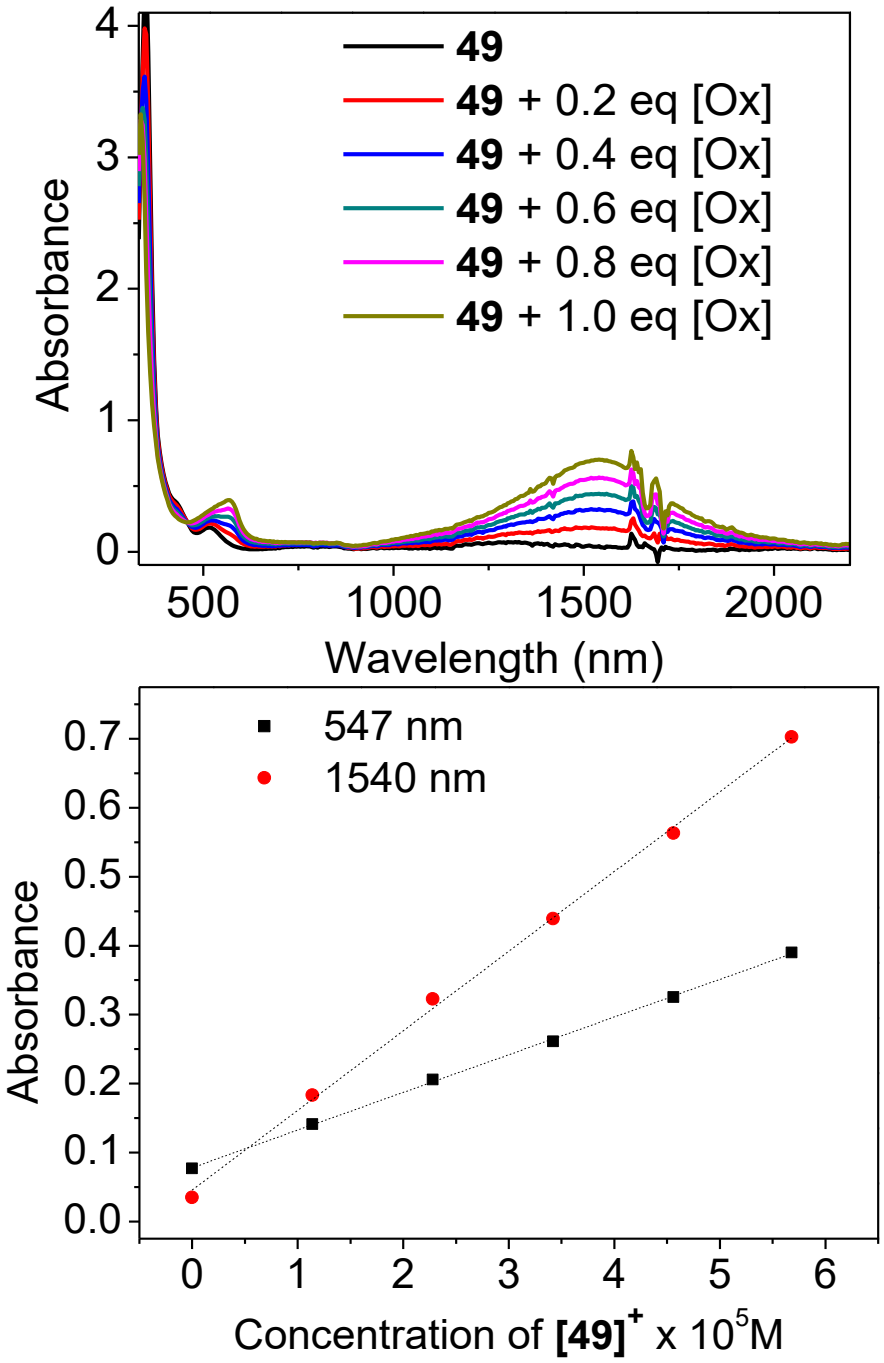

Figure II-16. UV-vis-NIR spectrum of **49** titrated by [Fc]$CH_{12}B_{11}$ as the oxidant [Ox]. Plot of absorbance *vs.* concentration of [**49**] $CH_{12}B_{11}$. According to Lambert-Beer law: λ_{max}: 567 nm; ε = 5464 $cm^{-1}M^{-1}$; λ_{max}: 1540 nm; ε = 11551 $cm^{-1}M^{-1}$.

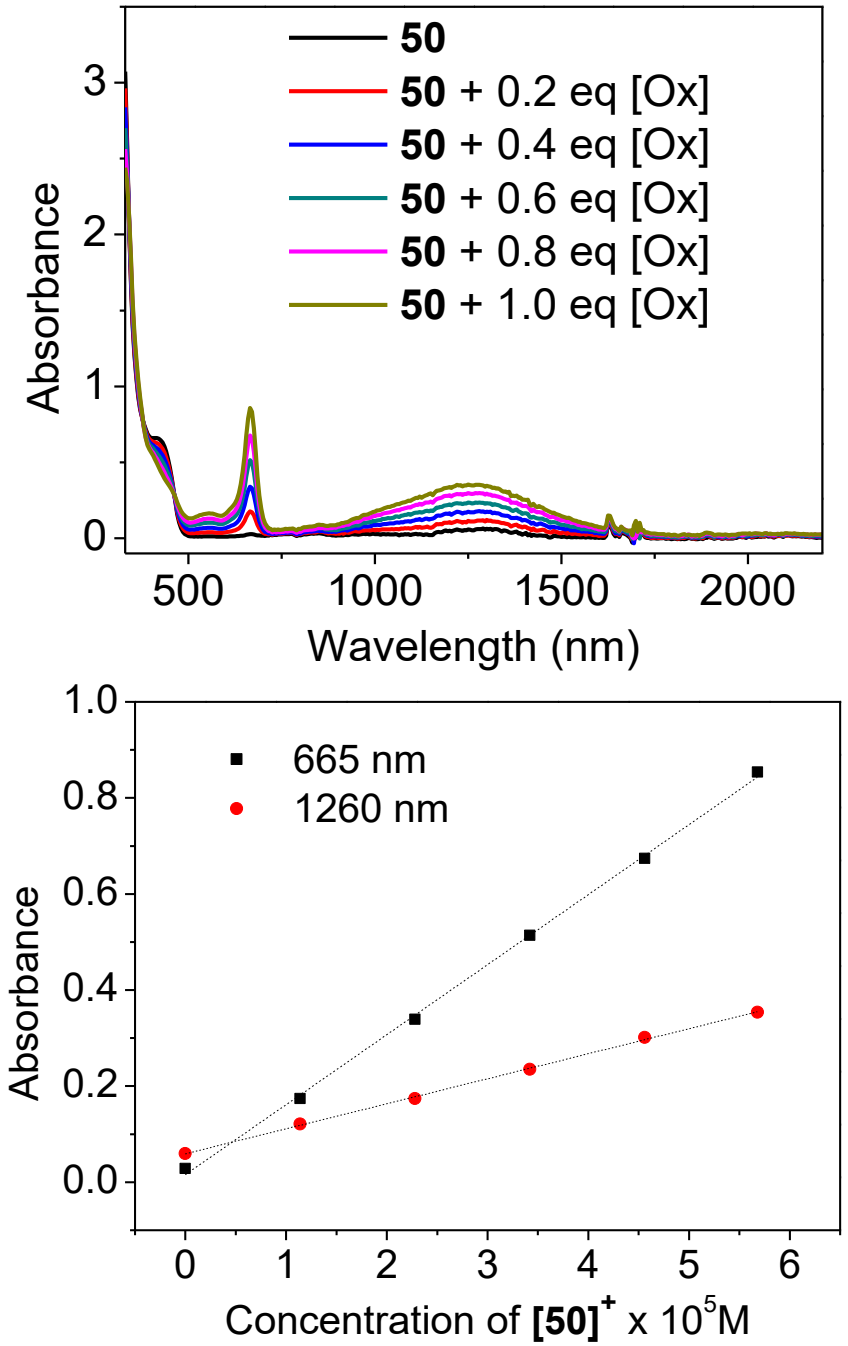

Figure II-17. UV-vis-NIR spectrum of **50** titrated by [Fc]$CH_{12}B_{11}$ as the oxidant [Ox]. Plot of absorbance *vs.* concentration of [**50**] $CH_{12}B_{11}$. According to Lambert-Beer law: λ_{max} : 665 nm; ε = 14572 $cm^{-1}M^{-1}$; : λ_{max} : 1260 nm; ε = 5207 $cm^{-1}M^{-1}$.

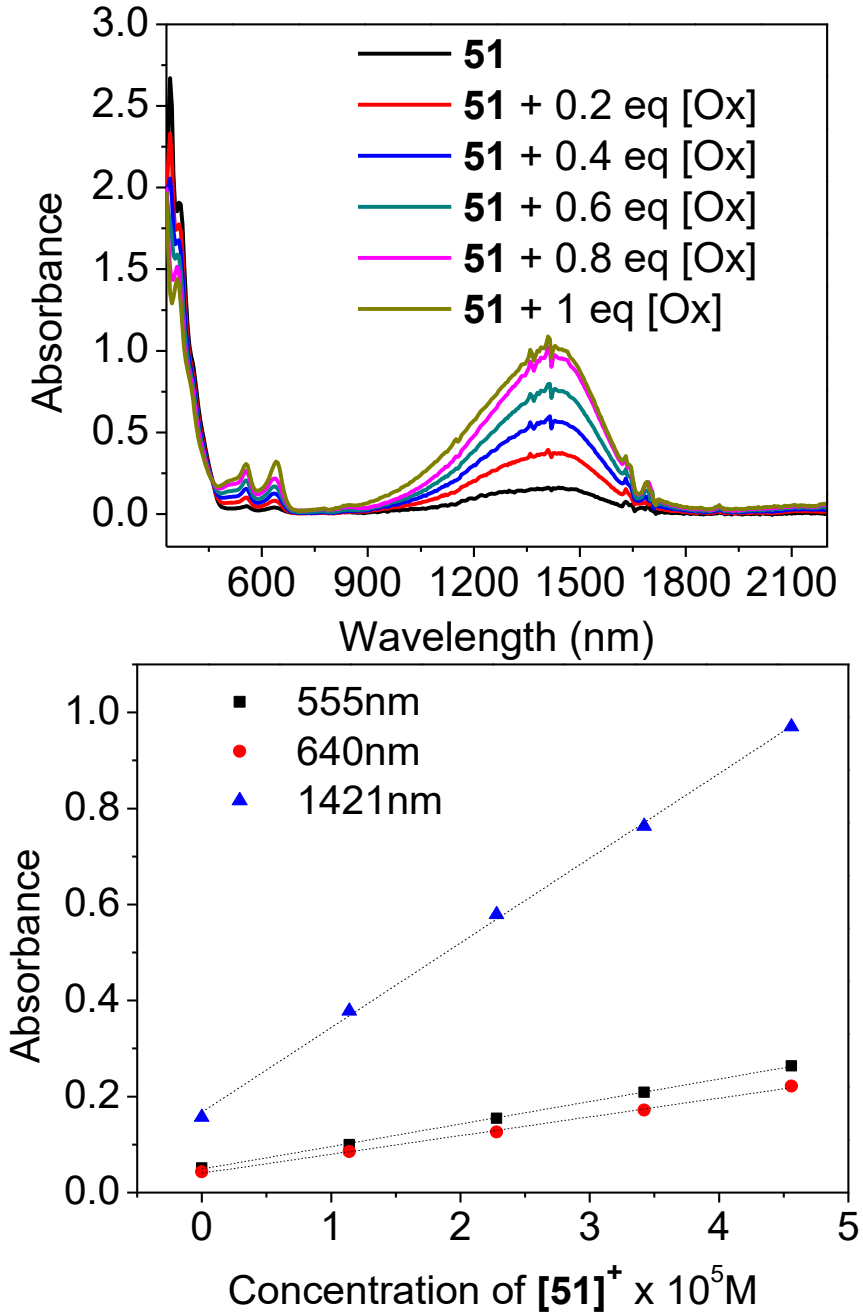

Figure II-18. UV-vis-NIR spectrum of **51** titrated by [Fc]$CH_{12}B_{11}$ as the oxidant [Ox]. Plot of absorbance *vs.* concentration of [**51**] $CH_{12}B_{11}$. According to Lambert-Beer law: λ_{max} : 555 nm; ε = 4686 $cm^{-1}M^{-1}$; λ_{max} : 640 nm; ε = 3904 $cm^{-1}M^{-1}$; λ_{max} : 1421 nm; ε = 17640 $cm^{-1}M^{-1}$.

2.4.6 Theoretical Calculation.

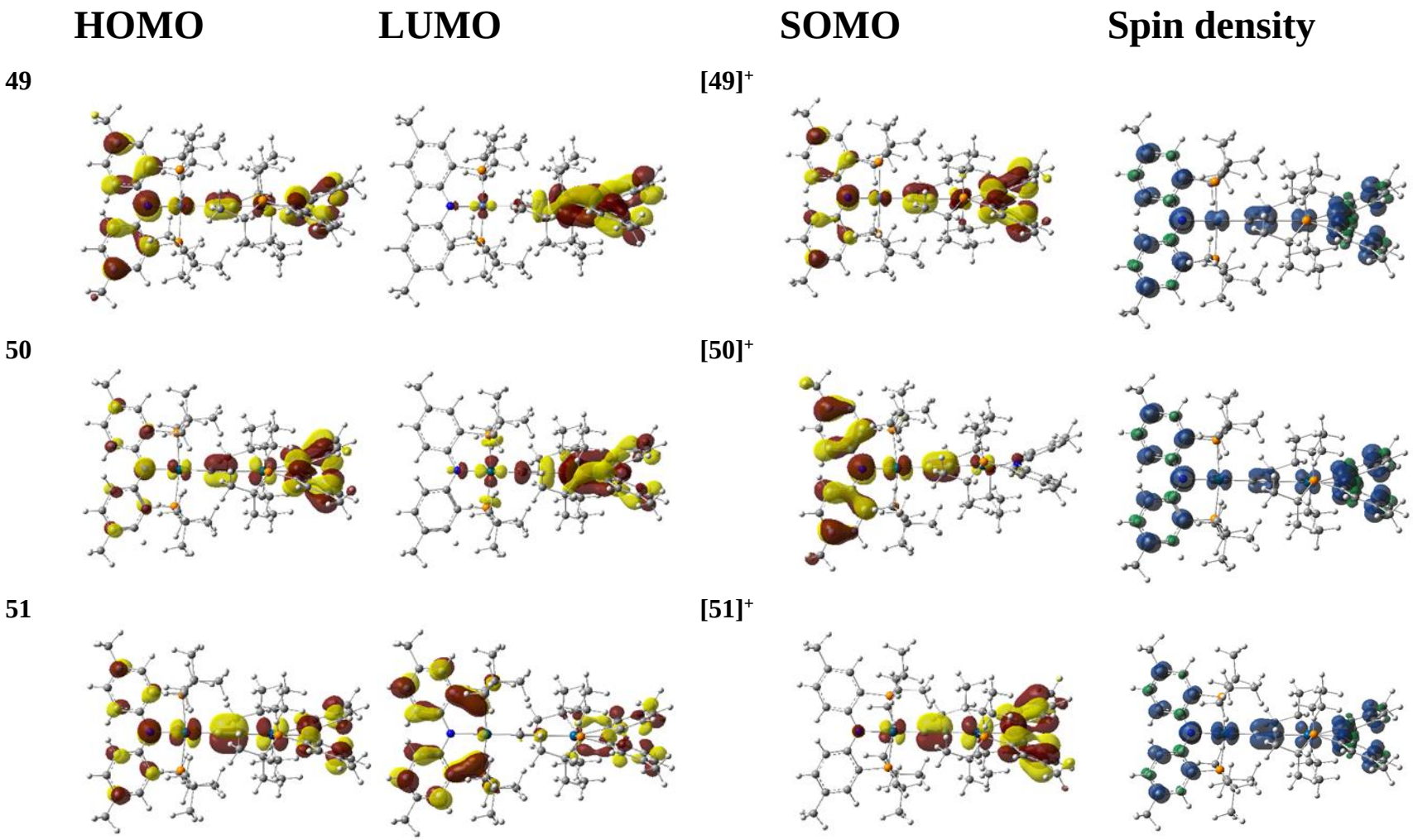

Figure II-19. Calculated HOMOs and LUMOs of complexes **49-51**; SOMOs and spin density plots of **[49-51]$^+$.**

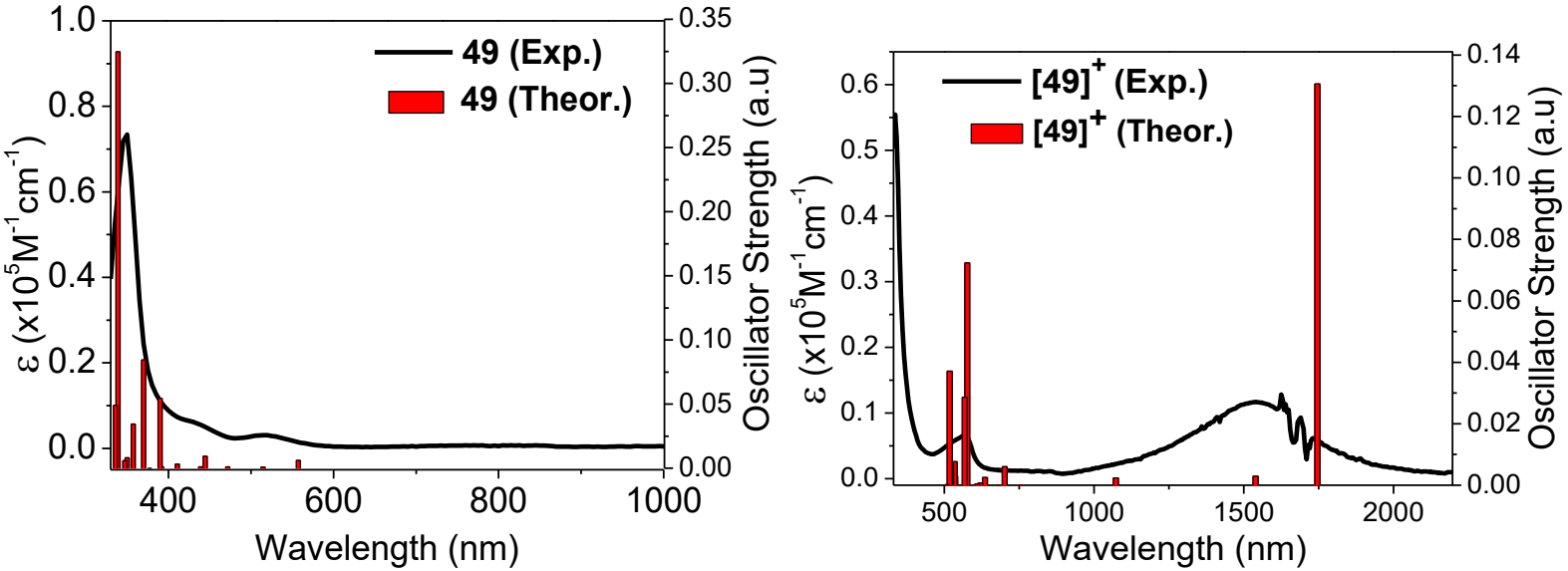

Figure II-20. An overlay of experimental spectra of **49** and **[49]**$^{+}$ and TD-DFT calculated oscillator strengths in CH_2Cl_2.

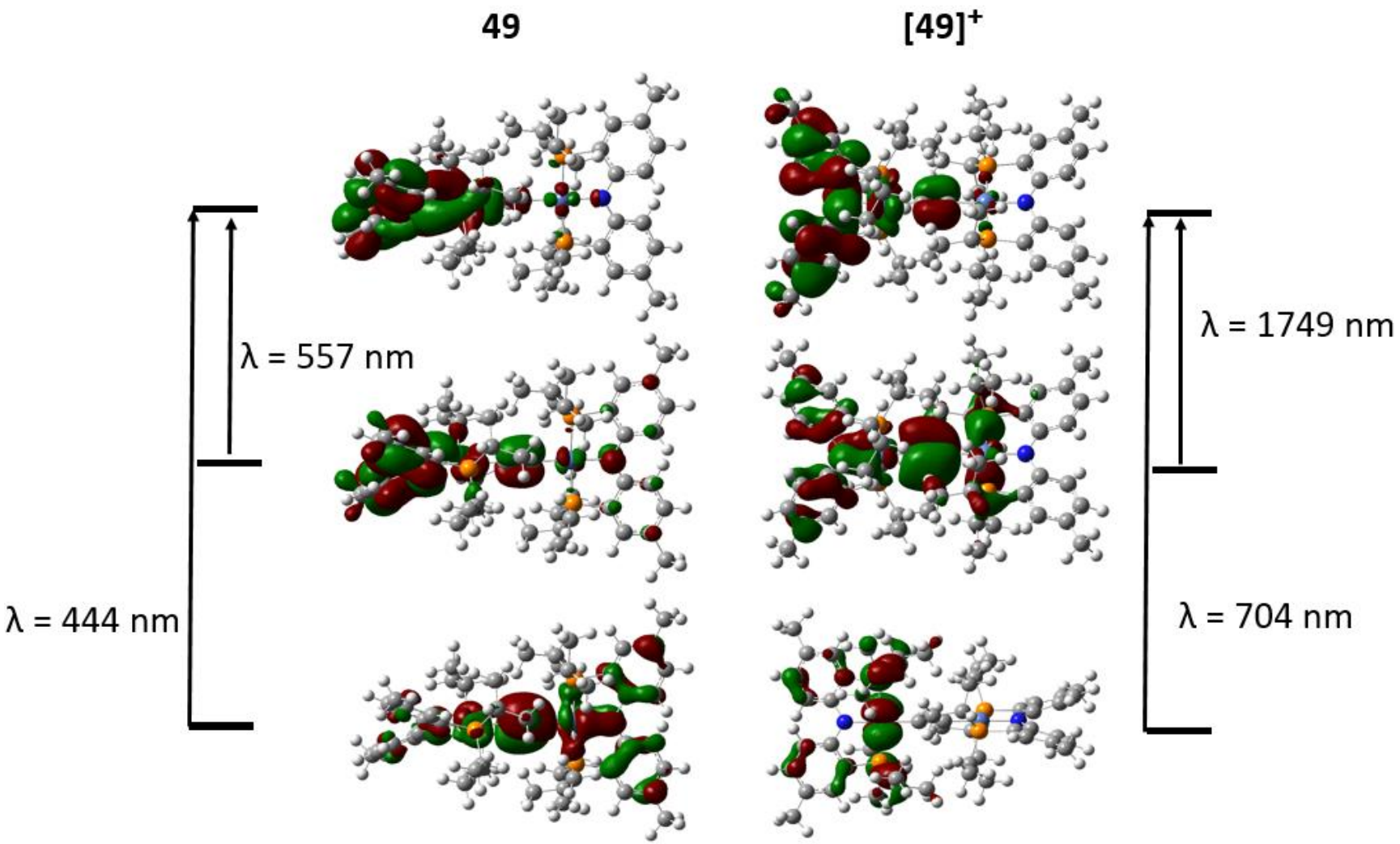

Figure II-21. MO diagrams of selected TD-DFT calculated transitions.

2.4.7 Solvent-Dependent NIR Absorption.

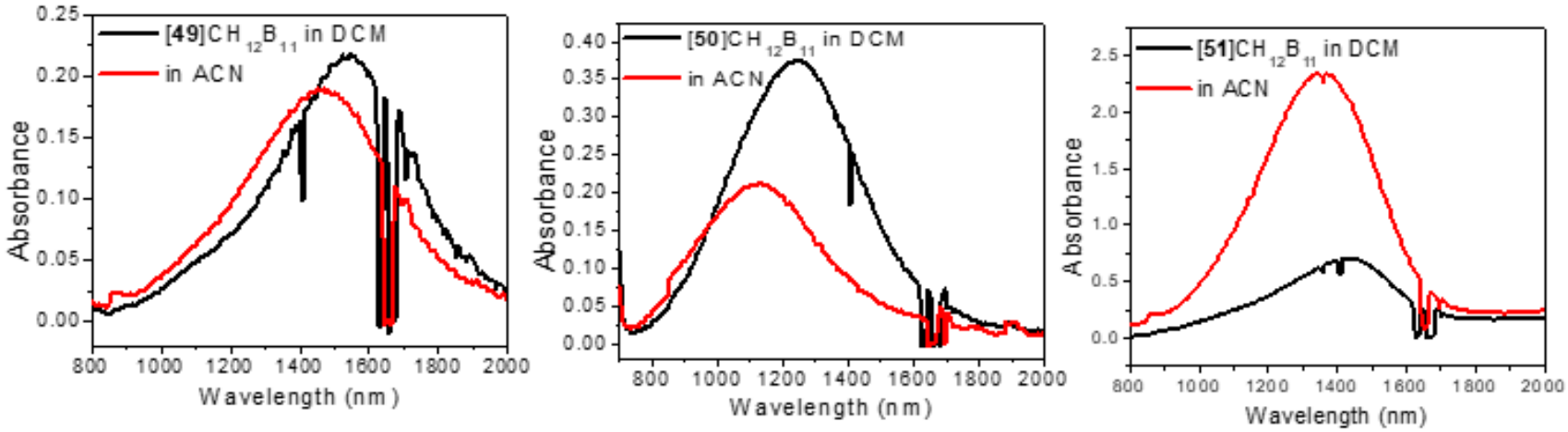

Figure II-22. NIR region spectra of [**49-51**]$CH_{12}B_{11}$ in dichloromethane (DCM) and acetonitrile (ACN) solution. Crude [**49-51**]$CH_{12}B_{11}$ were prepared by oxidizing complexes **49-51** with 0.9 equivalent of [Fc]$CH_{12}B_{11}$ in DCM. The ACN solutions were prepared by removing the volatiles in [**49-51**]$CH_{12}B_{11}$ DCM solution and re-dissolving with ACN.

Table I-11. Spectral data of [**49-51**]$^{+}$**.**

Complex	λ_{max} in DCM (nm)	$\tilde{\nu}_{max}$ in DCM (cm^{-1})	λ_{max} in ACN (nm)	$\tilde{\nu}_{max}$ in ACN (cm^{-1})	$\Delta\tilde{\nu}$(cm^{-1})
[49]$^{+}$	1540	6494	1460	6850	356
[50]$^{+}$	1245	8032	1120	8929	897
[51]$^{+}$	1420	7042	1355	7380	338

*2.4.8 IR Spectrum of Monocationic [**49**] and [**51**].*

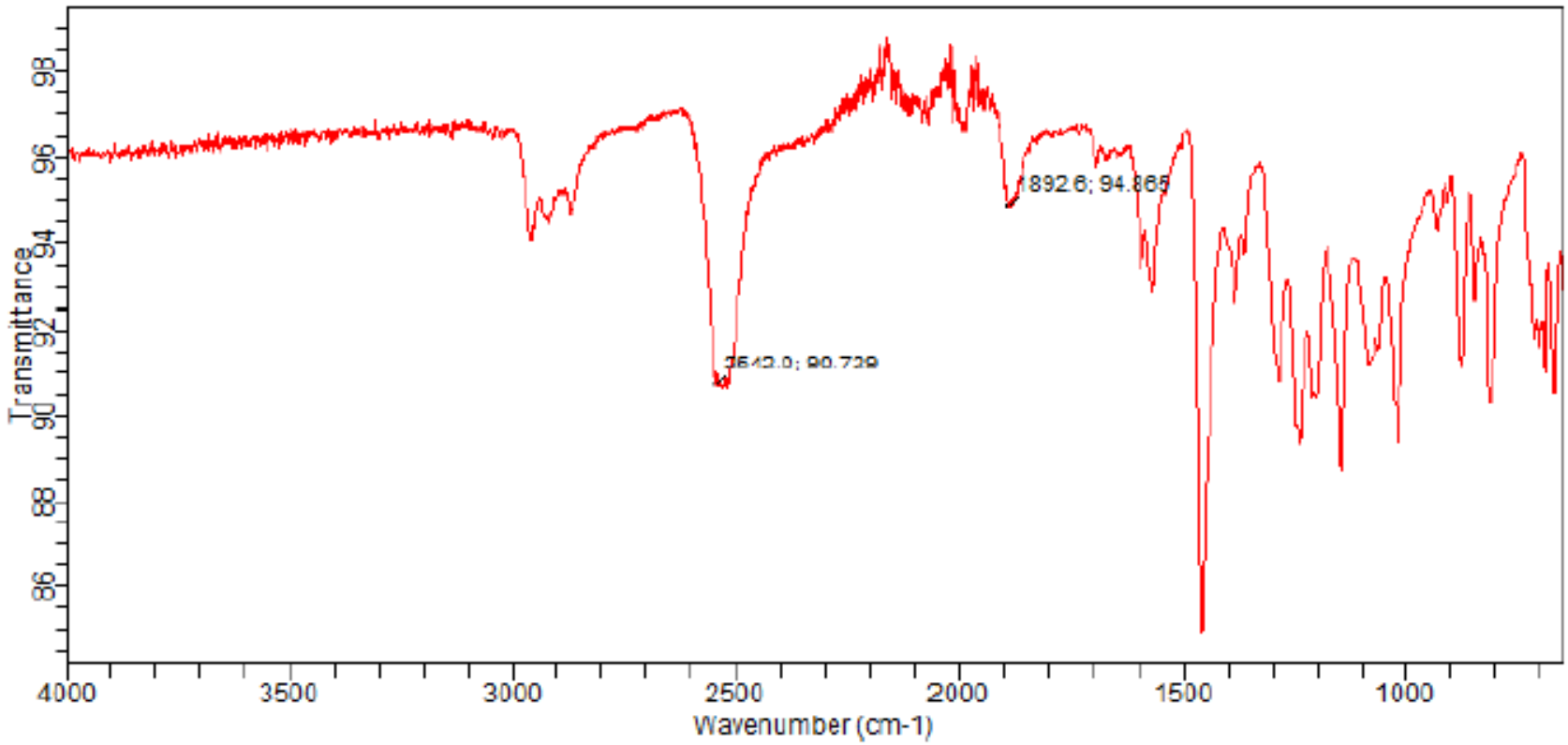

Figure II-23. ATR-IR spectrum (solid) of crude [**49**]$CH_{12}B_{11}$.

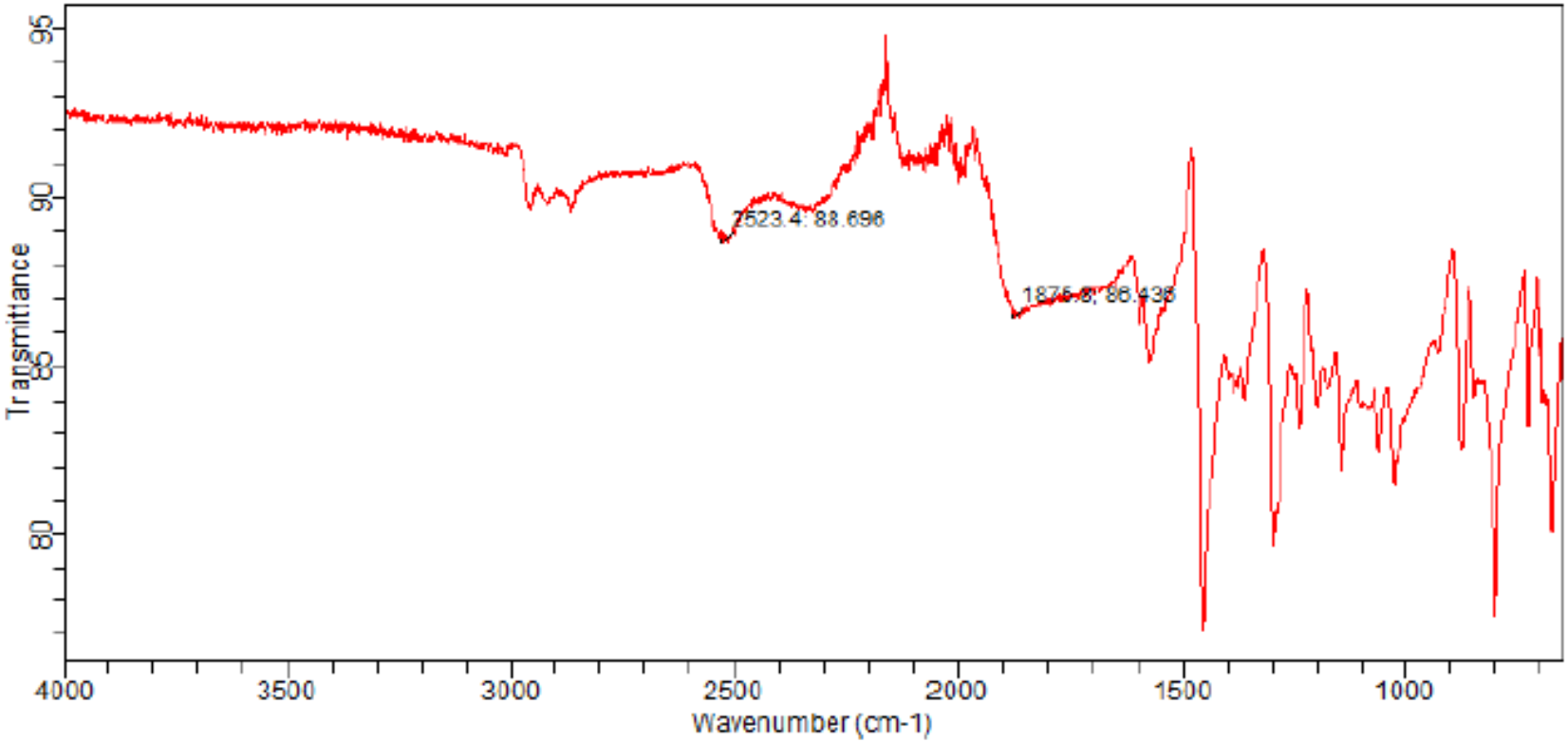

Figure II-24. ATR-IR spectrum (solid) of crude [**51**]$CH_{12}B_{11}$.

CHAPTER III

Palladium Bis(pincer) Complexes with Controlled Rigidity and Inter-Metal Distance*

3.1 Introduction

Arylamine derivatives are one of the most widely used structural components in the designs of organic functional materials for applications, such as electrochromic devices,[129,130] solar cells,[131,132] and light-emitting diodes.[133,134] Due to their electron-rich nature, arylamine derivatives can be readily oxidized into radical cations, whose persistence is dependent on the chemical environment and essential for the performance of organic electronic devices.[135,136] The electronic structures and properties of organic aminyl radical cations can be modulated by coordination with transition metals.[12] The inductive effect of the transition metal as a substituent, the geometric consequences of the incorporation of the organic fragment into the coordination sphere of the metal, and the π-interactions between the p-orbital on the nitrogen atom and a d_π orbital of the metal center may all play a role. As a result, incorporating transition metals drastically changes the optical and electronic properties of such an organic radical. Transition metal-decorated analogues serve as promising unconventional building blocks in the development of organic electronic materials because they may allow a range of properties not attainable with organic molecules alone.[81,82,137–139] In addition, amido donors have in particular attracted attention as redox-non-innocent auxiliaries in the design of oxidizable pincer (tridentate, meridional) ligands.[21,38,39,97,98,140–142] Redox-active ligands in transition metal complexes have typically been studied in the context of supplementing the reactivity of the metal center in catalysis and in novel

Reproduced in part from "Palladium Bis-Pincer Complexes with Controlled Rigidity and Inter-Metal Distance" submitted to *Chemical Science*. Synthesis of compound **72**, theoretical calculations, and the spectroelectrochemical experiment was done by Dr. Congzhi Zhu, Dr. Wei Hu and Xiaozhou Ji in Dr. Lei Fang's group and the EPR computational simulation was done by Dr. Haomiao Xie.

chemical transformations.[143–146] In a broader sense, we were interested in using coordination chemistry as a lynchpin to bring about new structures possessing extended conjugation in ligands, exotic redox activities, and synthetic potential for further connectivity.[147–149]

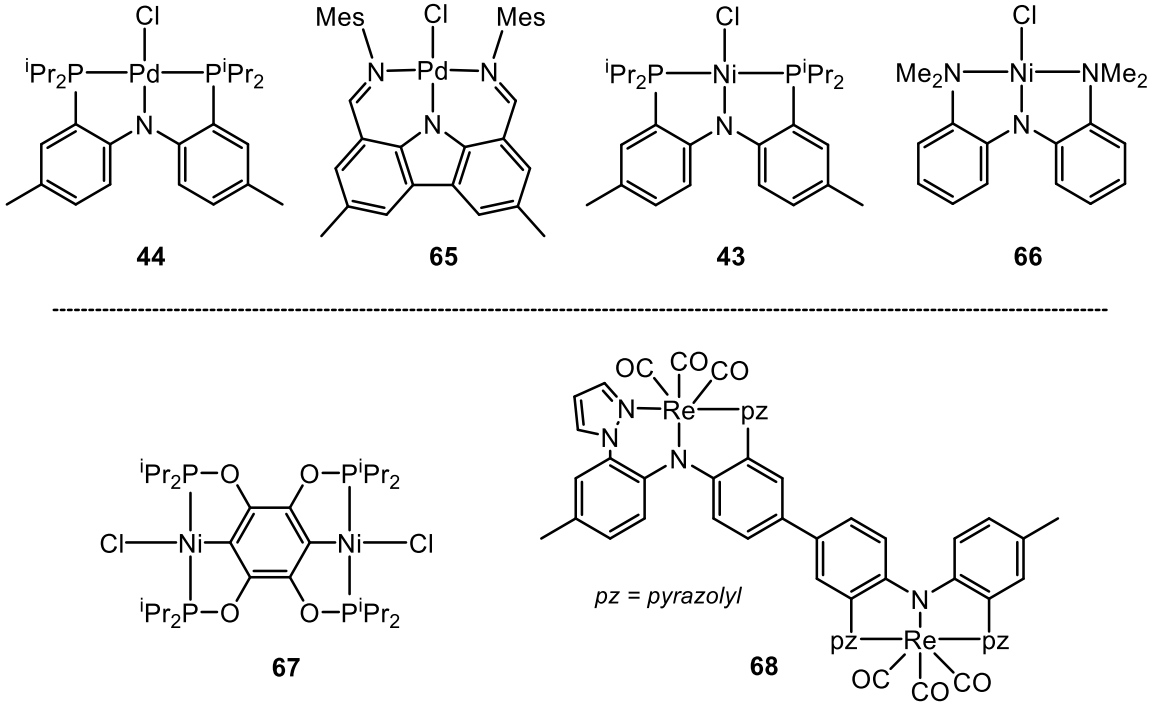

Figure III-1. Top: selected examples of diarylamido-centered pincer complexes, whose reversible redox properties have been studied previously. Bottom: recent examples of Janus pincers in the literature.

Complexes of diarylamido-centered pincer ligands with two neutral side donors are a particularly well-behaved set of examples of ligand-based of redox-activity (Figure III-1, top).[21,38,39,94,97,98] A broad synthetic variation of possible donor sets is possible, while maintaining reversibility of the oxidation and the apparent stability of the corresponding radical cation. The optical properties of these pincers in the complexes of group 10 metals (Ni, Pd, Pt) are strongly dependent on the identity of the transition metal, while the redox properties are affected by a change in the metal to only a modest degree because the oxidation primarily takes place at the ligand, with minimal electronic involvement of the metal.[21,38,97,98]

With this background in mind, we became interested in exploring molecules that combine multiple diarylamido-centered pincer-complex sites and in the electronic coupling possible between these different redox moieties. A few years ago, we explored bimetallic bis-(PNN)M complexes in which the two pincer cores were connected by a non-conjugating linker to a side arm donor.[92] More recently, we reported on the electronic communication in the bimetallic complexes where two (^{Me}PNP)M cores are connected by ynediyl linkers, i.e., via metal-ligand bonds.[150] In this work, we set out to explore bimetallic complexes where the two redox sites are connected via organic ligand-to-ligand linkers that modulate the degree of separation between the redox sites. We targeted the four systems depicted in Figure III-2. In this report, we present their syntheses and characterization of the degree of electronic coupling. Complexes **69** and **70** represent two (^{Me}PNP)M cores connected via the *para*-positions of the individual PNP ligands, either by an oxygen atom (**69**) or by a direct aryl-aryl bond (**70**). Complex 71 brings the two core PNP units even closer by means of them sharing one of the aromatic rings. Complex **72** is related to **71** in that the two pincer cores share a central ring substituted by two *para*-nitrogens, but **72** is based on an indolo[3,2-*b*]carbazole, a high-performance *p*-type organic semiconducting molecule.[151] Consequently, **72** possesses a rigid and planar ligand, with a more extended conjugation in the backbone. We utilized thiazole side donors in **72** instead of phosphines for reasons of synthetic feasibility and also to create a less electron-rich system vs PNP. This results in two (NNN)M cores which can be related to the mononuclear complex **65**.

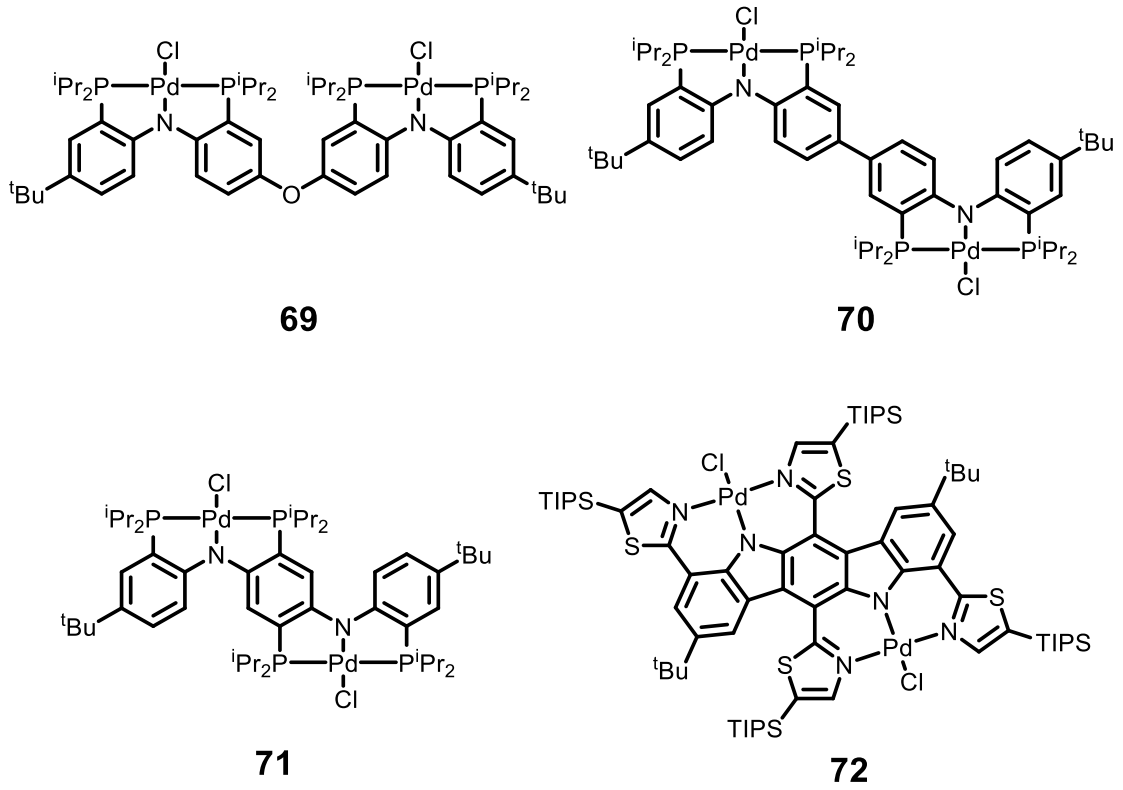

Figure III-2. Bis(pincer) complexes synthesized and studied in this work.

Complexes **69**-**72** are examples of the so-called Janus pincer systems, with two pincer cores on either end of the molecule "facing" in opposite directions. Janus pincer complexes have been studied previously, but the majority of reported systems are based on aryl-centered pincers[152–156] that are not intrinsically redox-active in a well-behaved, reversible fashion. The most recent example is the work by the Guan group on the Ni complexes of a Janus bis-POCOP ligand (**67**, Figure III-2, bottom).[157] Gardinier et al. studied a Re complex of Janus bis-NNN pincer (**68**, Figure III-2) that was built by connecting diarylamido cores similarly to **70**, although the fused analogues to **71** and **72** were not explored.[158] The bis-rhenium complex could be reversibly oxidized. However, the NNN ligand in Gardinier's compound adopted facial geometry about Re, thus not acting structurally as a pincer and disrupting potential conjugation with the lone pair at N,

especially in contrast to a system such as **72**. Thus, while Gardinier's pioneering example was instructive, we were motivated to explore complexes with enhanced planarity and chose a square-planar Pd center with a low-spin d^8 configuration. The use of a divalent metal with monoanionic pincer cores additionally offers an "extra" Pd-Cl coordination site. Although it was not attempted in this work, the Pd-Cl moiety offers potential for facile further functionalization, something that is not easily possible with a $Re(CO)_3$ terminus.

3.2 Results and discussion

3.2.1 Preparation of Bis(pincer) Pd Complexes

The syntheses of the bis-PNP pincer ligands and their Pd complexes were carried out as depicted in Scheme 1 and followed the general protocols we have previously established for the synthesis of mono-nuclear PNP ligands.[21,159,160] First, Buchwald-Hartwig coupling[161–163] was utilized to couple dibromoarenes **73-75** with two equiv. of *tert*-butylaniline to give the bis(diarylamines) **76-78** in good yields. Bromination of **76-78** with *N*-bromosuccinimide (NBS) in CH_2Cl_2 proceeded selectively to give good yields of the desired quadruply *ortho*-brominated compounds **79-81** under mild conditions. Except for the more electron-rich central benzene in **78**, each aromatic unit was brominated only once under these conditions. N-methylation of **79-81** was accomplished through deprotonation with NaH followed by treatment with methyl iodide, affording **82-84** in nearly quantitative yields.

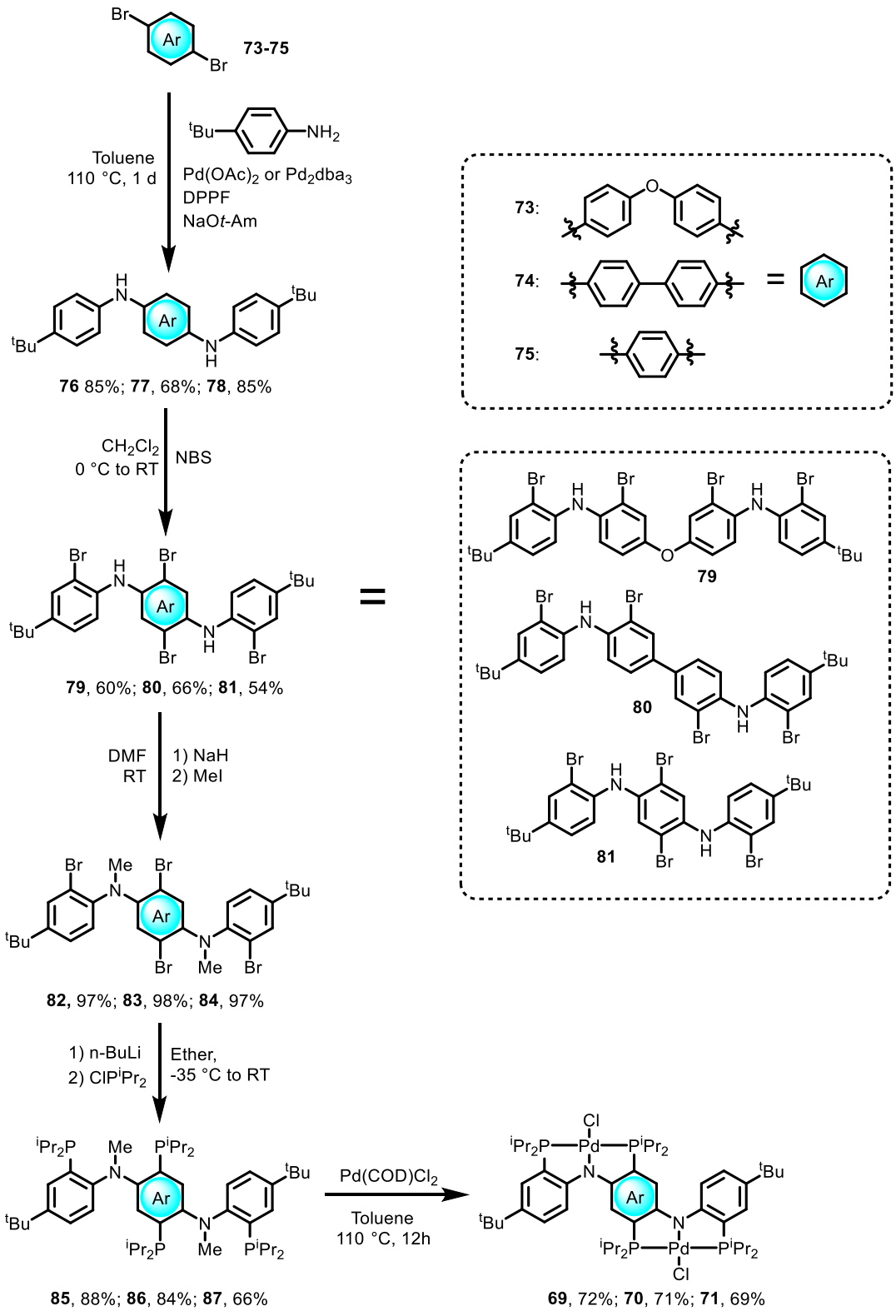

Scheme III-1. Synthesis of compound **60-71**.

Lithiation of **82-84** with ^{n}BuLi in diethyl ether followed by the addition of chlorodiisopropylphosphine led to the synthesis of **85-87**. Recrystallization from CH_2Cl_2/MeCN at -35 ºC afforded **69-71** in good isolated yields. We elected to pursue the syntheses of the N-methylated proto-pincers such as **85-87** as opposed to using **79-81** directly in the lithiation step for two reasons. Firstly, past work showed that the lithiation and the following phosphination of the mononuclear N-methylated brominated diarylamines proceeded cleanly and in many cases close to quantitatively, whereas the analogous lithiation/phosphination of the N-H versions typically did not.[21,159,160] The high selectivity towards the production of **85-87** was especially important because of the presence of the two pincer sites and because of the high lipohilicity and solubility of the products in organic solvents rendering any potential separation a challenge. Secondly, it was expected that the cleavage of methyl groups would proceed cleanly with Pd(II) reagents, as observed for the mononuclear PNP ligands with –P^{i}Pr$_2$ groups.[21,159] Indeed, this expectation was justified and thermolysis of **85-87** with (COD)$PdCl_2$ afforded isolated yields of the desired bis-Pd complexes **69-71** of around 70% after workup.

The ligands **85-87** and the dipalladium complexes **69-71** each possess two inequivalent phosphine sites, which can be thought of as the "outer" and the "inner" phosphines. This was reflected in the ^{31}P NMR spectra of these compounds, which displayed pairs of closely spaced, but inequivalent ^{31}P resonances in the ranges of chemical shifts that were similar to the known mono-PNP analogues. The coupling between the two ^{31}P sites was 10 Hz in **85-87**, but significantly increased to above 410 Hz in **69-71**. Large $^{2}J_{P\text{-}P}$ values are typical for two *trans*-disposed phosphines in a late transition metal coordination sphere. (Table III-1).

Table III-1. Selected ^{31}P NMR data for **69-71, 85-87** in C_6D_6.

	Ligand (δ ppm)	J_{P-P} (Hz)		Complex (δ ppm)	J_{P-P} (Hz)
85	-5.70, -5.90	10	**69**	49.45, 47.45	418
86	-5.74, -6.02	10	**70**	48.86, 48.83	N/A
87	-4.34, -6.54	10	**71**	49.49, 44.66	414

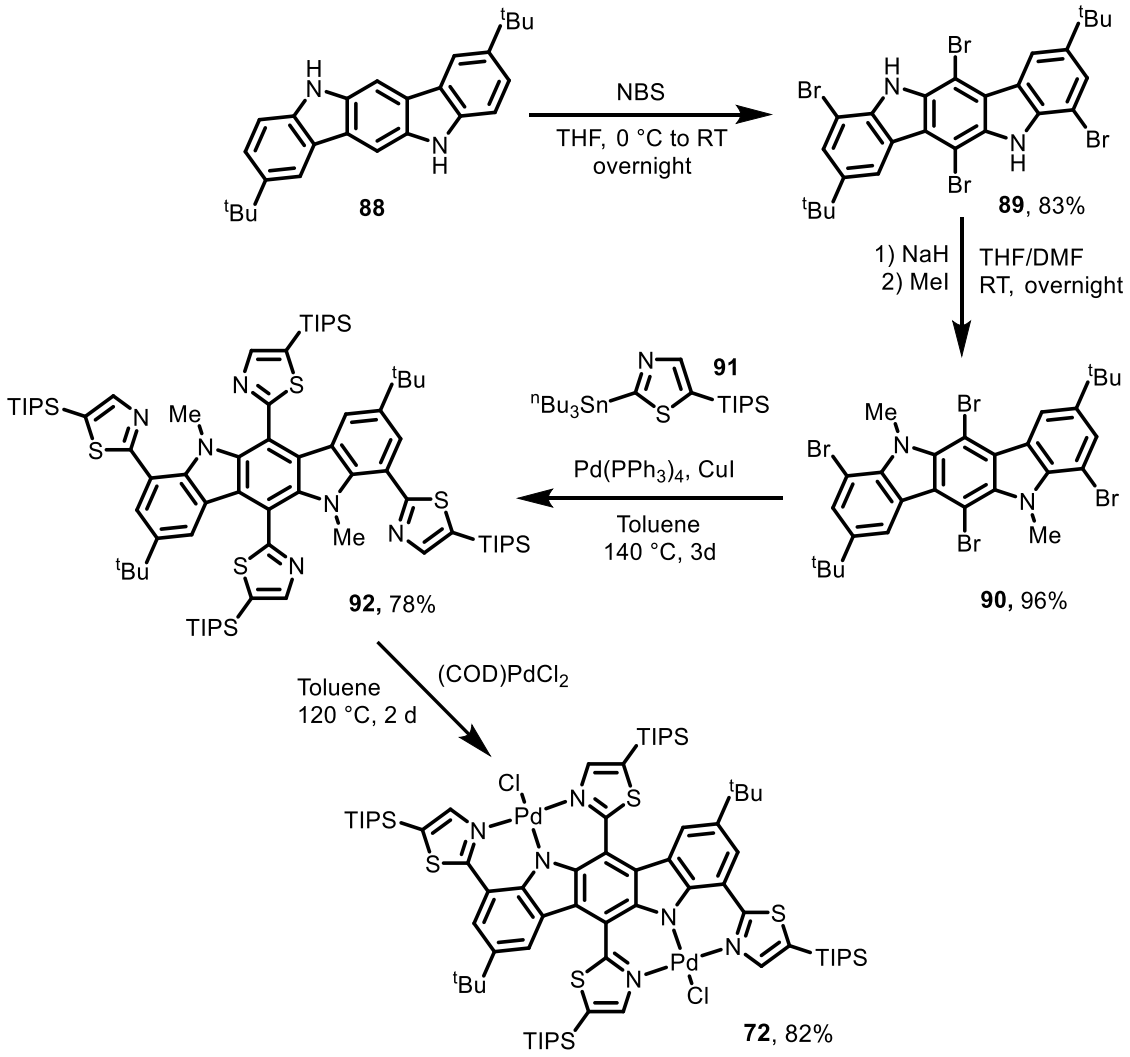

Scheme III-2. Synthesis of compound **72**.

Complex **72** was synthesized through a logically similar sequence (Scheme III-2). The indolo[3,2-*b*]carbazole precursor **88** with *tert*-butyl groups was prepared according to a reported procedure.[147] Bromination of **88** with NBS proceeded selectively for all the positions *ortho* to the amine moieties, resulting in **89** in an excellent yield. N-methylation of **89** progressed smoothly to give **90**. Stille coupling[164,165] with the thiazole unit **91** proceeded well at 130 °C, and gave **92** in a high yield. Triisopropylsilyl (TIPS) groups were pre-installed on **91** to endow the rigid and framework of **72** with high solubility. Gratifyingly, thermolysis of **91** with (COD)$PdCl_2$ did result in effective cleavage of the methyl groups,[94] and installation of two Pd(II) centers into the pincer clefts. The bimetallic complex **72** was air-stable under ambient conditions, and was purified by normal-phase silica gel chromatography.

3.2.2 Electrochemical Analysis

Cyclic voltammetry (CV) studies of complexes **69-72** were performed in CH_2Cl_2. The resulting CV plots are shown in Figure III-3 and the corresponding electrochemical parameters are summarized in Table III-2. All of the complexes **69-72** showed two quasi-reversible oxidation waves. The oxidation of complexes **69-71** can be compared with the oxidation of the analogous mononuclear (^{Me}PNP)PdCl complex **44**, which gives rise to a single quasi-reversible wave at -0.08 V vs the Fc/Fc^+ couple. As can be seen from Table III-2, the increasing proximity of the two redox sites in the **69-71** series leads to the ever more negative potential for the first oxidation and the greater potential difference (ΔE) between the first and the second oxidation potential. This is especially pronounced for compound **71**, which possesses a central *p*-diaminobenzene unit. Compound **72** is more difficult to oxidize relative to **69-71**, because of the presence of the electron-deficient (relative to phosphines) thiazole units and because a carbazole framework is generally

harder to oxidize than a diarylamido framework. Compound **72** can be compared with the (NNN)PdCl complex **65**, with its $E_{1/2}$ value of 0.69 V.[94] As was the case for **69-71** vs **44**, the first oxidation in **72** is considerably easier than in **65**.

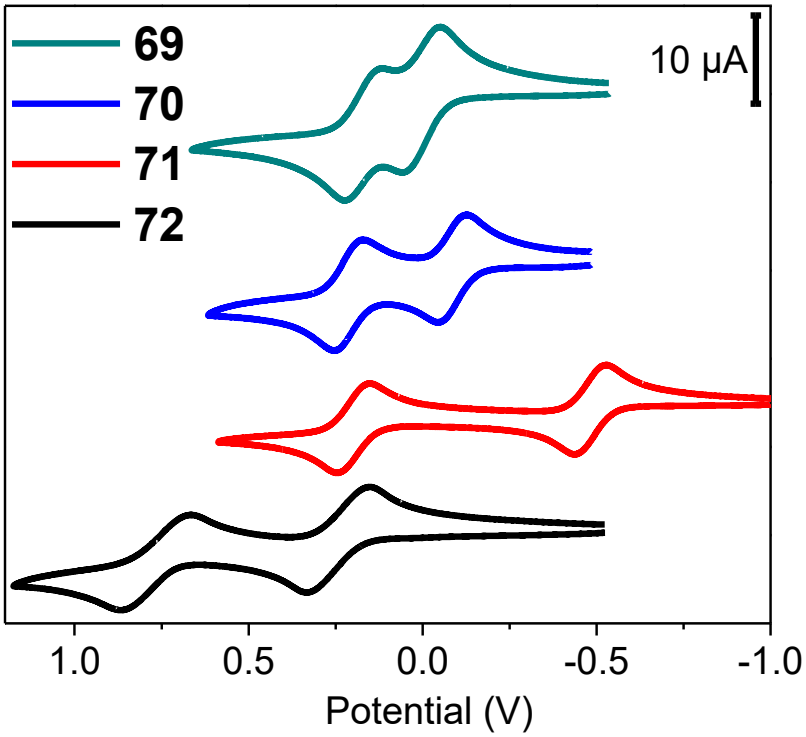

Figure III-3. Cyclic voltammograms of complexes **69-72** (ca. 0.001 M in CH_2Cl_2) with $^nBu_4NPF_6$ electrolyte (0.1 M), scan rate 100 mV/s, potentials referenced to Fc^+/Fc at 0 V.

Table III-2 Summary of oxidation potentials.

	$E^1_{1/2}$ (V)	$E^2_{1/2}$ (V)	ΔE (V)	Kc
69	-0.12	0.05	0.17	7.5×10^2
70	-0.22	0.08	0.30	1.2×10^5
71	-0.49	0.21	0.70	6.8×10^{11}
72	0.17	0.67	0.50	2.8×10^8

The ΔE values can be related to the comproportionation constant K_c.[72,107,108] These values are consistent with compounds **70, 71** and **72** belonging to the Robin-Day class III,[44,45] whereas the value for compound **69** falls into the range for class II. Considerable caution must be exercised when evaluating electronic communication based only on the ΔE values, as was amply discussed by Winter.[72] The smaller ΔE value for **72** compared against **71** was surprising at first.[166] One might have expected **72** to display a greater stabilization effect toward $\mathbf{72}^+$ because **72** contains a π-system that is more coplanar and extended. However, it is possible that the more extended conjugation in **72** results in significant electron delocalization over the organic conjugated ligand, whereas in **71**, the redox events are more "concentrated" in the central *p*-diaminobenzene unit. This view is supported by the results of the DFT calculations (*vide infra*).

3.2.3 Solid-State Structural Characterization

Single-crystal diffraction was used to establish solid-state structures of compounds **69** and **71**, as well the oxidized derivatives **[70][$CB_{11}H_{12}$]$_2$**, **[71]$CB_{11}H_{12}$**, and **[71][$SbCl_6$]$_2$**. Single crystals were obtained from solutions of **70** or **71** treated with an appropriate oxidant ($[Cp_2Fe]CB_{11}H_{12}$ or $[(p\text{-}BrC_6H_4)_3N]SbCl_6$), although the oxidized complexes were not isolated on the preparative scale. The structures of **69** and **71** (Figure III-4) confirmed the presence of two square-planar (^{Me}PNP)PdCl moieties in these molecules. The metrics associated with the coordination environment of Pd in **69** and **71** closely mimicked those in the previously reported mononuclear (^{Me}PNP)PdCl structure **44**.[89] Interestingly, the overall shape of the bis(pincer) unit was very similar in the structure of **71** and in its oxidized derivatives **[71]$CB_{11}H_{12}$** and **[71][$SbCl_6$]$_2$** (see Figures and). The geometric differences among these structures lie mainly in the changes in the bond distances associated with the central *p*-diaminobenzene unit (Table III-3). The XRD data do

not permit a finer analysis of the changes upon one-electron vs two-electron oxidation because of the relatively high esd values resulting from the solution of the structure of **[71]$CB_{11}H_{11}$**. Nonetheless, oxidation clearly leads to the adoption of a more quinoidal structure with substantial C-C bond length alternation within the central ring and the shortening of the N-C bond to the central ring. In contrast, the aromaticity of the outer rings, the Pd-P and the Pd-N bond lengths are not significantly affected. On the other hand, the C-N distance to the outer ring elongates upon oxidation. These metric data support the notion of the dominance of the conjugation with the inner ring upon oxidation of **71**, illustrated in Figure III-5 with the dominant quinoidal resonance structure for the doubly oxidized form of **71**.

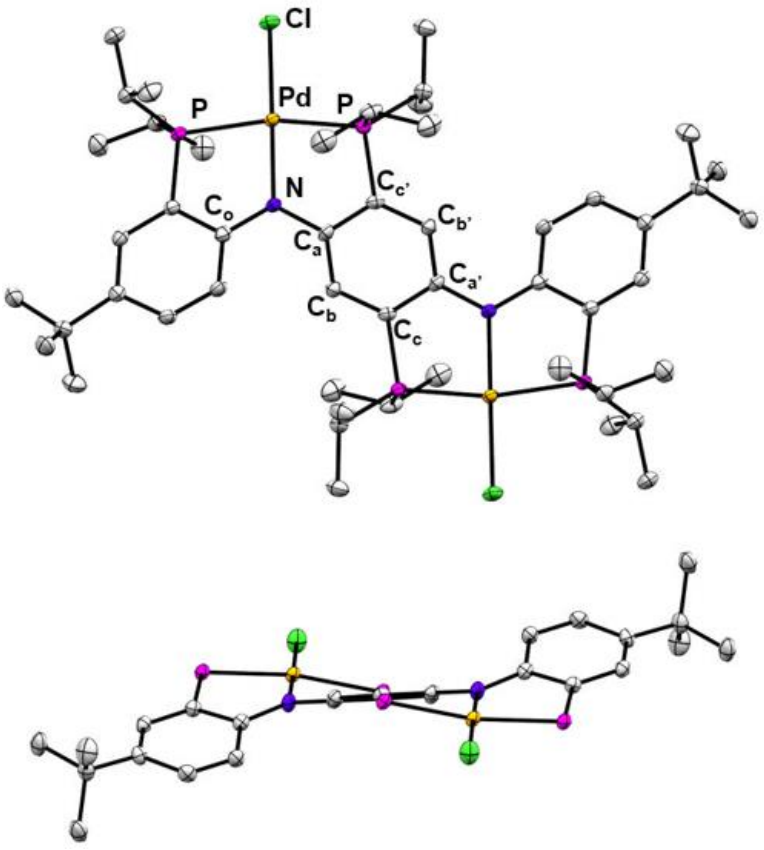

Figure III-4. ORTEP drawings depicting the structure of **71**. Displacement ellipsoids are shown at the 50% probability level and hydrogen atoms have been removed for clarity.

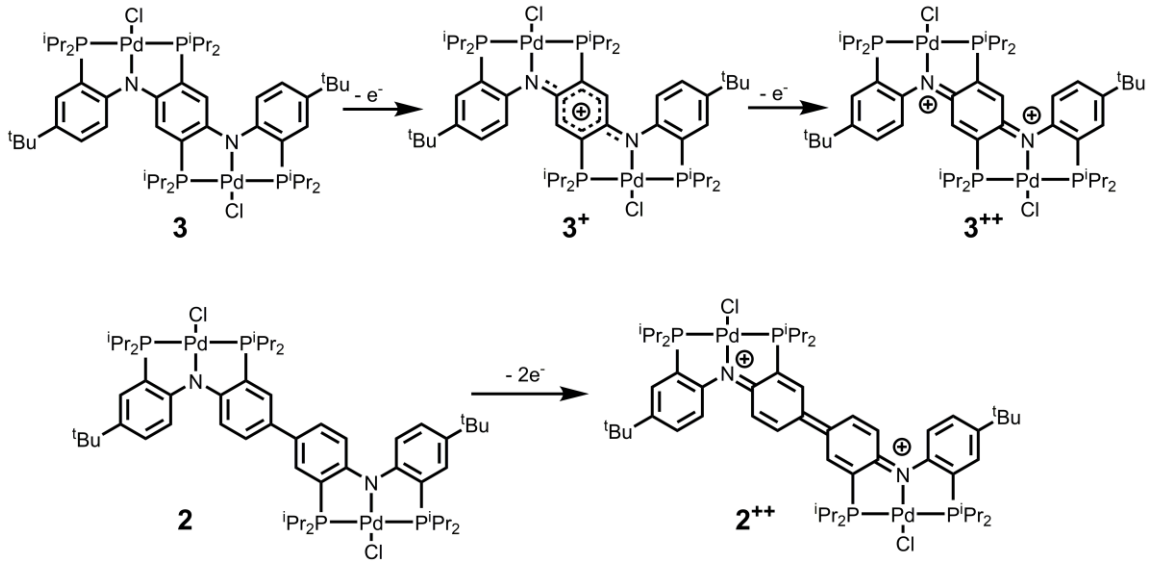

Figure III-5. Dominant resonance forms upon oxidation of **70** and **71**.

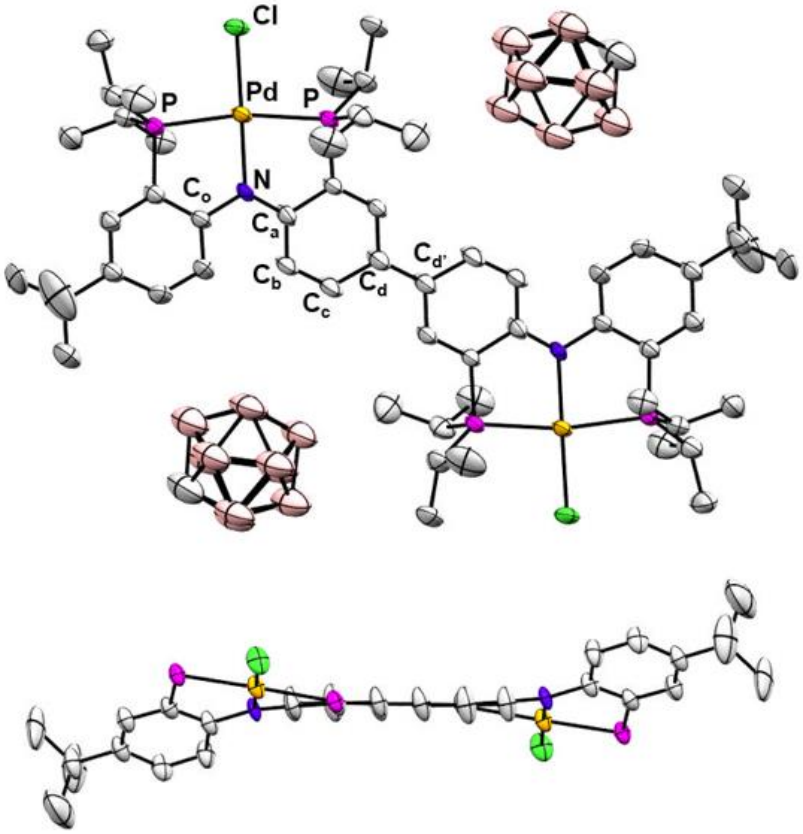

Figure III-6. ORTEP drawings depicting the structure of **[70][CB$_{11}$H$_{12}$]$_2$**. Displacement ellipsoids are shown at the 50% probability level and all hydrogen atoms have been removed for clarity.

Similar arguments can be applied to the structure of **[70][$CB_{11}H_{12}$]$_2$** (Figure III-6). The most striking features of the structure are the coplanarity of the two central aromatic rings and the distinct bond length alternation within the doubly oxidized central diaminobiphenyl unit. Figure III-5 depicts the dominant quinoidal resonance structure for the **70^{2+}** dication that dictates the coplanarity of the central rings.

Table III-3 Selected bond distances (Å) in **71, [71]$CB_{11}H_{12}$**, **[71][$SbCl_6$]$_2$** and **[70][$CB_{11}H_{12}$]** (see Figure III-7 for the numbering).

	71	**[71$^+$]**	**[71^{++}]**	**[70^{++}]^a**
Pd−N	2.0187(15)	2.024(9)	2.015(2)	2.027(5)
N−Ca	1.403(2)	1.350(17)	1.341(3)	1.339(7)
N−Co	1.383(2)	1.445(14)	1.419(3)	1.424(8)
Ca−Cb	1.403(3)	1.434(16)	1.441(4)	1.420(10)
Cb−Cc	1.397(3)	1.352(16)	1.360(4)	1.348(9)
Cc-Cd				1.44(1)
Cd-Cd’				1.430(9)

3.2.4 EPR Studies

Samples for the collection of EPR spectra (Figure III-8) were prepared via addition of 0.9 equiv of [(*p*-$BrC_6H_4)_3N$]$SbCl_6$ to the CH_2Cl_2 solutions of the neutral compounds **69-72**, thus generating the monooxidized derivatives in situ. The recorded *g* values are close to the value for the free electron (*g* = 2.00232), consistent with the primarily ligand-based nature of the unpaired electron. Meanwhile, the *g* value decreasing (and approaches the free electron value) in the order **69** > **70** ≈ **71** > **72** was observed.

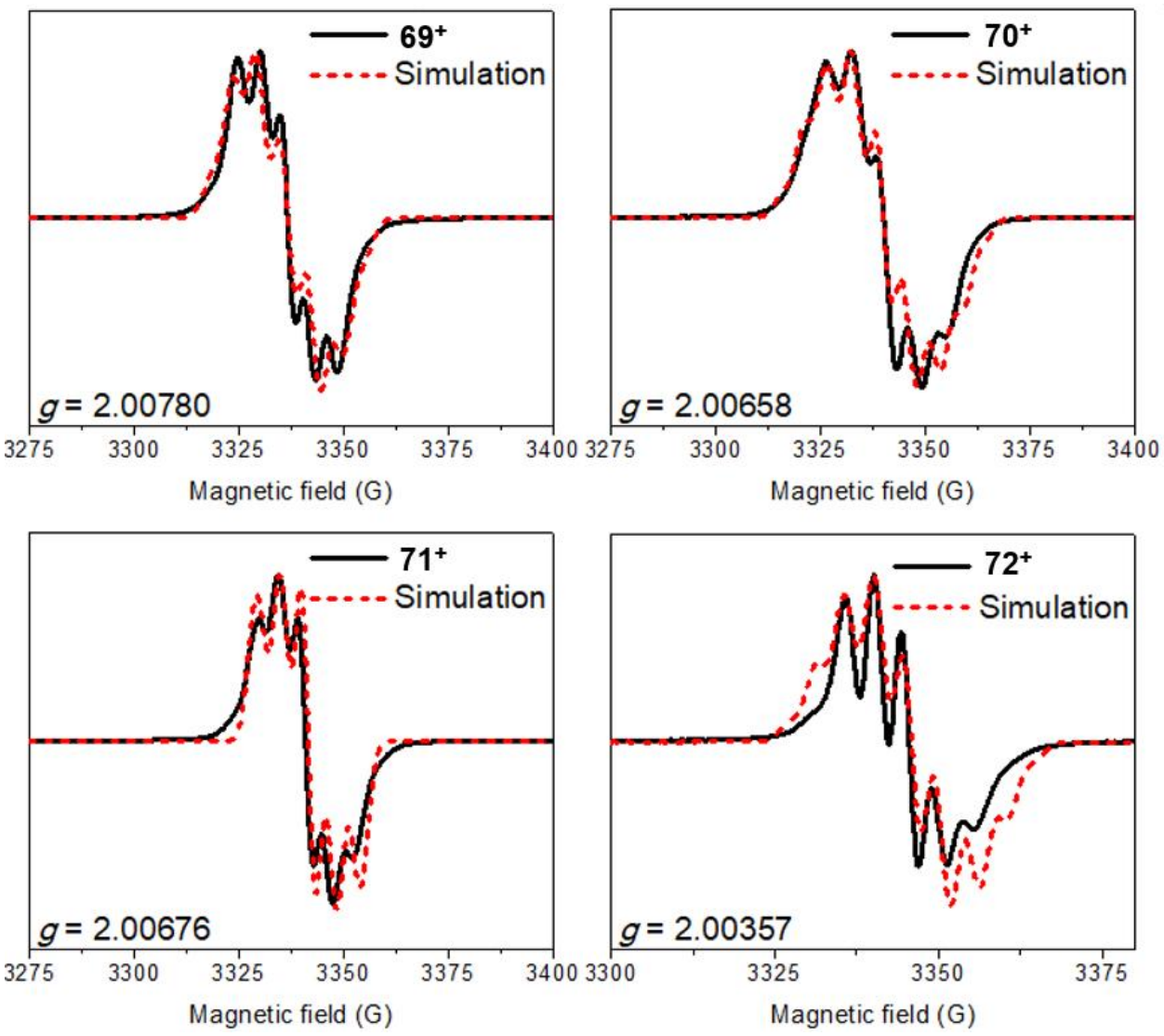

Figure III-7. X-band EPR spectra (in black) of monocations [**69-72**] (ca. 0.01 M in CH_2Cl_2) generated in situ by treating complexes **69-72** with 0.9 equiv. of $[(p\text{-}BrC_6H_4)_3N][SbCl_6]$. Instrumental parameters: T = 292 K; Freq = 9.38 GHz; Power = 0.6 mW, modulation 1 G. Simulations are shown in red (EasySpin).

Table III-4 Summary of simulated coupling constants (a) and line width (lw) (in G).

	a_N[a]	$a_{(P,H)}$[b]	$a_{(P,H)}$[b]	$a_{(P,H)}$[b]	$a_{(P,H)}$[b]	a_H[c]	a_H[c]
43$^+$	9.7	7.6	7.6	5.0	5.0	3.3	3.3
69$^+$	18.4	15.4	13.4	13.2	12.6		
70$^+$	18.6[d]	14.0	13.0	12.0	12.0		
71$^+$	14.5[d]	4.4	4.2	4.2	3.9		
72$^+$	27.8[d]					20.4[d]	20.2[d]

[a] Coupling constant to a $I = 1$ ^{14}N nucleus. [b] Coupling constant to an $I = ½$ nucleus (either ^{31}P or ^{1}H *ortho* to N_{amido}). [c] Coupling constant to an $I = ½$ nucleus assumed to be ^{1}H meta to N_{amido}. [d] Coupling to two nuclei.

EPR spectra were simulated using EasySpin[167] as the red dashed lines in Figure III-8, and the simulated coupling parameters are summarized in Table III-4. For complex **69**$^+$, the best fit involved coupling to one $I = 1$ nuclei (^{14}N), and as well as coupling to two kinds of $I = ½$ nuclei (^{1}H or ^{31}P, four each). Similarly to the 2008 study of the mononuclear analogue **43**$^+$, we interpret these coupling constants as arising from coupling to ^{31}P or *ortho*-^{1}H (attached to C2 and C8 in Figure III-7). For complex **70**$^+$ and **71**$^+$, the best fit required considering two $I = 1$ nuclei (^{14}N) with additional coupling to another set of four $I = ½$ nuclei. The resolution of the spectra does not permit further effective modeling to analyze hyperfine coupling in **70**$^+$ and **71**$^+$. The difference between a_N and the other coupling constants is largest in **71**$^+$. It could be the result of greater localization of the unpaired electron on the nitrogen sites.

Lastly, the spectrum of **72**$^+$ was fitted by considering coupling to two N nuclei and two pairs of H nuclei *meta*- to the nitrogens. Notably, the coupling constants observed in complex **72** are larger than in **69**-**71**. It could be a consequence of a structure that is more rigid, with enforced coplanarity

and enhanced π-orbital overlap, leading to the more effective delocalization of the unpaired electron.

3.2.5 Theoretical Studies

DFT calculations (Gaussian 09 at the M06/ LANL2DZp level)[168,169] were used to optimize the geometries of the neutral and monocationic complexes **69**-**72** to analyze their electronic structure. For the study of **72**, the $-Si^{i}Pr_3$ substituents on the thiazole rings were replaced with $-SiMe_3$, and the *tert*-butyl groups on the indolocarbazole were replaced with methyl groups for simplicity. The calculated geometries were generally in agreement with the results of the XRD structural determinations (*vide supra*). Figure III-9 illustrates the comparison between the frontier orbitals in **71** and **72** and their mono-oxidized derivatives. As expected, the HOMOs of both molecules and the corresponding SOMOs for the monocations are primarily ligand-based, with marginal contribution from a d_π orbital at Pd. This is consistent with the past investigations of the mononuclear diarylamido-based pincer complexes.[21,38,170] In both **71** and **72**, the HOMO and SOMO is most prominent in the central diaminobenzene ring. However, in the case **72**, there appears to be a greater degree of delocalization across the broader ligand π-system. The greater delocalization in **72** dovetails the observation of lesser ΔE values (vs **71**) in the electrochemical studies and possibly also the higher coupling constants observed in the EPR spectrum of $\mathbf{72}^+$ (*vide supra*). On the other hand, the LUMOs in compounds **71** and **72** were calculated to be of a different nature. In **71** (as well as **69** and **70**), the LUMO can be thought of as the antibonding orbital corresponding to the σ-bonding in the plane of the Pd coordination sphere with the central contribution from the d_{z2} orbital of Pd.[170] However, in **72**, the LUMO corresponds to a π* orbital of the organic ligand system. This is likely owing to the conjugation with the electron-deficient

thiazole, leading to the lower orbital energies of the π-system. Only the central pair of the thiazole rings contributes to the LUMO.

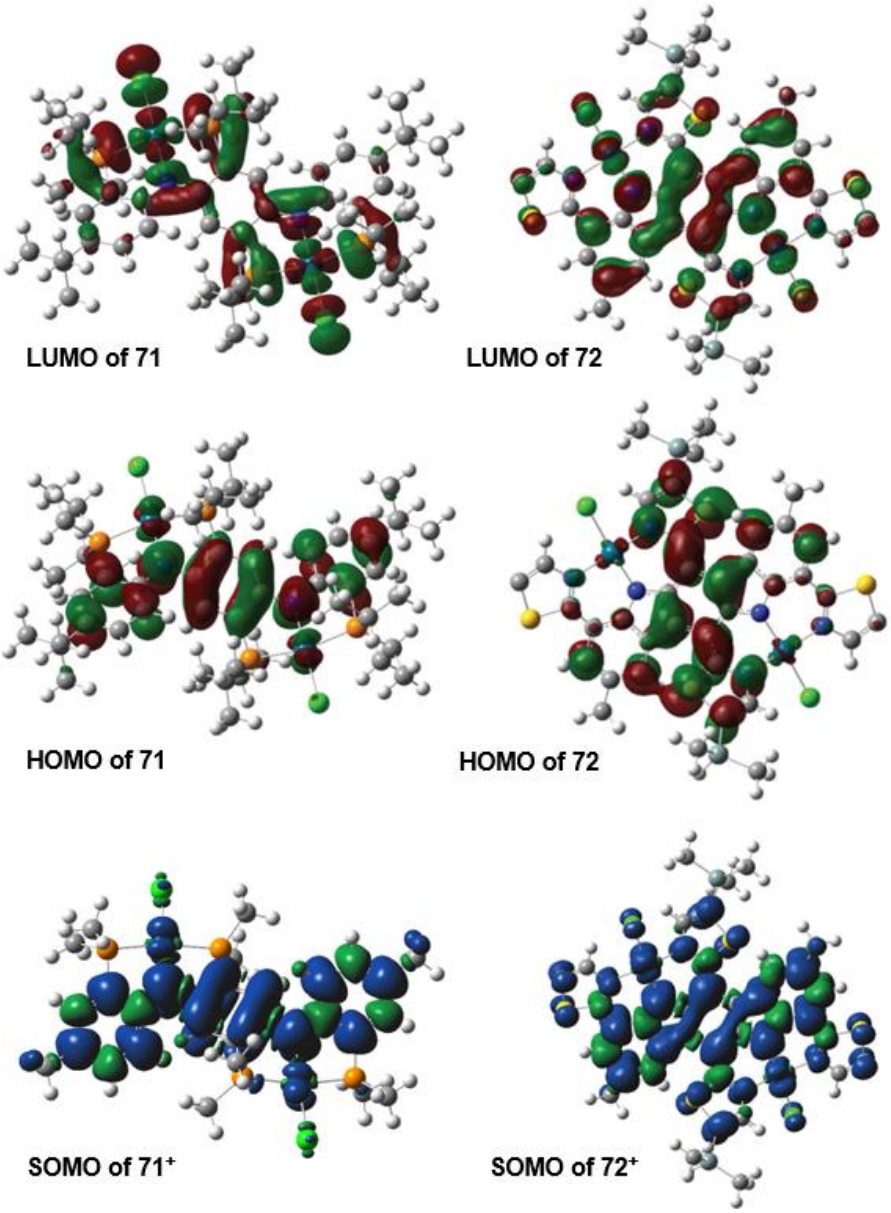

Figure III-8. Depictions of the calculated LUMO, HOMO and SOMO for **71**/**71**$^{+}$ (left) and **72**/**72**$^{+}$ (right) (isovalue = 0.02). The silyl groups on the outer thiazole rings of **72**/**72**$^{+}$ have been removed from the graphic for clarity.

3.2.6 UV-vis-NIR Spectroscopic Analysis

The UV-vis-NIR spectra of complexes **69-72** and of their mono-oxidized derivatives **69**$^+$-**72**$^+$ were collected in CH_2Cl_2 (Figure III-10). In the spectra of the neutral compounds **69-71**, the feature at ca. 500 nm appears at a wavelength similar to that observed in **44**. This is in concert with the similar colors of the compounds: like **44**, compounds **69** and **70** are red, while compound **71** is purple. On the other hand, compound **72** is green and consequently shows a maximum at a higher wavelength. These observations are consistent with the different nature of the LUMO for **72** vs **69-71**, as revealed by the DFT studies. The HOMO-LUMO transition in **69-71** can be viewed as LMCT, while in **72** it is a π-π* transition for the ligand system, corresponding to lower energy. Notably the metal-free ligands **85-87** are colorless and **92** is yellow. The apparent red shift of absorptions upon the introduction of the Pd center is related to a few factors. Pd is less electronegative than CH_3 and may be a modest π-donor towards the nitrogen which serves to raise the overall energy of the HOMO. For **69-71**, the introduction of the Pd center introduces a new, lower-energy, metal-based LUMO. In **72** the lowering of the LUMO energy is likely owing to the enforcement of the approximate coplanarity and thus improved conjugation of the electron-deficient thiazole units with the indolo[3,2-*b*]carbazole backbone.

The spectra of **69**$^+$-**72**$^+$ were recorded in order to provide insight in to the nature of the electronic coupling in the monocations. According to Hush theory,[45,46] a NIR-range intervalence charge-transfer (IVCT) absorption is expected for the sufficiently delocalized mixed-valence state. Complex **69**$^+$ showed no strong absorption in the NIR region, suggesting that the unpaired electron is largely localized in one of the pincer units and placing **69**$^+$ into the Robin-Day class I. [44,45] Complex **70**$^+$ had multiple intensive but broad peaks in NIR region. In the purely organic analogue **93**[71] and the rhenium complex **68** (Figure III-11), which have been assigned as class III mixed-

valence compounds, the Hush electron coupling integral $V = \nu_{max}/2$ are 3180 and 3715 cm^{-1}, respectively. In our case, *V* of complex $\mathbf{70}^{+}$ is 2924 cm^{-1}. Aside from the smaller *V,* **70** can be tentatively assigned as class III due to its electronic similarity and high K_c. Complex **71** and **72** are easier to assign since their *V* are 4799 and 3519 cm^{-1}, values that are squarely in the range of class III. Notably, the trend **71** > **72** > **70** > **69** suggested by the NIR absorption spectroscopy is consistent with the K_c measurement in electrochemistry.

Addition of the second equivalent of the oxidant $[(p\text{-}BrC_6H_4)_3N]SbCl_6$ permitted in-situ observation of $\mathbf{1}^{++}$, $\mathbf{2}^{++}$, and $\mathbf{3}^{++}$. The major absorption feature of $\mathbf{1}^{++}$ was similar to $\mathbf{1}^{+}$, as should be expected if its charges are largely isolated. On the other hand, the intense absorptions in the NIR region of $\mathbf{2}^{+}$ and $\mathbf{3}^{+}$ disappeared and no new NIR features such as in $\mathbf{C}^{+}$ and the dications of ethynyl-bridged PNP dimers were evident.[38,149] The domination quinoidal structures of $\mathbf{2}^{++}$ and $\mathbf{3}^{++}$ (Figure III-5) results in an electronic environment of ligand π* orbitals that is quite different from a radical species such as $\mathbf{C}^{+}$. On the other hand, the MLCT bands at around 600-700 nm increased in intensity upon second oxidation.

Treatment of **4** with $[(p\text{-}BrC_6H_4)_3N]SbCl_6$ did not lead to the clean formation of $\mathbf{4}^{++}$, consistent with the high 2nd oxidation potential determined for **4** in CV studies. Therefore, complex **4** was further studied using spectroelectrochemical measurements (Figure III-16). A series of optical spectra was collected after subjecting a solution of **4** containing $^{n}Bu_4NPF_6$ as the electrolyte to different constant voltages for 5 min. This experiment allowed the observation of the spectrum of $\mathbf{4}^{+}$ (matching that obtained by chemical oxidation, Figure III-8), and at higher potential, the spectrum of $\mathbf{4}^{++}$. The observed series of spectra displayed multiple isosbestic points, indicating quantitative oxidation processes and thus high stability of the oxidized cations.

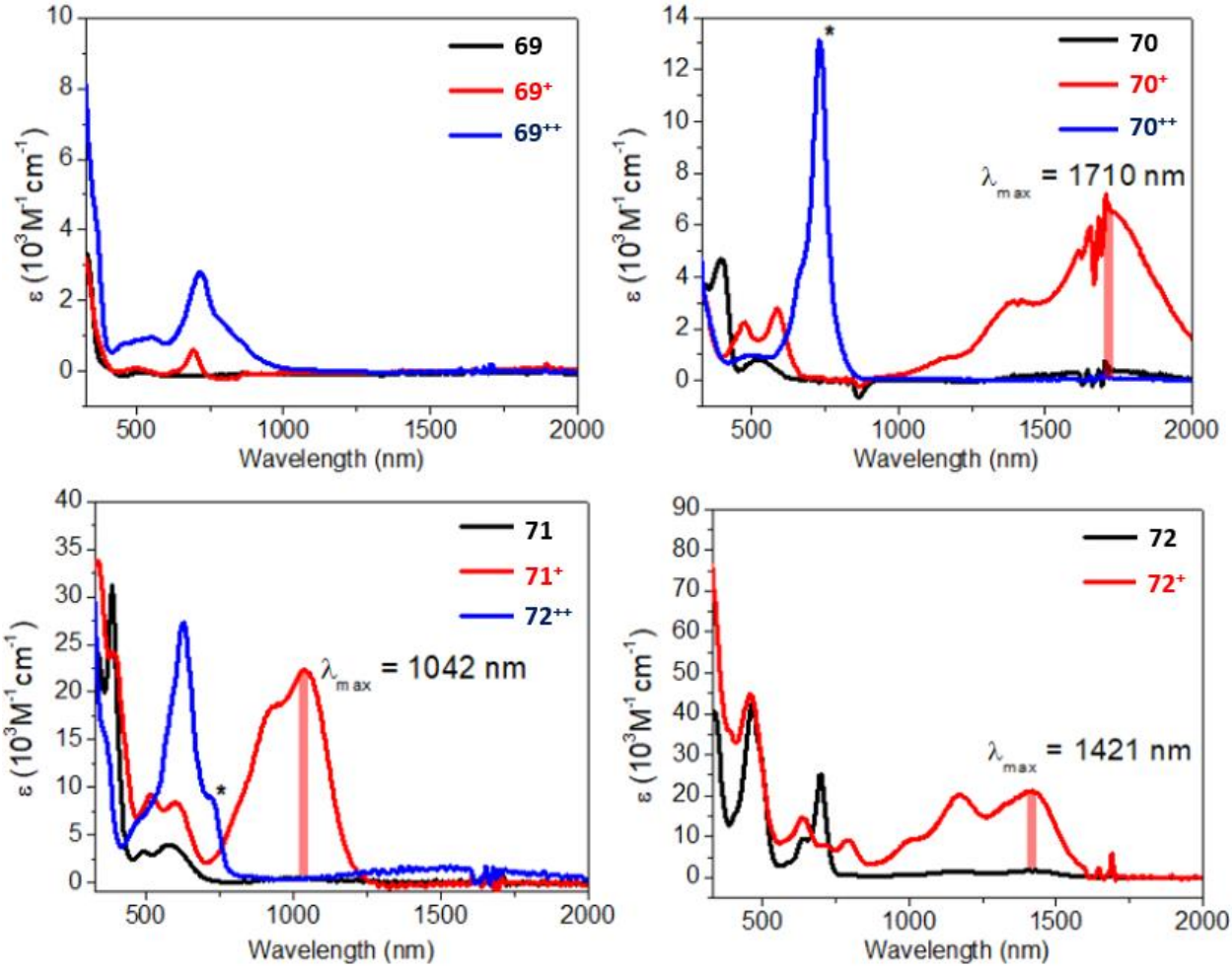

Figure III-9. UV-vis-NIR spectra of compounds **69**-**72** and their mono-oxidized derivatives **69**$^{+}$-**72**$^{+}$. The monocations were produced in situ via addition of 1 equiv. of oxidant ([Ox] = [*p*-(BrC_6H_4)$_3$N]$SbCl_6$) to solutions of **69**-**71** in CH_2Cl_2. The asterisk labeled the overlapping at 732 nm of **70**$^{+}$ and [*p*-(BrC_6H_4)$_3$N]$SbCl_6$.

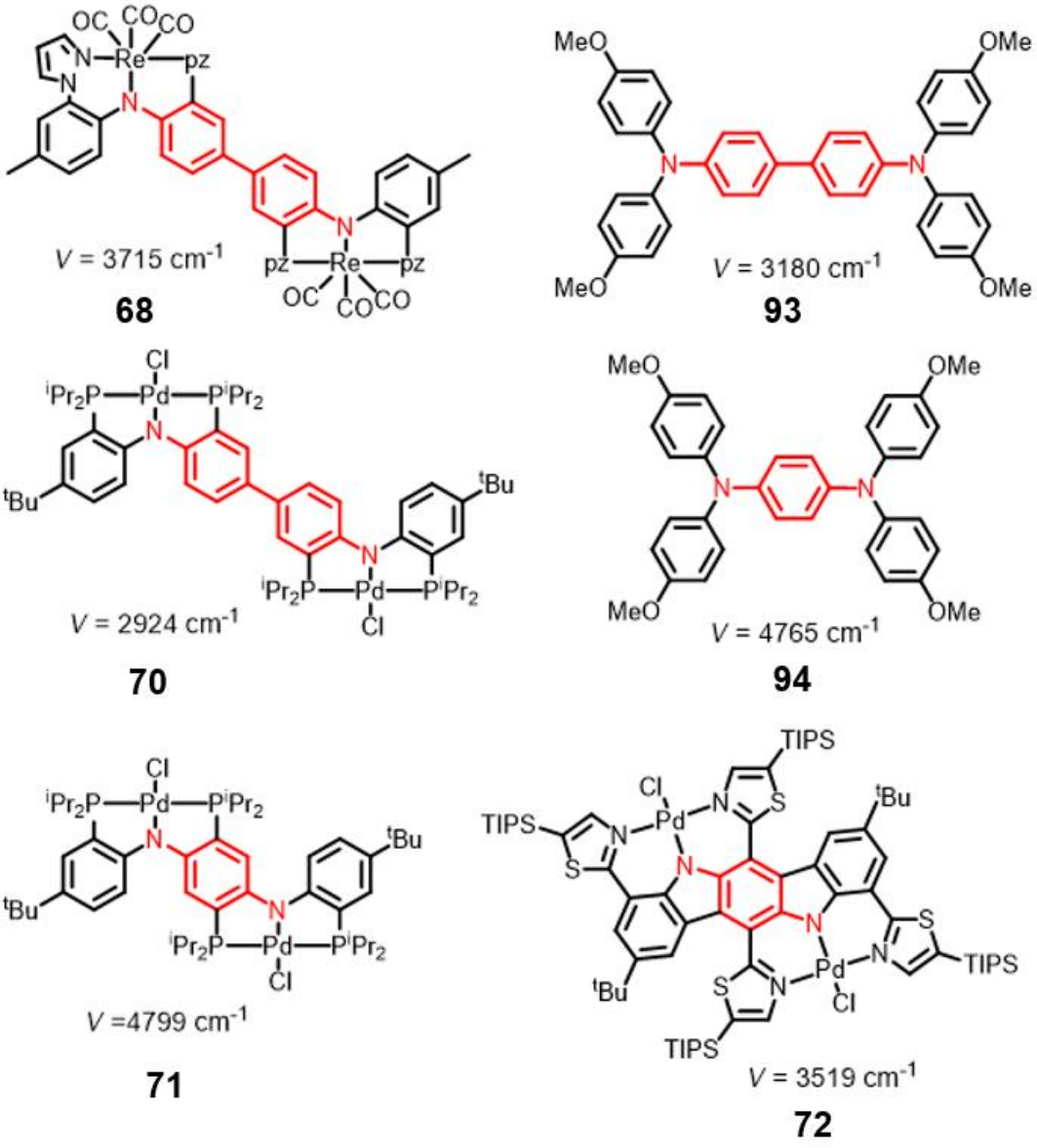

Figure III-10. Hush coupling constants comparison.

3.3 Conclusions

In summary, we described how novel, highly conjugated and delocalized systems with two reversible redox events can be obtained from the linkage or fusion of two pincer complexes into a single molecule. Analysis of the bis-palladium complexes by X-ray diffraction, cyclic voltammetry, UV-vis-NIR and EPR spectroscopies, as well as DFT calculations suggests that in

two or possibly three of the four systems, the mono-oxidized radical cation can be viewed as a highly delocalized mixed-valence state. The square-planar, divalent Pd center imposes a more rigid geometry on the organic ligand that leads to at least partial coplanarization of the aromatic rings of the extended system. The presence of the metal center is important in stabilizing the mono- and bis-oxidized forms of the molecule, even though the participation of metal d-orbitals in electronic delocalization is modest.

The greatest degree of electronic coupling was observed in the two fused bis(pincer) complexes built around a central *p*-diaminobenzene or an indolo[3,2-*b*]carbazole framework. The latter in particular contains an extended, flat and highly conjugated π-system that can be thought of as a fragment of a ladder metallapolymer. The bis(pincer) complexes studied in this work are potential building blocks for more complex conjugated molecules and potentially polymers. These complexes possess two Pd-Cl functionalities that should allow for straightforward synthetic modification in further studies.

3.4 Experimental details

3.4.1 General Considerations

Glovebox or standard Schlenk line operations were performed under argon or dinitrogen. Toluene, diethyl ether, pentane, tetrahydrofuran (THF) and isooctane were dried and deoxygenated (by purging) using a solvent purification system (Innovative Technology Pure Solv MD-5 Solvent Purification System) and stored over molecular sieves in an Ar-filled glovebox. For the synthesis of complex 72, diethyl ether was dried over Na/K, and distilled under nitrogen before usage. THF was dried over Na, and distilled under nitrogen before usage. C_6D_6 was dried over NaK/Ph_2CO/18-crown-6, distilled or vacuum transferred and stored over molecular sieves in an Ar-filled glovebox.

CH_2Cl_2, $CDCl_3$, and CD_2Cl_2 were dried over CaH_2, distilled or vacuum transferred and stored over molecular sieves in an Ar-filled glovebox. 2,8-di-*tert*-butyl-5,11-dihydroindolo[3,2-b]carbazole (**88**) and 2-bromo-5-(triisopropylsilyl)thiazole (**93**) were synthesized according to a modified procedure from the literature.[1,2] Ferrocenium carba-*closo*-dodecaborate $[Fc][CH_{12}B_{11}]$ was synthesized by the procedure from the literature.[3] All other chemicals were used as received from commercial vendors.

3.4.2 Physical Methods

NMR spectra were recorded on a Varian Inova 300, Mercury 300 (^{1}H NMR, 299.952 MHz; ^{13}C NMR, 75.421 MHz; ^{31}P NMR, 121.422 MHz), Bruker 400 (^{1}H NMR, 399.535 MHz; ^{13}C NMR, 100.582 MHz; ^{31}P NMR, 161.734 MHz) and Varian Inova 500 (^{1}H NMR, 499.703 MHz; ^{13}C NMR, 125.697 MHz; ^{31}P NMR, 202.265 MHz) spectrometer. Chemical shifts are reported in δ (ppm). For ^{1}H and ^{13}C NMR spectra, the residual solvent peak was used as an internal reference (^{1}H NMR: δ 7.16 for C_6D_6, 7.26 for $CDCl_3$; ^{13}C NMR: δ 128.06 for C_6D_6, 77.23 for $CDCl_3$). ^{31}P NMR spectra were referenced externally with 85% phosphoric acid at δ 0. UV-vis-NIR spectra were collected on a Hitachi U-4100 UV-vis-NIR spectrophotometer. Electron paramagnetic resonance spectra were recorded in a continuous wave X-band EleXsys EPR spectrometer at 288 K. Electrochemical studies were carried out using a CH Instruments Model 700 D Series Electrochemical Analyzer and Workstation in conjunction with a three electrode cell. The working electrode was a CHI 104 glassy carbon disk with a 3.0 mm diameter and the auxiliary electrode was composed of platinum wire. The third electrode, the reference electrode, was an $Ag/AgNO_3$ electrode. This was prepared as a bulk solution composed of 0.01 M $AgNO_3$ and 0.1 M $^nBu_4NPF_6$ in dichloromethane. This was separated from solution by a fine porosity frit. CVs were conducted

in dichloromethane with 0.1 M $^{n}Bu_4NPF_6$ as the general supporting electrolyte if not specifically mentioned and were reported with a scan rate of 100 mV/s. The concentration of the analyte solutions were approximately 1.00×10^{-3} M. CVs were referenced to $Fe(\eta^5\text{-}Cp)_2$/ $Fe(\eta^5\text{-}Cp)^+$ redox couple. ACPI-MS and ESI-MS data were performed by Texas A&M University Chemistry Mass Spectrometry Laboratory. Preparative GPC was performed in chloroform solution at room temperature, using a JAI recycling preparative HPLC (LC-92XXII NEXT SERIES) through a JAIGEL-2H-40 column. Column chromatography was carried out using Biotage® IsoleraTM Prime instrument with various size of SiO_2 Biotage ZIP® cartridge. Elemental analyses were performed by CALI Labs, Inc. (Highland Park, NJ).

3.4.3 *Synthesis and Characterization*

4,4'-oxybis(*N*-(4-(*tert*-butyl)phenyl)aniline) (76). 4,4'-Dibromodiphenyl ether (**73**, 5.0 g, 15.2 mmol) and *tert*-butylaniline (6.8 g, 45.7 mmol) were mixed with 300 mL of toluene in a 1 L flask. In another vial, $Pd_2(dba)_3$ (70 mg, 0.076 mmol) and 1,1'-bis(diphenylphosphino)ferrocene (DPPF, 126 mg, 0.228 mmol) were pre-mixed with 20 mL toluene. Then the yellow suspension solution was combined to the flask. Sodium *tert*-pentoxide (5.0 g, 45.6 mmol) was added into the flask and the solution immediately turned red. The reaction mixture was heated to reflux for two days. After completion, the solution was directly poured into a separation funnel and extracted with water, diluted $HCl_{(aq)}$, and $NaHCO_{3(aq)}$. The organic layer was collected and dried with $Na_2SO_{4(s)}$. The solution was then filtered through a plug of silica gel. The filtrate was pumped down under vacuum, re-dissolved in CH_2Cl_2, layered with ethanol and put into a -35 ºC freezer for one day. The supernatant was decanted and the solid was dried under vacuum to yield light yellow powder (6.0 g, 85%). ^{1}H NMR (400 MHz, C_6D_6): δ 7.21 (d, $J_{H\text{-}H}$ = 8 Hz, 2H, Ar-*H*), 6.98 (d, $J_{H\text{-}H}$ = 8 Hz,

2H, Ar-*H*), 6.86 (d, $J_{H\text{-}H}$ = 8 Hz, 2H, Ar-*H*), 6.82 (d, $J_{H\text{-}H}$ = 8 Hz, 2H, Ar-*H*), 4.98 (s, 1H, N-*H*), 1.27 (s, 9H, C*Me*$_3$).^{13}C{^{1}H} NMR (101 MHz, C_6D_6): δ. 152.6 (s, Ar-*C*), 143.4 (s, Ar-*C*), 141.9 (s, Ar-*C*), 139.4 (s, Ar-*C*), 126.4 (s, Ar-*C*), 120.0 (s, Ar-*C*), 119.9 (s, Ar-*C*), 117.6 (s, Ar-*C*), 34.2 (s, *C*Me$_3$), 31.7 (s, C*Me*$_3$). ESI-MS: m/z $[M+H]^+$ Calcd. For $C_{32}H_{36}N_2O$: 464.2900; Found: 465.2894.

4,4'-oxybis(2-bromo-*N*-(2-bromo-4-(*tert*-butyl)phenyl)aniline) (79). 76 (1.0 g, 2.15 mmol) was dissolved in 100 mL of dried, degassed CH_2Cl_2 under argon atmosphere. N-bromosuccinimide (NBS, 1.53 g, 8.61 mmol) was added in 4 portions during 4 h. Three hours after the addition of the final portion, the volatiles were removed under vacuum. The residue was then re-dissolved in 1:1 hexanes/toluene and carefully passed through a plug of silica gel collecting only the light-colored portion. The volatiles were removed from the filtrate under vacuum, the residue was re-dissolved in CH_2Cl_2, layered with ethanol and put into a -35 ºC freezer for one day. The supernatant was decanted and the solid was dried under vacuum to yield light-yellow powder (1.0 g, 60%). ^{1}H NMR (400 MHz, C_6D_6): δ 7.63 (d, $J_{H\text{-}H}$ = 4 Hz, 1H, Ar-*H*), 7.28 (d, $J_{H\text{-}H}$ = 4 Hz, 1H, Ar-*H*), 7.00-6.92 (m, 3H, Ar-*H*), 6.67 (dd, $J_{H\text{-}H}$ = 8 Hz, 4 Hz, 1H, Ar-*H*), 6.37 (s, 1H, N-*H*), 1.12 (s, 9H, C*Me*$_3$).^{13}C{^{1}H} NMR (101 MHz, C_6D_6): δ. 152.3 (s, Ar-*C*), 146.0 (s, Ar-*C*), 138.5 (s, Ar-*C*), 136.9 (s, Ar-*C*), 130.4 (s, Ar-*C*), 125.54 (s, Ar-*C*), 123.7 (s, Ar-*C*), 120.0 (s, Ar-*C*), 118.9 (s, Ar-*C*), 117.9 (s, Ar-*C*), 115.6 (s, Ar-*C*), 114.5 (s, Ar-*C*), 34.2 (s, *C*Me$_3$), 31.3 (s, C*Me*$_3$). ESI-MS: m/z $[M+H]^+$ Calcd. For $C_{32}H_{32}Br_4N_2O$: 780.9280; Found: 780.9275.

4,4'-oxybis(2-bromo-*N*-(2-bromo-4-(*tert*-butyl)phenyl)-*N*-methylaniline) (82). 79 (1.0 g, 1.28 mmol) was dissolved in 50 mL of dried, degassed DMF under argon atmosphere. NaH (94 mg, 3.84 mmol) was added slowly. After 10 min, methyl iodide (MeI, 545 mg, 3.84 mmol) was added

and the solution was stirred overnight. After completion, the solution was poured into a separation funnel and extracted with water and $NaCl_{(aq)}$. The organic layer was collected and dried with $Na_2SO_{4(s)}$. The solution was then filtered through a plug of silica gel and the volatiles were removed from the filtrate under vacuum to yield a white powder (1.0 g, 97%). ^{1}H NMR (400 MHz, C_6D_6): δ 7.70 (d, $J_{H\text{-}H}$ = 4 Hz, 1H, Ar-*H*), 7.36 (d, $J_{H\text{-}H}$ = 4 Hz, 1H, Ar-*H*), 7.08 (dd, $J_{H\text{-}H}$ = 8 Hz, 4 Hz, 1H, Ar-*H*), 6.77 (d, $J_{H\text{-}H}$ = 8 Hz, 1H, Ar-*H*), 6.67 (dd, $J_{H\text{-}H}$ = 8 Hz, 4 Hz, 1H, Ar-*H*), 6.61 (d, $J_{H\text{-}H}$ = 8 Hz, 1H, Ar-*H*), 2.93 (s, 3H, N-*Me*), 1.11 (s, 9H, C*Me*$_3$).^{13}C{^{1}H} NMR (101 MHz, C_6D_6): δ. 153.8 (s, Ar-*C*), 148.0 (s, Ar-*C*), 146.5 (s, Ar-*C*), 145.3 (s, Ar-*C*), 131.8 (s, Ar-*C*), 125.3 (s, Ar-*C*), 125.3 (s, Ar-*C*), 124.9 (s, Ar-*C*), 123.2 (s, Ar-*C*), 122.0 (s, Ar-*C*), 120.3 (s, Ar-*C*), 118.5 (s, Ar-*C*), 41.5 (s, N-*Me*), 34.2 (s, *C*Me$_3$), 31.3 (s, C*Me*$_3$). ESI-MS: m/z $[M+H]^+$ Calcd. For $C_{34}H_{36}Br_4N_2O$: 808.9593; Found: 808.9586.

^{tBu}PNPOPNP (85). In a glovebox, **82** (1.0 g, 1.04 mmol) was dissolved in 50 mL of dried, degassed ether in a Schlenk flask and cooled to -35 ºC. *n*BuLi (1.83 mL, 4.58 mmol) was added slowly by syringe. After 2 h, ^{i}Pr$_2$PCl (700 mg , 4.58 mmol) was added and the solution was stirred overnight. After completion, the volatiles was removed under vacuum and the residue was re-dissolved in pentane. The solution was filtered through a plug of silica gel and the volatiles were removed from the filtrate under vacuum to leave behind a colorless oil. The oil was re-dissolved in CH_2Cl_2, layered with acetonitrile and put into a -35 ºC freezer for one day. The supernatant was decanted and the solid was dried under vacuum to yield white powder (630 mg, 63%). ^{1}H NMR (400 MHz, C_6D_6): δ 7.55 (s, 1H, Ar-*H*), 7.32 (s, 1H, Ar-*H*), 7.14 (s, 1H, Ar-*H*), 6.89 (m, 3H, Ar-*H*), 3.47 (s, 3H, N-*Me*), 2.13 (m, 2H, C*H*Me$_2$), 1.95 (s, 3H, C*H*Me$_2$),1.28 (s, 9H, C*Me*$_3$), 1.21 (dd, 6H, CH*Me*$_2$), 1.13 (dd, 6H, CH*Me*$_2$) 1.01 (m, 12H, CH*Me*$_2$). ^{31}P{^{1}H} NMR (202 MHz, C_6D_6): δ -

5.70 (d, $J_{P\text{-}P}$ = 10 Hz, 1P, Ar-*P*(^{i}Pr$_2$)), -5.90 (d, $J_{P\text{-}P}$ = 10 Hz, 1P, Ar-*P*(^{i}Pr$_2$)).^{13}C{^{1}H} NMR (101 MHz, C_6D_6): δ. 158.0 (d, $J_{C\text{-}P}$ = 10 Hz, Ar-*C*), 156.3 (d, $J_{C\text{-}P}$ = 10 Hz, Ar-*C*), 145.1 (s, Ar-*C*), 135.3 (s, Ar-*C*), 132.9 (d, $J_{C\text{-}P}$ = 4 Hz, Ar-*C*), 132.2 (d, $J_{C\text{-}P}$ = 23 Hz, Ar-*C*), 132.0 (d, $J_{C\text{-}P}$ = 23 Hz, Ar-*C*), 131.4 (d, $J_{C\text{-}P}$ = 4 Hz, Ar-*C*), 126.5 (s, Ar-*C*), 124.2 (d, $J_{C\text{-}P}$ = 24 Hz, Ar-*C*), 46.4 (t, $J_{C\text{-}P}$ = 10 Hz, N-*Me*), 34.4 (s, *C*Me$_3$), 31.6 (s, C*Me*$_3$), 25.0 (d, $J_{C\text{-}P}$ = 10 Hz, *C*HMe$_2$), 24.8 (d, $J_{C\text{-}P}$ = 10 Hz, *C*HMe$_2$), 21.2 (dd, $J_{C\text{-}P}$ = 14 Hz, 3 Hz, CH*Me*$_2$), 20.9 (dd, $J_{C\text{-}P}$ = 14 Hz, 3 Hz, CH*Me*$_2$), 20.4 (dd, $J_{C\text{-}P}$ = 7 Hz, 1 Hz, CH*Me*$_2$), 20.2 (dd, $J_{C\text{-}P}$ = 7 Hz, 1 Hz, CH*Me*$_2$). ESI-MS: m/z $[M+H]^+$ Calcd. For $C_{58}H_{92}N_2OP_4$: 957.6233; Found: 957.6217.

$^{t\text{Bu}}$(PNPOPNP)PdCl (69). In a glovebox, **85** (200 mg, 209 μmol) was dissolved in 10 mL of dried, degassed toluene in a screw cap culture tube. Pd(COD)Cl_2 (119 mg, 417 μmol) was added and the tube was brought outside the glovebox. After heating at 100 ^{o}C for 3 h, the tube was taken in the glovebox. Volatiles were then removed under vacuum and the residue was re-dissolved in ether. The solution was filtered through a plug of silica gel and the volatiles were removed from the filtrate under vacuum to give a red powder. The powder can be further purified by re-dissolving in CH_2Cl_2, layering with acetonitrile and placing into a -35 ºC freezer for one day. The supernatant was decanted and the solid was dried under vacuum to yield a red powder (253 mg, 72%). ^{1}H NMR (400 MHz, C_6D_6): δ 7.66 (m, 2H, Ar-*H*), 7.13 (s, 1H, Ar-*H*), 7.04 (d, 1H, $J_{H\text{-}H}$ = 8 Hz, Ar-*H*), 6.91 (m, 2H, Ar-*H*), 2.37 (m, 2H, C*H*Me$_2$), 2.21 (m, 2H, C*H*Me$_2$), 1.42 (m, 12H, CH*Me*$_2$),1.25 (s, 9H, C*Me*$_3$), 1.13 (m, 12H, CH*Me*$_2$). ^{31}P{^{1}H} NMR (202 MHz, C_6D_6): δ 49.45 (d, $J_{P\text{-}P}$ = 418 Hz, 1P, Ar-*P*(^{i}Pr$_2$)), 47.50 (d, $J_{P\text{-}P}$ = 418 Hz, 1P, Ar-*P*(^{i}Pr$_2$)).^{13}C{^{1}H} NMR (101 MHz, C_6D_6): δ 162.0 (dd, $J_{C\text{-}P}$ = 5 Hz, 17 Hz, Ar-*C*), 160.2 (dd, $J_{C\text{-}P}$ = 5 Hz, 17 Hz, Ar-*C*), 149.1 (dd, $J_{C\text{-}P}$ = 6 Hz, 2 Hz, Ar-*C*), 139.7 (d, $J_{C\text{-}P}$ = 5 Hz, Ar-*C*), 129.1 (d, $J_{C\text{-}P}$ = 6 Hz, Ar-*C*), 122.1 (d, $J_{C\text{-}P}$ = 5 Hz, Ar-*C*),

120.8 (dd, $J_{C\text{-}P}$ = 10 Hz, 5 Hz, Ar-*C*), 119.2 (dd, $J_{C\text{-}P}$ = 10 Hz, 5 Hz, Ar-*C*), 116.9 (d, $J_{C\text{-}P}$ = 13 Hz, Ar-*C*), 115.7 (d, $J_{C\text{-}P}$ = 10 Hz, Ar-*C*), 33.9 (s, *C*Me$_3$), 31.6 (s, C*Me*$_3$), 25.1 (dd, $J_{C\text{-}P}$ = 4 Hz, 8Hz, *C*HMe$_2$), 18.7 (dd, $J_{C\text{-}P}$ = 4 Hz, 8Hz, *C*HMe$_2$), 18.0 (s, CH*Me*$_2$). Elem. Anal. Calcd for $C_{56}H_{86}Cl_2N_2OP_4Pd_2$: C, 55.54; H, 7.16; N, 2.31. Found: C, 55.48; H, 7.15; N, 2.18.

***N*^{4},*N*$^{4'}$-bis(4-(*tert*-butyl)phenyl)-[1,1'-biphenyl]-4,4'-diamine (77).** 4,4'-Dibromobiphenyl (**74**, 5.0 g, 16.0 mmol) and *tert*-butylaniline (7.2 g, 48.0 mmol) were dissolved in 300 mL of toluene in a 1 L flask. In another vial, $Pd(OAc)_2$ (35.9 mg, 0.16 mmol) and DPPF (133 mg, 0.24 mmol) were pre-mixed with 20 mL toluene. The resultant yellow suspension was added to the flask. Sodium *tert*-pentoxide (5.3 g, 48.0 mmol) was then added into the flask and the contents immediately turned red. The reaction mixture was heated to reflux for two days. After completion, the solution was poured into a separation funnel and extracted with water, diluted $HCl_{(aq)}$, and $NaHCO_{3(aq)}$. The organic layer was collected and dried with $Na_2SO_{4(s)}$. The solution was then filtered through a plug of silica gel. The volatiles were removed from the filtrate under vacuum; the residue was re-dissolvedin CH_2Cl_2, layered with ethanol and put into a -35 ºC freezer for one day. The supernatant was decanted and the solid was dried under vacuum to yield grey powder (4.9 g, 68%). ^{1}H NMR (400 MHz, C_6D_6): δ 7.48 (d, $J_{H\text{-}H}$ = 8 Hz, 2H, Ar-*H*), 7.24 (d, $J_{H\text{-}H}$ = 8 Hz, 2H, Ar-*H*), 6.96 (d, $J_{H\text{-}H}$ = 8 Hz, 4H, Ar-*H*), 5.09 (s, 1H, N-*H*), 1.28 (s, 9H, C*Me*$_3$).^{13}C{^{1}H} NMR (101 MHz, C_6D_6): δ. 144.0 (s, Ar-*C*), 143.0 (s, Ar-*C*), 141.0 (s, Ar-*C*), 133.8 (s, Ar-*C*), 127.7 (s, Ar-*C*), 126.4 (s, Ar-*C*), 118.7 (s, Ar-*C*), 118.0 (s, Ar-*C*), 34.2 (s, *C*Me$_3$), 31.7 (s, C*Me*$_3$). ESI-MS: m/z $[M+H]^+$ Calcd. For $C_{32}H_{36}N_2$: 449.2951; Found: 449.2942.

3,3'-dibromo-*N*^{4},*N*$^{4'}$-bis(2-bromo-4-(*tert*-butyl)phenyl)-[1,1'-biphenyl]-4,4'-diamine (80). 77 (1.0 g, 2.22 mmol) was dissolved in 100 mL of dried, degassed CH_2Cl_2 under argon atmosphere. NBS (1.59 g, 8.92 mmol) was added in 4 portions during 4 h. Three hours after the final portion was added, the volatiles were removed under vacuum. The residue was then re-dissolved in 1:1 hexanes/toluene and carefully passed through a plug of silica gel while collecting only the light-colored portion. The volatiles were removed from the filtrate under vacuum; the residue was re-dissolved in CH_2Cl_2, layered with ethanol and put into a -35 ºC freezer for one day. The supernatant was decanted and the solid was dried under vacuum to yield light-yellow powder (1.1 g, 66%). ^{1}H NMR (400 MHz, C_6D_6): δ 7.65 (d, $J_{H\text{-}H}$ = 4 Hz, 1H, Ar-*H*), 7.64 (d, $J_{H\text{-}H}$ = 4 Hz, 1H, Ar-*H*), 7.14-6.99 (m, 4H, Ar-*H*), 6.64 (s, 1H, N-*H*), 1.12 (s, 9H, C*Me*$_3$).^{13}C{^{1}H} NMR (101 MHz, C_6D_6): δ. 146.9 (s, Ar-*C*), 140.0 (s, Ar-*C*), 137.7 (s, Ar-*C*), 133.8 (s, Ar-*C*), 131.3 (s, Ar-*C*), 130.5 (s, Ar-*C*), 126.5 (s, Ar-*C*), 125.5 (s, Ar-*C*), 119.5 (s, Ar-*C*), 117.4 (s, Ar-*C*), 115.7 (s, Ar-*C*), 114.3 (s, Ar-*C*), 34.3 (s, *C*Me$_3$), 31.3 (s, C*Me*$_3$). ESI-MS: m/z $[M+H]^+$ Calcd. For $C_{32}H_{32}Br_4N_2$: 764.9331; Found: 764.5726.

3,3'-dibromo-*N*^{4},*N*$^{4'}$-bis(2-bromo-4-(*tert*-butyl)phenyl)-*N*^{4},*N*$^{4'}$-dimethyl-[1,1'-biphenyl]-4,4'-diamine (83). 80 (1.0 g, 1.31 mmol) was dissolved in 50 mL of dried, degassed DMF under argon atmosphere. NaH (94 mg, 3.92 mmol) was added slowly. After 10 min, MeI (557 mg , 3.92 mmol) was added. The resultant solution was stirred overnight, then poured into a separation funnel and extracted with water and $NaCl_{(aq)}$. The organic layer was collected and dried with $Na_2SO_{4(s)}$. The solution was then filtered through a plug of silica gel and the volatiles were removed from the filtrate under vacuum to yield a white powder (1.0 g, 96%). ^{1}H NMR (400 MHz, C_6D_6): δ 7.75 (d, $J_{H\text{-}H}$ = 4 Hz, 2H, Ar-*H*), 7.08 (d, $J_{H\text{-}H}$ = 8 Hz, 2H, Ar-*H*), 6.79 (d, $J_{H\text{-}H}$ = 8 Hz, 2H, Ar-

H), 6.77 (d, J_{H-H} = 8 Hz, 2H, Ar-*H*), 3.00 (s, 3H, N-*Me*), 1.12 (s, 9H, C*Me*$_3$).^{13}C{^{1}H} NMR (101 MHz, C_6D_6): δ. 148.6 (s, Ar-*C*), 148.4 (s, Ar-*C*), 146.5 (s, Ar-*C*), 136.0 (s, Ar-*C*), 132.9 (s, Ar-*C*), 131.7 (s, Ar-*C*), 126.5 (s, Ar-*C*), 125.5 (s, Ar-*C*), 124.2 (s, Ar-*C*), 124.1 (s, Ar-*C*), 121.1 (s, Ar-*C*), 120.9 (s, Ar-*C*), 41.4 (s, N-*Me*), 34.3 (s, *C*Me$_3$), 31.2 (s, C*Me*$_3$). ESI-MS: m/z $[M+H]^+$ Calcd. For $C_{32}H_{32}Br_4N_2$: 808.9593; Found: 808.9579.

^{tBu}PNP$_B$PNP (86). In a glovebox, **83** (1.0 g, 1.26 mmol) was dissolved in 50 mL of dried, degassed ether in a Schlenk flask and cooled to -35ºC. *n*BuLi (2.22 mL, 5.54 mmol) was added slowly by syringe. After 2 h, ^{i}Pr$_2$PCl (845 mg, 5.54 mmol) was added and the solution was stirred overnight. Subsequently, the volatiles were removed under vacuum and the residue was re-dissolved in pentane. The solution was filtered through a plug of silica gel and the volatiles were removed from the filtrate under vacuumto result in a colorless oil. The oil was re-dissolved in CH_2Cl_2, layered with acetonitrile and put into a -35 ºC freezer for one day. The supernatant was decanted and the solid was dried under vacuum to yield a white powder (1.0 g, 84%). ^{1}H NMR (400 MHz, C_6D_6): δ 7.91 (s, 1H, Ar-*H*), 7.60 (s, 1H, Ar-*H*), 7.47 (dd, J_{H-H} = 8 Hz, 4 Hz, 1H, Ar-*H*), 7.14 (d, J_{H-H} = 4 Hz, 1H, Ar-*H*), 7.00 (dd, J_{H-H} = 8 Hz, 4 Hz, 1H, Ar-*H*), 6.95 (dd, J_{H-H} = 8 Hz, 4 Hz, 1H, Ar-*H*), 3.56 (s, 3H, N-*Me*), 2.18 (m, 4H, C*H*Me$_2$), 1.30 (s, 9H, C*Me*$_3$), 1.23 (dd, 12H, CH*Me*$_2$), 1.06 (dd, 12H, CH*Me*$_2$). ^{31}P{^{1}H} NMR (202 MHz, C_6D_6): δ -5.74 (d, J_{P-P} = 10 Hz, 1P, Ar-*P*(^{i}Pr$_2$)), -6.02 (d, J_{P-P} = 10 Hz, 1P, Ar-*P*(^{i}Pr$_2$)).^{13}C{^{1}H} NMR (101 MHz, C_6D_6): δ 157.96 (d, J_{C-P} = 10 Hz, Ar-*C*), 156.28 (d, J_{C-P} = 10 Hz, Ar-*C*), 145.14 (s, Ar-*C*), 135.34 (s, Ar-*C*), 132.85 (d, J_{C-P} = 4 Hz, Ar-*C*), 132.24 (d, J_{C-P} = 23 Hz, Ar-*C*), 132.00 (d, J_{C-P} = 23 Hz, Ar-*C*), 131.41 (d, J_{C-P} = 4 Hz, Ar-*C*), 126.46 (s, Ar-*C*), 124.22 (d, J_{C-P} = 24 Hz, Ar-*C*), 46.21 (t, J_{C-P} = 10 Hz, N-*Me*), 34.46 (s, *C*Me$_3$), 31.61 (s, C*Me*$_3$), 24.91 (d, J_{C-P} = 20 Hz, *C*HMe$_2$), 24.71(d, J_{C-P} = 20 Hz, *C*HMe$_2$), 21.12 (dd, J_{C-P}

= 6 Hz, 2 Hz, CH*Me*$_2$), 20.98 (dd, $J_{C\text{-}P}$ = 6 Hz, 2 Hz, CH*Me*$_2$), 20.34 (s, CH*Me*$_2$), 20.17(s, CH*Me*$_2$). ESI-MS: m/z $[M+H]^+$ Calcd. For $C_{58}H_{92}N_2P_4O$: 957.6233; Found: 957.6212.

$^{t\text{Bu}}$PNP$_\text{B}$PNPPdCl (70). In a glovebox, **86** (200 mg, 212 μmol) was dissolved in 10 mL of dried, degassed toluene in a screw cap culture tube. Pd(COD)Cl_2 (121 mg, 425 μmol) was added to the solution and the tube was brought outside the glovebox. After heating at 100 ºC for 3 h, the tube was taken in the glovebox. Volatiles were then removed under vacuum and the residue was re-dissolved in ether. The solution was filtered through a plug of silica gel and the volatiles were removed from the filtrate under vacuum to give a red powder. The powder was further purified by re-dissolving it in THF, layering with pentane and placing in a -35 ºC freezer for one day. The supernatant was decanted and the solid was dried under vacuum to yield red powder (180 mg, 71%). ^{1}H NMR (400 MHz, C_6D_6): δ 7.88 (d, $J_{H\text{-}H}$ = 8 Hz, 1H, Ar-*H*), 7.81 (d, $J_{H\text{-}H}$ = 8 Hz, 1H, Ar-*H*), 7.43 (s, 1H, Ar-*H*), 7.37 (d, $J_{H\text{-}H}$ = 8 Hz, 1H, Ar-*H*), 7.16 (s, 1H, Ar-*H*), 7.10 (d, $J_{H\text{-}H}$ = 8 Hz, 1H, Ar-*H*), 2.41 (m, 4H, C*H*Me$_2$), 1.45 (dd, $J_{H\text{-}P}$ = 20 Hz, $J_{H\text{-}H}$ = 8 Hz, 12H, CH*Me*$_2$), 1.26 (s, 9H, C*Me*$_3$), 1.19 (m, 12H, CH*Me*$_2$). ^{31}P{^{1}H} NMR (202 MHz, C_6D_6): δ 48.86 (s, 1P, Ar-*P*(^{i}Pr$_2$)), 48.83 (s, 1P, Ar-*P*(^{i}Pr$_2$)). ^{13}C{^{1}H} NMR (101 MHz, C_6D_6): δ 162.9 (dd, $J_{C\text{-}P}$ = 12 Hz, 9 Hz, Ar-*C*), 161.7 (dd, $J_{C\text{-}P}$ = 12 Hz, 9 Hz, Ar-*C*), 140.3 (s, Ar-*C*), 130.4 (s, Ar-*C*), 130.2 (t, $J_{C\text{-}P}$ = 3 Hz, Ar-*C*), 129.8 (s, Ar-*C*), 129.2 (s, Ar-*C*), 129.0 (s, Ar-*C*), 128.6 (s, Ar-*C*), 120.6 (dd, $J_{C\text{-}P}$ = 20 Hz, 14 Hz, Ar-*C*), 119.7 (dd, $J_{C\text{-}P}$ = 20 Hz, 15 Hz, Ar-*C*), 116.8 (dd, $J_{C\text{-}P}$ = 7 Hz, 6 Hz, Ar-*C*), 116.5 (dd, $J_{C\text{-}P}$ = 7 Hz, 6 Hz, Ar-*C*), 34.0 (s, *C*Me$_3$), 31.6 (s, C*Me*$_3$), 25.1 (m, *C*HMe$_2$), 18.7 (s, CH*Me*$_2$), 18.0 (s, CH*Me*$_2$). Elem. Anal. Calcd. for $C_{56}H_{86}Cl_2N_2P_4Pd_2$: C, 56.29; H, 7.25; N, 2.34. Found: C, 56.56; H, 7.26; N, 2.29.

***N*[1],*N*[4]-bis(4-(*tert*-butyl)phenyl)benzene-1,4-diamine (78).** 1,4-Dibromobenzene (**75**, 5.0 g, 21.2 mmol) and *tert*-butylaniline (9.5 g, 63.6 mmol) were dissolved in 300 mL of toluene in a 1 L flask. In another vial, $Pd(OAc)_2$ (49.4 mg, 0.22 mmol) and DPPF (183 mg, 0.33 mmol) were pre-mixed with 20 mL toluene. The resultant yellow suspension was added to the flask, followed by sodium *tert*-pentoxide (7.0 g, 63.6 mmol). The reaction mixture immediately turned red; it was then heated at reflux for two days. Subsequently, the solution was poured into a separation funnel and extracted with water, diluted $HCl_{(aq)}$, and $NaHCO_{3(aq)}$. The organic layer was collected and dried with $Na_2SO_{4(s)}$. The solution was then filtered through a plug of silica gel. The volatiles were removed from the filtrate under vacuum, the residue was re-dissolved in CH_2Cl_2, layered with ethanol and placed into a -35 ºC freezer for one day. The supernatant was decanted and the solid was dried under vacuum to yield a light-red powder (6.7 g, 85%). ^{1}H NMR (400 MHz, C_6D_6): δ 7.21 (d, $J_{H\text{-}H}$ = 8 Hz, 2H, Ar-*H*), 6.98 (d, $J_{H\text{-}H}$ = 8 Hz, 2H, Ar-*H*), 6.86 (d, $J_{H\text{-}H}$ = 8 Hz, 2H, Ar-*H*), 6.82 (d, $J_{H\text{-}H}$ = 8 Hz, 2H, Ar-*H*), 4.98 (s, 1H, N-*H*), 1.27 (s, 9H, C*Me*$_3$).^{13}C{^{1}H} NMR (101 MHz, C_6D_6): δ. 142.9 (s, Ar-*C*), 142.5 (s, Ar-*C*), 138.0 (s, Ar-*C*), 126.4 (s, Ar-*C*), 120.6 (s, Ar-*C*), 117.1 (s, Ar-*C*), 34.2 (s, *C*Me$_3$), 31.7 (s, C*Me*$_3$). ESI-MS: m/z $[M+H]^+$ Calcd. For $C_{26}H_{32}N_2$: 372.2560; Found: 372.2554.

2,5-dibromo-*N*[1],*N*[4]-bis(2-bromo-4-(*tert*-butyl)phenyl)benzene-1,4-diamine (81). 78 (1.0 g, 2.68 mmol) was dissolved in 100 mL of dried, degassed CH_2Cl_2 under argon atmosphere. NBS (1.91 g, 10.74 mmol) was added in 4 portions during 4 h. Three hours after the addition of the final portion, the volatiles were removed under vacuum. The residue was then re-dissolved in 1:1 hexanes/toluene and carefully passed through a plug of silica gel while collecting only the light-colored portion. The volatiles were removed from the filtrate under vacuum, the residue was re-

dissolved in CH_2Cl_2, layered with ethanol and placed into a -35 ºC freezer for one day. The supernatant was decanted and the solid was dried under vacuum to yield a light-red powder (1.0 g, 54%). ^{1}H NMR (400 MHz, C_6D_6): δ 7.62 (d, J_{H-H} = 4 Hz, 1H, Ar-*H*), 7.37 (s, 1H, Ar-*H*), 6.93-6.85 (m, 2H, Ar-*H*), 6.29 (s, 1H, N-*H*), 1.09 (s, 9H, C*Me*$_3$).^{13}C{^{1}H} NMR (101 MHz, C_6D_6): δ. 146.1 (s, Ar-*C*), 138.2 (s, Ar-*C*), 135.9 (s, Ar-*C*), 130.4 (s, Ar-*C*), 125.7 (s, Ar-*C*), 123.4 (s, Ar-*C*), 117.6 (s, Ar-*C*), 114.9 (s, Ar-*C*), 114.2 (s, Ar-*C*), 34.2 (s, *C*Me$_3$), 31.3 (s, C*Me*$_3$). ESI-MS: m/z $[M+H]^+$ Calcd. For $C_{26}H_{28}Br_4N_2$: 687.8940; Found: 687.8919.

2,5-dibromo-*N*^{1},*N*^{4}-bis(2-bromo-4-(*tert*-butyl)phenyl)-*N*^{1},*N*^{4}-dimethylbenzene-1,4-diamine (84). 81 (1.0 g, 1.45 mmol) was dissolved in 50 mL of dried, degassed DMF under argon atmosphere. NaH (105 mg , 4.36 mmol) was added slowly. After 10 minutes, MeI (620 mg , 4.36 mmol) was added and the solution was stirred overnight, then poured into a separation funnel, and extracted with water and $NaCl_{(aq)}$. The organic layer was collected and dried with $Na_2SO_{4(s)}$. The solution was then filtered through a plug of silica gel and the volatiles were removed from the filtrate under vacuum to yield a white powder (1.0 g, 97%). ^{1}H NMR (400 MHz, C_6D_6): δ 7.68 (d, J_{H-H} = 4 Hz, 1H, Ar-*H*), 7.30 (s, 1H, Ar-*H*), 7.02 (dd, J_{H-H} = 8 Hz, 4 Hz, 2H, Ar-*H*), 6.71 (d, J_{H-H} = 8 Hz, 1H, Ar-*H*), 2.85 (s, 3H, N-*Me*) 1.07 (s, 9H, C*Me*$_3$).^{13}C{^{1}H} NMR (101 MHz, C_6D_6): δ. 148.6 (s, Ar-*C*), 146.2 (s, Ar-*C*), 145.6 (s, Ar-*C*), 131.7 (s, Ar-*C*), 129.0 (s, Ar-*C*), 125.6 (s, Ar-*C*), 124.1 (s, Ar-*C*), 120.9 (s, Ar-*C*), 119.6 (s, Ar-*C*), 41.4 (s, N-*Me*), 34.2 (s, *C*Me$_3$), 31.2 (s, C*Me*$_3$). ESI-MS: m/z $[M+H]^+$ Calcd. For $C_{28}H_{32}Br_4N_2$: 715.9523; Found: 715.9230.

$^{t\text{Bu}}$PNPPNP (87). In a glovebox, **84** (1.0 g, 1.40 mmol) was dissolved in 50 mL of dried, degassed ether in a Schlenk flask and cooled to -35 ^{o}C. *n*BuLi (2.46 mL , 6.16 mmol) was added slowly by syringe. After 2 h, ^{i}Pr$_2$PCl (940 mg, 6.16 mmol) was added and the solution was stirred overnight. Subsequently, the volatiles were removed under vacuum and the residue was re-dissolved in pentane. The resultant solution was filtered through a plug of silica gel and the volatiles were removed from the filtrate under vacuum to produce a colorless oil. The oil was re-dissolved in CH_2Cl_2, layered with acetonitrile and placed into a -35 ºC freezer for one day. The supernatant was decanted and the solid was dried under vacuum to yield a light-brown powder (800 mg, 66%). ^{1}H NMR (400 MHz, C_6D_6): δ 7.57 (s, 1H, Ar-*H*), 7.27 (s, 1H, Ar-*H*), 7.19 (d, $J_{H\text{-}H}$ = 8 Hz, 1H, Ar-*H*), 7.02 (dd, $J_{H\text{-}H}$ = 8 Hz, 4Hz, 1H, Ar-*H*), 3.59 (s, 3H, N-*Me*), 2.25 (m, 2H, C*H*Me$_2$), 2.00 (m, 2H, C*H*Me$_2$), 1.30 (s, 9H, C*Me*$_3$), 1.59 (m, 6H, CH*Me*$_2$), 1.13 (m, 12H, CH*Me*$_2$), 1.01 (dd, $J_{H\text{-}H}$ = 12 Hz, 8 Hz, 6H, CH*Me*$_2$). ^{31}P{^{1}H} NMR (202 MHz, C_6D_6): δ -4.34 (d, $J_{P\text{-}P}$ = 10 Hz, 1P, Ar-*P*(^{i}Pr$_2$)), -6.54 (d, $J_{P\text{-}P}$ = 10 Hz, 1P, Ar-*P*(^{i}Pr$_2$)). ^{13}C{^{1}H} NMR (101 MHz, C_6D_6): δ 156.6 (d, $J_{C\text{-}P}$ = 5 Hz Ar-*C*), 153.3 (d, $J_{C\text{-}P}$ = 5 Hz Ar-*C*), 144.7 (s, Ar-*C*), 134.5 (d, $J_{C\text{-}P}$ = 13 Hz, Ar-*C*), 131.3 (s, Ar-*C*), 131.0 (s, Ar-*C*), 129.9 (s, Ar-*C*), 126.1 (s, Ar-*C*), 124.1 (m, Ar-*C*), 46.5 (m, N-*Me*), 34.4 (s, *C*Me$_3$), 31.6 (s, C*Me*$_3$), 24.8 (d, $J_{C\text{-}P}$ = 17 Hz, *C*HMe$_2$), 21.0 (d, $J_{C\text{-}P}$ = 13 Hz, *C*HMe$_2$), 20.4 (d, $J_{C\text{-}P}$ = 18 Hz, CH*Me*$_2$), 20.2 (d, $J_{C\text{-}P}$ = 18 Hz, CH*Me*$_2$). ESI-MS: m/z $[M+H]^+$ Calcd. For $C_{52}H_{88}N_2P_4$: 865.5971; Found: 865.5953.

$^{t\text{Bu}}$(PNPPNP)PdCl (71). In a glovebox, **87** (200 mg, 231 μmol) was dissolved in 10 mL of dried, degassed toluene in a screw cap culture tube followed by the addition of Pd(COD)Cl_2 (132 mg, 462 μmol). The tube was taken out of the glovebox and was heated at 100 ºC for 3 h. After heating, the tube was taken in the glovebox. The volatiles were then removed under vacuum and the residue

was re-dissolved in THF. The resultant solution was filtered through a plug of silica gel and the volatiles were removed from the filtrate under vacuum to give a purple powder. The powder was further purified by re-dissolving in THF, layering with pentane and placing into a -35 ºC freezer for one day. The supernatant was decanted and the solid was dried under vacuum to yield a purple powder (212 mg, 82%). ^{1}H NMR (400 MHz, C_6D_6): δ 7.74 (dd, J_{H-H} = 8 Hz, 4 Hz, 1H, Ar-*H*), 7.57 (dd, J_{H-H} = 8 Hz, 4 Hz, 1H, Ar-*H*), 7.21 (d, J_{H-H} = 12 Hz, 1H, Ar-*H*), 2.45 (m, 2H, C*H*Me$_2$), 2.13 (m, 2H, C*H*Me$_2$), 1.49 (dd, J_{H-H} = 16 Hz, 8 Hz, 6H, CH*Me$_2$*), 1.41 (dd, J_{H-H} = 16 Hz, 8 Hz, 6H, CH*Me$_2$*), 1.25 (s, 9H, C*Me$_3$*), 1.20 (dd, J_{H-H} = 16 Hz, 8 Hz, 6H, CH*Me$_2$*), 1.11 (dd, J_{H-H} = 16 Hz, 8 Hz, 6H, CH*Me$_2$*).^{31}P{^{1}H} NMR (202 MHz, C_6D_6): δ 49.49 (d, J_{P-P} = 10 Hz, 1P, Ar-*P*(^{i}Pr$_2$)), 44.66 (d, J_{P-P} = 10 Hz, 1P, Ar-*P*(^{i}Pr$_2$)). ^{13}C{^{1}H} NMR (126 MHz, THF with trace amount of C_6D_6): δ 161.4 (d, J_{C-P} = 21 Hz, Ar-*C*), 155.2 (dd, J_{C-P} = 6 Hz, 21 Hz, Ar-*C*), 138.2 (d, J_{C-P} = 5 Hz, Ar-*C*), 129.0 (s, Ar-*C*), 128.1 (s, Ar-*C*), 122.5 (d, J_{C-P} = 37 Hz, Ar-*C*), 118.4 (d, J_{C-P} = 15 Hz, Ar-*C*), 117.1 (d, J_{C-P} = 37 Hz, Ar-*C*), 114.5 (d, J_{C-P} = 13 Hz, Ar-*C*), 33.4 (s, *C*Me$_3$), 30.9 (s, C*Me$_3$*), 17.9 (d, J_{C-P} = 5 Hz, CH*Me$_2$*), 17.8 (d, J_{C-P} = 5 Hz, CH*Me$_2$*), 17.3 (d, J_{C-P} = 3 Hz, CH*Me$_2$*), 17.2 (d, J_{C-P} = 3 Hz, CH*Me$_2$*). Elemental Analysis: C, 53.68; H, 7.39; N, 2.50. Found: C, 53.44; H, 7.51; N, 2.56.

2-bromo-5-(triisopropylsilyl)thiazole (93).[171] To a solution of ^{i}PrMgCl•LiCl (12.0 mL, 15.6 mmol, 1.3 M in THF), anhydrous 2,2,6,6-tetramethylpiperidine (TMPH, 16.0 mmol, 2.26 g) was added dropwise at room temperature. The resulting mixture was stirred for 2 d to give a TMPMgCl•LiCl THF solution, which is directly used for the following synthesis. A solution of 2-bromothiazole (10.0 mmol, 1.64 g) in anhydrous THF (20 mL) was stirred at −78 °C. The freshly prepared TMPMgCl•LiCl solution was added dropwise over 15 min. The resulting mixture was stirred at −78 °C for 2 h, and triisopropylsilylchloride was added in one portion. The mixture was

slowly warmed up to room temperature and stirred overnight. The reaction mixture was extracted with CH_2Cl_2. The organic solution was washed with water extensively, and dried over $MgSO_4$. The crude product was purified by column chromatography (SiO_2, hexane/CH_2Cl_2 = 2/1), to give **93** as pale yellow oil (1.73 g, 54%). ^{1}H NMR (500 MHz, $CDCl_3$): δ 7.63 (s, 1H, Ar-*H*), 1.30 (sept, $J_{H\text{-}H}$ = 7.5 Hz, 3H, C*H*Me$_2$), 1.09 (d, $J_{H\text{-}H}$ = 7.5 Hz, 18H, CH*Me$_2$*). ^{13}C{^{1}H} NMR (101 MHz, $CDCl_3$): δ 150.1 (s, Ar-*C*), 140.6 (s, Ar-*C*), 132.9 (s, Ar-*C*), 18.6 (m, *C*HMe$_2$), 11.8 (m, *C*H*Me$_2$*). APCI-MS: m/z $[M+H]^+$ Calcd. for $C_{12}H_{23}BrNSSi$: 320.0498; Found: 320.0489.

2-(tributylstannyl)-5-(triisopropylsilyl)thiazole (91). To a solution of **93** (1.19 mmol, 380 mg) in anhydrous Et_2O (3 mL) at −78 °C, *n*BuLi (1.0 mL, 1.6 M in hexane) was added dropwise. After the addition of *n*BuLi, anhydrous THF (0.3 mL) was added. The resulting mixture was stirred at −78 °C for 1 h, before ^{n}Bu$_3$SnCl (1.6 mmol, 520 mg) was added in one portion. The mixture was slowly warmed up to room temperature and stirred overnight. The reaction mixture was extracted with CH_2Cl_2. The organic solution was washed with water extensively, and dried over $MgSO_4$. The crude product was purified by GPC, to give **91** as brown oil (500 mg, 79%). ^{1}H NMR (500 MHz, $CDCl_3$): δ 8.22 (s, 1H, Ar-*H*), 1.60 (m, 6H), 1.36~1.31 (m, 9H), 1.22 (m, 6H), 1.09 (d, $J_{H\text{-}H}$ = 7.5 Hz, 18H, CH*Me$_2$*), 0.88 (t, $J_{H\text{-}H}$ = 7.5 Hz, 9H, Sn*^{n}Bu$_3$*). ^{13}C{^{1}H} NMR (101 MHz, $CDCl_3$): δ 178.4 (s, Ar-*C*), 152.4 (s, Ar-*C*), 128.6 (s, Ar-*C*), 29.1, 27.4, 18.7, 13.8, 12.2, 11.4. APCI-MS: m/z $[M+H]^+$ Calcd. for $C_{24}H_{50}NSSiSn$: 532.2450; Found: 532.2434.

4,6,10,12-tetrabromo-2,8-di-*tert*-butyl-5,11-dihydroindolo[3,2-b]carbazole (89). 2,8-di-*tert*-butyl-5,11-dihydroindolo[3,2-b]carbazole (**88**, 1.0 mmol, 369 mg) was dissolved in anhydrous

THF (20 mL) at 0 °C. A solution of NBS (6.0 mmol, 1.07 g) in anhydrous THF (15 mL) was added. The resulting mixture was warmed up to room temperature and stirred overnight. After removal of volatiles under reduced pressure, the crude product was washed with methanol, to give **89** (568 mg, 83%) as a grey solid. ^{1}H NMR (500 MHz, $CDCl_3$): δ 8.74 (d, $J_{H\text{-}H}$ = 1.5 Hz, 2H, Ar-*H*), 8.27 (s, 2H, N-*H*), 7.73 (d, $J_{H\text{-}H}$ = 1.5 Hz, 2H, Ar-*H*), 1.48 (s, 18H, C*Me*$_3$). ^{13}C{^{1}H} NMR (100 MHz, $CDCl_3$): δ 144.7 (s, Ar-*C*), 137.3 (s, Ar-*C*), 134.9 (s, Ar-*C*), 127.6 (s, Ar-*C*), 124.4 (s, Ar-*C*), 122.0 (s, Ar-*C*), 118.3 (s, Ar-*C*), 35.2 (s, *C*Me$_3$), 32.1 (s, C*Me*$_3$). APCI-MS: m/z $[M+H]^+$ Calcd. for $C_{26}H_{25}Br_4N_2$: 684.8707; Found: 684.8701.

90. 89 (1.10 g, 1.61 mmol) was dissolved in a mixed solvent of DMF (100 mL) and THF (20 mL) at room temperature. NaH (116 mg) was added in one portion. The mixture was stirred at room temperature for 30 min before MeI (680 mg, 4.79 mmol) was added. After the addition of MeI, a yellow precipitate was formed, and the suspension was stirred overnight. The suspension was filtered, and the resulting yellow solids were washed extensively with water and acetone, to give **90** (1.10 g, 96%). ^{1}H NMR (500 MHz, $CDCl_3$): δ 9.01 (d, $J_{H\text{-}H}$ = 1.5 Hz, 2H, Ar-*H*), 7.75 (d, $J_{H\text{-}H}$ = 1.5 Hz, 2H, Ar-*H*), 4.30 (s, 6H, N-*Me*), 1.45 (s, 18H, C*Me*$_3$). ^{13}C{^{1}H} NMR (125 MHz, $CDCl_3$): δ 145.0 (s, Ar-*C*), 142.4 (s, Ar-*C*), 141.1 (s, Ar-*C*), 130.4 (s, Ar-*C*), 127.4 (s, Ar-*C*), 125.0 (s, Ar-*C*), 119.2 (s, Ar-*C*), 104.6 (s, Ar-*C*), 98.8 (s, Ar-*C*), 39.1 (s, N-*Me*), 35.0 (s, *C*Me$_3$), 32.0 (s, C*Me*$_3$). APCI-MS: m/z $[M+H]^+$ Calcd. For $C_{28}H_{29}Br_4N_2$: 712.9021; Found: 712.9002.

92. A thick-wall reaction vessel filled with **90** (99.7 mg, 0.14 mmol) and **91** (509.2 mg, 0.96 mmol) was taken into an N_2-filled glovebox, where $Pd(PPh_3)_4$ (40.4 mg, 0.035 mmol), CuI (6.7 mg, 0.035 mmol) and toluene (4 mL) were added. The reaction vessel was sealed and taken out of

the glovebox. The reaction mixture was stirred at 140 °C for 3 d. After cooling to room temperature, volatiles were removed under reduced pressure. The mixture was further extracted with CH_2Cl_2. The organic solution was washed with water extensively, and dried over $MgSO_4$. The crude product was purified by column chromatography (SiO_2, hexane/ethyl acetate = 19/1 ~ 7/3), to give **92** as yellow solids (148 mg, 78%). ^{1}H NMR (500 MHz, $CDCl_3$): δ 8.26 (s, 2H, Ar-*H*), 7.91 (s, 2H, Ar-*H*), 7.53 (d, J_{H-H} = 1.5 Hz, 2H, Ar-*H*), 7.05 (d, J_{H-H} = 1.5 Hz, 2H, Ar-*H*), 2.94 (s, 6H, N-*Me*), 1.45 (sept, 6H, C*H*Me$_2$), 1.36 (sept, 6H, C*H*Me$_2$), 1.24 (s, 18H, C*Me*$_3$), 1.18 (d, J_{H-H} = 7.5 Hz, 36H, CH*Me*$_2$), 1.12 (d, J_{H-H} = 7.5 Hz, 36H, CH*Me*$_2$). ^{13}C{^{1}H} NMR (125 MHz, $CDCl_3$): δ 171.5 (s, Ar-*C*), 169.4 (s, Ar-*C*), 150.4 (s, Ar-*C*), 150.0 (s, Ar-*C*), 141.6 (s, Ar-*C*), 140.6 (s, Ar-*C*), 137.9 (s, Ar-*C*), 131.0 (s, Ar-*C*), 128.5 (s, Ar-*C*), 127.2 (s, Ar-*C*), 124.3 (s, Ar-*C*), 123.3 (s, Ar-*C*), 120.5 (s, Ar-*C*), 117.2 (s, Ar-*C*), 111.8 (s, Ar-*C*), 36.3 (s, N-*Me*), 34.6, 32.0, 18.8 (two s), 12.0. APCI-MS: m/z $[M+H]^+$ Calcd. for $C_{76}H_{117}N_6S_4Si_4$: 1354.7300; Found: 1354.7334.

72. 92 (13.5 mg, 0.01 mmol) was mixed with $Pd(COD)Cl_2$ (6.3 mg, 0.022 mmol) in anhydrous toluene (1.0 mL). The mixture was stirred at 120 °C for two days. After cooling to room temperature, the volatiles were removed under reduced pressure. The residue was extracted with CH_2Cl_2. The organic solution was washed with water extensively, and dried over $MgSO_4$. The crude product was purified by column chromatography (SiO_2, hexane/ CH_2Cl_2 = 9/1 ~ 8/2), to give **72** as green solids (13.2 mg, 82%). ^{1}H NMR (500 MHz, $CDCl_3$): δ 9.33 (s, 2H, Ar-*H*), 9.14 (d, J_{H-H} = 1.5 Hz, 2H, Ar-*H*), 9.11 (s, 2H, Ar-*H*), 8.08 (d, J_{H-H} = 1.5 Hz, 2H, Ar-*H*), 1.48 (s, 18H, C*Me*$_3$), 1.44 (m, 6H, C*H*Me$_2$), 1.37 (m, 6H, C*H*Me$_2$), 1.20 (d, J_{H-H} = 7.5 Hz, 36H, CH*Me*$_2$), 1.14 (d, J_{H-H} = 7.5 Hz, 36H, CH*Me*$_2$). ^{13}C{^{1}H} NMR (125 MHz, $CDCl_3$): δ 168.7 (s, Ar-*C*), 164.0 (s, Ar-*C*), 153.2 (s, Ar-*C*), 152.8 (s, Ar-*C*), 140.4 (s, Ar-*C*), 138.4 (s, Ar-*C*), 137.2 (s, Ar-*C*), 124.4 (s, Ar-*C*),

124.2 (s, Ar-*C*), 124.1 (s, Ar-*C*), 123.7 (s, Ar-*C*), 122.5 (s, Ar-*C*), 121.4 (s, Ar-*C*), 114.5 (s, Ar-*C*), 112.5 (s, Ar-*C*), 35.0, 32.3, 18.7, 18.7, 11.9. Elemental Analysis: C, 55.27; H, 6.90; N, 5.23. Found: C, 54.79; H, 6.79; 5.07.

[70][$CH_{12}B_{11}]_2$ crystal. In a glovebox, **70** (10 mg, 8 μmol) was dissolved in CH_2Cl_2 and mixed with approximately 1 equiv. of ferrocenium carba-*closo*-dodecaborate (2.6 mg, 8 μmol) in a glass vial. The solution color changed from red to black immediately. The reaction mixture was layered with isooctane and placed into a -35 ºC freezer overnight, yielding black crystals. A suitable crystal was selected and subjected to an X-ray diffraction study.

[71][$CH_{12}B_{11}^-$] crystal. In a glovebox, **71** (10 mg, 9 μmol) was dissolved in CH_2Cl_2 and mixed with approximately 0.9 equiv. of ferrocenium carba-*closo*-dodecaborate (2.6 mg, 8 μmol) in a glass vial. The solution color changed from purple to black immediately. The reaction mixture was layered with isooctane and placed into a -35 ºC freezer overnight, yielding black crystals. A suitable crystal was selected and subjected to an X-ray diffraction study.

[71][$SbCl_6]_2$ crystal. In a glovebox, **71** (10 mg, 9 μmol) was dissolved in CH_2Cl_2 and mixed with approximately 2.2 equiv. of tris(4-bromophenyl)aminium hexachloroantimonate, [(*p*-$BrC_6H_4)_3N]SbCl_6$ (16 mg, 18 μmol), in a glass vial. The solution color changed from purple to deep blue immediately. The reaction mixture was layered with isooctane and placed into a -35 ºC freezer overnight, yielding blue crystals. A suitable crystal was selected and subjected to an X-ray diffraction study.

3.4.4 X-Ray Structural Determination Details

X-Ray data collection, solution, and refinement for (69). (CCDC number: 2003991)

A Leica MZ 75 microscope was used to identify a suitable red block with very well defined faces with dimensions (max, intermediate, and min) 0.182 x 0.153 x 0.124 mm^3 from a representative sample of crystals of the same habit. The crystal mounted on a nylon loop was then placed in a cold nitrogen stream (Oxford) maintained at 110 K. A BRUKER APEX 2 Duo X-ray (three-circle) diffractometer was employed for crystal screening, unit cell determination, and data collection. The X-ray radiation employed was generated from a Mo sealed X-ray tube (K_α = 0.71073Å with a potential of 40 kV and a current of 40 mA). All diffractometer manipulations, including data collection, integration and scaling were carried out using the Bruker APEX3 software.[122] An absorption correction was applied using SADABS.[123] Systematic reflection conditions and statistical tests of the data suggested the space group $P2_1/c$. A solution was obtained readily using XT/XS in APEX3.[122,124] Hydrogen atoms were placed in idealized positions and were set riding on the respective parent atoms. All non-hydrogen atoms were refined with anisotropic thermal parameters. Absence of additional symmetry and voids were confirmed using PLATON (ADDSYM). The structure was refined (weighted least squares refinement on F^2) to convergence.[124,125] ORTEP-3 and POV-Ray were employed for the final data presentation and structure plots.[126,127]

X-Ray data collection, solution, and refinement for [70][$CH_{12}B_{11}$]$_2$. (CCDC number: 2003992)

A Leica MZ 75 microscope was used to identify a suitable brown plate with very well defined faces with dimensions (max, intermediate, and min) 0.132 x 0.052 x 0.013 mm^3 from a

representative sample of crystals of the same habit. The crystal mounted on a nylon loop was then placed in a cold nitrogen stream (Oxford) maintained at 140 K. A BRUKER Venture X-ray (kappa geometry) diffractometer was employed for crystal screening, unit cell determination, and data collection. The X-ray radiation employed was generated from a Cu-Iμs X-ray tube (K_α = 1.5418Å with a potential of 50 kV and a current of 1.0mA). All diffractometer manipulations, including data collection, integration and scaling were carried out using the Bruker APEX3 software.[122] An absorption correction was applied using SADABS.[123] Systematic reflection conditions and statistical tests of the data suggested the space group *P*-1. A solution was obtained readily (Z=1; Z'=0.5) using XT/XS in APEX3.[122,124] Hydrogen atoms were placed in idealized positions and were set riding on the respective parent atoms. All non-hydrogen atoms were refined with anisotropic thermal parameters. The structure showed presence of partially occupied and/or disordered solvent molecules; both dichloromethane and pentane. Our efforts to model the solvents resulted in high reliability factors. For the final refinement cycles, these solvent molecules were MASKed using OLEX2.[125] Absence of additional symmetry or void were confirmed using PLATON (ADDSYM). The structure was refined (weighted least squares refinement on F^2) to convergence.[124,125] ORTEP-3 and POV-Ray were employed for the final data presentation and structure plots.[126,127]

X-Ray data collection, solution, and refinement for (71). (CCDC number: 1915569)

A Leica MZ 75 microscope was used to identify a suitable dark brown block with very well defined faces with dimensions (max, intermediate, and min) 0.182 x 0.042 x 0.027 mm^3 from a representative sample of crystals of the same habit. The crystal mounted on a nylon loop was then placed in a cold nitrogen stream (Oxford) maintained at 110 K. A BRUKER Venture X-ray (kappa

geometry) diffractometer was employed for crystal screening, unit cell determination, and data collection. The X-ray radiation employed was generated from a Cu-Iμs X-ray tube (K_α = 1.5418Å with a potential of 50 kV and a current of 1.0mA). All diffractometer manipulations, including data collection, integration and scaling were carried out using the Bruker APEX3 software.[122] An absorption correction was applied using SADABS.[123] Systematic reflection conditions and statistical tests of the data suggested the space group *P*-1. A solution was obtained readily using XT/XS in APEX3.[122,124] Hydrogen atoms were placed in idealized positions and were set riding on the respective parent atoms. All non-hydrogen atoms were refined with anisotropic thermal parameters. PLATON suggests presence of voids (~47 $Å^3$), however with no electron density. Additionally, no residual electron density were found corresponding at the voids. Absence of additional symmetry was confirmed using PLATON (ADDSYM). The structure was refined (weighted least squares refinement on F^2) to convergence.[124,125] ORTEP-3 and POV-Ray were employed for the final data presentation and structure plots.[126,127]

X-Ray data collection, solution, and refinement for [71][$CH_{12}B_{11}$]. (CCDC number: 1915570)

A Leica MZ 75 microscope was used to identify a suitable black block with very well defined faces with dimensions (max, intermediate, and min) 0.402 x 0.385 x 0.376 mm^3 from a representative sample of crystals of the same habit. The crystal mounted on a nylon loop was then placed in a cold nitrogen stream (Oxford) maintained at 110 K. A BRUKER APEX 2 Duo X-ray (three-circle) diffractometer was employed for crystal screening, unit cell determination, and data collection. The X-ray radiation employed was generated from a Mo sealed X-ray tube (K_α = 0.71073Å with a potential of 40 kV and a current of 40 mA). All diffractometer manipulations, including data collection, integration and scaling were carried out using the Bruker APEX3

software.[122] An absorption correction was applied using SADABS.[123] Systematic reflection conditions and statistical tests of the data suggested the space group *C*2/*c*. A solution was obtained readily (Z=4; Z'=0.5) using XT/XS in APEX3.[4,6] Hydrogen atoms were placed in idealized positions and were set riding on the respective parent atoms. The C1a atom of the carborane could not be located due to the symmetry. Initially all the carborane atoms were assigned boron. C1a was assigned based on the thermal ellipsoid and was set as disorder. Hydrogen atoms could not be located on the carborane from the residual electron density map, and were placed only to satisfy geometry. All non-hydrogen atoms were refined with anisotropic thermal parameters. Solvent molecules (dichloromethane) which were partially occupied and disordered, could not be modeled and were MASKed using OLEX2.[125] Absence of additional symmetry were confirmed using PLATON (ADDSYM). The structure was refined (weighted least squares refinement on F^2) to convergence.[124,125] ORTEP-3 and POV-Ray were employed for the final data presentation and structure plots.[126,127]

X-Ray data collection, solution, and refinement for [71][$SbCl_6$]$_2$. (CCDC number: 1915571)

A Leica MZ 75 microscope was used to identify a suitable brown needle with very well defined faces with dimensions (max, intermediate, and min) 0.192 x 0.042 x 0.027 mm^3 from a representative sample of crystals of the same habit. The crystal mounted on a nylon loop was then placed in a cold nitrogen stream (Oxford) maintained at 110 K. A BRUKER Quest X-ray (fixed-Chi geometry) diffractometer with a PHOTON II detector was employed for crystal screening, unit cell determination, and data collection. The X-ray radiation employed was generated from a Mo-Iμs X-ray tube (K_α = 0.71073Å). All diffractometer manipulations, including data collection, integration and scaling were carried out using the Bruker APEX3 software.[122] An absorption

correction was applied using SADABS.[123] Systematic reflection conditions and statistical tests of the data suggested the space group $P2_1/n$. A solution was obtained readily (Z=2; Z'=0.5) using XT/XS in APEX3.[122,124] A molecule of dichloromethane was found solvated. Hydrogen atoms were placed in idealized positions and were set riding on the respective parent atoms. All non-hydrogen atoms were refined with anisotropic thermal parameters. Elongated ellipsoids on atoms C25, C20-C22, and the solvent Cl1s, Cl2s, C3s suggested disorder which were successfully modeled between two positions each with an occupancy ratio of 0.64:0.36. Appropriate restraints and constraints were applied to keep the bond distances, angles, and thermal ellipsoids meaningful. Final formula: $C_{50}H_{82}Cl_2N_2P_4Pd_2 \cdot 2(CH_2Cl_2) \cdot 2(SbCl_6)$. Absence of additional symmetry and voids were confirmed using PLATON (ADDSYM). The structure was refined (weighted least squares refinement on F^2) to convergence.[124,125] ORTEP-3 and POV-Ray were employed for the final data presentation and structure plots.[126,127]

3.4.5 ORTEP Graphs

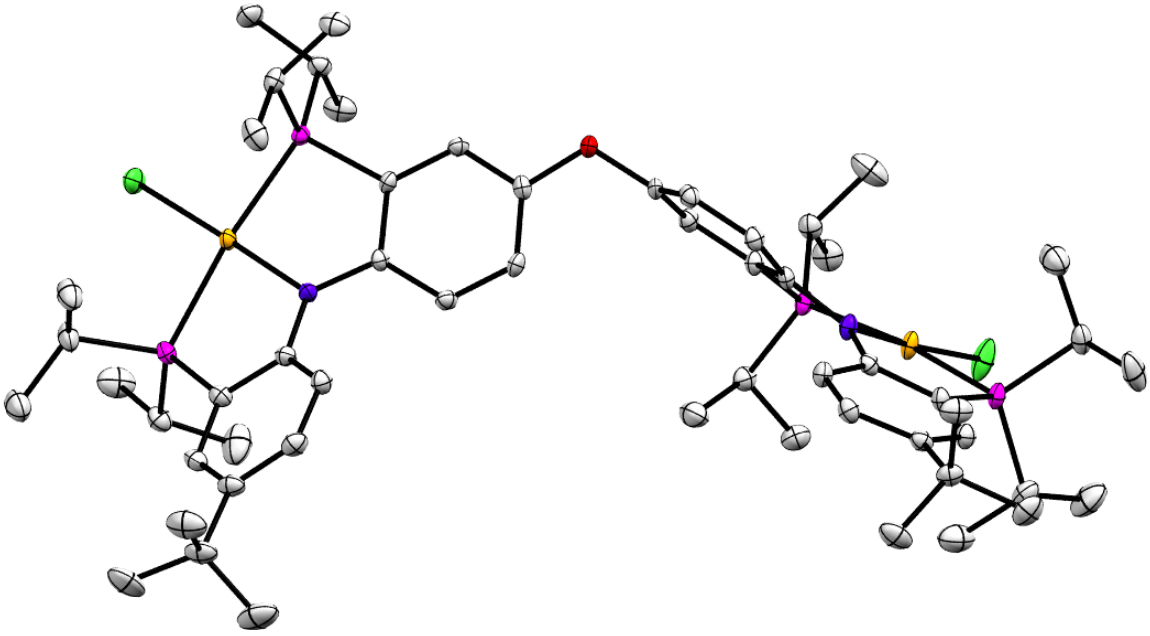

Figure III-11. ORTEP of complex **69**. The ellipsoids are set at the 50% probability level, and hydrogen atoms are omitted for clarity.

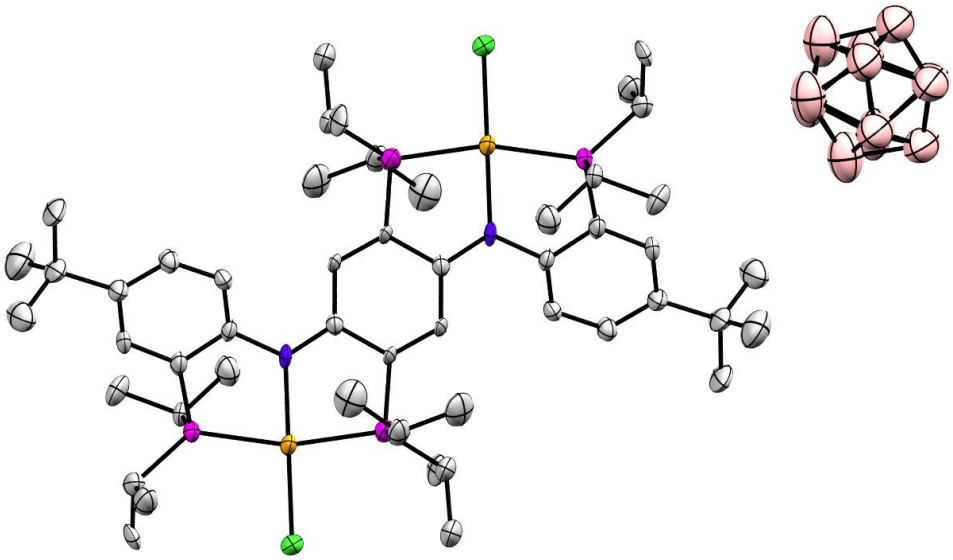

Figure III-12. ORTEP of complex [**71**]$CH_{12}B_{11}$. The ellipsoids are set at the 50% probability level, and hydrogen atoms are omitted for clarity.

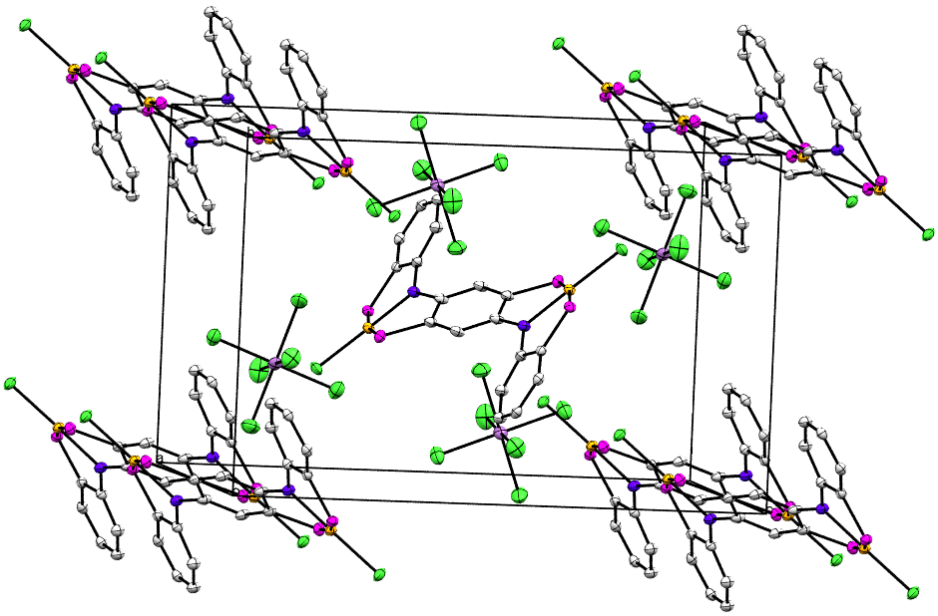

Figure III-13. ORTEP of [**3**][$SbCl_6$]$_2$ unit cell. The ellipsoids are set at the 50% probability level. The diisopropryl groups on phosphine, tert-butyl groups, solvents and hydrogen atoms are omitted for clarity.

3.4.6 UV-vis-NIR Spectrum

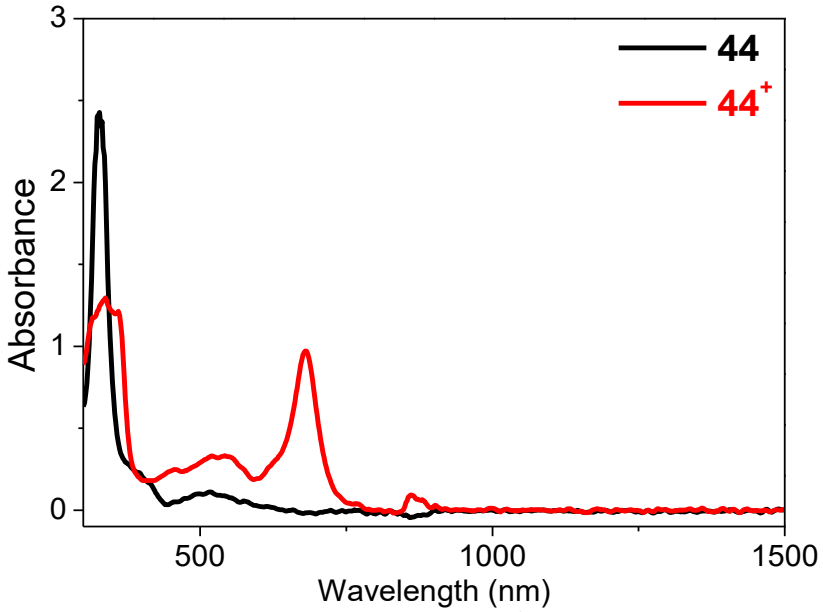

Figure III-14. UV-vis-NIR spectrum of approx. 1 x 10^{-4} M **44** in CH_2Cl_2, where the **44**$^+$ was in situ generated by addition of 1.2 eq of [Fc]$CH_{12}B_{11}$ as the oxidant.

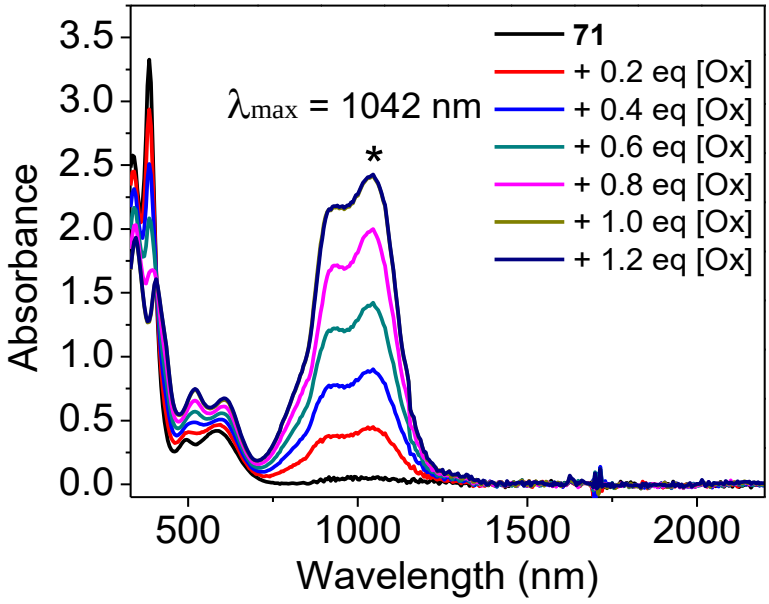

Figure III-15. UV-vis-NIR spectrum of approx. 1 x 10^{-4} M complex **71** in CH_2Cl_2, where the [**71**] $CH_{12}B_{11}$ was in situ generated by stepwise addition of 1.2 eq of [Fc]$CH_{12}B_{11}$ as the oxidant [Ox].

*3.4.7 Spectroelectrochemical Analysis of Complex **4***

Spectroelectrochemical measurements were conducted with a Shimadzu UV3600 UV−vis-NIR spectrophotometer and a 273A potentiostat (Princeton Applied Research). The measurement was carried out in a honeycomb spectroelectrochemical cell (Pine Research Instrumentation, Inc.) composed of a quartz UV-vis cell (path length = 1.7 mm), a gold electrode chip and a mini Ag/AgCl reference electrode. Before taking a scan of an absorption spectrum, the potential was held at a constant voltage for 300 seconds. The range of potentials vs the Ag/AgCl reference electrode applied in these spectroelectrochemical experiments is consistent with the redox potentials vs Fc/Fc^{+} determined in cyclic voltammetry experiments.

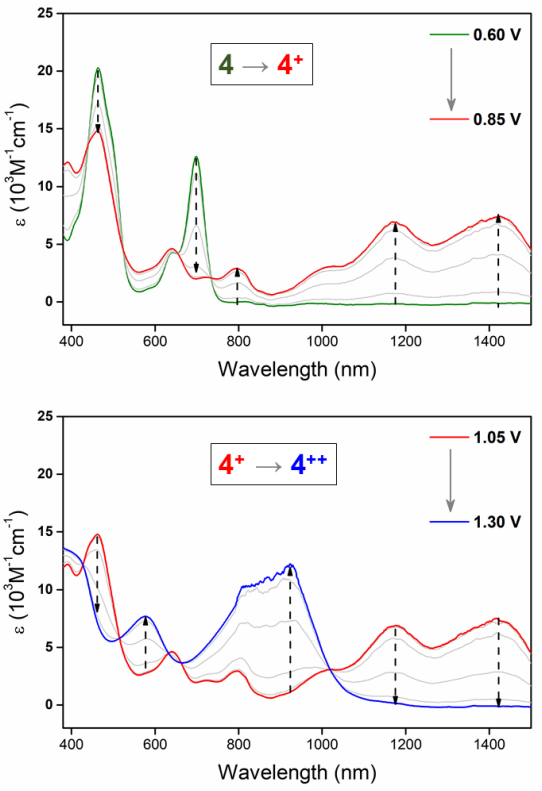

Figure III-16. UV-vis-NIR absorption changes of the solution of **4** in CH_2Cl_2 (7.6×10^{-4} M), with 0.10 M $^{n}Bu_4NPF_6$ as the electrolyte, upon stepwise applications of potentials on the working electrode (Step height: 0.05 V, *vs* Ag/AgCl) from +0.60 V to +0.85 V (top), +1.05 V to +1.30 V (bottom).

3.4.8 Theoratical Calculations

DFT calculations were carried out using Gaussian 09.[10] Geometry optimizations were performed with the M06[11] functional with the LANL2DZp[12] basis set for all atoms. To simplify the computations, –Si(*i*Pr)$_3$ groups were replaced by –Si(CH$_3$)$_3$ groups and the *t*Bu groups were replaced by methyl groups.

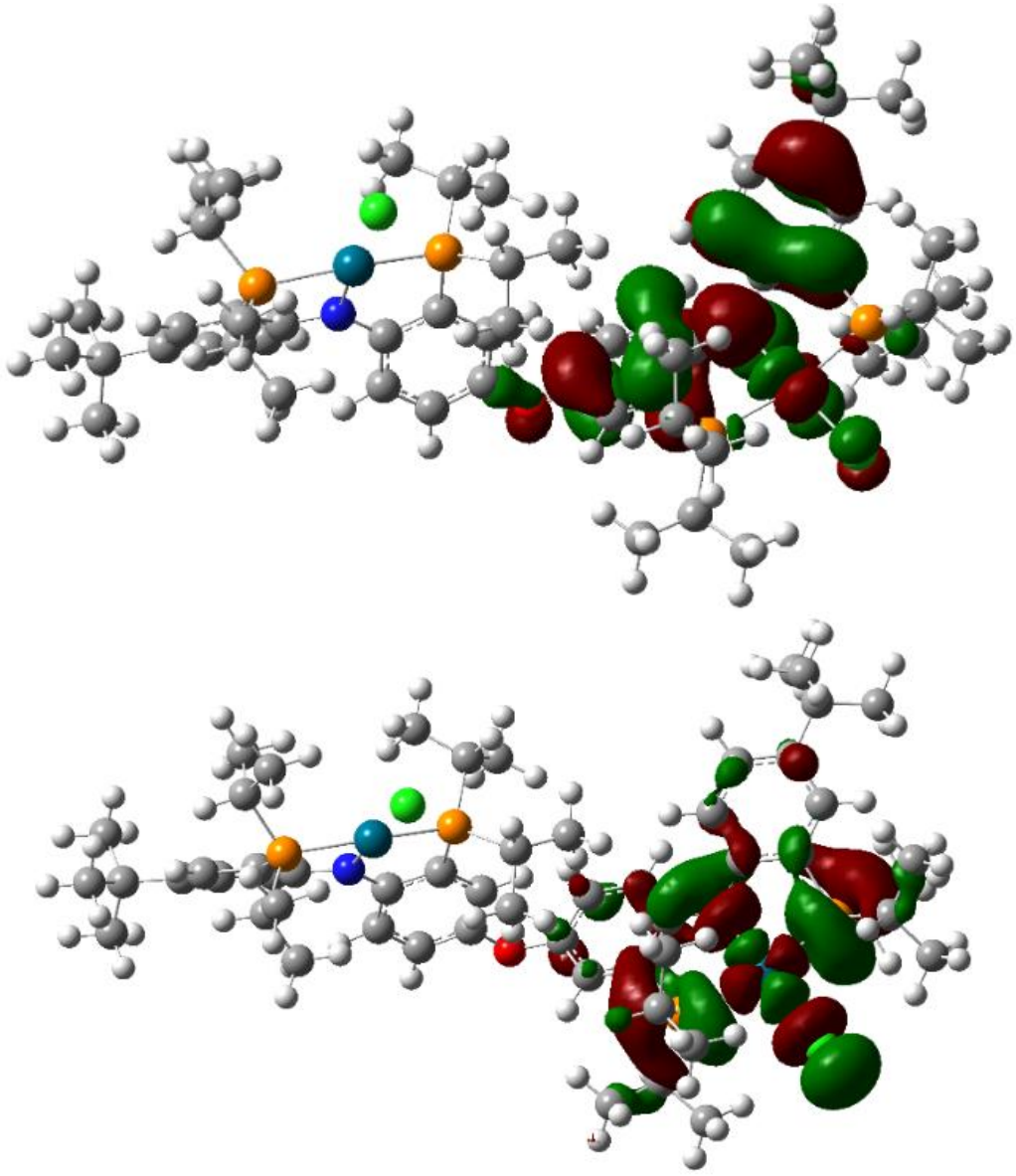

Figure III-17. HOMO (upper) and LUMO (lower) for complex **69** (isovalue = 0.02).

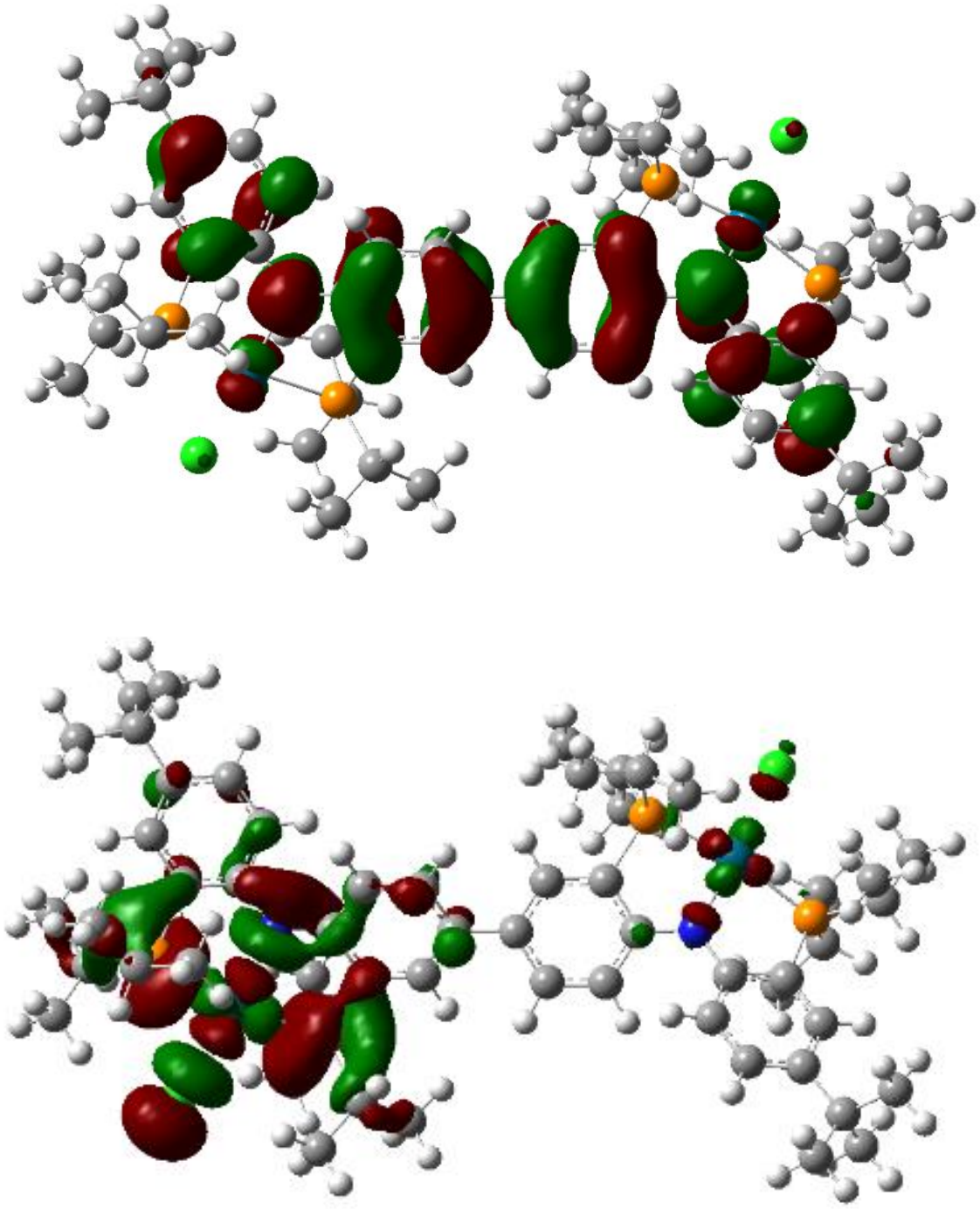

Figure III-18. One of the two degenerate HOMOs (upper) and one of the two degenerate LUMOs (lower) for complex **70** (isovalue = 0.02).

CHAPTER IV

Approaches to Group 10 Metallapolymers Derived from Bis(pincer) Complexes

4.1 Introduction

Design of novel conducting metallapolymers is an intriguing field for chemists. This platform, built up by three major components: metal, ligand, and π-conjugated polymer backbone, enables amalgamation of multiple functional moieties.[139,172–174] Desired properties arising from the metal and π-conjugated backbone can also be approached synergistically. That is, one could take advantage of the properties from the complex and polymer independently, or craft a new function through their cooperation.[173,175] The many possibilities allow numerous applications such as light-harvesting,[75,176] luminescent,[177–180] chemical sensing,[181,182] memory storage,[66,183,184] and solar cell.[185] Metallapolymers containing a transition metal in the main chain should be highly signal-responsive. Perturbation of the electronic nature of the metal centers such as changing the oxidation state or additional ligand binding will strongly influence the conductive current. For example, in Figure IV-1, a cobalt (II) chelated salen metallapolymer was situated in between two electrodes. After exposure to nitric oxide, Co(II) was steadily converted to Co(III) thereby interrupting the conducting current and resulting in an increased resistance.

Although the idea is fascinating, applicable conjugated metallapolymers of this type are rare due to the challenges in polymerization methodology. Constructing polymer via metal-ligand coordination is not as common as via organic covalent bond since the bond could be labile or the metal center can undergo an undesired side reaction such as oxidative addition or reductive elimination. Multi-dentate ligands such as porphyrins,[186] salens,[81,181,187] or terpyridines,[65,188,189] are good candidates to address the bond lability problem. However, this will often cause low solubility

due to the large peripheral π-arenes. Overall, it is essential to augment the toolbox by developing more available metal complexes as the polymer precursors.

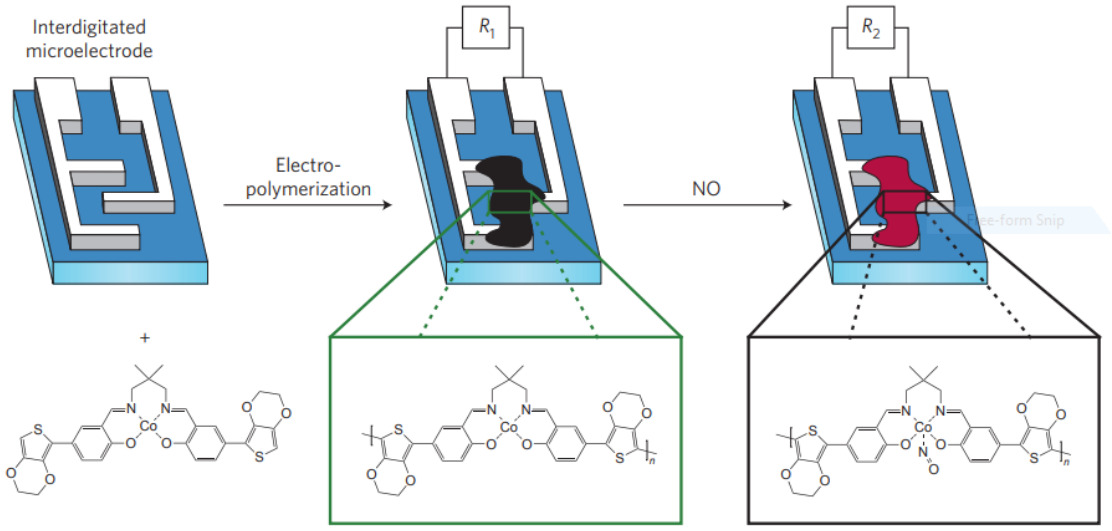

Figure IV-1. A cobalt-containing metallapolymer for sensing nitric oxide. Reproduced with permission from ref. 181.

Pincer ligands are tridentate and prefer to coordinate metals in the meridional fashion.[15,16,160] The planar structure and multi denticity are both promising features for metallapolymer preparation.[15–17] In addition, the diarylamido PNP pincer ligand[160] our group has been interested in has a metal-stabilized ligand-based redox center. The organic analogue of this type are arylamines, which have been widely used as a charge carrier in p-type semiconducting material.[27,38,94,190] In addition, it is also important to develop methods for establishing strong covalent σ-bonds with π-conjugation, such as the metal-alkynyl bond,[73,74,84,150] between pincer complexes and bridging ligands. If only weak coordination interaction for self-assembly is given, it could cause a structural instability during the charge accumulation or dissociation at high temperature. Recently, we reported on connecting two (^{Me}PNP) complexes with ynediyl bridges, which are proper units for π-conjugation extension.[150] Another piece of work was the synthesis of bis(pincer) PNP complexes (**69-72** in

Section 3.2.1). It had two potential functional sites for building up the ynediyl bridges. We anticipated that with the combination of these two methods, a novel type of redox-active PNP metallapolymer could be achieved. In this work, we would like to demonstrate the preliminary results stemming from this approach. Additionally, a notation of bis(pincer) ligands is introduced for convenience. The ligand backbone of compound **85** is called PNPOPNP; **86** is called PNPbPNP; **87** is called PNPpPNP; **92** is called NNNpNNN.

4.2 Results and Discussion

4.2.1 Synthesis of Bis(pincer) Polymerization Precursors

The synthesis of bis(pincer) complexes as the precursors of polymerization was accomplished as shown in Scheme IV-1, IV-2 and IV-3. First, the oxygen-bridged bis(pincer) ligand PNPOPNP (**85)** reported in the previous chapter was utilized to install group 10 metals by N–Methyl cleavage metalation. $NiCl_2$, $Pd(COD)Cl_2$, and $Pt(COD)Cl_2$, were then used as metal sources to obtain compounds **93**, **69**, and **94** by thermolysis in toluene solution. The crude products after workup can be recrystallized from $MeOH/CH_2Cl_2$ as we discovered in the synthesis of compound **69.** The yields of Ni (**93**) and Pt (**94**) bis(pincer) complexes were 71% and 83%, respectively. The Pd complexes with different backbones, PNPOPNP (**69)** and PNPbPNP (**70)** were selected to undergo ethynylation in order to build up M–C≡C–M in the desired polymers. Reactions of **67** and **70** with slight excess of LiCCH resulted in the formation of ethynyl complexes **95** and **96**. The purification method was the same as that reported[150] for monomeric (^{Me}PNP)MCCH pincer complexes.

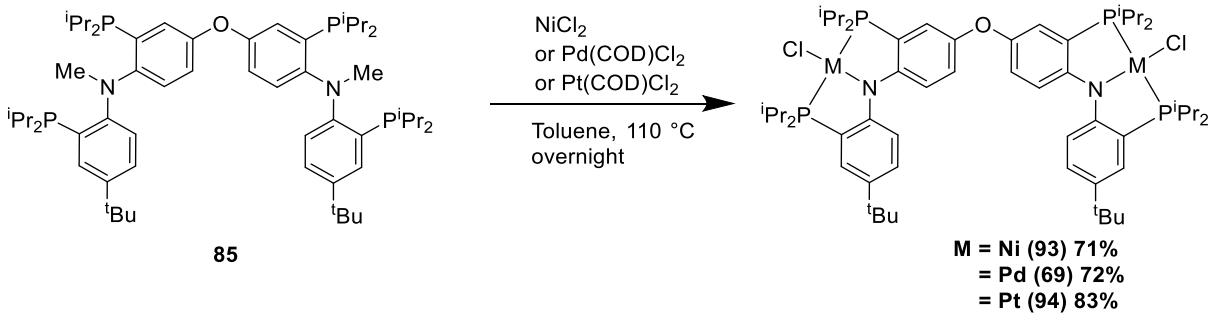

Scheme IV-1. Synthesis of **93**, **69** and **94**.

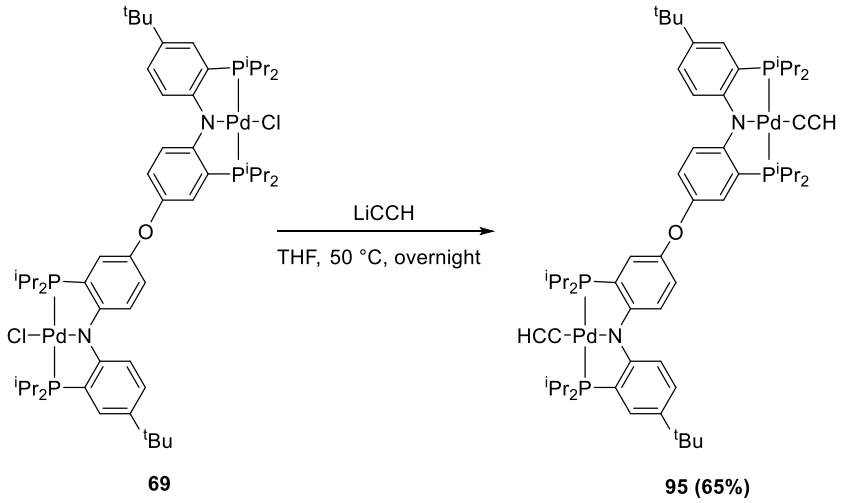

Scheme IV-2. Synthesis of **95**.

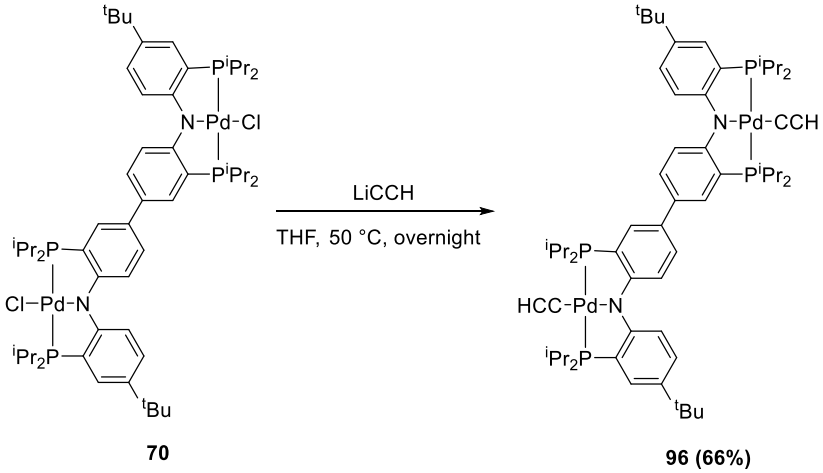

Scheme IV-3. Synthesis of **96**.

4.2.2 Synthesis of Tetrametallic Pincer Complexes

The tetrametallic complexes were prepared to better understand charge transport in M–C≡C–M metallapolymers. Two bis(pincer) cores, PNPOPNPPd and PNPbPNPPd were selected. First, two equivalents of (^{Me}PNP)PdCCH (**47**) was deprotonated by LDA. After 5 to 10 min, the solution was combined with **69** or **70** and was heated to 50º C for 3 hours to yield tetrametallic pincer complexes **97** and **98**, respectively. In addition, one interesting observation was that while conducting the reactions for 15 hours under room temperature instead of heating, the reaction with compound **47** and **69** can still result in an apparently complete conversion to **97** but the reaction with **47** and **70** does not fully give compound **98** (Figure IV-10) and the rest of **47** was observed.

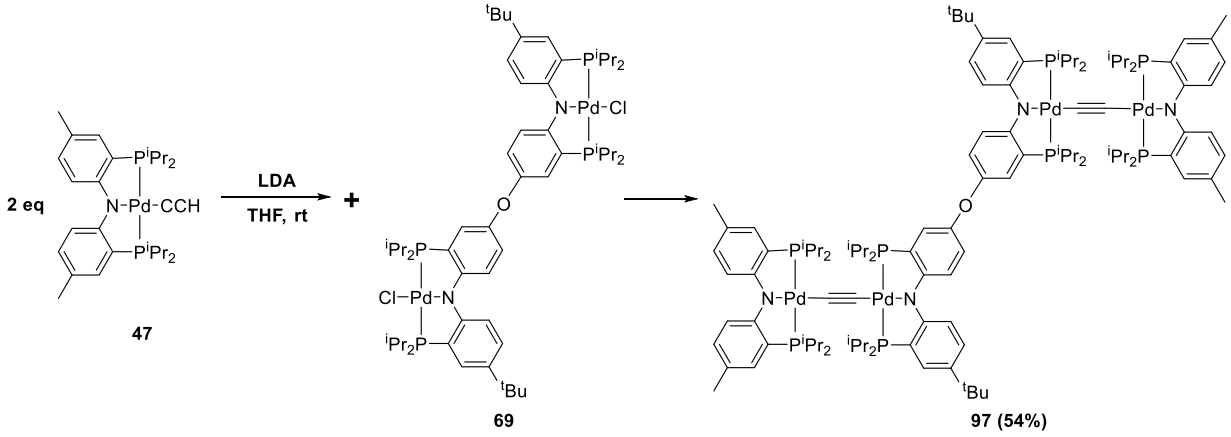

Scheme IV-4. Synthesis of tetrametallic pincer complex **97**.

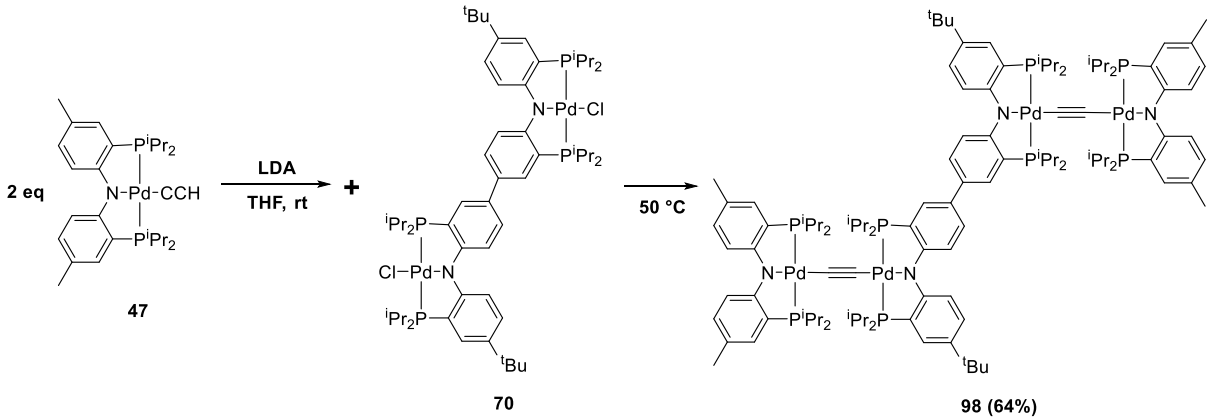

Scheme IV-5. Synthesis of of tetrametallic pincer complex **98**.

4.2.3 Polymerization of PNPOPNP(MCl)$_2$ with 1,4-Diethynylbenzene

In order to test if a metallapolymer can be made by reacting bis(pincer) complexes with dialkynes and LDA, 1,4-diethynylbenzene was selected as a model of dialkynes. A J. Young was loaded with LDA, 1,4-diethynylbenzene and the PNPOPNP(MCl)$_2$ complex (**69**, **93**, or **94**), followed by the addition of THF . The resulting concentration was 0.05 M in THF. After 15 hours under room temperature, ^{31}P NMR spectra were recorded. The ^{31}P NMR signals of the Ni (**99**) polymer product were observed at 46.0 and 45.6 ppm and the ^{31}P NMR signals of the Pd (**100**) polymer were observed at 51.2 and 50.9 ppm (Figure IV-11). Together with the absence of ^{31}P chemical shifts of the starting materials, we assumed those reaction were completed. On the other hand, no obvious ^{31}P NMR signals were detected from the THF solution of Pt bis(pincer) reaction mixtures**.** The crude products were diluted by 5 mL THF and analyzed by gel permeation chromatography (GPC) (Table IV-1). The repeating unit *n* for the Ni (**99**) and Pd (**100**) polymers reached 8, whereas with Pt (**101**) it was only 4. It was observed that the Pt (**101**) reaction mixture formed large amounts of yellow precipitate after few minutes, whereas the Ni (**99**) and Pd (**100**) did not form observable precipitates in solution. Although LiCl as the byproduct can potentially preticipate out, the amount of it should be too small to be observed in those highly colored solutions. The observation of a significant amounf of precipitate implies that the solubility of Pt (**101**) was significantly lower than Ni (**99**), and Pd (**100**). Other polymerization reactions were conducted by changing the reaction temperature to 70 ºC. The results showed the repeating unit of Pd (**100**) polymer increased by 2 but those of Ni (**99**) and Pt (**101**) did not significantly increase.

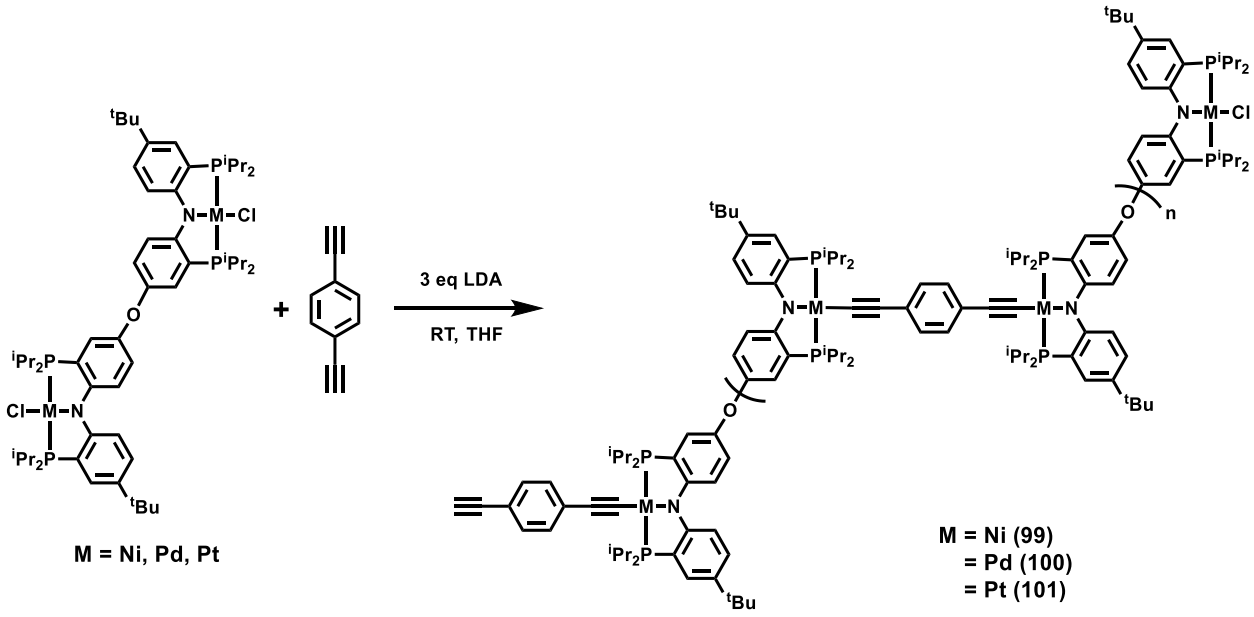

Scheme IV-6. Polymerization of PNPOPNP(MCl)$_2$ with 1,4-diethynylbenzene.

Table IV-1. GPC results for polymer **99-101**.

Complex	Reaction Temp.	M_n	M_w	n	$Đ$
Ni (**99**)	25 ºC	10103	11894	8.63	1.177
Ni (**99**)	70 ºC	3213	3289	2.74	1.024
Pd (**100**)	25 ºC	10436	14503	8.24	1.390
Pd (**100**)	70 ºC	12891	13739	10.2	1.069
Pt (**101**)	25 ºC	6030	6935	4.18	1.15
Pt (**101**)	70 ºC	6727	7302	4.66	1.086

4.2.4 Preparation of μ-Ethynediyl-Bridged Bis(pincer) Pd Metallapolymers.

The preparation of μ-ethynediyl-bridged bis(pincer) Pd metallapolymers was conducted imilarly to the method described in Section 4.2.3. First, for polymer **102**, a J. Young was loaded with LDA, PNPOPNP(PdCCH)$_2$ (**95**) and PNPOPNP(PdCl)$_2$ (**69)**. THF solvent was added last, resulting in a

0.05 M solution. This method was also used to prepare polymer **103** (**96**+**69**) and **104** (**96**+**70**), as shown in Scheme IV-6. After heating the mixture at 70 ºC for 15 h, ^{31}P NMR spectra were recored. Polymer **102**, which contained only PNPOPNP units, gave rise to two ^{31}P NMR signals at 46.6 and 46.0 ppm (Figure IV-12). Polymer **104** containing only PNPbPNP units also displayed just two ^{31}P NMR resonancesat 46.7 and 46.5 ppm.For the polymer **103** containing two different units, PNPOPNP and PNPbPNP, two ^{31}P peaks were found at 46.5 and 46.0 ppm with the integral ratio close to 3 : 1. It could be due to the accidental overlap of ^{31}P peaks. The ^{31}P NMR signals of the starting materials were not observed in those reaction mixtures. The solutions containing the reaction mixtures were then filtered through a plug of celite and the filtrate were analyzed by GPC. The results (Table IV-2) showed that polymer **104** had the highest M_n. The repeating unit *n* was determined to be around 8-9. The polymer **103** had thesecond highest M_n and the M_n of polymer **102** was the lowest. Another set of experiments for synthesizing polymer **102** and **104** was conducted with the concentration of **95** and **69** increased to 0.1 M. These reactions resulted in M_n values for **102** and **104** that were higher than those prepared from 0.05 M of **95** and **69**.

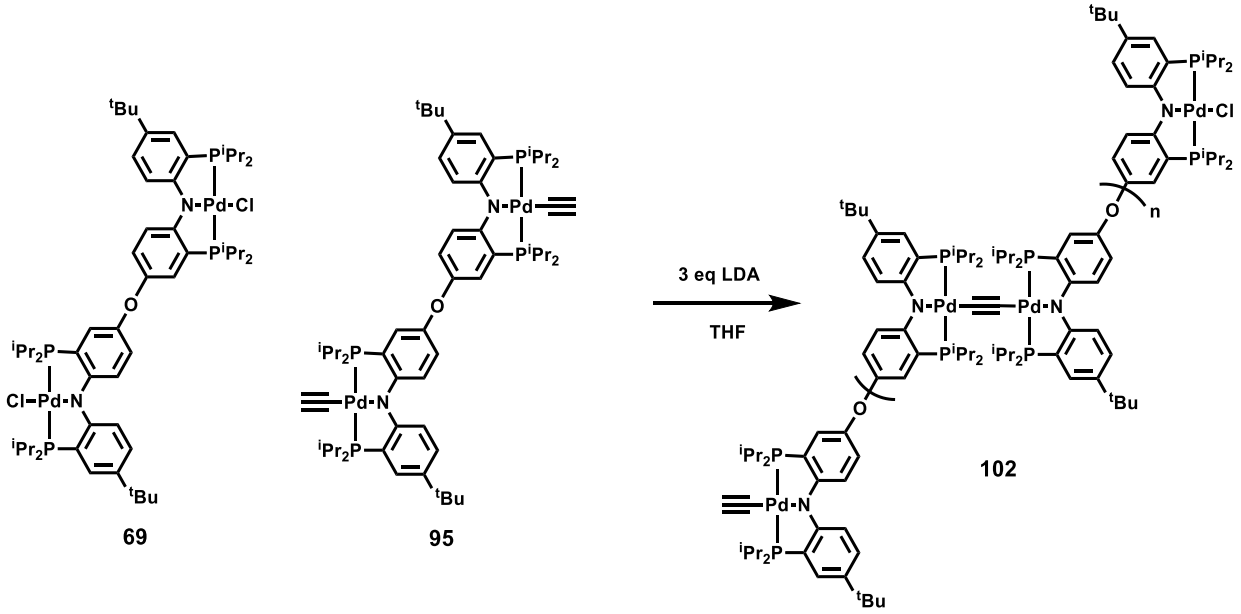

69 95 102

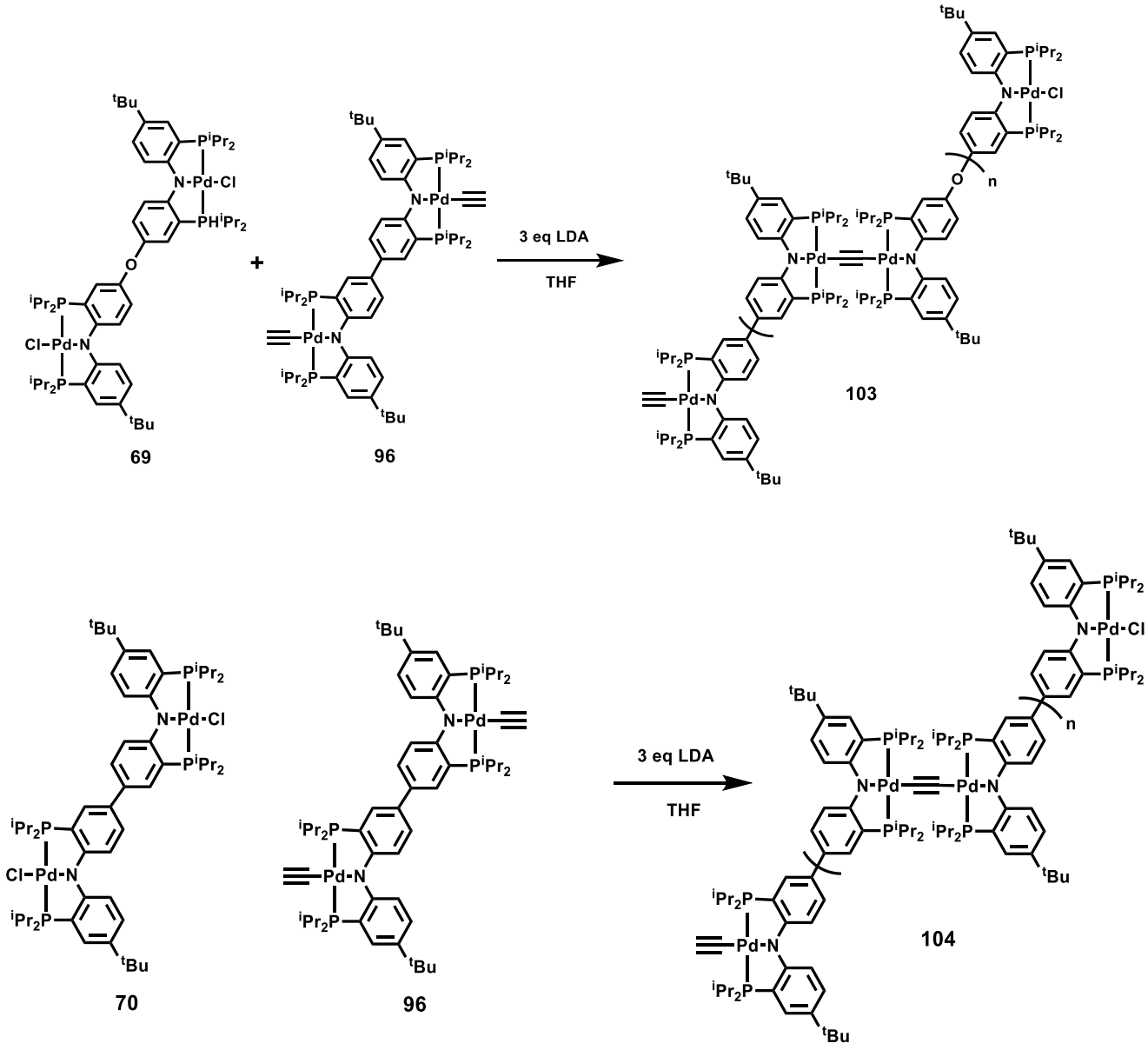

Scheme IV-7. Polymerization of μ-ethynediyl-bridged bis(pincer) complexes **102-104**.

Table IV-2. GPC results of **102-104** polymers.

Polymer	*Conc.*	M_n	M_w	*n*	*Đ*
95 + 69 (102)	0.05 M	7344	8174	6.30	1.107
96 + 69 (103)	0.05 M	8987	11075	7.77	1.235
96 + 70 (104)	0.05 M	9989	11334	8.69	1.120
95 + 69 (102)	0.1 M	18908	25343	16.2	1.340
96 + 70 (104)	0.1 M	12974	16488	11.3	1.302

4.2.5 Electrochemical Studies

Cyclic votammograms of tetrametallic complexes **97** and **98**, as well as the metallapolymers **102** and **104** were collected (Figures IV-2 and Table IV-3) with 0.1 M $^{n}Bu_4NPF_6$ as the supporting electrolyte in CH_2Cl_2. In complex **97**, multiple quasi-reversible waves were observed. Differential pulse voltammogram (DPV) was conducted to confirm the current intensities (Figure IV-4). Four peaks at 1:1:1:1 ratio were found. The first and second oxidation potentials were close to μ-ethynediyl-bridged (^{Me}PNP)PdC≡CPd(PNP^{Me}) (**50)**. We proposed a pathway in Scheme IV-7 based on these results. The first oxidation event happens on the (^{Me}PNP)Pd wings and the second happens on the other side of PNPOPNP central core. The oxidation potentials of these two should be intrinsically close and we found the difference, 0.04 V to be quite small. The third and fourth oxidation events could happen on the central PNPOPNP backbone first, then on the (^{Me}PNP)Pd wings or the other way around. The available information was not sufficient to distinguish these two possibilities. Polymer **102**, which is mostly composed of the –Pd(PNPOPNP)PdC≡C–

repeating unit, should have oxidation potentials close to the first and the last of **97**. Indeed, that was what we observed for polymer **102** (-0.34 and -0.06 V, respectively).

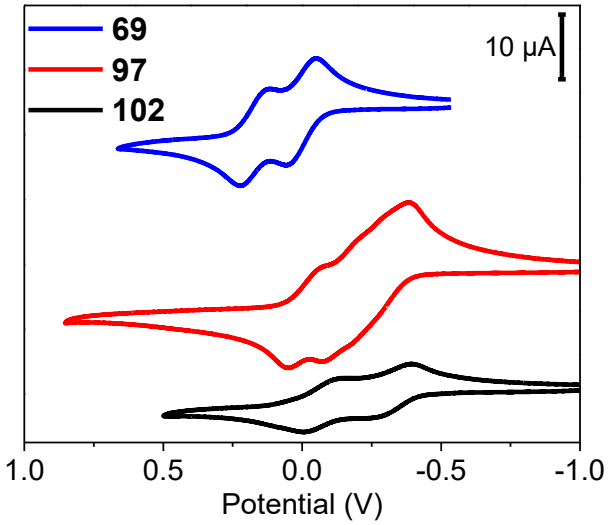

Figure IV-2. Cyclic voltammograms of ca. 1 x 10^{-3} M **69**, **97** and **102** ($^{n}Bu_4NPF_6$ 0.1 M in CH_2Cl_2, 100 mV s^{-1}, vs Fc^{+}/Fc).

Table IV-3. Summary of oxidation potential in Figure IV-2.

Compound	$E^{1}_{1/2}$ (V)	$E^{2}_{1/2}$ (V)	$E^{3}_{1/2}$ (V)	$E^{4}_{1/2}$ (V)	ΔE (V)
69	0.00	0.17	-	-	0.17
97	-0.33	-0.27	-0.18	-0.05	0.04, 0.09, 0.13
102	-0.34	-0.06	-	-	0.28
50*	-0.40	-0.25			0.15

***with** nBu$_4$NBAr$^{F}_4$ as the supporting electrolyte.

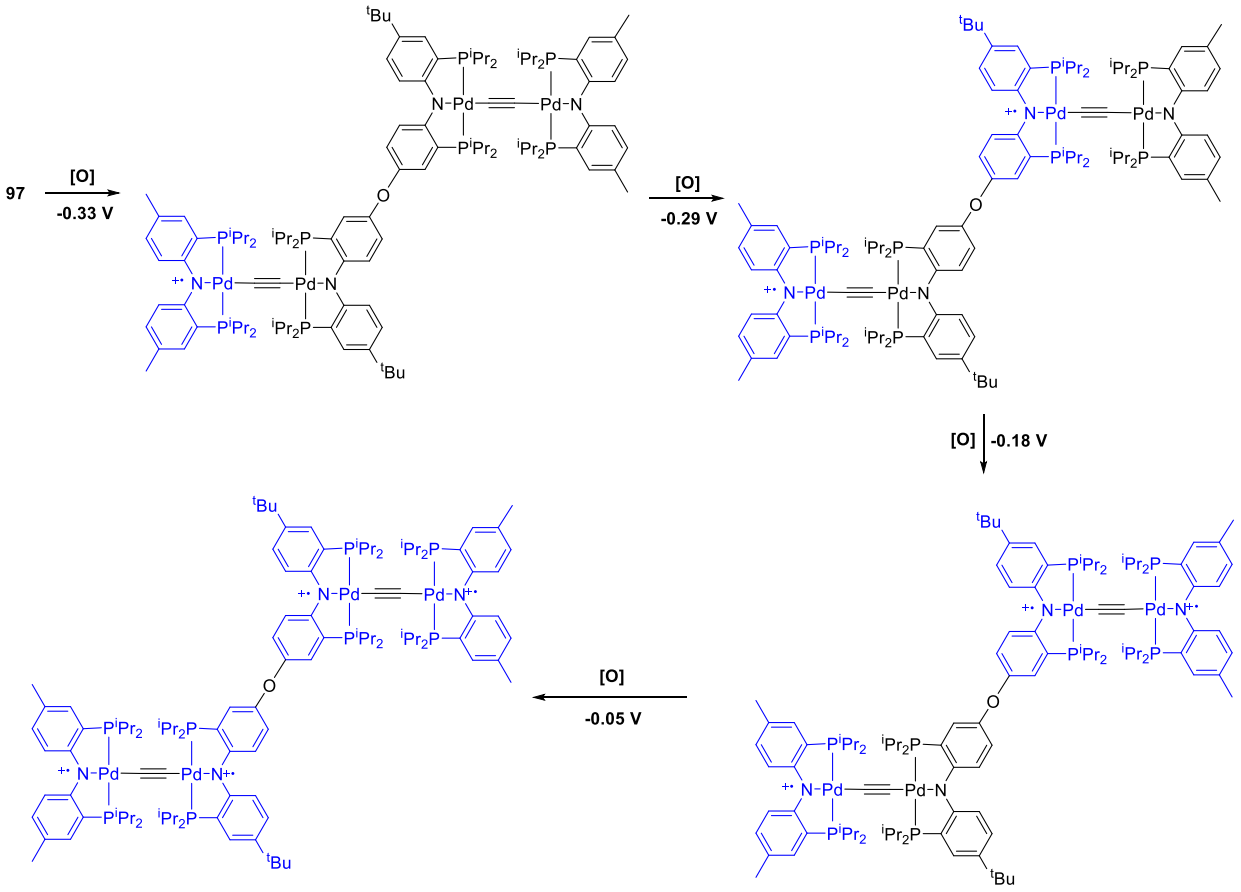

Scheme IV-8. Proposed oxidation pathway of compound **97**.

Cyclic votammogram of **98** showed three oxidation events: -0.40, -0.17, 0.00 V. In this case, the separation of first and second events was higher than that of **97** and the current of second peak was significantly higher than the other two. The DPV result also confirmed that the ratio of current intensities was close to 1:2:1. Based on this observation, we proposed in compound **98**, the first oxidation happened not on the (^{Me}PNP)Pd wings but on the central PNPbPNP backbone (Scheme IV-8). It is also supported by the fact that the first oxidation potential of **70** (-0.13 V) is lower than **69** (0.00 V). The strong redox coupling of the central bis-amido diphenyl moiety would create a totally delocalized MV state that leaded the two (^{Me}PNP)Pd outside wings electronically equivalent. Thus the next two electrons are removed from the outside wings at the same potential,

while the last oxidation then happens on the central backbone. The oxidation potentials of polymer **104**, observed at -0.50 and -0.12 V, were comparable to compound **98**. Notably, the peak separation of **102** and **104** were close to the "addition" from each separated units. For example, $\Delta \boldsymbol{E}$ of **104** is 0.38 V and the sum of $\Delta \boldsymbol{E}$ of compound **70** and **50** is 0.45 V.

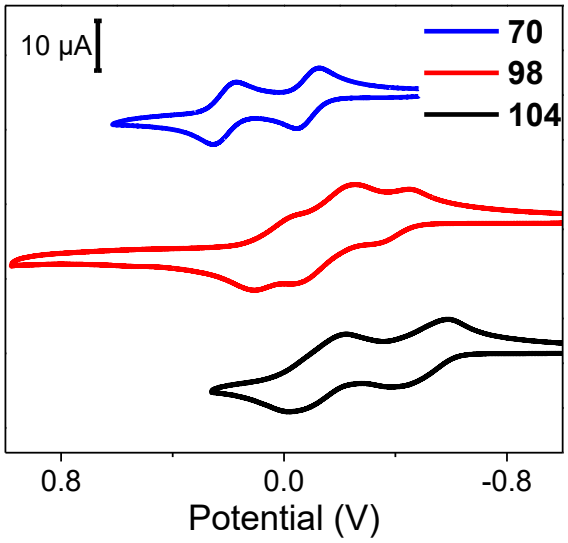

Figure IV-3. Cyclic voltammograms of ca. 1 x 10^{-3} M **70, 98,** and **104** ($^{n}Bu_4NPF_6$ 0.1 M in CH_2Cl_2, 100 mV s^{-1}, vs Fc^{+}/Fc).

Table IV-4. Summary of oxidation potential in Figure IV-3.

Compound	$\boldsymbol{E^1_{1/2}}$ **(V)**	$\boldsymbol{E^2_{1/2}}$ **(V)**	$\boldsymbol{E^3_{1/2}}$ **(V)**	$\Delta \boldsymbol{E}$ **(V)**
70	-0.13	0.21	-	0.34
98	-0.40	-0.17	0.00	0.23, 0.17
104	-0.50	-0.12	-	0.38
50*	-0.40	-0.25		0.15

***with** $n$$Bu_4NBAr^F{}_4$ as the supporting electrolyte.

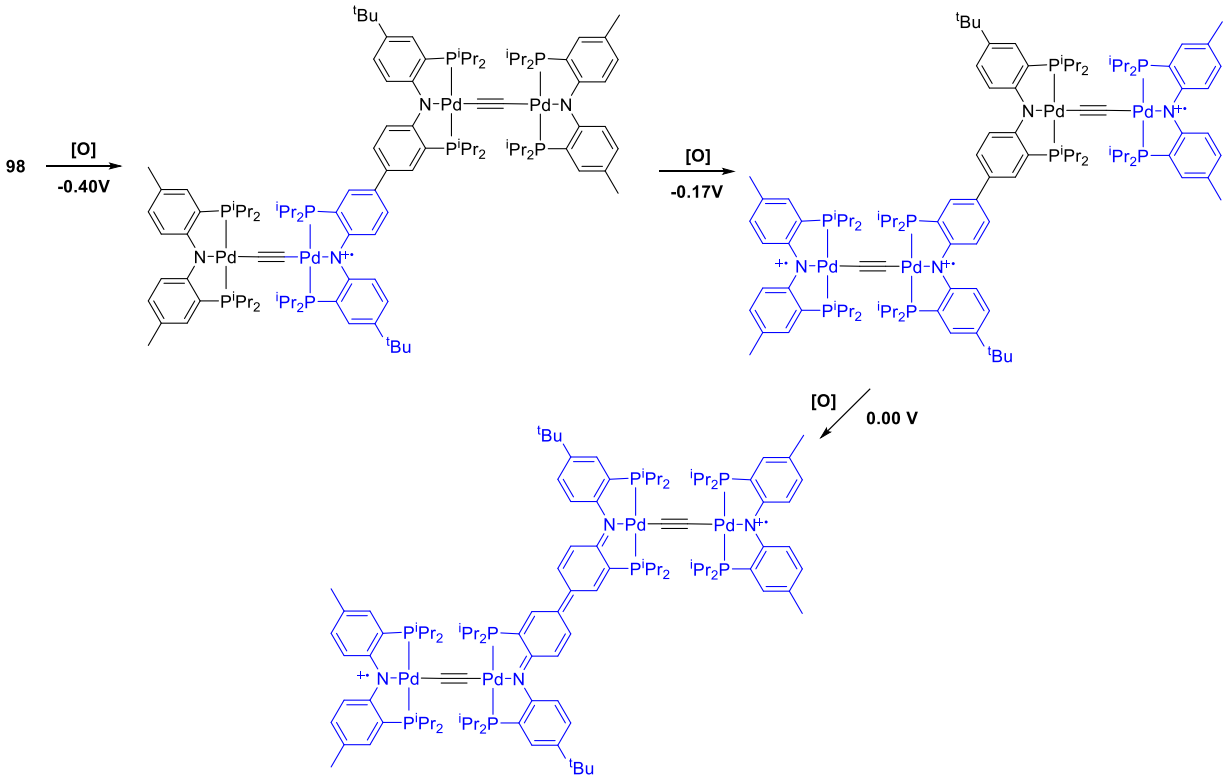

Scheme IV-9. Proposed oxidation pathway of compound **98**.

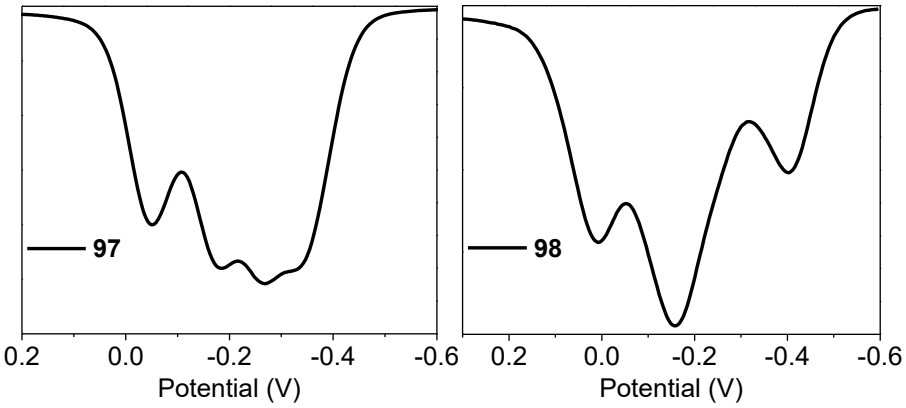

Figure IV-4. Differential pulse voltammograms of ca. 1 x 10^{-3} M **97** and **98** ($^{n}Bu_4NPF_6$ 0.1 M in CH_2Cl_2, 100 mV s^{-1}, vs Fc^{+}/Fc).

4.2.6 UV-vis-NIR Spectroscopy

The UV-vis-NIR spectra of complexes **97** and **98** and of their mono-oxidized derivatives **97**$^{+}$-**98**$^{+}$ were collected in CH_2Cl_2 solution (Figure IV-5 and Figure IV-6). The spectrum of neutral **97** did contain intensive characteristic features similar to **69.** After one electron oxidation, two bands at 670 and 1190 nm appeared. The absorption at 670 nm is proposed to be MLCT band[27,38,150] and the band at 1190 nm is proposed to be the IVCT of outside PNPPdCCPdPNP moieties.[150] Notably, the IVCT band of **97** is blue-shifted about 100 nm comparing to 1290 nm of compound **50** and the band shape deviates from Gaussian, indicating different electronic environment and asymmetrical nature. On the other hand, the spectrum of neutral **98** was partially oxidized by CH_2Cl_2 solvent or small amount of air. That is generally easy to happen given its high oxidation potential. After removal of one electron, the spectrum of **98**$^{+}$ was similar to mono-cationic PNPbPNP(PdCl)$_2$ (**70**$^{+}$) and the IVCT of outside PNPPdCCPdPNP moieties at around 1200 nm did not show up. This result implied the charge was mainly located at the more delocalized state on the central backbone, supporting what we proposed in Scheme IV-8.

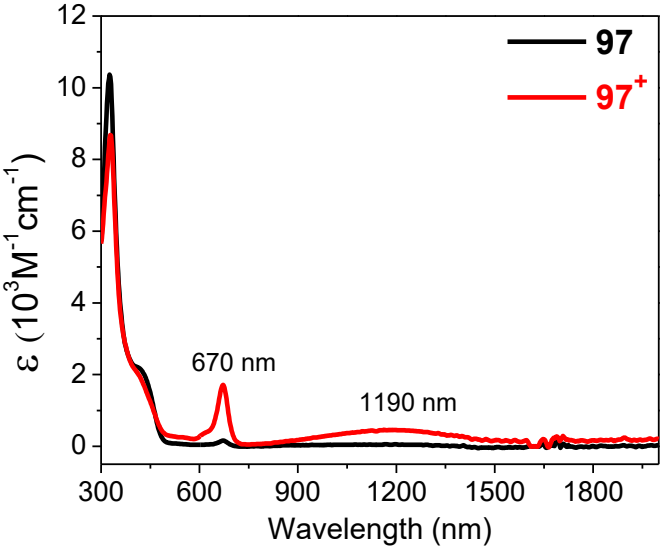

Figure IV-5. UV-vis-NIR spectrum of ca. 2 x 10^{-5} M complex **97** in CH_2Cl_2, where the [**97**] $CH_{12}B_{11}$ was in situ generated by addition of [Fc]$CH_{12}B_{11}$ as the oxidant [Ox].

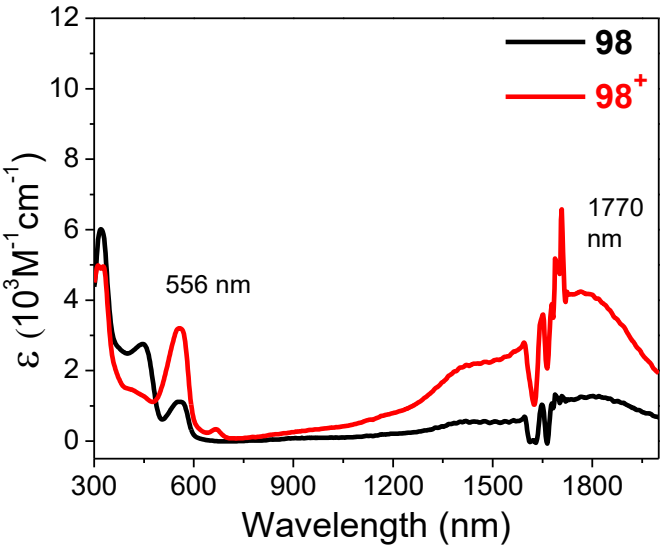

Figure IV-6. UV-vis-NIR spectrum of ca. 2 x 10^{-5} M complex **98** in CH_2Cl_2, where the [**98**] $CH_{12}B_{11}$ was in situ generated by addition of [Fc]$CH_{12}B_{11}$ as the oxidant [Ox].

The UV-vis-NIR spectroscopy experiments of polymer **102-104** were also conducted, shown in Figure IV-7. The overall absorption features of them are close to the tetrametallic pincer analogues **97** and **98**. The polymer **103** showed an intensive peak at around 300 nm, which presented in polymer **102** but not **104**. This feature could be the contribution from PNPOPNP backbone. The polymers could be steadily oxidized by adding one equivalent [Fc]$CH_{12}B_{11}$. The spectra of these cationic species were collected (Figure IV-8). Similarly, we observed the increase of MLCT at 688 nm and charge resonance band at 1710 nm for polymer **103** and **104** containing the biphenyl backbone. The MLCT absorptivity of polymers were found to be higher than those of **69** and **70** and tetrametallic complexes **97** and **98**. Adding another equivalent [Fc]$CH_{12}B_{11}$ in those solutions resulted in further oxidation (Figure IV-9). Polymers **103** and **104** would be expected to have the quinoidal close-shell structure (Figure III-5). Therefore, the charge resonance bands of them at 1710 nm were decreased, accompanied by the rise of MLCT band as we found in compound **70**$^{++}$. On the other hand, the broad peak in **102** at around 939 nm could be the π-π* transition of radical cationic complex that was observed in **50**$^{++}$ at around 950 nm.

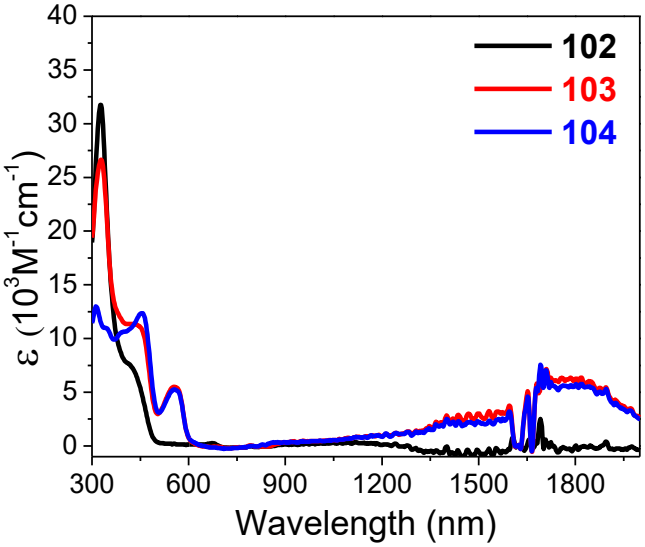

Figure IV-7. UV-vis-NIR spectrum of ca. 2 x 10^{-5} M polymers **102-104** in CH_2Cl_2.

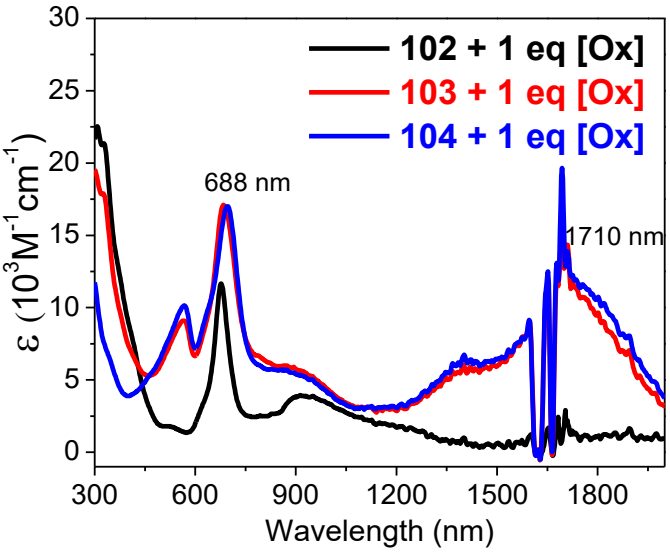

Figure IV-8. UV-vis-NIR spectrum of ca. 2 x 10^{-5} M polymer [**102-104**]$CH_{12}B_{11}$, which were in situ generated by addition of [Fc]$CH_{12}B_{11}$ as the oxidant [Ox].

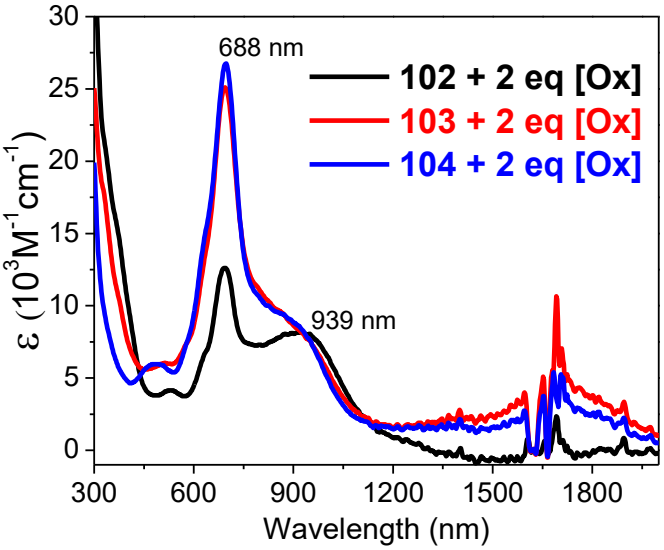

Figure IV-9. UV-vis-NIR spectrum of ca. 2 x 10^{-5} M polymer [**102-104**][$CH_{12}B_{11}$]$_2$, which were *in situ* generated by addition of [Fc][$CH_{12}B_{11}$]$_2$ as the oxidant [Ox].

4.3 Conclusion

In summary, we demonstrated the step-growth polymerization reaction for preparing novel group 10 metallapolymers based on two bis(pincer) ligand backbones, bis-amidodiphenyl ether, PNPOPNP, and bis-amidobiphenyl, PNPbPNP. For polymerization of PNPOPNP(MCl)$_2$ (M = Ni, Pd, Pt) with 1,4-diethynylbenzene, the [Ni] and [Pd] polymers reached 8 repeating units. For the PNPOPNP backbone metallapolymer (–Pd(PNPOPNP)PdC ≡ C–)$_n$, the repeating unit was determined to be ca. 16. On the other hand, for the metallapolymer (–Pd(PNPbPNP)PdC≡C–)$_n$, the repeating unit was 11.

The tetrametallic pincer complexes based on the PNPOPNP or PNPbPNP central backbone were synthesized with (^{Me}PNP)PdC≡C– as side wings. With four possible oxidation sites, the multiple peaks observed on CV and DPV illustrated the order of oxidation events happened on PNP. The PNPOPNP backbone tetrametallic complex has the outside-center-outside-center order and the PNPbPNP backbone tetrametallic complex has the center-outside-center order. This proposed

pathway is relating to the extent of delocalization on central backbone and also supported by spectroscopical evidences.

4.4 Experimental Details

4.4.1 General Considerations

Unless specified otherwise, all manipulations were performed under an Ar atmosphere using standard Schlenk line or glovebox techniques. Toluene, diethyl ether, pentane, and isooctane were dried and deoxygenated (by purging) using a solvent purification system (Innovative Technology Pure Solv MD-5 Solvent Purification System) and stored over molecular sieves in an Ar-filled glove box. C_6D_6 was dried over NaK/Ph_2CO/18-crown-6, distilled or vacuum transferred and stored over molecular sieves in an Ar-filled glovebox. CH_2Cl_2, $CDCl_3$, and CD_2Cl_2 were dried over CaH_2, distilled or vacuum transferred and stored over molecular sieves in an Ar-filled glove box. **85**, **86**, **69**, **70** were prepared via literature procedures. All other chemicals were used as received from commercial vendors.

4.4.2 Physical Methods

NMR spectra were recorded on a Varian Inova 300, Mercury 300 (^{1}H NMR, 299.952 MHz; ^{13}C NMR, 75.421 MHz; ^{31}P NMR, 121.422 MHz), Bruker 400 (^{1}H NMR, 399.535 MHz; ^{11}C NMR, 100.582 MHz; ^{31}P NMR, 161.734 MHz) and Varian Inova 500 (^{1}H NMR, 499.703 MHz; ^{13}C NMR, 125.697 MHz; ^{31}P NMR, 202.265 MHz) spectrometer. Chemical shifts are reported in δ (ppm). For ^{1}H and ^{13}C NMR spectra, the residual solvent peak was used as an internal reference (^{1}H NMR: δ 7.16 for C_6D_6, 7.24 for $CDCl_3$; ^{13}C NMR: δ 128.06 for C_6D_6, 77.16 for $CDCl_3$). ^{31}P NMR spectra were referenced externally with 85% phosphoric acid at δ 0. Infrared spectra were

collected on an Agilent CARY FT-IR spectrometer. UV-Vis-NIR spectra were collected on a Hitachi U-4100 UV-Vis-NIR spectrophotometer. Electrochemical studies were carried out using a CH Instruments Model 700 D Series. Electrochemical Analyzer and Workstation in conjunction with a three electrode cell. The working electrode was a CHI 104 glassy carbon disk with a 3.0 mm diameter and the auxiliary electrode was composed of platinum wire. The third electrode, the reference electrode, was a $Ag/AgNO_3$ electrode. This was prepared as a bulk solution composed of 0.01 M $AgNO_3$ and 0.1 M $n Bu_4NPF_6$ in dichloromethane. This was separated from solution by a fine porosity frit. CVs and DPVs were conducted in dichloromethane with 0.1 supporting electrolyte mentioned in footnotes and were reported with a scan rate of 100 mV/s. The concentration of the analyte solutions were approximately 1.00×10^{-3} M. CVs were referenced to $Fe(\eta^5\text{-}Cp)_2$/ $Fe(\eta^5\text{-}Cp)^+$ redox couple. Elemental analyses were performed by CALI Labs, Inc. (Highland Park, NJ). Size exclusion chromatography (SEC) was performed on a TOSOH EcoSEC (HLC-8320GPC) chromatography at 40 ºC with THF as the eluent. The molecular weights were calculated using a calibration curve based on polystyrene standards. The SEC columns were TSKgel SuperHM-M and TSKgel SuperH-RC.

4.4.3 Synthesis and Characterization Details

Synthesis of 93

In a glovebox, **85** (500 mg, 0.522 mmol) was dissolved in 20 mL of dried, degassed toluene in a screw cap culture tube. Anhydrous $NiCl_2$ (151 mg, 1.150 mmol) was added to the solution and the tube was brought outside the glovebox. After heating at 100 ºC for 3 h, the tube was taken in the glovebox. Volatiles were then removed under vacuum and the residue was re-dissolved in ether. The solution was filtered through a plug of silica gel and the volatiles were removed from the

filtrate under vacuum to give a green powder. The powder was further purified by re-dissolving it in CH_2Cl_2, layering with MeOH and placing in a -35 ºC freezer for one day. The supernatant was decanted and the solid was dried under vacuum to yield green powder (410 mg, 71%). ^{1}H NMR (500 MHz, C_6D_6): δ 7.49 (m, 2H, Ar-*H*), 7.22 (m, 1H, Ar-*H*), 6.99 (s, 2H, Ar-*H*), 6.85 (m, 1H, Ar-*H*), 2.31 (m, 2H, C*H*Me$_2$), 2.16 (m, 2H, C*H*Me$_2$), 1.51 (m, 12H, CH*Me*$_2$), 1.25 (s, 9H, C*Me*$_3$), 1.33 -1.18 (m, 12H, CH*Me*$_2$). ^{31}P{^{1}H} NMR (202 MHz, C_6D_6): δ 34.67 (d, $J_{P\text{-}P}$ = 313 Hz, 1P, Ar-*P*(^{i}Pr$_2$)), 34.23 (d, $J_{P\text{-}P}$ = 313 Hz, 1P, Ar-*P*(^{i}Pr$_2$)). ^{13}C{^{1}H} NMR (126 MHz, C_6D_6): δ 162.1 (dd, $J_{C\text{-}P}$ = 7 Hz, 19 Hz, Ar-*C*), 160.1 (dd, $J_{C\text{-}P}$ = 7 Hz, 19 Hz, Ar-*C*), 148.7 (d, $J_{C\text{-}P}$ = 6 Hz, Ar-*C*), 139.1 (d, $J_{C\text{-}P}$ = 5 Hz, Ar-*C*), 128.8 (s, Ar-*C*), 122.0 (s, Ar-*C*), 121.8 (dd, $J_{C\text{-}P}$ = 31 Hz, 6 Hz, Ar-*C*), 120.1 (dd, $J_{C\text{-}P}$ = 31 Hz, 6 Hz, Ar-*C*), 117.2 (d, $J_{C\text{-}P}$ = 10 Hz, Ar-*C*), 116.0 (d, $J_{C\text{-}P}$ = 10 Hz, Ar-*C*), 33.9 (s, *C*Me$_3$), 31.7 (s, C*Me*$_3$), 24.1 (dt, $J_{C\text{-}P}$ = 6 Hz, 18 Hz, *C*HMe$_2$), 18.6 (dd, $J_{C\text{-}P}$ = 3 Hz, 11 Hz, *C*HMe$_2$), 17.8 (d, *J* = 5.2 Hz, CH*Me*$_2$).

Synthesis of 94

In a glovebox, **85** (500 mg, 0.522 mmol) was dissolved in 20 mL of dried, degassed toluene in a screw cap culture tube. Pt(COD)Cl_2 (437 mg, 1.150 mmol) was added to the solution and the tube was brought outside the glovebox. After heating at 100 ºC for 3 h, the tube was taken in the glovebox. Volatiles were then removed under vacuum and the residue was re-dissolved in ether. The solution was filtered through a plug of silica gel and the volatiles were removed from the filtrate under vacuum to give a yellow powder. (600 mg, 83%). ^{1}H NMR (500 MHz, C_6D_6): δ 7.75 (dd, $J_{H\text{-}H}$ = 3 Hz, 9 Hz, 1H, Ar-*H*), 7.71 (dd, $J_{H\text{-}H}$ = 3 Hz, 9 Hz, 1H, Ar-*H*), 7.19 (dt, $J_{H\text{-}H}$ = 2 Hz, 6 Hz, 1H, Ar-*H*), 7.02 (dd, $J_{H\text{-}H}$ = 2 Hz, 9 Hz, 1H, Ar-*H*), 6.98 (dt, $J_{H\text{-}H}$ = 3 Hz, 6 Hz, 1H, Ar-*H*), 6.89 (dd, $J_{H\text{-}H}$ = 3 Hz, 9 Hz, 1H, Ar-*H*), 2.59 (m, 2H, C*H*Me$_2$), 2.43 (m, 2H, C*H*Me$_2$), 1.41 (ddt, *J*

= 7 Hz, 12 Hz, 17 Hz, 12H, CH*Me*$_2$), 1.26 (s, 9H, C*Me*$_3$), 1.16 (ddd, *J* = 5 Hz, 7 Hz, 11 Hz, 6H, CH*Me*$_2$), 1.09 (ddd, *J* = 5 Hz, 7 Hz, 11 Hz, 6H, CH*Me*$_2$). ^{31}P{^{1}H} NMR (202 MHz, C_6D_6): δ 42.44 (d, $J_{P\text{-}P}$ = 384 Hz, $J_{P\text{-}Pt}$ = 1315 Hz, 1P, Ar-*P*(^{i}Pr$_2$)), 40.76 (d, $J_{P\text{-}P}$ = 384 Hz, $J_{P\text{-}Pt}$ = 1315 Hz, 1P, Ar-*P*(^{i}Pr$_2$)).

Synthesis of 95

69 (100 mg, 83 μmol) was dissolved in THF solution (3 mL) and lithium acetylide, ethylene diamine complex (LiCCH · $NH_2CH_2CH_2NH_2$) (19 mg, 206 μmol) was added to it under room temperature. The solution color changed immediately from red to yellow. After stirring for 1 hour, the volatiles were removed under vacuum, and the residue was extracted with toluene and filtered through a plug of silica gel. The filtrate was collected and the volatiles were removed under vacuum, yielding a yellow solid (64 mg, 65%). ^{1}H NMR (500 MHz, C_6D_6): δ 7.76 (dd, $J_{H\text{-}H}$ = 4 Hz, 9 Hz, 1H, Ar-*H*), 7.72 (dd, $J_{H\text{-}H}$ = 4 Hz, 9 Hz, 1H, Ar-*H*), 7.17 (s, 1H, Ar-*H*), 7.08 (d, $J_{H\text{-}H}$ = 9 Hz, 1H, Ar-*H*), 7.00-6.93 (s, 2H, Ar-*H*), 2.63 (s, 1H, CC-*H*), 2.41 (m, 2H, C*H*Me$_2$), 2.23 (m, 2H, C*H*Me$_2$), 1.42 (m, 12H, CH*Me*$_2$), 1.27 (s, 9H, C*Me*$_3$), 1.14 (m, 6H, CH*Me*$_2$), 1.08 (m, 6H, CH*Me*$_2$). ^{31}P{^{1}H} NMR (202 MHz, C_6D_6): δ 49.8 (d, $J_{P\text{-}P}$ = 378 Hz, 1P, Ar-*P*(^{i}Pr$_2$)), 51.0 (d, $J_{P\text{-}P}$ = 378 Hz, 1P, Ar-*P*(^{i}Pr$_2$)). ^{13}C{^{1}H} NMR (126 MHz, C_6D_6): δ 161.6 (dd, $J_{C\text{-}P}$ = 5 Hz, 16 Hz, Ar-*C*), 159.8 (dd, $J_{C\text{-}P}$ = 5 Hz, 16 Hz, Ar-*C*), 148.8 (d, $J_{C\text{-}P}$ = 6 Hz, Ar-*C*), 138.6 (d, $J_{C\text{-}P}$ = 5 Hz, Ar-*C*), 129.3 (s, Ar-*C*), 129.0 (s, Ar-*C*), 122.5 (s, Ar-*C*), 122.0 (s, Ar-*C*), 121.5 (dd, $J_{C\text{-}P}$ = 7 Hz, 28 Hz, Ar-*C*), 119.9 (dd, $J_{C\text{-}P}$ = 7 Hz, 29 Hz, Ar-*C*), 116.3 (d, $J_{C\text{-}P}$ = 12 Hz, Ar-*C*), 115.1 (d, $J_{C\text{-}P}$ = 10 Hz, Ar-*C*), 101.59 (s, Pd*C*CH), 88.32 (t, $J_{C\text{-}P}$ = 16 Hz, PdC*C*H), 33.9 (s, *C*Me$_3$), 31.7 (s, C*Me*$_3$), 25.3 (dd, $J_{C\text{-}P}$ = 7 Hz, 18 Hz, *C*HMe$_2$), 19.1 (d, $J_{C\text{-}P}$ = 12 Hz, *C*HMe$_2$), 18.2 (d, *J* = 7 Hz, CH*Me*$_2$).

Synthesis of 95

70 (100 mg, 84 μmol) was dissolved in THF solution (3 mL) and lithium acetylide, ethylene diamine complex ($LiCCH \cdot NH_2CH_2CH_2NH_2$) (19 mg, 210 μmol) was added to it at room temperature. The solution color changed immediately from red to yellow and the tube was brought outside the glovebox. After heating at 50 ºC for 3 hours, the tube was taken in the box and the volatiles were removed under vacuum, and the residue was extracted with THF and filtered through a plug of silica gel. The filtrate was collected and the volatiles were removed under vacuum, yielding a yellow solid (65 mg, 66%). ^{1}H NMR (500 MHz, C_6D_6): δ 7.98 (dt, $J_{H\text{-}H}$ = 2 Hz, 9 Hz, 1H, Ar-*H*), 7.91 (dd, $J_{H\text{-}H}$ = 2 Hz, 9 Hz, 1H, Ar-*H*), 7.49 (m, 1H, Ar-*H*), 7.46 (dd, $J_{H\text{-}H}$ = 2 Hz, 9 Hz, 1H, Ar-*H*), 7.22 (m, 1H, Ar-*H*), 7.14 (m, 1H, Ar-*H*), 2.68 (s, 1H, CC-*H*), 2.45 (m, 4H, C*H*Me_2), 1.50-1.44 (m, 12H, CH*Me*$_2$), 1.29 (s, 9H, C*Me*$_3$), 1.17 (ddd, $J_{H\text{-}H}$ = 7 Hz, 13 Hz, 16 Hz, 12H, CH*Me*$_2$). ^{31}P{^{1}H} NMR (202 MHz, C_6D_6): δ 46.7 (s, 1P, Ar-*P*(^{i}Pr$_2$)), 46.5 (s, 1P, Ar-*P*(^{i}Pr$_2$)).

Synthesis of 97

In a glovebox, **47** (46 mg, 84 μmol) was dissolved in THF solution (2.0 mL) in a culture tube and fresh prepared lithium diisopropylamide (11 mg, 100 μmol) was added to it. After stirring for 1 minute, **69** (50 mg, 42 μmol) was added. Further after stirring overnight, the volatiles were removed under vacuum and the product was extracted with THF and filtered through a plug of silica gel. The filtrate was collected and the volatiles were removed under vacuum. The powder was further purified by re-dissolving it in CH_2Cl_2, layering with MeOH and placing in a -35 ºC freezer for one day. The supernatant was decanted and the solid was dried under vacuum to yield a yellow solid (51 mg, 54 %). ^{1}H NMR (500 MHz, C_6D_6): δ 7.88-7.83 (m, 6H, Ar-*H*), 7.81 (dd,

J_{H-H} = 4 Hz, 9 Hz, 2H, Ar-*H*), 7.26 (dt, J_{H-H} = 2 Hz, 7 Hz, 2H, Ar-*H*), 7.11 (dd, J_{H-H} = 2 Hz, 9 Hz, 4H, Ar-*H*), 7.01 (dd, J_{H-H} = 3 Hz, 9 Hz, 2H, Ar-*H*), 6.98 (m, 4H, Ar-*H*), 6.87 (d, J_{H-H} = 7 Hz, 4H, Ar-*H*), 2.61-2.52 (m, 4H, C*H*Me$_2$), 2.52-2.43 (m, 8H, CH*Me*$_2$), 2.43-2.36 (m, 4H, CH*Me*$_2$), 2.21 (s, 12H, Ar-*Me*), 1.66-1.55 (m, 48H, CH*Me*$_2$), 1.32 (s, 18H, C*Me*$_3$), 1.30-1.19 (m, 48H, CH*Me*$_2$). $^{31}P\{^1H\}$ NMR (202 MHz, C_6D_6): δ 46.3 (s, 2P, Ar-*P*(^{i}Pr$_2$)), 46.0 (s, 4P, Ar-*P*(^{i}Pr$_2$)).

Synthesis of 98

In a grove box, **47** (47 mg, 84 μmol) was dissolved in THF solution (2.0 mL) in a culture tube and fresh prepared lithium diisopropylamide (11 mg, 100 μmol) was added to it. After stirring 1 minutes, **70** (50 mg, 42 μmol) was added and the tube was brought outside the glovebox. After heating at 50 ºC for 3 hours, the tube was taken into the glovebox. The volatiles were removed under vacuum and the product was extracted with THF and filtered through a plug of silica gel. The filtrate was collected and the volatiles were removed under vacuum. The powder was further purified by re-dissolving it in CH_2Cl_2, layering with MeOH and placing in a -35 ºC freezer for one day. The supernatant was decanted and the solid was dried under vacuum to yield an orange solid (50 mg, 53 %). ^1H NMR (500 MHz, C_6D_6)*: δ 8.05 (dt, J_{H-H} = 2 Hz, 9 Hz, 2H, Ar-*H*), 7.97 (dt, J_{H-H} = 2 Hz, 9 Hz, 2H, Ar-*H*), 7.86 (d, J_{H-H} = 9 Hz, 4H, Ar-*H*), 7.61 (m, 2H, Ar-*H*), 7.53 (dd, J_{H-H} = 2 Hz, 9 Hz, 2H, Ar-*H*), 7.30 (m, 2H, Ar-*H*), 6.99 (m, 4H, Ar-*H*), 6.87 (d, J_{H-H} = 9 Hz, 4H, Ar-*H*), 2.60 (m, 8H, C*H*Me$_2$), 2.48 (m, 8H, CH*Me*$_2$), 2.21 (s, 12H, Ar-*Me*), 1.63 (m, 48H, CH*Me*$_2$), 1.34 (s, 18H, C*Me*$_3$), 1.37-1.19 (m, 48H, CH*Me*$_2$). $^{31}P\{^1H\}$ NMR (202 MHz, C_6D_6): δ 46.4 (s, Ar-*P*(^{i}Pr$_2$)), 46.0 (s, Ar-*P*(^{i}Pr$_2$)).

*Two Ar-*H* might overlap with C_6D_6 at 7.16 ppm.

*4.4.4 Observation of Incomplete Reaction of **98***

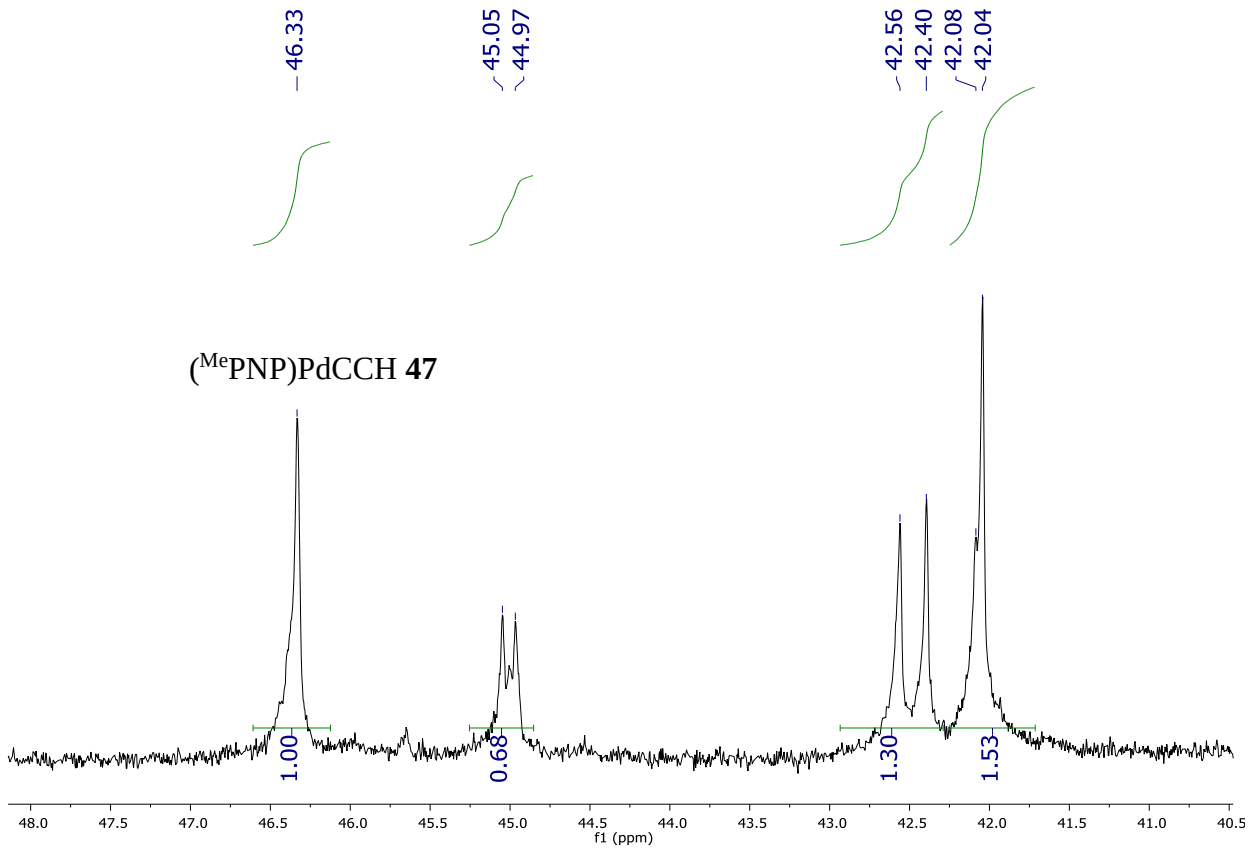

Figure IV-10. In situ $^{31}P\{^{1}H\}$ NMR in THF solution of the reaction mixtures for compound **98** synthesis under room temperature after 18 hours.

4.4.5 Polymerization Details

Synthesis of polymer 99-101

In a glovebox, 1,4-diethynylbenzene (1.3 mg, 10 μmol), freshly prepared lithium diisopropylamide (3 mg, 29 μmol) and **PNPOPNPMCl** (**69, 93** and **94,** 29 μmol respectively) were added into a J-Young tube and THF was syringed into the tube. The J. Young tube was brought outside the box and was heated to 70 ^{o}C overnight. After that, the solution was diluted with THF and the M_n was measured by GPC. Before further CV and UV measurement, the volatiles

were removed under vacuum and the crude products were washed with methanol and pentane. The residues were then dried under vacuum again.

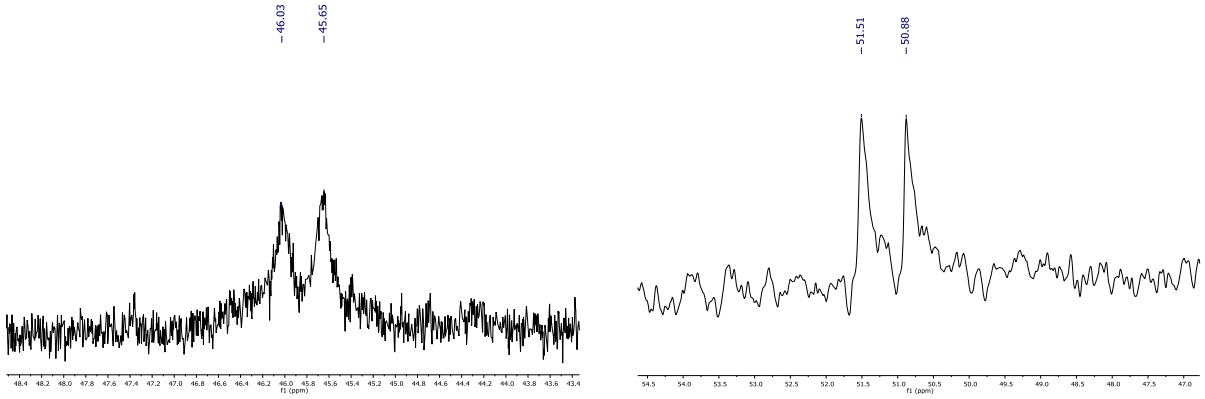

Figure IV-11. In situ $^{31}P\{^{1}H\}$ NMR in THF solution of the reaction mixtures for polymer **99** (room temperature, left) and **100** (70^{o}C, right) synthesis after 18 hours.

Synthesis of polymer 102-104

In a glovebox, bis(pincer) **[Pd]CCH** (**95** and **96**) (10 μmol), freshly prepared lithium diisopropylamide (3 mg, 29 μmol) and bis(pincer) **[Pd]Cl** (**69** and **70**) (10 μmol) were added into a J. Young tube and 100 μL (0.1 M) or 200 μL (0.05 M) THF added to the tube by means of a syringe. The J. Young tube was brought outside the box and was heated to 70 ^{o}C overnight. After that, the solution was diluted with THF and the M_n was measured by GPC. Before further CV and UV measurement, the volatiles were removed under vacuum and the crude product was washed with methanol and pentane. The residue was then dried under vacuum again. The yields of polymers **102**, **103** and **104** were 60%, 39%, 70%, respectively.

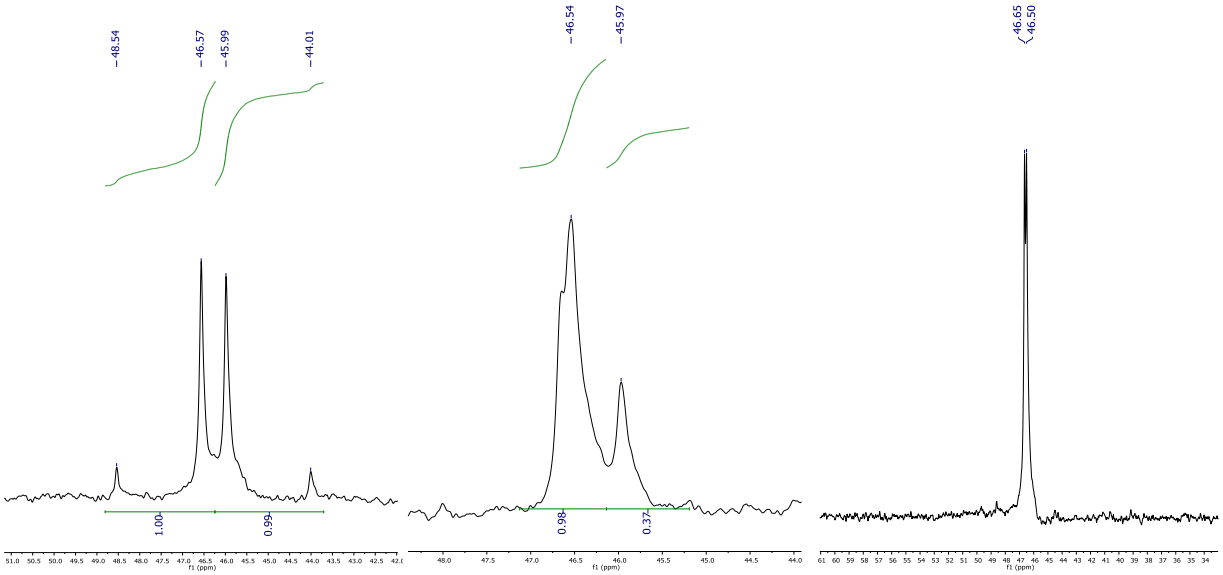

Figure IV-12. In situ $^{31}P\{^{1}H\}$ NMR in THF solution of the reaction mixtures for polymer **102**, **103** and **104** (from left to right) synthesis under 70 ^{o}C after 18 hours.

Figure IV-13. A J.-Young tube that being used to set up the polymerization reaction.

CHAPTER V

SUMMARY AND CONCLUSIONS

The method of bridging two diarylamido/bis(phosphine) (^{Me}PNP)M (M = Ni, Pd, Pt) moieties by ynediyl linkers has been demonstrated. The linkers that were utilized, from short to long, were the μ-ethynediyl, μ-butadiynediyl, and μ-diethynylbenzenediyl. Redox communication behavior of the μ-ethynediyl-bridged compounds were studied by X-ray crystallography, EPR, CV, DFT calculation and UV-vis-NIR spectroscopy. Single crystals of the neutral form (^{Me}PNP)MCCM(^{Me}PNP) and the one-electron oxidized, radical cationic form were obtained and structural characterization via X-ray diffraction crystallography was conducted. The N–M and M–C bond lengths along the N-M-C≡C-M-N axis were decreased upon oxidation with the overall asymmetrical structures. The dissymmetry cannot be guaranteed to be the result only from the localized charge since the uncertainities in the metric data and the distortion from crystal packing could be responsible. The potentials measured by CV showed significant separation between the first and second oxidation events due to the redox coupling. The order of ΔE in (^{Me}PNP)MCCM(^{Me}PNP) was found to be M = Pt ≈ Ni > Pd. Further analysis was carried out by examining the IV-CT band of radical cationic species appearing in NIR region and established the order of Hush coupling integral *V* as Pt > Ni > Pd, which is in agreement with the analysis in (salen)M (M = Ni, Pd, Pt) complexes by Shimazaki et al. The Hush coupling energies *V* were calculated. The Pd complex (**50**) was classified as Robin-Day class II and the Ni (**49**) and Pt (**51**) were at the borderline of II-III. The significance of this work is discovering the methodology of bridging two (^{Me}PNP)M (M = Ni, Pd, Pt) moieties as well as extending the original redox coupling studies from the divalent monoatomic group 10 metal to the M–C≡C–M linkage.

Bis(pincer) diarylamido/bis(phosphine) (PNP) and carbarzolidyl/bis(imido) (NNN) palladium complexes with the conjugated connection on the ligand backbone were successfully synthesized. The ligand connections between the nitrogens for bis(pincer) PNP were the diphenylether (PNPOPNP), biphenyl (PNPbPNP), and phenylene (PNPpPNP) linkage. On the other hand, the NNN bis(pincer) backbone was based on indolo[3,2-*b*]carbazole (NNNpNNN). The metal chelation was believed to enhance the stability of bis(pincer) oxidized species. As the result, we successfully isolated the dicationic PNPbPNP$(PdCl)_2$ and monocationic as well as dicationic PNPpPNP$(PdCl)_2$ single crystals. In addition, the first and second oxidation peaks of those complexes on CV all showed quasireversible. The order of collected ΔE was PNPpPNP$(PdCl)_2$ > NNNpNNN$(PdCl)_2$ > PNPbPNP$(PdCl)_2$ > PNPOPNP$(PdCl)_2$, implying the stability gain of their monocationic form. Except $[PNPOPNP(PdCl)_2]^+$, which had no absorption in the NIR region, the other three, $[PNPpPNP(PdCl)_2]^+$, $[NNNpNNN(PdCl)_2]^+$ and $[PNPbPNP(PdCl)_2]^+$ exhibited intense bands at 1024, 1421, and 1710 nm, respectively. According to the interpretation of similar optical features in related cases in the literature, these compounds were tentatively assigned to Robin-Day class III, meaning that the charge was totally delocalized.

The polymerization of bis(pincer) palladium complexes was conducted using, –C≡C–, as the connecting linker. The preliminary results showed the PNPOPNPPd was the most promising polymerization candidate, which the average molecular weight M_n can reach 18900, which corresponded to 16 repeating units. The PNPbPNPPd polymer was also promising. Its M_n was determined to be ca. 13000, corresponding to 11 repeat units. The tetrametallic palladium pincer complexes with PNPOPNP and PNPbPNP were synthesized as a model fragment of the metallapolymers to understand their electronic properties. Step-wise oxidation events were

observed in CV and DPV and analyzed for the likely order of oxidation events in the tetrametallic models and the polymers.

REFERENCES

(1) Eisenberg, R.; Gray, H. B. Noninnocence in Metal Complexes: A Dithiolene Dawn. *Inorg. Chem.* **2011**, *50*, 9741–9751.

(2) Schrauzer, G. N.; Mayweg, V. P. Preparation, Reactions, and Structure of Bisdithio-α-Diketone Complexes of Nickel, Palladium, and Platinum1,2. *J. Am. Chem. Soc.* **1965**, *87*, 1483–1489.

(3) Bachler, V.; Olbrich, G.; Neese, F.; Wieghardt, K. Theoretical Evidence for the Singlet Diradical Character of Square Planar Nickel Complexes Containing Two O-Semiquinonato Type Ligands. *Inorg. Chem.* **2002**, *41*, 4179–4193.

(4) Szilagyi, R. K.; Lim, B. S.; Glaser, T.; Holm, R. H.; Hedman, B.; Hodgson, K. O.; Solomon, E. I. Description of the Ground State Wave Functions of Ni Dithiolenes Using Sulfur K-Edge X-Ray Absorption Spectroscopy. *J. Am. Chem. Soc.* **2003**, *125*, 9158–9169.

(5) Wang, K.; Stiefel, E. I. Toward Separation and Purification of Olefins Using Dithiolene Complexes: An Electrochemical Approach. *Science* **2001**, *291*, 106.

(6) Wu, J.-Y.; Yu, C.-H.; Wen, J.-J.; Chang, C.-L.; Leung, M. Pyrrolo-[3,2-b]Pyrroles for Photochromic Analysis of Halocarbons. *Anal. Chem.* **2016**, *88* (2), 1195–1201.

(7) Gomberg, M. An Instance Of Trivalent Carbon: Triphenylmethyl. *J. Am. Chem. Soc.* **1900**, *22*, 757–771.

(8) Neumann, W. P.; Uzick, Wolfram.; Zarkadis, A. K. Sterically Hindered Free Radicals. 14. Substituent-Dependent Stabilization of Para-Substituted Triphenylmethyl Radicals. *J. Am. Chem. Soc.* **1986**, *108*, 3762–3770.

(9) Veciana, J.; Carilla, J.; Miravitlles, C.; Molins, E. Free Radicals as Clathrate Hosts: Crystal and Molecular Structure of 1: 1 Perchlorotriphenylmethyl Radical–Benzene. *J. Chem. Soc. Chem. Commun.* **1987**, 812–814.

(10) Ballester, M. Inert Free Radicals (IFR): A Unique Trivalent Carbon Species. *Acc. Chem. Res.* **1985**, *18*, 380–387.

(11) Kobayashi, K.; Ohtsu, H.; Wada, T.; Kato, T.; Tanaka, K. Characterization of a Stable Ruthenium Complex with an Oxyl Radical. *J. Am. Chem. Soc.* **2003**, *125*, 6729–6739.

(12) Büttner, T.; Geier, J.; Frison, G.; Harmer, J.; Calle, C.; Schweiger, A.; Schönberg, H.; Grützmacher, H. A Stable Aminyl Radical Metal Complex. *Science* **2005**, *307*, 235.

(13) Liang, H. W.; Kroll, T.; Nordlund, D.; Weng, T.-C.; Sokaras, D.; Pierpont, C. G.; Gaffney, K. J. Charge and Spin-State Characterization of Cobalt Bis(o-Dioxolene) Valence Tautomers Using Co Kβ X-Ray Emission and L-Edge X-Ray Absorption Spectroscopies. *Inorg. Chem.* **2017**, *56*, 737–747.

(14) Shimazaki, Y.; Yajima, T.; Tani, F.; Karasawa, S.; Fukui, K.; Naruta, Y.; Yamauchi, O. Syntheses and Electronic Structures of One-Electron-Oxidized Group 10 Metal(II)−(Disalicylidene)Diamine Complexes (Metal = Ni, Pd, Pt). *J. Am. Chem. Soc.* **2007**, *129*, 2559–2568.

(15) Peris, E.; Crabtree, R. H. Key Factors in Pincer Ligand Design. *Chem. Soc. Rev.* **2018**, *47*, 1959–1968.

(16) Maser, L.; Vondung, L.; Langer, R. The ABC in Pincer Chemistry – From Amine- to Borylene- and Carbon-Based Pincer-Ligands. *Polyhedron* **2018**, *143*, 28-42.

(17) Dupont, J.; Consorti, C. S.; Spencer, J. CHAPTER 1 - Organometallic Pincer-Type Complexes: Recent Applications in Synthesis and Catalysis. In *The Chemistry of Pincer*

Compounds; Morales-Morales, D., Jensen, C. M., Eds.; Elsevier Science B.V.: Amsterdam, 2007; pp 1–24.

(18) Moulton, C. J.; Shaw, B. L. Transition Metal–Carbon Bonds. Part XLII. Complexes of Nickel, Palladium, Platinum, Rhodium and Iridium with the Tridentate Ligand 2,6-Bis[(Di-t-Butylphosphino)Methyl]Phenyl. *J. Chem. Soc. Dalton Trans.* **1976**, 1020–1024.

(19) Al-Salem, N. A.; Empsall, H. D.; Markham, R.; Shaw, B. L.; Weeks, B. Formation of Large Chelate Rings and Cyclometallated Products from Diphosphines of Type $Bu^t_2P(CH_2)_nPBu^t_2$(n = 5–8) and $Ph_2P(CH_2)_5PPh_2$ with Palladium and Platinum Chlorides: Factors Affecting the Stability and Conformation of Large Chelate Rings. *J. Chem. Soc. Dalton Trans.* **1979**, 1972–1982.

(20) van Koten, G.; Timmer, K.; Noltes, J. G.; Spek, A. L. A Novel Type of Pt–C Interaction and a Model for the Final Stage in Reductive Elimination Processes Involving C–C Coupling at Pt; Synthesis and Molecular Geometry of [1,N,N′-η-2,6-Bis{(Dimethylamino)Methyl}-Toluene]Iodoplatinum(II) Tetrafluoroborate. *J. Chem. Soc. Chem. Commun.* **1978**, 250–252.

(21) Davidson, J. J.; DeMott, J. C.; Douvris, C.; Fafard, C. M.; Bhuvanesh, N.; Chen, C.-H.; Herbert, D. E.; Lee, C.-I.; McCulloch, B. J.; Foxman, B. M.; Ozerov, O. V. Comparison of the Electronic Properties of Diarylamido-Based PNZ Pincer Ligands: Redox Activity at the Ligand and Donor Ability Toward the Metal. *Inorg. Chem.* **2015**, *54*, 2916–2935.

(22) You, F.; Liu, H.; Luo, G.; Shi, X. Tridentate Diarylamido-Based Pincer Complexes of Nickel and Palladium: Sidearm Effects in the Polymerization of Norbornene. *Dalton Trans.* **2019**, *48*, 12219–12227.

(23) Brunel, P.; Lhardy, C.; Mallet-Ladeira, S.; Monot, J.; Martin-Vaca, B.; Bourissou, D. Palladium Pincer Complexes Featuring an Unsymmetrical SCN Indene-Based Ligand with a Hemilabile Pyridine Sidearm. *Dalton Trans.* **2019**, *48*, 9801–9806.

(24) Mancano, G.; Page, M. J.; Bhadbhade, M.; Messerle, B. A. Hemilabile and Bimetallic Coordination in Rh and Ir Complexes of NCN Pincer Ligands. *Inorg. Chem.* **2014**, *53*, 10159–10170.

(25) Churusova, S. G.; Aleksanyan, D. V.; Vasil'ev, A. A.; Nelyubina, Y. V.; Novikov, V. V.; Pavlov, A. A.; Denisov, G. L.; Klemenkova, Z. S.; Kozlov, V. A. 5,6- and 6,6-Membered Palladium(II) Pincer Complexes Based on Functionalized Carboxamides with Ancillary Sulfur and Nitrogen Donors. *Eur. J. Inorg. Chem.* **2016**, *2016*, 5271–5280.

(26) Ma, L.; Woloszynek, R. A.; Chen, W.; Ren, T.; Protasiewicz, J. D. A New Twist on Pincer Ligands and Complexes. *Organometallics* **2006**, *25*, 3301–3304.

(27) Schneck, F.; Finger, M.; Tromp, M.; Schneider, S. Chemical Non-Innocence of an Aliphatic PNP Pincer Ligand. *Chem. – Eur. J.* **2017**, *23*, 33–37.

(28) Lindley, B. M.; Bruch, Q. J.; White, P. S.; Hasanayn, F.; Miller, A. J. M. Ammonia Synthesis from a Pincer Ruthenium Nitride via Metal–Ligand Cooperative Proton-Coupled Electron Transfer. *J. Am. Chem. Soc.* **2017**, *139*, 5305–5308.

(29) Gregor, L. C.; Chen, C.-H.; Fafard, C. M.; Fan, L.; Guo, C.; Foxman, B. M.; Gusev, D. G.; Ozerov, O. V. Heterolytic Splitting of H-X Bonds at a Cationic (PNP)Pd Center. *Dalton Trans* **2010**, *39*, 3195–3202.

(30) Cao, Y.; Shih, W.-C.; Ozerov, O. V. Addition of O–H, N–H, and F–H Bonds across a Boryl–Iridium Unit. *Organometallics* **2019**, *38*, 4076–4081.

(31) Ben-Ari, E.; Leitus, G.; Shimon, L. J. W.; Milstein, D. Metal−Ligand Cooperation in C−H and H_2 Activation by an Electron-Rich PNP Ir(I) System: Facile Ligand Dearomatization−Aromatization as Key Steps. *J. Am. Chem. Soc.* **2006**, *128*, 15390–15391.

(32) Tang, S.; von Wolff, N.; Diskin-Posner, Y.; Leitus, G.; Ben-David, Y.; Milstein, D. Pyridine-Based PCP-Ruthenium Complexes: Unusual Structures and Metal–Ligand Cooperation. *J. Am. Chem. Soc.* **2019**, *141*, 7554–7561.

(33) Zhang, J.; Leitus, G.; Ben-David, Y.; Milstein, D. Efficient Homogeneous Catalytic Hydrogenation of Esters to Alcohols. *Angew. Chem. Int. Ed.* **2006**, *45*, 1113–1115.

(34) Gunanathan, C.; Milstein, D. Bond Activation and Catalysis by Ruthenium Pincer Complexes. *Chem. Rev.* **2014**, *114*, 12024–12087.

(35) Anaby, A.; Feller, M.; Ben-David, Y.; Leitus, G.; Diskin-Posner, Y.; Shimon, L. J. W.; Milstein, D. Bottom-Up Construction of a CO2-Based Cycle for the Photocarbonylation of Benzene, Promoted by a Rhodium(I) Pincer Complex. *J. Am. Chem. Soc.* **2016**, *138*, 9941–9950.

(36) Kosanovich, A. J.; Komatsu, C. H.; Bhuvanesh, N.; Pérez, L. M.; Ozerov, O. V. Dearomatization of the PCP Pincer Ligand in a ReV Oxo Complex. *Chem. – Eur. J.* **2018**, *24*, 13754–13757.

(37) Chirik, P. J.; Wieghardt, K. Radical Ligands Confer Nobility on Base-Metal Catalysts. *Science* **2010**, *327*, 794-795.

(38) Adhikari, D.; Mossin, S.; Basuli, F.; Huffman, J. C.; Szilagyi, R. K.; Meyer, K.; Mindiola, D. J. Structural, Spectroscopic, and Theoretical Elucidation of a Redox-Active Pincer-Type Ancillary Applied in Catalysis. *J. Am. Chem. Soc.* **2008**, *130*, 3676–3682.

(39) Radosevich, A. T.; Melnick, J. G.; Stoian, S. A.; Bacciu, D.; Chen, C.-H.; Foxman, B. M.; Ozerov, O. V.; Nocera, D. G. Ligand Reactivity in Diarylamido/Bis(Phosphine) PNP Complexes of $Mn(CO)_3$ and $Re(CO)_3$. *Inorg. Chem.* **2009**, *48*, 9214–9221.

(40) Bart, S. C.; Chłopek, K.; Bill, E.; Bouwkamp, M. W.; Lobkovsky, E.; Neese, F.; Wieghardt, K.; Chirik, P. J. Electronic Structure of Bis(Imino)Pyridine Iron Dichloride, Monochloride, and Neutral Ligand Complexes: A Combined Structural, Spectroscopic, and Computational Study. *J. Am. Chem. Soc.* **2006**, *128*, 13901–13912.

(41) Manuel, T. D.; Rohde, J.-U. Reaction of a Redox-Active Ligand Complex of Nickel with Dioxygen Probes Ligand-Radical Character. *J. Am. Chem. Soc.* **2009**, *131*, 15582–15583.

(42) Creutz, C.; Taube, H. Direct Approach to Measuring the Franck-Condon Barrier to Electron Transfer between Metal Ions. *J. Am. Chem. Soc.* **1969**, *91*, 3988–3989.

(43) Allen, G. C.; Hush, N. S. Intervalence-Transfer Absorption. Part 1. Qualitative Evidence for Intervalence-Transfer Absorption in Inorganic Systems in Solution and in the Solid State. In *Progress in Inorganic Chemistry*; John Wiley & Sons, Ltd, 2007; pp 357–389.

(44) Robin, M. B.; Day, P. Mixed Valence Chemistry-A Survey and Classification. In *Advances in Inorganic Chemistry and Radiochemistry*; Emeléus, H. J., Sharpe, A. G., Eds.; Academic Press, 1968; Vol. 10, pp 247–422.

(45) Demadis, K. D.; Hartshorn, C. M.; Meyer, T. J. The Localized-to-Delocalized Transition in Mixed-Valence Chemistry. *Chem. Rev.* **2001**, *101*, 2655–2686.

(46) Hush, N. S. Distance Dependence of Electron Transfer Rates. *Coord. Chem. Rev.* **1985**, *64*, 135–157.

(47) Szeghalmi, A. V.; Erdmann, M.; Engel, V.; Schmitt, M.; Amthor, S.; Kriegisch, V.; Nöll, G.; Stahl, R.; Lambert, C.; Leusser, D.; Stalke, D.; Zabel, M.; Popp, J. How Delocalized Is

N,N,N‘,N‘-Tetraphenylphenylenediamine Radical Cation? An Experimental and Theoretical Study on the Electronic and Molecular Structure. *J. Am. Chem. Soc.* **2004**, *126*, 7834–7845.

(48) Lindeman, S. V.; Rosokha, S. V.; Sun, D.; Kochi, J. K. X-Ray Structure Analysis and the Intervalent Electron Transfer in Organic Mixed-Valence Crystals with Bridged Aromatic Cation Radicals. *J. Am. Chem. Soc.* **2002**, *124*, 843–855.

(49) Hansmann, M. M.; Melaimi, M.; Bertrand, G. Organic Mixed Valence Compounds Derived from Cyclic (Alkyl)(Amino)Carbenes. *J. Am. Chem. Soc.* **2018**, *140*, 2206–2213.

(50) Cowan, D. O.; LeVanda, C.; Park, J.; Kaufman, F. Organic Solid State. VIII. Mixed-Valence Ferrocene Chemistry. *Acc. Chem. Res.* **1973**, *6*, 1–7.

(51) Levanda, Carole.; Bechgaard, Klaus.; Cowan, D. O. Mixed Valence Cations. Chemistry of .Pi.-Bridged Analogues of Biferrocene and Biferrocenylene. *J. Org. Chem.* **1976**, *41*, 2700–2704.

(52) Todorova, T.; Delley, B. The Creutz−Taube Complex Revisited: DFT Study of the Infrared Frequencies. *Inorg. Chem.* **2008**, *47*, 11269–11277.

(53) Parthey, M.; Kaupp, M. Quantum-Chemical Insights into Mixed-Valence Systems: Within and beyond the Robin–Day Scheme. *Chem. Soc. Rev.* **2014**, *43*, 5067–5088.

(54) Parthey, M.; Gluyas, J. B. G.; Fox, M. A.; Low, P. J.; Kaupp, M. Mixed-Valence Ruthenium Complexes Rotating through a Conformational Robin–Day Continuum. *Chem. – Eur. J.* **2014**, *20*, 6895–6908.

(55) Coropceanu, V.; Gruhn, N. E.; Barlow, S.; Lambert, C.; Durivage, J. C.; Bill, T. G.; Nöll, G.; Marder, S. R.; Brédas, J.-L. Electronic Couplings in Organic Mixed-Valence

Compounds: The Contribution of Photoelectron Spectroscopy. *J. Am. Chem. Soc.* **2004**, *126*, 2727–2731.

(56) Lee, J.; Kalin, A. J.; Yuan, T.; Al-Hashimi, M.; Fang, L. Fully Conjugated Ladder Polymers. *Chem. Sci.* **2017**, *8*, 2503–2521.

(57) Zhu, C.; Kalin, A. J.; Fang, L. Covalent and Noncovalent Approaches to Rigid Coplanar π-Conjugated Molecules and Macromolecules. *Acc. Chem. Res.* **2019**, *52*, 1089–1100.

(58) Teo, Y. C.; Lai, H. W. H.; Xia, Y. Synthesis of Ladder Polymers: Developments, Challenges, and Opportunities. *Chem. – Eur. J.* **2017**, *23*, 14101–14112.

(59) Yu, Z.-D.; Lu, Y.; Wang, J.-Y.; Pei, J. Conformation Control of Conjugated Polymers. *Chem. – Eur. J.* **2020**, accepted author manuscript. doi:10.1002/chem.202000220.

(60) Yu, L.; Chen, M.; Dalton, L. R. Ladder Polymers: Recent Developments in Syntheses, Characterization, and Potential Applications as Electronic and Optical Materials. *Chem. Mater.* **1990**, *2*, 649–659.

(61) Zheng, T.; Cai, Z.; Ho-Wu, R.; Yau, S. H.; Shaparov, V.; Goodson, T.; Yu, L. Synthesis of Ladder-Type Thienoacenes and Their Electronic and Optical Properties. *J. Am. Chem. Soc.* **2016**, *138*, 868–875.

(62) Goldfinger, M. B.; Swager, T. M. Fused Polycyclic Aromatics via Electrophile-Induced Cyclization Reactions: Application to the Synthesis of Graphite Ribbons. *J. Am. Chem. Soc.* **1994**, *116*, 7895–7896.

(63) Zou, Y.; Yuan, T.; Yao, H.; Frazier, D. J.; Stanton, D. J.; Sue, H.-J.; Fang, L. Solution-Processable Core-Extended Quinacridone Derivatives with Intact Hydrogen Bonds. *Org. Lett.* **2015**, *17*, 3146–3149.

(64) Deraedt, C.; Pinaud, N.; Astruc, D. Recyclable Catalytic Dendrimer Nanoreactor for Part-Per-Million CuI Catalysis of "Click" Chemistry in Water. *J. Am. Chem. Soc.* **2014**, *136*, 12092–12098.

(65) Elmas, S.; Beelders, W.; Bradley, S. J.; Kroon, R.; Laufersky, G.; Andersson, M.; Nann, T. Platinum Terpyridine Metallopolymer Electrode as Cost-Effective Replacement for Bulk Platinum Catalysts in Oxygen Reduction Reaction and Hydrogen Evolution Reaction. *ACS Sustain. Chem. Eng.* **2017**, *5*, 10206–10214.

(66) Choi, T.-L.; Lee, K.-H.; Joo, W.-J.; Lee, S.; Lee, T.-W.; Chae, M. Y. Synthesis and Nonvolatile Memory Behavior of Redox-Active Conjugated Polymer-Containing Ferrocene. *J. Am. Chem. Soc.* **2007**, *129*, 9842–9843.

(67) Marcus, R. A. Chemical and Electrochemical Electron-Transfer Theory. *Annu. Rev. Phys. Chem.* **1964**, *15*, 155–196.

(68) Barbara, P. F.; Meyer, T. J.; Ratner, M. A. Contemporary Issues in Electron Transfer Research. *J. Phys. Chem.* **1996**, *100*, 13148–13168.

(69) Gray, H. B.; Winkler, J. R. Electron Transfer in Proteins. *Annu. Rev. Biochem.* **1996**, *65*, 537–561.

(70) Facchetti, A. π-Conjugated Polymers for Organic Electronics and Photovoltaic Cell Applications. *Chem. Mater.* **2011**, *23*, 733–758.

(71) Lambert, C.; Nöll, G. The Class II/III Transition in Triarylamine Redox Systems. *J. Am. Chem. Soc.* **1999**, *121*, 8434–8442.

(72) Winter, R. F. Half-Wave Potential Splittings $\Delta E_{1/2}$ as a Measure of Electronic Coupling in Mixed-Valent Systems: Triumphs and Defeats. *Organometallics* **2014**, *33*, 4517–4536.

(73) Paul, F.; Meyer, W. E.; Toupet, L.; Jiao, H.; Gladysz, J. A.; Lapinte, C. A "Conjugal" Consanguineous Family of Butadiynediyl-Derived Complexes: Synthesis and Electronic Ground States of Neutral, Radical Cationic, and Dicationic Iron/Rhenium C4 Species. *J. Am. Chem. Soc.* **2000**, *122*, 9405–9414.

(74) Jiao, H.; Costuas, K.; Gladysz, J. A.; Halet, J.-F.; Guillemot, M.; Toupet, L.; Paul, F.; Lapinte, C. Bonding and Electronic Structure in Consanguineous and Conjugal Iron and Rhenium Sp Carbon Chain Complexes $[MC_4M']^{n+}$: Computational Analyses of the Effect of the Metal. *J. Am. Chem. Soc.* **2003**, *125*, 9511–9522.

(75) Lin, V.; DiMagno, S.; Therien, M. Highly Conjugated, Acetylenyl Bridged Porphyrins: New Models for Light-Harvesting Antenna Systems. *Science* **1994**, *264*, 1105.

(76) Jones, S. C.; Coropceanu, V.; Barlow, S.; Kinnibrugh, T.; Timofeeva, T.; Brédas, J.-L.; Marder, S. R. Delocalization in Platinum−Alkynyl Systems: A Metal-Bridged Organic Mixed-Valence Compound. *J. Am. Chem. Soc.* **2004**, *126*, 11782–11783.

(77) Liddle, B. J.; Wanniarachchi, S.; Hewage, J. S.; Lindeman, S. V.; Bennett, B.; Gardinier, J. R. Electronic Communication Across Diamagnetic Metal Bridges: A Homoleptic Gallium(III) Complex of a Redox-Active Diarylamido-Based Ligand and Its Oxidized Derivatives. *Inorg. Chem.* **2012**, *51*, 12720–12728.

(78) Hewage, J. S.; Wanniarachchi, S.; Morin, T. J.; Liddle, B. J.; Banaszynski, M.; Lindeman, S. V.; Bennett, B.; Gardinier, J. R. Homoleptic Nickel(II) Complexes of Redox-Tunable Pincer-Type Ligands. *Inorg. Chem.* **2014**, *53*, 10070–10084.

(79) Shimazaki, Y.; Stack, T. D. P.; Storr, T. Detailed Evaluation of the Geometric and Electronic Structures of One-Electron Oxidized Group 10 (Ni, Pd, and Pt) Metal(II)-(Disalicylidene)Diamine Complexes. *Inorg. Chem.* **2009**, *48*, 8383–8392.

(80) Rotthaus, O.; Thomas, F.; Jarjayes, O.; Philouze, C.; Saint-Aman, E.; Pierre, J.-L. Valence Tautomerism in Octahedral and Square-Planar Phenoxyl–Nickel(II) Complexes: Are Imino Nitrogen Atoms Good Friends? *Chem. – Eur. J.* **2006**, *12*, 6953–6962.

(81) Nguyen, M. T.; Jones, R. A.; Holliday, B. J. Understanding the Effect of Metal Centers on Charge Transport and Delocalization in Conducting Metallopolymers. *Macromolecules* **2017**, *50*, 872–883.

(82) Holliday, B. J.; Swager, T. M. Conducting Metallopolymers: The Roles of Molecular Architecture and Redox Matching. *Chem Commun* **2005**, 23–36.

(83) Kingsborough, R. P.; Swager, T. M. Polythiophene Hybrids of Transition-Metal Bis(Salicylidenimine)s: Correlation between Structure and Electronic Properties. *J. Am. Chem. Soc.* **1999**, *121*, 8825–8834.

(84) Ho, C.-L.; Yu, Z.-Q.; Wong, W.-Y. Multifunctional Polymetallaynes: Properties, Functions and Applications. *Chem. Soc. Rev.* **2016**, *45*, 5264–5295.

(85) Oyaizu, K.; Nishide, H. Radical Polymers for Organic Electronic Devices: A Radical Departure from Conjugated Polymers? *Adv. Mater.* **2009**, *21*, 2339–2344.

(86) Shirota, Y.; Kageyama, H. Charge Carrier Transporting Molecular Materials and Their Applications in Devices. *Chem. Rev.* **2007**, *107*, 953–1010.

(87) Himo, F.; Siegbahn, P. E. M. Quantum Chemical Studies of Radical-Containing Enzymes. *Chem. Rev.* **2003**, *103*, 2421–2456.

(88) Stubbe, J.; van der Donk, W. A. Protein Radicals in Enzyme Catalysis. *Chem. Rev.* **1998**, *98*, 705–762.

(89) Fan, L.; Foxman, B. M.; Ozerov, O. V. N−H Cleavage as a Route to Palladium Complexes of a New PNP Pincer Ligand. *Organometallics* **2004**, *23*, 326–328.

(90) Ozerov, O. V.; Guo, C.; Fan, L.; Foxman, B. M. Oxidative Addition of N−C and N−H Bonds to Zerovalent Nickel, Palladium, and Platinum. *Organometallics* **2004**, *23*, 5573–5580.

(91) Fafard, C. M.; Adhikari, D.; Foxman, B. M.; Mindiola, D. J.; Ozerov, O. V. Addition of Ammonia, Water, and Dihydrogen Across a Single Pd−Pd Bond. *J. Am. Chem. Soc.* **2007**, *129*, 10318–10319.

(92) Herbert, D. E.; Ozerov, O. V. Binuclear Palladium Complexes Supported by Bridged Pincer Ligands. *Organometallics* **2011**, *30*, 6641–6654.

(93) Harkins, S. B.; Mankad, N. P.; Miller, A. J. M.; Szilagyi, R. K.; Peters, J. C. Probing the Electronic Structures of $[Cu_2(\mu\text{-}XR_2)]^{n+}$ Diamond Cores as a Function of the Bridging X Atom (X = N or P) and Charge (n = 0, 1, 2). *J. Am. Chem. Soc.* **2008**, *130*, 3478–3485.

(94) Hollas, A. M.; Gu, W.; Bhuvanesh, N.; Ozerov, O. V. Synthesis and Characterization of Pd Complexes of a Carbazolyl/Bis(Imine) NNN Pincer Ligand. *Inorg. Chem.* **2011**, *50*, 3673–3679.

(95) Barbe, J.-M.; Habermeyer, B.; Khoury, T.; Gros, C. P.; Richard, P.; Chen, P.; Kadish, K. M. Three-Metal Coordination by Novel Bisporphyrin Architectures. *Inorg. Chem.* **2010**, *49*, 8929–8940.

(96) Wanniarachchi, S.; Liddle, B. J.; Toussaint, J.; Lindeman, S. V.; Bennett, B.; Gardinier, J. R. Chemical Switching Behaviour of Tricarbonylrhenium(i) Complexes of a New Redox Active 'Pincer' Ligand. *Dalton Trans.* **2010**, *39*, 3167–3169.

(97) Kieltsch, I.; Dubinina, G. G.; Hamacher, C.; Kaiser, A.; Torres-Nieto, J.; Hutchison, J. M.; Klein, A.; Budnikova, Y.; Vicic, D. A. Magnitudes of Electron-Withdrawing Effects of the

Trifluoromethyl Ligand in Organometallic Complexes of Copper and Nickel. *Organometallics* **2010**, *29*, 1451–1456.

(98) Madhira, V. N.; Ren, P.; Vechorkin, O.; Hu, X.; Vicic, D. A. Synthesis and Electronic Properties of a Pentafluoroethyl-Derivatized Nickel Pincer Complex. *Dalton Trans.* **2012**, *41*, 7915–7919.

(99) Rodríguez-Lugo, R. E.; de Bruin, B.; Trincado, M.; Grützmacher, H. A Stable Aminyl Radical Coordinated to Cobalt. *Chem. – Eur. J.* **2017**, *23*, 6795–6802.

(100) Haque, A.; Al-Balushi, R. A.; Al-Busaidi, I. J.; Khan, M. S.; Raithby, P. R. Rise of Conjugated Poly-Ynes and Poly(Metalla-Ynes): From Design Through Synthesis to Structure–Property Relationships and Applications. *Chem. Rev.* **2018**, *118*, 8474–8597.

(101) Ogawa, Hiroo.; Onitsuka, Kiyotaka.; Joh, Takashi.; Takahashi, Shigetoshi.; Yamamoto, Yasuhiro.; Yamazaki, Hiroshi. Synthesis, Characterization, and Molecular Structure of .Mu.-Ethynediyl Complexes [X(PR_3)MC.Ident.CM(PR_3)$_2$X] (M = Pd, Pt; R = Me, Et, n-Bu; X = Cl, I). *Organometallics* **1988**, *7*, 2257–2260.

(102) Mohaček-Grošev, V.; Furić, K. Low Temperature Raman Study of Bis(Trimethylsilyl)Acetylene. *Mol. Spectrosc. Mol. Struct.* **2007**, 270–275.

(103) Carty, A. J.; Efraty, A. Coordination Complexes of Acetylene Diphosphines. I. Diphosphine-Bridged Binuclear Copper(I) and Gold(I) Complexes of Bis(Diphenylphosphino)Acetylene. *Inorg. Chem.* **1969**, *8*, 543–550.

(104) Edwards, H. G. M. Vibration—Rotational Raman Spectra of Acetylene, 12C2H2. *Spectrochim. Acta Part Mol. Spectrosc.* **1990**, *46*, 97–106.

(105) Herzberg, G.; Stoicheff, B. P. Carbon–Carbon and Carbon–Hydrogen Distances in Simple Polyatomic Molecules. *Nature* **1955**, *175*, 79–80.

(106) Owen, G. R.; Stahl, J.; Hampel, F.; Gladysz, J. A. Coordination-Driven Self-Assembly, Structures, and Dynamic Properties of Diplatinum Hexatriynediyl and Butadiynediyl Complexes in Which the Sp Carbon Chains Are Shielded by Sp3 Carbon Chains: Towards Endgroup–Endgroup Interactions. *Chem. – Eur. J.* **2008**, *14*, 73–87.

(107) Crutchley, R. J. Intervalence Charge Transfer and Electron Exchange Studies of Dinuclear Ruthenium Complexes. In *Advances in Inorganic Chemistry*; Sykes, A. G., Ed.; Academic Press, 1994; Vol. 41, pp 273–325.

(108) D'Alessandro, D. M.; Keene, F. R. A Cautionary Warning on the Use of Electrochemical Measurements to Calculate Comproportionation Constants for Mixed-Valence Compounds. *Dalton Trans.* **2004**, 3950–3954.

(109) Carrasco, R.; Cano, J.; Ottenwaelder, X.; Aukauloo, A.; Journaux, Y.; Ruiz-García, R. Molecular and Electronic Structure of Square-Planar Nickel(Ii), Nickel(Iii) and Nickel(Iii) π-Cation Radical Complexes with a Tetradentate o-Phenylenedioxamidate Redox-Active Ligand. *Dalton Trans.* **2005**, 2527–2538.

(110) Ray, K.; Bill, E.; Weyhermüller, T.; Wieghardt, K. Redox-Noninnocence of the S,S'-Coordinated Ligands in Bis(Benzene-1,2-Dithiolato)Iron Complexes. *J. Am. Chem. Soc.* **2005**, *127*, 5641–5654.

(111) Xu, G.-L.; Zou, G.; Ni, Y.-H.; DeRosa, M. C.; Crutchley, R. J.; Ren, T. Polyyn-Diyls Capped by Diruthenium Termini: A New Family of Carbon-Rich Organometallic Compounds and Distance-Dependent Electronic Coupling Therein. *J. Am. Chem. Soc.* **2003**, *125*, 10057–10065.

(112) Sarkar, P.; Mukherjee, C. A Non-Innocent Pincer H3LONS Ligand and Its Corresponding Octahedral Low-Spin Fe(III) Complex Formation via Ligand-Centric Homolytic S–S Bond Scission. *Dalton Trans.* **2018**, *47*, 13337–13341.

(113) Nelsen, S. F.; Ismagilov, R. F.; Trieber, D. A. Adiabatic Electron Transfer: Comparison of Modified Theory with Experiment. *Science* **1997**, *278*, 846.

(114) Barlow, S.; Risko, C.; Chung, S.-J.; Tucker, N. M.; Coropceanu, V.; Jones, S. C.; Levi, Z.; Brédas, J.-L.; Marder, S. R. Intervalence Transitions in the Mixed-Valence Monocations of Bis(Triarylamines) Linked with Vinylene and Phenylene−Vinylene Bridges. *J. Am. Chem. Soc.* **2005**, *127*, 16900–16911.

(115) Fan, L.; Ozerov, Oleg. V. Efficient Nickel Catalyst for Coupling of Acetonitrile with Aldehydes. *Chem. Commun.* **2005**, 4450–4452.

(116) Ono, T.; Ohta, M.; Sada, K. Ionic Polymers Act as Polyelectrolytes in Nonpolar Media. *ACS Macro Lett.* **2012**, *1*, 1270–1273.

(117) M. J. Frisch et al. *Gaussian09, RevisionD.01*; Gaussian, Inc.: Wallingford CT, 2009.

(118) Bailey, W. D.; Luconi, L.; Rossin, A.; Yakhvarov, D.; Flowers, S. E.; Kaminsky, W.; Kemp, R. A.; Giambastiani, G.; Goldberg, K. I. Pyrazole-Based PCN Pincer Complexes of Palladium(II): Mono- and Dinuclear Hydroxide Complexes and Ligand Rollover C–H Activation. *Organometallics* **2015**, *34*, 3998–4010.

(119) Mandapati, P.; Giesbrecht, P. K.; Davis, R. L.; Herbert, D. E. Phenanthridine-Containing Pincer-like Amido Complexes of Nickel, Palladium, and Platinum. *Inorg. Chem.* **2017**, *56*, 3674–3685.

(120) Huckaba, A. J.; Cao, B.; Hollis, T. K.; Valle, H. U.; Kelly, J. T.; Hammer, N. I.; Oliver, A. G.; Webster, C. E. Platinum CCC-NHC Benzimidazolyl Pincer Complexes: Synthesis,

Characterization, Photostability, and Theoretical Investigation of a Blue-Green Emitter. *Dalton Trans.* **2013**, *42*, 8820.

(121) Zhao, Y.; Truhlar, D. G. The M06 Suite of Density Functionals for Main Group Thermochemistry, Thermochemical Kinetics, Noncovalent Interactions, Excited States, and Transition Elements: Two New Functionals and Systematic Testing of Four M06-Class Functionals and 12 Other Functionals. *Theor. Chem. Acc.* **2008**, *120*, 215–241.

(122) Weigend, F.; Ahlrichs, R. Balanced Basis Sets of Split Valence, Triple Zeta Valence and Quadruple Zeta Valence Quality for H to Rn: Design and Assessment of Accuracy. *Phys. Chem. Chem. Phys.* **2005**, *7*, 3297.

(123) APEX3 "Program for Data Collection on Area Detectors" BRUKER AXS Inc.: Madison, WI, USA, 2016.

(124) Sheldrick, G.M. SADABS: Program for Absorption Correction of Area Detector Frames; BRUKER AXS Inc.: Madison, WI, USA, 2008.

(125) (A) Sheldrick, G. M. A Short History of SHELX. *Acta Cryst.* **2008**, A64, 112-122. (b) Sheldrick, G. M. SHELXT – Integrated Space-Group and Crystal-Structure Determination. *Acta Cryst*. **2015**, A71, 3-8. (c) Sheldrick, G. M. Crystal Structure Refinement with SHELXL. *Acta Cryst.* **2015**, C71, 3-8. (d) XT, XS, BRUKER AXS Inc.: Madison, WI, USA.

(126) Dolomanov, O. V.; Bourhis, L. J.; Gildea, R. J.; Howard, J. A. K.; Puschmann, H. OLEX2: A Complete Structure Solution, Refinement and Analysis Program. *J. Appl. Cryst.* **2009**, *42*, 339-341.

(127) Farrugia, L. J. WinGX and ORTEP for Windows: An Update *J. Appl. Cryst.* **2012**, *45*, 849-854.

(128) POV-Ray home page http://www.povray.org/ (qccessed March 26, 2018).

(129) Chen, W.-H.; Wang, K.-L.; Liaw, D.-J.; Lee, K.-R.; Lai, J.-Y. N,N,N′,N′- Tetraphenyl-1,4-Phenylenediamine−Fluorene Alternating Conjugated Polymer: Synthesis, Characterization, and Electrochromic Application. *Macromolecules* **2010**, *4*3, 2236–2243.

(130) Yen, H.-J.; Liou, G.-S. Recent Advances in Triphenylamine-Based Electrochromic Derivatives and Polymers. *Polym. Chem.* **2018**, *9*, 3001–3018.

(131) Jeon, N. J.; Lee, J.; Noh, J. H.; Nazeeruddin, M. K.; Grätzel, M.; Seok, S. I. Efficient Inorganic–Organic Hybrid Perovskite Solar Cells Based on Pyrene Arylamine Derivatives as Hole-Transporting Materials. *J. Am. Chem. Soc.* **2013**, *135*, 19087–19090.

(132) Liang, M.; Chen, J. Arylamine Organic Dyes for Dye-Sensitized Solar Cells. *Chem. Soc. Rev.* **2013**, *42*, 3453–3488.

(133) Tao, Y.; Yang, C.; Qin, J. Organic Host Materials for Phosphorescent Organic Light-Emitting Diodes. *Chem. Soc. Rev.* **2011**, *40*, 2943–2970.

(134) Shimizu, M.; Kaki, R.; Takeda, Y.; Hiyama, T.; Nagai, N.; Yamagishi, H.; Furutani, H. 1,4-Bis(Diarylamino)-2,5-Bis(4-Cyanophenylethenyl)Benzenes: Fluorophores Exhibiting Efficient Red and Near-Infrared Emissions in Solid State. *Angew. Chem. Int. Ed.* **2012**, *51*, 4095–4099.

(135) Jonsson, M.; Wayner, D.; Lusztyk, J. *Redox and Acidity Properties of Alkyl and Arylamine Radical Cations and the Corresponding Aminyl Radicals 1*; 1996; Vol. 100.

(136) Hioe, J.; Šakić, D.; Vrček, V.; Zipse, H. The Stability of Nitrogen-Centered Radicals. *Org. Biomol. Chem.* **2015**, *13*, 157–169.

(137) Fortier, S.; Moral, O. G.; Chen, C.-H.; Pink, M.; Le Roy, J. J.; Murugesu, M.; Mindiola, D. J.; Caulton, K. G. Probing the Redox Non-Innocence of Dinuclear, Three-Coordinate

Co(II) Nindigo Complexes: Not Simply β-Diketiminate Variants. *Chem. Commun.* **2012**, *48*, 11082–11084.

(138) Gallei, M.; Rüttiger, C. Recent Trends in Metallopolymer Design: Redox-Controlled Surfaces, Porous Membranes, and Switchable Optical Materials Using Ferrocene-Containing Polymers. *Chem. – Eur. J.* **2018**, *24*, 10006–10021.

(139) Eloi, J.-C.; Chabanne, L.; Whittell, G. R.; Manners, I. Metallopolymers with Emerging Applications. *Mater. Today* **2008**, *11*, 28–36.

(140) Nguyen, A. I.; Zarkesh, R. A.; Lacy, D. C.; Thorson, M. K.; Heyduk, A. F. Catalytic Nitrene Transfer by a Zirconium(IV) Redox-Active Ligand Complex. *Chem. Sci.* **2011**, *2*, 166–169.

(141) Heyduk, A. F.; Zarkesh, R. A.; Nguyen, A. I. Designing Catalysts for Nitrene Transfer Using Early Transition Metals and Redox-Active Ligands. *Inorg. Chem.* **2011**, *50*, 9849–9863.

(142) Zarkesh, R. A.; Ziller, J. W.; Heyduk, A. F. Four-Electron Oxidative Formation of Aryl Diazenes Using a Tantalum Redox-Active Ligand Complex. *Angew. Chem. Int. Ed.* **2008**, *47*, 4715–4718.

(143) Chirik, P. J. Preface: Forum on Redox-Active Ligands. *Inorg. Chem.* **2011**, *50*, 9737–9740.

(144) Lyaskovskyy, V.; de Bruin, B. Redox Non-Innocent Ligands: Versatile New Tools to Control Catalytic Reactions. *ACS Catal.* **2012**, *2*, 270–279.

(145) de Bruin, B.; Gualco, P.; Paul, N. D. Redox Non-Innocent Ligands. In *Ligand Design in Metal Chemistry*; John Wiley & Sons, Ltd, 2016; pp 176–204.

(146) Chirik, P. J.; Wieghardt, K. Radical Ligands Confer Nobility on Base-Metal Catalysts. *Science* **2010**, *327*, 794.

(147) Zhu, C.; Ji, X.; You, D.; Chen, T. L.; Mu, A. U.; Barker, K. P.; Klivansky, L. M.; Liu, Y.; Fang, L. Extraordinary Redox Activities in Ladder-Type Conjugated Molecules Enabled by B ← N Coordination-Promoted Delocalization and Hyperconjugation. *J. Am. Chem. Soc.* **2018**, *140*, 18173–18182.

(148) Arumugam, K.; Shaw, M. C.; Chandrasekaran, P.; Villagrán, D.; Gray, T. G.; Mague, J. T.; Donahue, J. P. Synthesis, Structures, and Properties of 1,2,4,5-Benzenetetrathiolate Linked Group 10 Metal Complexes. *Inorg. Chem.* **2009**, *48*, 10591–10607.

(149) Deibel, N.; Sommer, M. G.; Hohloch, S.; Schwann, J.; Schweinfurth, D.; Ehret, F.; Sarkar, B. Dinuclear Quinonoid-Bridged D8 Metal Complexes with Redox-Active Azobenzene Stoppers: Electrochemical Properties and Electrochromic Behavior. *Organometallics* **2014**, *33*, 4756–4765.

(150) Yu, C.-H.; Yang, X.; Ji, X.; Wang, C.-H.; Lai, Q.; Bhuvanesh, N.; Ozerov, O. V. Redox Communication between Two Diarylamido/Bis(Phosphine) (PNP)M Moieties Bridged by Ynediyl Linkers (M = Ni, Pd, Pt). *Inorg. Chem.* **2020**, 59, 10153-10162.

(151) Li, Y.; Wu, Y.; Ong, B. S. Polyindolo[3,2-b]Carbazoles: A New Class of p-Channel Semiconductor Polymers for Organic Thin-Film Transistors. *Macromolecules* **2006**, *39*, 6521–6527.

(152) Steenwinkel, P.; Kooijman, H.; Smeets, W. J. J.; Spek, A. L.; Grove, D. M.; van Koten, G. Intramolecularly Stabilized 1,4-Phenylene-Bridged Homo- and Heterodinuclear Palladium and Platinum Organometallic Complexes Containing N,C,N-Coordination

Motifs; η^1-SO_2 Coordination and Formation of an Organometallic Arenium Ion Complex with Two Pt−C σ-Bonds. *Organometallics* **1998**, *17*, 5411–5426.

(153) Jeon, S. L.; Loveless, D. M.; Yount, W. C.; Craig, S. L. Thermodynamics of Pyridine Coordination in 1,4-Phenylene Bridged Bimetallic (Pd, Pt) Complexes Containing Two N,C,N‘ Motifs, 1,4-M_2-[$C_6(CH_2NR_2)_4$-2,3,5,6]. *Inorg. Chem.* **2006**, *45*, 11060–11068.

(154) Loeb, S. J.; Shimizu, G. K. H. Dimetallated Thioether Complexes as Building Blocks for Organometallic Coordination Polymers and Aggregates. *J. Chem. Soc. Chem. Commun.* **1993**, 1395–1397.

(155) Loeb, S. J.; Shimizu, G. K. H.; Wisner, J. A. Mono- versus Dipalladation of the Durene-Based Tetrathioether Ligand 1,2,4,5-(^{t}BuSCH$_2$)$_4$C$_6$H$_2$. Structures of [PdCl((^{t}BuSCH$_2$)$_4$C$_6$H)] and [Pd$_2$((^{t}BuSCH$_2$)$_4$C$_6$)(MeCN)$_2$][BF$_4$]$_2$. *Organometallics* **1998**, *17*, 2324–2327.

(156) Das, D.; Singh, P.; Singh, M.; Singh, A. K. Tetradentate Selenium Ligand as a Building Block for Homodinuclear Complexes of Pd(II) and Ru(II) Having Seven Membered Rings or Bis-Pincer Coordination Mode: High Catalytic Activity of Pd-Complexes for Heck Reaction. *Dalton Trans.* **2010**, *39*, 10876–10882.

(157) Wellala, N. P. N.; Dong, H. T.; Krause, J. A.; Guan, H. Janus POCOP Pincer Complexes of Nickel. *Organometallics* **2018**, *37*, 4031–4039.

(158) Gardinier, J. R.; Hewage, J. S.; Bennett, B.; Wang, D.; Lindeman, S. V. Tricarbonylrhenium(I) Complexes of Dinucleating Redox-Active Pincer Ligands. *Organometallics* **2018**, *37*, 989–1000.

(159) Fan, L.; Yang, L.; Guo, C.; Foxman, B. M.; Ozerov, O. V. N−C Cleavage in Pincer PNP Complexes of Palladium. *Organometallics* **2004**, *23*, 4778–4787.

(160) Ozerov, O. V. CHAPTER 13 - Rigid PNP Pincer Ligands and Their Transition Metal Complexes. In *The Chemistry of Pincer Compounds*; Morales-Morales, D., Jensen, C. M., Eds.; Elsevier Science B.V.: Amsterdam, 2007; pp 287–309.

(161) Yang, B. H.; Buchwald, S. L. Palladium-Catalyzed Amination of Aryl Halides and Sulfonates. *J. Organomet. Chem.* **1999**, *576*, 125–146.

(162) Hartwig, J. F. Carbon−Heteroatom Bond-Forming Reductive Eliminations of Amines, Ethers, and Sulfides. *Acc. Chem. Res.* **1998**, *31*, 852–860.

(163) Hartwig, J. F. Transition Metal Catalyzed Synthesis of Arylamines and Aryl Ethers from Aryl Halides and Triflates: Scope and Mechanism. *Angew. Chem. Int. Ed.* **1998**, *37*, 2046–2067.

(164) Cordovilla, C.; Bartolomé, C.; Martínez-Ilarduya, J. M.; Espinet, P. The Stille Reaction, 38 Years Later. *ACS Catal.* **2015**, *5*, 3040–3053.

(165) Hämmerle, J.; Schnürch, M.; Iqbal, N.; Mihovilovic, M. D.; Stanetty, P. A Guideline for the Arylation of Positions 4 and 5 of Thiazole via Pd-Catalyzed Cross-Coupling Reactions. *Tetrahedron* **2010**, *66*, 8051–8059.

(166) Lamm, W.; Pragst, F.; Jugelt, W. Untersuchungen Zum Anodischen Verhalten von Carbazolen Und Indolo[3,2-b]Carbazolen in Acetonitril. *J. Für Prakt. Chem.* **1975**, *317*, 995–1004.

(167) Stoll, S.; Schweiger, A. EasySpin—A Comprehensive Software Package for Spectral Simulation and Analysis in EPR. *J. Magn. Reson. San Diego Calif 1997* **2006**, *178*, 42–55.

(168) Hay, P. J.; Wadt, W. R. Ab Initio Effective Core Potentials for Molecular Calculations. Potentials for K to Au Including the Outermost Core Orbitals. *J. Chem. Phys.* **1985**, *82*, 299–310.

(169) Ke, X.-S.; Hong, Y.; Tu, P.; He, Q.; Lynch, V. M.; Kim, D.; Sessler, J. L. Hetero Cu(III)–Pd(II) Complex of a Dibenzo[g,p]Chrysene-Fused Bis-Dicarbacorrole with Stable Organic Radical Character. *J. Am. Chem. Soc.* **2017**, *139*, 15232–15238.

(170) DeMott, J. C.; Bhuvanesh, N.; Ozerov, O. V. Frustrated Lewis Pair-like Splitting of Aromatic C–H Bonds and Abstraction of Halogen Atoms by a Cationic $[(^{F}PNP)Pt]^{+}$ Species. *Chem. Sci.* **2013**, *4*, 642–649.

(171) Stangeland, E. L.; Sammakia, T. Use of Thiazoles in the Halogen Dance Reaction: Application to the Total Synthesis of WS75624 B. *J. Org. Chem.* **2004**, *69*, 2381–2385.

(172) Swager, T. M. 50th Anniversary Perspective: Conducting/Semiconducting Conjugated Polymers. A Personal Perspective on the Past and the Future. *Macromolecules* **2017**, *50*, 4867–4886.

(173) Holliday, B. J.; Swager, T. M. Conducting Metallopolymers: The Roles of Molecular Architecture and Redox Matching. *Chem. Commun.* **2005**, 23–36.

(174) Whittell, G. R.; Hager, M. D.; Schubert, U. S.; Manners, I. Functional Soft Materials from Metallopolymers and Metallosupramolecular Polymers. *Nat. Mater.* **2011**, *10*, 176–188.

(175) Nguyen, M. T.; Jones, R. A.; Holliday, B. J. Recent Advances in the Functional Applications of Conducting Metallopolymers. *Coord. Chem. Rev.* **2018**, *377*, 237–258.

(176) Vinoth, R.; Babu, S. G.; Bharti, V.; Gupta, V.; Navaneethan, M.; Bhat, S. V.; Muthamizhchelvan, C.; Ramamurthy, P. C.; Sharma, C.; Aswal, D. K.; Hayakawa, Y.; Neppolian, B. Ruthenium Based Metallopolymer Grafted Reduced Graphene Oxide as a New Hybrid Solar Light Harvester in Polymer Solar Cells. *Sci. Rep.* **2017**, *7*, 43133.

(177) Carrara, S.; Mauro, M.; Hogan, C. F. Metallopolymers as Nanostructured Solid-State Platforms for Electrochemiluminescence Applications. *ChemElectroChem* **2019**, *6*, 5790–5796.

(178) Chan, M. H.-Y.; Ng, M.; Leung, S. Y.-L.; Lam, W. H.; Yam, V. W.-W. Synthesis of Luminescent Platinum(II) 2,6-Bis(N-Dodecylbenzimidazol-2′-Yl)Pyridine Foldamers and Their Supramolecular Assembly and Metallogel Formation. *J. Am. Chem. Soc.* **2017**, *139*, 8639–8645.

(179) de Hatten, X.; Bell, N.; Yufa, N.; Christmann, G.; Nitschke, J. R. A Dynamic Covalent, Luminescent Metallopolymer That Undergoes Sol-to-Gel Transition on Temperature Rise. *J. Am. Chem. Soc.* **2011**, *133*, 3158–3164.

(180) Stanley, J. M.; Holliday, B. J. Luminescent Lanthanide-Containing Metallopolymers. *19th Int. Symp. Photophysics Photochem. Coord. Compd.* **2012**, *256*, 1520–1530.

(181) Holliday, B. J.; Stanford, T. B.; Swager, T. M. Chemoresistive Gas-Phase Nitric Oxide Sensing with Cobalt-Containing Conducting Metallopolymers. *Chem. Mater.* **2006**, *18*, 5649–5651.

(182) Zhou, C.; Zhao, W.; You, F.; Geng, Z.; Peng, H. Highly Stable and Luminescent Oxygen Nanosensor Based on Ruthenium-Containing Metallopolymer for Real-Time Imaging of Intracellular Oxygenation. *ACS Sens.* **2019**, *4*, 984–991.

(183) Dzhardimalieva, G. I.; Yadav, B. C.; Singh, S.; Uflyand, I. E. Self-Healing and Shape Memory Metallopolymers: State-of-the-Art and Future Perspectives. *Dalton Trans.* **2020**, *49*, 3042–3087.

(184) Liu, S.-J.; Lin, Z.-H.; Zhao, Q.; Ma, Y.; Shi, H.-F.; Yi, M.-D.; Ling, Q.-D.; Fan, Q.-L.; Zhu, C.-X.; Kang, E.-T.; Huang, W. Flash-Memory Effect for Polyfluorenes with On-Chain Iridium(III) Complexes. *Adv. Funct. Mater.* **2011**, *21*, 979–985.

(185) Ashford, D. L.; Gish, M. K.; Vannucci, A. K.; Brennaman, M. K.; Templeton, J. L.; Papanikolas, J. M.; Meyer, T. J. Molecular Chromophore–Catalyst Assemblies for Solar Fuel Applications. *Chem. Rev.* **2015**, *115*, 13006–13049.

(186) Dong, Q.; Qu, W.; Liang, W.; Tai, F.; Guo, K.; Leung, C.-W.; Lo, Y. H.; Wong, W.-Y. Porphyrin-Based Metallopolymers: Synthesis, Characterization and Pyrolytic Study for the Generation of Magnetic Metal Nanoparticles. *J. Mater. Chem. C* **2016**, *4*, 5010–5018.

(187) Mejía, M. L.; Reeske, G.; Holliday, B. J. Gallium-Containing Conducting Metallopolymers Which Display Chemically Tunable Reactivity for the Growth of Ga2S3 Semiconducting Nanoparticles. *Chem. Commun.* **2010**, *46*, 5355–5357.

(188) Bode, S.; Bose, R. K.; Matthes, S.; Ehrhardt, M.; Seifert, A.; Schacher, F. H.; Paulus, R. M.; Stumpf, S.; Sandmann, B.; Vitz, J.; Winter, A.; Hoeppener, S.; Garcia, S. J.; Spange, S.; van der Zwaag, S.; Hager, M. D.; Schubert, U. S. Self-Healing Metallopolymers Based on Cadmium Bis(Terpyridine) Complex Containing Polymer Networks. *Polym. Chem.* **2013**, *4*, 4966–4973.

(189) Liang, Y.; Strohecker, D.; Lynch, V.; Holliday, B. J.; Jones, R. A. A Thiophene-Containing Conductive Metallopolymer Using an Fe(II) Bis(Terpyridine) Core for Electrochromic Materials. *ACS Appl. Mater. Interfaces* **2016**, *8*, 34568–34580.

(190) DeMott, J. C.; Dekarske, J. R.; McCulloch, B. J.; Ozerov, O. V. Cyclometallation of the NNN Pincer Ligand in Complexes of Platinum. *Inorg. Chem. Front.* **2015**, *2*, 912–916.

APPENDIX A

SYNTHESIS OF DIPHENYL AND PHENYLTOLYLAMIDO PNP PLATINUM(II) PINCER COMPLEXES AND OBSERVATION OF OXIDATIVE COUPLING

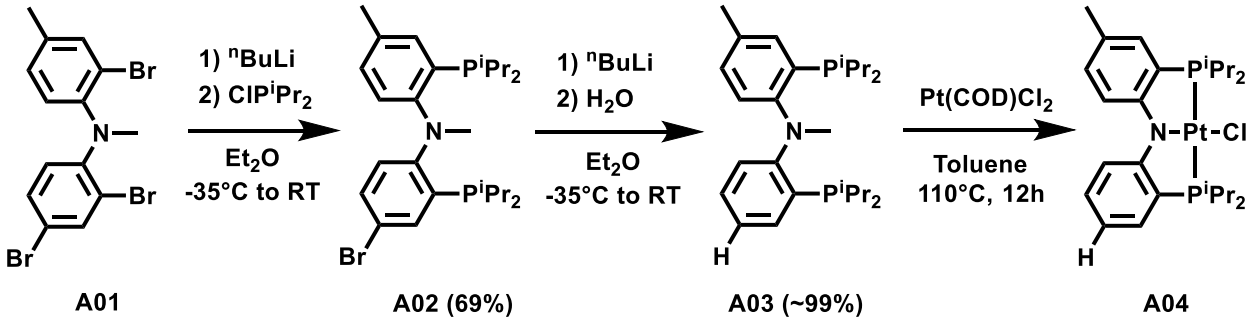

Scheme A-1. Synthesis of phenyltolyl PNPPtCl complex **A06.**

A02. In a glovebox, **A01** (1.5 g, 3.46 mmol) was dissolved in 50 mL of dried, degassed ether in a Schlenk flask and cooled to -35 ºC. ^{n}BuLi (2.77 mL, 6.9 mmol) was added slowly by a syringe. After 3 hours, $^{i}Pr_2PCl$ (1.06 g, 6.9 mmol) was added and the solution was stirred overnight. After completion, the volatiles was removed under vacuum and the residue was re-dissolved in pentane. The solution was filtered through a plug of silica gel and the volatiles were removed from the filtrate under vacuum to leave behind a colorless oil. The oil was re-dissolved in CH_2Cl_2, layered with acetonitrile and put into a -35 ºC freezer for one day. The supernatant was decanted and the solid was dried under vacuum to yield white powder (1.21 g, 69%). ^{1}H NMR (500 MHz, C_6D_6): δ 7.65 (s, 1H, Ar-*H*), 7.24 (s, 1H, Ar-*H*), 7.19 (dd, $J_{H\text{-}H}$ = 2 Hz, 9 Hz, 1H, Ar-*H*), 6.92 (d, $J_{H\text{-}H}$ = 9 Hz, 1H, Ar-*H*), 6.80 (dd, $J_{H\text{-}H}$ = 4 Hz, 8 Hz, 1H, Ar-*H*), 6.58 (dd, $J_{H\text{-}H}$ = 4 Hz, 9 Hz, 1H, Ar-*H*), 3.40 (s, 3H, N-*Me*), 2.16 (s, 3H, Ar-*Me*), 2.06-1.96 (m, 2H, C*H*Me$_2$), 1.94-1.84 (m, 2H, C*H*Me$_2$), 1.15 (dd, *J* = 7 Hz, 13 Hz, 6H, CH*Me*$_2$), 1.09 (dd, *J* = 7 Hz, 13 Hz, 6H, CH*Me*$_2$), 0.94 (dd, *J* = 7

Hz, 13 Hz, 12H, CH*Me*$_2$). ^{31}P{^{1}H} NMR (202 MHz, C_6D_6): δ -4.50 (d, $J_{P\text{-}P}$ = 9 Hz, 1P, Ar-*P*(^{i}Pr$_2$)), -7.12 (d, $J_{P\text{-}P}$ = 9 Hz, 1P, Ar-*P*(^{i}Pr$_2$)).

A03. In a glovebox, **A02** (1.0 g, 1.97 mmol) was dissolved in 50 mL of dried, degassed ether in a Schlenk flask and cooled to -35 ºC. ^{n}BuLi (0.88 mL, 2.20 mmol) was added slowly by a syringe. After 3 hours, H_2O (50 μL, 2.78 mmol) was added and the solution was stirred overnight. After completion, the volatiles was removed under vacuum and the residue was re-dissolved in pentane. The solution was filtered through a plug of silica gel and the volatiles were removed from the filtrate under vacuum to leave behind a pale oil. (with solvents, 880 mg, ~99%). ^{1}H NMR (500 MHz, C_6D_6): δ 7.36 (d, $J_{H\text{-}H}$ = 9 Hz, 1H, Ar-*H*), 7.26 (s, 1H, Ar-*H*), 7.06 (t, $J_{H\text{-}H}$ = 8 Hz, 1H, Ar-*H*), 6.97-6.82 (m, 4H, Ar-*H*), 3.48 (s, 3H, N-*Me*), 2.17 (s, 3H, Ar-*Me*), 2.06 (m, 4H, C*H*Me$_2$), 1.18 (m, 12H, C*H*Me$_2$), 0.98 (m, 12H, CH*Me*$_2$). ^{31}P{^{1}H} NMR (202 MHz, C_6D_6): δ -6.10 (d, $J_{P\text{-}P}$ = 10 Hz, 1P, Ar-*P*(^{i}Pr$_2$)), -7.14 (d, $J_{P\text{-}P}$ = 10 Hz, 1P, Ar-*P*(^{i}Pr$_2$)).

A04. In a glovebox, **A03** (200 mg, 0.466 mmol) was dissolved in 20 mL of dried, degassed toluene in a screw cap culture tube. Pt(COD)Cl_2 (187 mg, 0.500 mmol) was added to the solution and the tube was brought outside the glovebox. After heating at 110 ^{o}C for 12 h, the tube was taken in the glovebox. Volatiles were then removed under vacuum and the residue was re-dissolved in ether. The solution was filtered through a plug of silica gel and the volatiles were removed from the filtrate under vacuum to give a yellow powder. (250 mg, 82%). ^{1}H NMR (500 MHz, C_6D_6): δ 7.79 (d, $J_{H\text{-}H}$ = 8 Hz, 1H, Ar-*H*), 7.74 (d, $J_{H\text{-}H}$ = 8 Hz, 1H, Ar-*H*), 7.01-6.86 (m, 3H, Ar-*H*), 6.73 (d, $J_{H\text{-}H}$ = 8 Hz, 1H, Ar-*H*), 6.47 (t, $J_{H\text{-}H}$ = 7 Hz, 1H, Ar-*H*), 2.50 (m, 4H, C*H*Me$_2$), 2.13 (s, 3H, Ar-

Me), 1.49-1.35 (m, 12H, CH*Me*$_2$), 1.18-1.02 (m, 12H, CH*Me*$_2$). $^{31}P\{^1H\}$ NMR (202 MHz, C_6D_6): δ 41.7 (s, $J_{P\text{-}Pt}$ = 1331 Hz, 1P, Ar-*P*(^{i}Pr$_2$)), 41.5 (s, $J_{P\text{-}Pt}$ = 1331 Hz, 1P, Ar-*P*(^{i}Pr$_2$)).

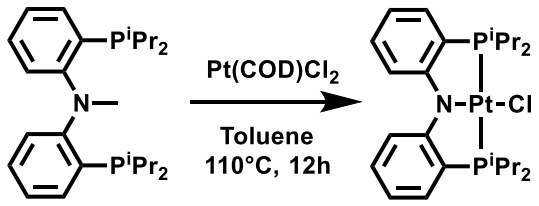

A05 **A06**

Scheme A-2. Synthesis of diphenyl PNPPtCl complex **A05.**

A06. In a glovebox, **A05** (200 mg, 0.451 mmol) was dissolved in 20 mL of dried, degassed toluene in a screw cap culture tube. $Pt(COD)Cl_2$ (187 mg, 0.500 mmol) was added to the solution and the tube was brought outside the glovebox. After heating at 110 ^oC for 12 h, the tube was taken in the glovebox. Volatiles were then removed under vacuum and the residue was re-dissolved in ether. The solution was filtered through a plug of silica gel and the volatiles were removed from the filtrate under vacuum to give a yellow powder. (145 mg, 51%). ^1H NMR (500 MHz, C_6D_6): δ 7.78 (d, $J_{H\text{-}H}$ = 9 Hz, 2H, Ar-*H*), 6.96 (dt, $J_{H\text{-}H}$ = 4 Hz, 7 Hz, 2H, Ar-*H*), 6.90 (t, $J_{H\text{-}H}$ = 8 Hz, 2H, Ar-*H*), 6.48 (d, $J_{H\text{-}H}$ = 7 Hz, 2H, Ar-*H*), 2.49 (m, 4H, C*H*Me$_2$), 1.40 (q, $J_{H\text{-}H}$ = 8 Hz, 12H, CH*Me*$_2$), 1.08 (q, $J_{H\text{-}H}$ = 7 Hz, 12H, CH*Me*$_2$). $^{31}P\{^1H\}$ NMR (202 MHz, C_6D_6): δ 41.6 (s, $J_{P\text{-}Pt}$ = 1325 Hz, 1P, Ar-*P*(^{i}Pr$_2$)).

Oxidative coupling experiment.

In a glovebox, **A05** or **A06** (0.158 mmol) was dissolved in 20 mL of dried, degassed THF in a screw cap culture tube. The oxidant ($FeCl_3$, AgOTf, or magic blue, 0.634 mmol) and NaO^{t}Bu (0.317 mmol) were added to the solution and the tube was brought outside the glovebox. After

heating at 70 ^{o}C overnight, the tube was taken in the glovebox. The solution was filtered through a plug of celite and cobaltocene (0.317 mmol) was added to it. After 5 minutes, the solution was filtered through a plug of silica gel and the volatiles were removed from the filtrate. The NMR spectrum of the crude mixture was then collected.

Treatment of A04 with $FeCl_3$.

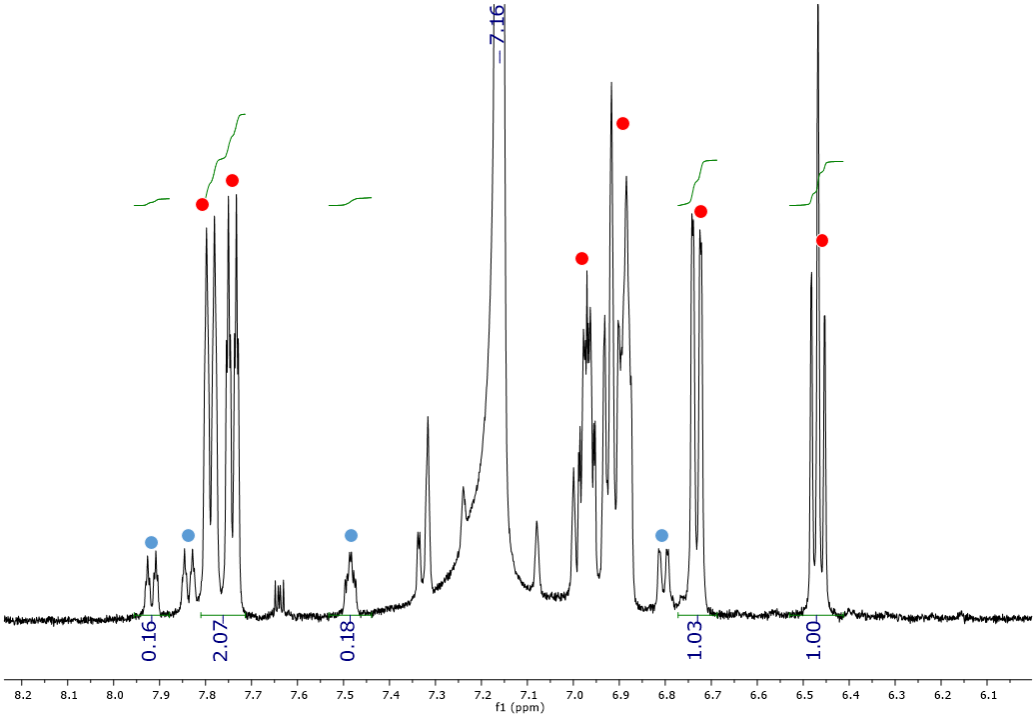

Figure A-1. Reaction of **A04** with $FeCl_3$ for 3 hours at room temperature. **A04** was labeled with red and the product was labeled with blue.

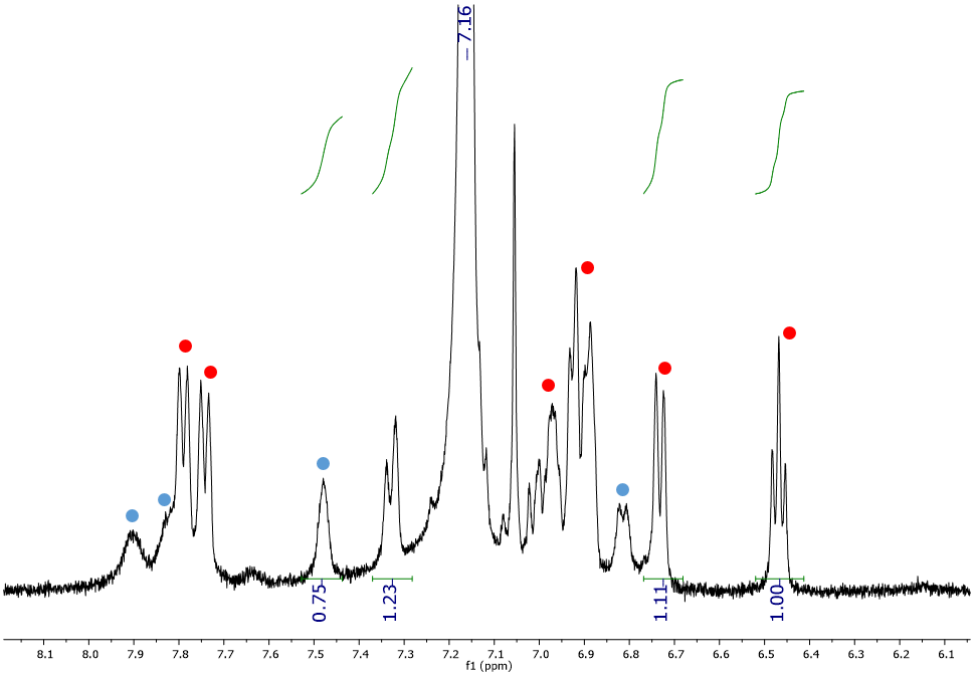

Figure A-2. Reaction of **A04** with $FeCl_3$ for 18 hours at 70 ºC. **A04** was labeled with red and the product was labeled with blue.

Treatment of A04 with magic blue.

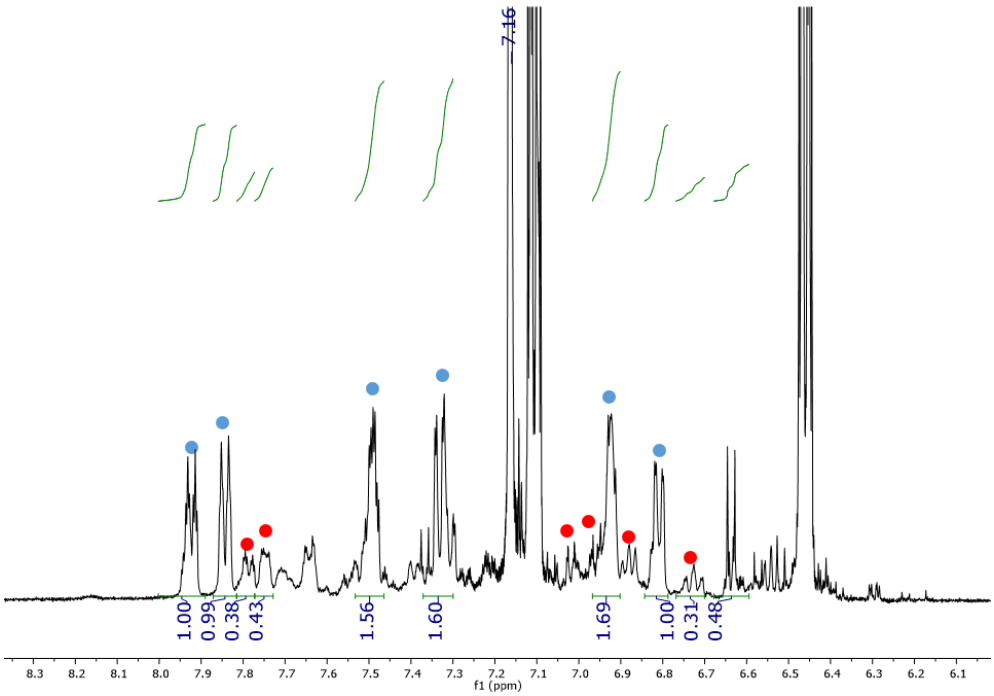

Figure A-3. Reaction of **A04** with $FeCl_3$ for 18 hours at 70 ºC. **A04** was labeled with red and the product was labeled with blue.

Treatment of A06 with AgOTf.

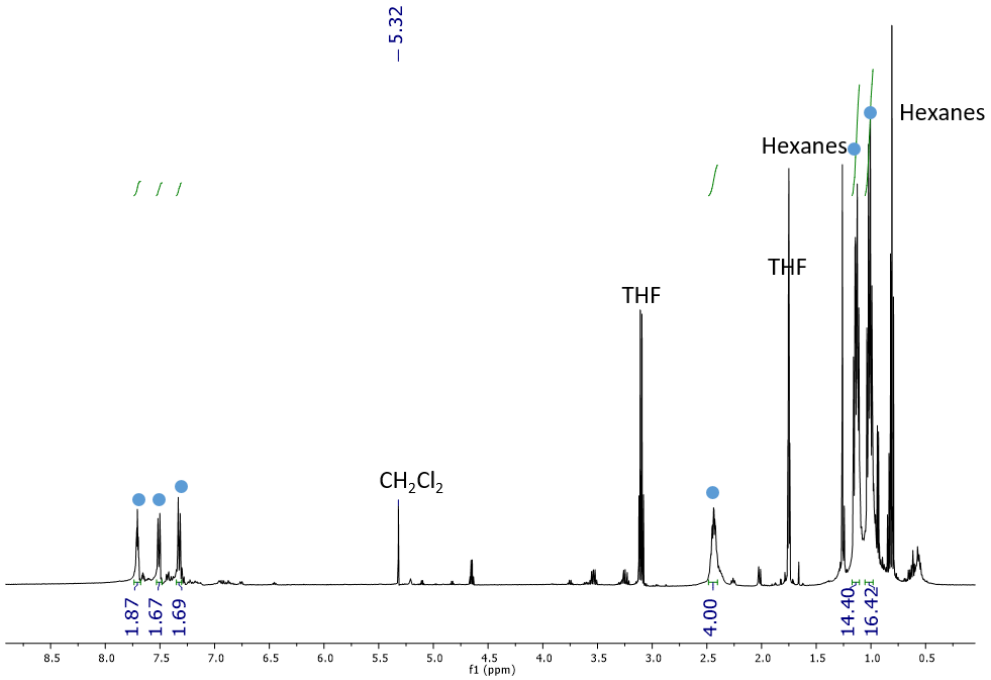

Figure A-4. Reaction of **A06** with AgOTf for 18 hours at 70 ºC. The product was labeled with blue.

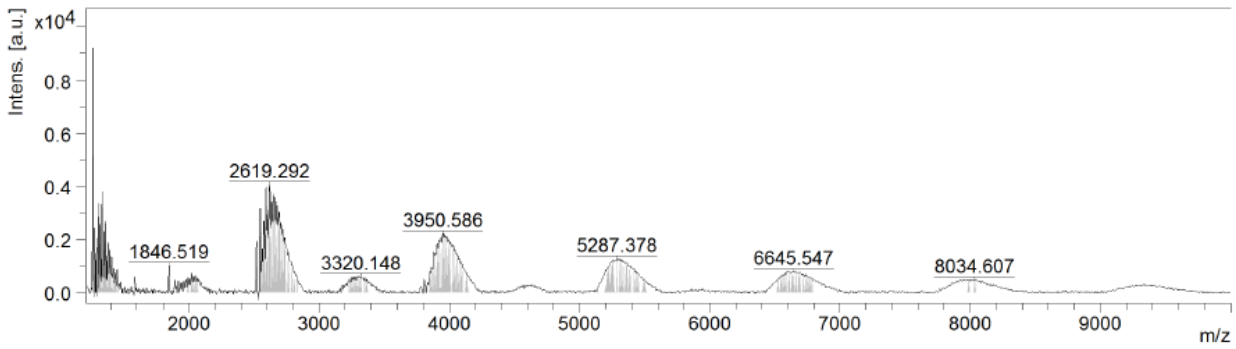

Figure A-5. MALDI-MS of the product from Figure A-4.

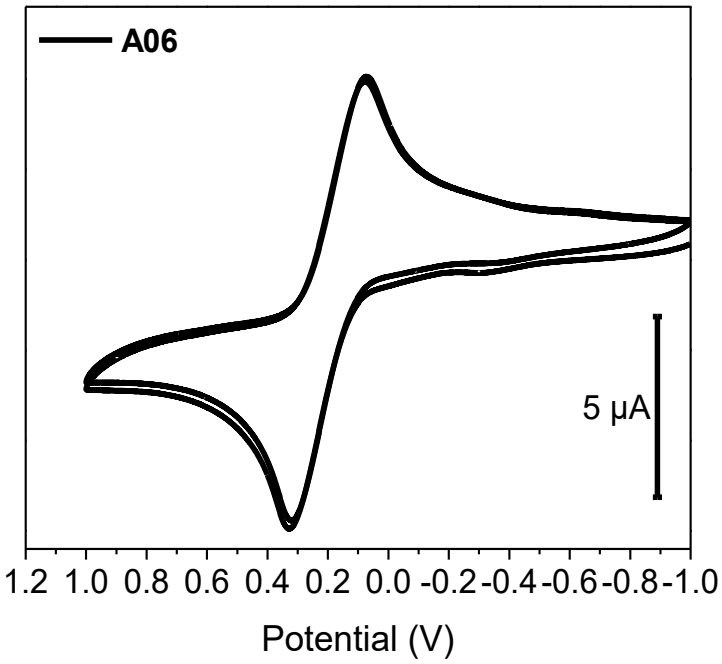

Figrue A-6. Multiple scanning cyclic voltammograms of complexes **A06** (ca. 0.001 M in CH_2Cl_2) with $^{n}Bu_4NPF_6$ electrolyte (0.1 M), scan rate 100 mV/s, potentials referenced to Fc^{+}/Fc at 0 V.

APPENDIX B

LIST OF PUBLICATIONS FROM THE PHD WORK

1. Yu, C.-H.; Yang, X.; Ji, X.; Wang, C.-H.; Lai, Q.; Bhuvanesh, N.; Ozerov, O. V. "Redox Communication between Two Diarylamido/Bis(Phosphine) (PNP)M Moieties Bridged by Ynediyl Linkers (M = Ni, Pd, Pt)" *Inorg. Chem.* **2020**, *59*, 10153-10162.
2. Yu, C.-H.; Zhu, C.; Ji, X.; Hu, W.; Xie, H.; Bhuvanesh, N.; Fang, L.; Ozerov, O. V. "Palladium Bis-Pincer Complexes with Controlled Rigidity and Inter-Metal Distance" submitted.